Université de Montréal

# Mucopolysaccharidosis type IIIC: Molecular defects and pathophysiological mechanism

*Par*

**Carla Isabel Ferraz Nunes Martins**

Département de biochimie et médecine moléculaire,

Centre de recherche du Centre Hospitalier Universitaire Ste-Justine,

Faculté de médecine, Université de Montréal

Thèse présentée en vue de l'obtention du grade de Doctorat

en Biochimie, spécialisation Génétique moléculaire

Août 2021

Université de Montréal

Unité académique: Département de Biochimie et Médecine Moléculaire, Faculté de Médecine

---

*Cette thèse intitulée*

# Mucopolysaccharidosis type IIIC: Molecular defects and pathophysiological mechanism

*Présenté par*

**Carla Isabel Ferraz Nunes Martins**

*A été évaluée par un jury composé des personnes suivantes*

**Stephen Michnick**
Président-rapporteur

**Alexey V. Pshezhetsky**
Directeur de recherche

**Przemyslaw (Mike) Sapieha**
Membre du jury

**John Mitchell**
Examinateur externe

# Résumé

La mucopolysaccharidose de type IIIC (MPS IIIC), ou le syndrome de Sanfilippo type C, est une maladie pédiatrique rare et grave, provoquant une détérioration neurologique progressive, affectant initialement l'acquisition de la parole et le comportement, et conduisant finalement à la démence, aux déficits moteurs et à une mort prématurée. Des variants pathogéniques dans le gène *HGSNAT* sont responsables de la déficience de l'enzyme héparane sulfate acetyl-CoA: α-glucosaminide N-acetyltransferase impliquée dans le catabolisme lysosomal de l'héparane sulfate (HS).

La connaissance limitée de la pathophysiologie de la maladie jusqu'à présent a empêché le développement de thérapies efficaces. Afin de mieux comprendre les mécanismes pathogéniques à l'origine de la maladie, en particulier la neurodégénerescence progressive, nous avons caractérisé le premier modèle animal du syndrome de Sanfilippo type C, une souris *Hgsnat* Knockout (chapitre II). Nous avons montré que le modèle murin de MPS IIIC reproduit les étapes progressives de la maladie humaine. Les souris affectées présentent une hyperactivité et une réduction de l'anxiété comme symptômes initiaux, suivis d'une déficience de la mémoire spatiale et de l'apprentissage, d'une démarche anormale à un stade ultérieur de la maladie et une espérance de vie réduite.

À travers cette étude, nous avons démontré que le déficit en HGSNAT entraîne la surcharge de HS dans les lysosomes des microglies depuis le plus jeune âge et déclenche une réponse neuroinflammatoire chronique, caractérisée par une micro- et astrogliose et la production de cytokines. Au niveau des neurones, l'accumulation d'HS est détecté plus tard et est accompagné de l'accumulation d'organelles dysfonctionnelles, y compris des mitochondries gonflées avec une structure anormale, ce qui entraîne probablement une déficience du métabolisme énergétique mitochondriale dans le cerveau des souris MPS IIIC. En outre, des niveaux accrus d'ubiquitine, LC3-II, des protéines tau phosphorylée et amyloïde-β susceptibles à l'agrégation, et des protéines modifiées par *O*-GlcNAc dans les neurones suggèrent une protéolyse cellulaire déficitaire. Nos résultats suggèrent que l'accumulation de mitochondries endommagées peut largement contribuer

à la perte neuronale détectée dans les souris MPS IIIC et serait la conséquence d'une neuroinflammation chronique et d'un déficit de la mitophagie.

Dans le deuxième projet de cette thèse, nous avons étudié et caractérisé les défauts génétiques d'une large cohorte de nouveaux patients Sanfilippo C de différentes origines géographiques, incluant des pays où des patients n'avait jamais encore été identifiés (chapitre III).

La caractérisation moléculaire de 27 nouveaux patients a permis, pour la première fois, l'identification de variants pathogéniques dans *HGSNAT* chez des patients du Brésil, d'Algérie, d'Azerbaïdjan et d'Iran et l'élargissement du spectre mutationnel au Canada, la Colombie, la Turquie et les USA. De plus, nous avons identifié six nouveaux variants causant la maladie, montrant, à travers des analyses *in silico* et d'études fonctionnelles *in vitro*, qu'ils interfèrent avec la production ou le repliement des protéines HGSNAT mutantes.

Cette étude nous a aussi permis de différencier deux groupes de patients en fonction de l'apparition et de la progression de la maladie, potentiellement associés à différents types de variants pathogéniques. Enfin, l'analyse d'haplotypes portant sur le plus grand groupe de patients étudiés à ce jour, 78 cas provenant de 22 pays différents, a révélé la même origine pour plusieurs variants pathogéniques du gène *HGSNAT* détectés dans différentes populations, et l'existence de plusieurs mutations fondatrices.

En conclusion, la caractérisation du premier modèle murin MPS IIIC a permis d'identifier différents mécanismes physiopathologiques sous-jacents à la maladie, qui peuvent représenter des cibles thérapeutiques clés. Ce modèle animal est également un outil utile pour l'évaluation de l'efficacité de nouvelles thérapies. En outre, cette thèse a ainsi contribué à la connaissance de la répartition géographique et de la fréquence des variants pathogéniques du gène *HGSNAT* et à l'identification des effets fondateurs, ce qui peut contribuer à un diagnostic précoce des patients atteints de MPS IIIC.

**Mots clés:** Mucopolysaccharidose, maladies lysosomales, héparane sulfate, héparane sulfate acetyl-CoA: α-glucosaminide N-acetyltransferase, neurodégénérescence, modèle souris knockout, mitochondrie, variants du gène *HGSNAT*, haplotype, effet foundateur.

# Abstract

Mucopolysaccharidosis III type C (MPS IIIC), or Sanfilippo syndrome type C, is a rare and severe pediatric disease causing progressive neurological deterioration, initially affecting speech acquisition and behavior, and ultimately leading to dementia, motor deficits and premature death. Pathogenic variants in the *HGSNAT* gene are responsible for the deficiency of heparan sulfate acetyl-CoA: α-glucosaminide N-acetyltransferase involved in the lysosomal catabolism of heparan sulfate (HS).

The limited knowledge of the pathophysiology of the disease has so far precluded the development of effective therapies. In order to understand the pathogenic mechanisms underlying the disease, in particular the neurodegenerative process, we have characterized the first animal model of Sanfilippo syndrome type C, an *Hgsnat* Knockout mouse (chapter II). We have shown that the MPS IIIC murine model recapitulates human disease progression, presenting hyperactivity and reduced anxiety as initial symptoms, followed by an impaired spatial memory and learning, abnormal gait at a later stage, and reduced lifespan.

Through this study, we have demonstrated that HGSNAT deficiency leads to the storage of HS in brain microglial lysosomes from an early age, triggering a chronic neuroinflammatory response characterized by micro- and astrogliosis and cytokine production. In neurons, the storage of HS is detected at a later stage and it is accompanied by the accumulation of dysfunctional organelles, including swollen, structurally abnormal mitochondria, likely responsible for the impaired mitochondrial energy metabolism in the brain of MPS IIIC mice. Furthermore, augmented levels of intraneuronal ubiquitin, LC3-II, the aggregate prone-proteins phosphorylated tau and amyloid-β, and *O*-GlcNAc-modified proteins are suggestive of a defective cellular proteolysis. Altogether, our findings suggest that accumulation of damaged mitochondria is the consequence of chronic neuroinflammation and mitophagy impairment, and may largely contribute to the neuronal loss detected in MPS IIIC mice.

In the second project of this thesis, we investigated and characterized the molecular defects in a large cohort of new Sanfilippo C patients from different geographic origins, including countries where MPS IIIC patients had not yet been reported (chapter III). The molecular characterization of the 27 new patients enabled, for the first time, the identification of *HGSNAT* disease-causing

variants in patients from Brazil, Algeria, Azerbaijan, and Iran and to extend their spectrum within Canada, Colombia, Turkey and the USA. Besides, we have identified six novel pathogenic variants showing, through *in silico* and *in vitro* functional studies, that they interfere with the production or folding of the resulting HGSNAT mutant proteins.

This study also allowed the differentiation of two groups of patients based on the onset and progression of the disease, potentially associated to different types of pathogenic variants. Finally, a haplotype study on the largest group of patients studied so far, 78 cases from 22 different countries, revealed the same origin for several *HGSNAT* pathogenic variants detected in different populations, and the existence of several founder mutations.

In conclusion, the characterization of the first MPS IIIC murine model enabled the identification of different pathophysiological mechanisms underlying the disease, which may represent key therapeutic targets. This animal model is also a useful tool for the evaluation of the effectiveness of novel therapies. Furthermore, this thesis has also contributed to the knowledge of the worldwide geographic distribution and frequency of *HGSNAT* disease-causing variants, and the identification of founder effects, which may contribute to an early diagnosis of MPS IIIC patients.

**Keywords:** Mucopolysaccharidosis, lysosomal storage disorder, heparan sulfate, heparan sulfate acetyl-CoA: α-glucosaminide N-acetyltransferase, neurodegeneration, knockout mouse model, mitochondria, *HGSNAT* variants, haplotype, founder effect.

# Table of contents

# List of Tables

# List of Figures

# List of abbreviations

2OST: 2-*O*-sulfotransferase
3OST: 3-*O*-sulfotransferase
6OST: 6-*O*-sulfotransferase
AAV: Adeno-associated virus
AAV-TT: Adeno-associated virus true type
AD: Alzheimer's disease
ALS: Amyotrophic lateral sclerosis
AMPK: 5' Adenosine monophosphate-activated protein kinase
Akt: Protein kinase B
AP: Adaptor protein
ATG: Autophagy related
ATP: Adenosine 5' triphosphate
ARSA: Arylsulfatase A
ARSG: N-sulphoglucosamine 3-*O*-sulfatase
ARSK: Arylsulfatase K
AV: Adenovirus
βGC: β-glucocerebrosidase
BBB: Blood-brain barrier
BDNF: Brain-derived neurotrophic factor
BM: Basement membrane
bp: Base pair
$Ca^{2+}$: Calcium cation
Cas9: CRISPR-associated protein 9
Casp: Caspase
C6S: Chondroitin 6-sulfate
cAMP: Cyclic adenosine monophosphate
CI-MPR: Cation-independent mannose 6-phophate receptor
CLEAR: Coordinated lysosomal expression and regulation
CMA: Chaperone-mediated autophagy
CMV: Cytomegalovirus
CNS: Central nervous system
CoQ10: Coenzyme Q10, or ubiquinone
Cox IV: Cytochrome c oxidase subunit IV
CRISPR: Clustered regularly interspaced short palindromic repeats
CS: Chondroitin sulfate

CSF: Cerebrospinal fluid
CTS: Cathepsin
Cytc: Cytochrome c
DAMP: Damage-associated molecular patterns
DBS: Dried blood spot
DS: Dermatan sulfate
DNA: Deoxyribonucleic acid
DMB: 1,9-dimethylmethylene blue
DMT: 1-Divalent metal transporter-1
ECM: Extracellular matrix
EET: Enzyme enhancement therapy
EGF: Epidermal growth factor
EL: Endolysosome
ER: Endoplasmic reticulum
ERAD: Endoplasmic reticulum-associated degradation pathway
ERT: Enzyme replacement therapy
ESCRT: Endosomal sorting complex required for transport
ESC: Embryonic stem cells
EXTL1, 2 or 3: Exostosin-like glycosyltransferase 1, 2 or 3
FDA: Food and drug administration
FGE: Formylglycine-generating enzyme
G6S: N-acetylglucosamine-6-sulfatase
GABA: Gamma-aminobutyric acid
GAG: Glycosaminoglycan
GAP43: Growth associated protein 43
GDS: Glucuronate-2-sulfatase
GFAP: Glial fibrillary acid protein
GGA: Golgi-localized, γ-ear-containing, ADP-ribosylation factor (Arf)-binding protein
GlcA: Glucuronic acid
GlcN: Glucosamine
GlcNAc: N-acetylglucosamine
GlcNS: Sulfated glucosamine units
GNS: N-acetylglucosamine-6-sulfatase
GT: Gene therapy
GUSB: β-D-glucuronidase
GSL: glycosphingolipids
HA: Hyaluronic acid
Hex A: Hexosaminidase A
Hex B: Hexosaminidase B
HD: Huntinton's disease
HGMD: Human Gene Mutation Database

HGSNAT: Heparan sulfate acetyl-CoA: α-glucosaminide N-acetyltransferase, or Heparan□α□glucosaminide N□acetyltransferase
HS: Heparan sulfate
HSBP: Heparan sulfate binding protein
HSC: Haematopoietic stem cell
HSCT: Haematopoietic stem cell transplant
HSO: HS-oligosaccharides
HSPG: Heparan sulfate proteoglycan
HSPC: Hematopoietic stem and progenitor cell
ICT: Intracisternal
ICV: Intracerebroventricular
IDDD: Intrathecal drug delivery device
IdoA: Iduronic Acid
IDS: Iduronate-2-sulfatase
IDUA: α-L-Iduronidase
IGF2: Insulin-like growth factor 2
IL1-β: Interleukin 1β
IL6: Interleukin 6
ILVs: Intraluminal vesicles
IFNγ: Interferon-γ
iNOS: Inducible nitric oxide synthase
IP: Intraparenchymal
iPSC: Induced pluripotent stem cell
IT: Intrathecal lumbar
IV: Intravenous
KO: Knockout
KS: Keratan sulfate
LAMP: Lysosomal-associated membrane protein
LC3: Microtubule-associated protein light chain 3
LC-MS/MS: Liquid chromatography tandem mass spectrometry
LE: Late endosomes
LIMP-2: Lysosomal integral membrane protein 2
LMP: Lysosomal membrane permeabilization
LPS: Lipopolysaccharide
LSD: Lysosomal storage disorder
LV: Lentivirus
M6P: Mannose-6-phosphate
M6PR: Mannose-6-phosphate receptor
MAP: Mitogen-activated protein
MAPK: Mitogen-activated protein kinase
MCOLN1: Mucolipin-1, or TRPML1

MCP1/CCL2: Monocyte chemoattractant protein 1/ C–C motif chemokine ligand 2
MYD88: Myeloid differentiation primary response 88
MEC: Medial entorhinal cortex
MEF: Murine embryonic fibroblasts
MIP-1α/CCL3: Macrophage Inflammatory Proteins 1α/ C–C motif chemokine ligand 3
MLKL: Mixed lineage kinase domain-like protein
MOMP: Mitochondrial outer membrane permeabilization
MPS: Mucopolysaccharidosis
MOMP: Mitochondrial outer membrane permeabilization
MS/MS: Tandem mass spectrometry
MSD: Multiple sulfatase deficiency
MVB: Multivesicular body
mTORC1: Mammalian target of rapamycin complex 1
NADPH: Reduced nicotinamide adenine dinucleotide phosphate
NAGLU: α-N-acetylglucosaminidase
NDST: N-deacetylase/N-sulfotransferase
NB-DNJ: N-butyl-deoxynojirimycin (Miglustat)
NF-κB: Nuclear Factor kappa-light-chain-enhancer of activated B cells
NLRP3: Nucleotide-binding oligomerization domain (NOD), leucine rich repeat (LRR) and pyrin domain containing 3
NGF: Nerve growth factor
NGS: Next-generation sequencing
NO: Nitric oxide
NPC Niemann-Pick disease type C
NSAID: Nonsteroidal anti-inflammatory drug
NSC: Neural stem cells
P62/SQSTM1: Sequestosome-1
PAMPs: Pathogen-associated molecular patterns
PC: Pharmacological chaperone
pH: Hydrogen potential
PI3K: Phosphatidylinositol-3-kinase
PI3P: Phosphatidylinositol 3-phosphate
PD: Parkinson's disease
PM: Plasma membrane
PNS: peripheral nervous system
PPS: Pentosan polysulfate
P-tau: Phosphorylated tau
PTPC: Permeability transition pore complex
RIPK3: Receptor-interacting serine/threonine-protein kinase 3
RME: Receptor-mediated endocytosis
Rheb: Ras homolog enriched in brain

RME: Receptor-mediated endocytosis
RNA: Ribonucleic acid
RP: Retinitis pigmentosa
ROS: Reactive oxygen species
RNS: Reactive nitrogen species
RV: Retroviral
SCMAS: Subunit c of mitochondrial ATP synthase
SGSH: N-sulphoglucosamine sulphohydrolase, or sulfamidase
SNARE: Soluble N-ethylmaleimide-sensitive factor attachment protein receptor
SNAP-29: Synaptosomal-associated protein 29
SNPs: Single nucleotide polymorphisms
SOD1: Superoxide dismutase 1
SP: Signal peptide
SRT: Substrate reduction therapy
STR: Short tandem repeat
SUMF1: Sulfatase Modifying Factor 1
Tau/MAPT: microtubule-associated protein tau
TFEB: Transcription factor EB
TfR: Transferrin receptor
TGF-β: Transforming growth factor β
TGN: Trans-Golgi network
TLR: Toll-like receptor
TNF-α: Tumor necrosis factor alpha
TNFR1: Tumor necrosis factor receptor 1
TRPML1: Transient receptor potential cation channel, mucolipin subfamily, member 1, or MCOLN1
UCB: Umbilical cord blood
uGAGs: Urinary glycosaminoglycans
UPR: Unfolded protein response
UPS: Ubiquitin-proteasome system
VAMP-7: Vesicle-associated membrane protein 7
VEGP: Vascular endothelial growth factor
VDAC1: Voltage-dependent anion-selective channel 1
VNTRs: Variable number of tandem repeats
WES: Whole exome sequencing
WGS: Whole genome sequencing
WT: Wild type
XYLT1 or 2: Xylosyltransferases 1 or 2

*I dedicate this thesis to the memory of my father, João, and to my mother, Maria de Lurdes.*

*I also dedicate it to Jonah, Joana, all the other MPS IIIC patients and their loving families.*

# Acknowledgements

This dissertation is the result of a long journey, only possible through the support of an extended group of people, to whom I am deeply grateful.

First, I would like to express my sincere gratitude to my supervisor, Professor Alexey Pshezhetsky, for giving me the opportunity to pursue my Doctoral studies his laboratory, enabling me to do research in the inspirational field of pediatric neurodegenerative disorders. I am deeply indebted for his invaluable guidance, unwavering support and patience, trust in my abilities and encouragement throughout these years.

I would like to acknowledge the PhD jury members, Professors Stephen Michnick, John Mitchell, Przemyslaw (Mike) Sapieha and Fernando Alvarez, for accepting to evaluate this dissertation.

I am also extremely thankful to the elements of my PhD advisory committee, Professors Jurgen Sygusch and Yves Durocher, for the supportive and insightful advice during my studies.

I gratefuly acknowledge the Fundação para a Ciência e Tecnologia (FCT, Lisboa - Portugal) for the 4-year PhD fellowship (SFRH/BD/84929/2012 financiada por fundos nacionais do orçamento de estado) and the Faculty of Medicine of the University of Montreal for funding my studies. I also thank Jonah Just Begun Foundation and Sanfilippo Children's Research Foundation for supporting the research in our laboratory.

I would like to express my deepest gratitude to all the collaborators for their contribution to the publications in this dissertation. I must thank Dr Damian Labuda for his contagious enthusiasm for population genetics and for offering me invaluable expertise and guidance in this area; Dr Roberto Giugliani, Dr Paula Frassinetti de Medeiros and Dr Nursel Elcioglu for their interest in the project and always being available to answer to my questions on the clinical history of MPS IIIC patients; Dr Brian Bigger and his team, as well as Dr Jerôme Ausseil, for technical assistance in different experiments, material and insightful discussions; Dr Helena Hůlková and Dr Martin Hrebícek for performing the electron microscopy experiments; Dr Graziella DiCristo and her group for the training in confocal microscopy and providing access to the microscopy facilities; Dr Edith Hamel for the training and granting access to the Morris water maze; Dr Hana Hansíková and her team for the measurement of mitochondrial enzymatic activities and CoQ10 content; Dr Carlos Morales for kindly providing the *GM2A* plasmid and anti-GM2AP antibody; Dr Grant A. Mitchell and his team for the clinical evaluation of the GM2-gangliosidosis, AB variant, patient.

I am deeply indebted to Dr Lucia Lacerda, who has been an example for me since my earliest steps in science, for her faith in my abilities, for encouraging me to pursue my Doctoral studies, being crucial for the start of this endeavour, and for her friendship.

This thesis would not be possible without the contribution of MPS IIIC patients and their families. I particularly thank Mrs Jill Wood (Jonah Just Begun Foundation) and Mrs Raquel Marques (Associação Sanfilippo Portugal), for also triggering my PhD adventure and for their support and motivation. They are truly inspirational, as they are an example that courage, resilience and love for the family allows facing the most difficult obstacles and, hopefully, changing the world. I am extremely grateful to the families that kindly answered my questions, allowing me to learn more about the disease.

Many thanks to all past and present colleagues in the laboratory, especially to Larbi Dridi and Mila Ashmarina, for contributing to my work, generously helping me during this journey, the interesting scientific discussions and enjoyable moments.

I am also thankful to my friends for their constant optimism and encouragement. Special thanks to Ana Maria, Cristina and Mafalda for being there for me, despite the distance.

I am very fortunate that my PhD studies in Canada allowed meeting wonderful people.

I will be forever grateful to Dª Fernanda, Sr. Jorge Campos and their family for receiving and treating me as a family member, and being always source of support and happiness over the years.

I really miss the joyful discussions with Fatima and Josianne at coffee and lunch in the research center as well as the wonderful time spent outside. Thank you for listening to me when I needed, your supportive advice, and your friendship!

Words cannot express the gratitude to my mother, Maria de Lurdes, for the love and everything that she has taught and done for me. Thank you for the endless support and encouragement to start and complete this venture! (Muito obrigada mãezinha, pelo amor e por tudo aquilo que me ensinaste e fizeste por mim, pelo apoio e incentivo para começar e finalizar esta etapa!).

I am forever indebted to Larbi, initially as a colleague in the lab, then a friend and finally a husband, for all the help along the way, essential for the success of this long enterprise. You were my greatest gift in Montreal, and my life, and I am profoundly thankful for your unconditional love, for your immense patience and understanding, for believing in me and being my biggest supporter!

# Chapter I. Introduction

## 1.1 Lysosomes

### 1.1.1 Discovery and general characteristics

Lysosomes are single membrane-bound intracellular organelles first described by Christian de Duve in 1955 (1). Due to their high content in acid hydrolases and role in localized intracellular digestion of macromolecules, De Duve suggested the Greek term 'lysosome', corresponding to 'digestive body', to name these cell structures. Since then the knowledge on the structure and cellular functions of the lysosome greatly expanded. Multiple studies have also revealed the important roles of these organelles in disease and aging.

The lysosomes are now defined as dynamic organelles present in all eukaryotic cells that may exhibit variation in size, shape (2), number and positioning in the cell (3). They interact with the plasma membrane and other organelles, and play an important role in intracellular signaling and communication between cells, as well as between cells and their external environment, e.g. during the immune response and cell death (Fig.1). The function of the lysosome as an important metabolic regulator has been recently unraveled, showing that these organelles sense and respond to environmental cues.

The lysosomes play a key role in the endolysosomal-autophagy network by ensuring the degradation of impaired organelles, other intra- and extracellular material and recycling of nutrients, essential for cell homeostasis (Fig.1).

### 1.1.2 Lysosomes: biogenesis and protein composition

#### 1.1.2.1 Biogenesis of lysosomes

The formation of lysosomes depends on both the biosynthetic and endocytic pathways of the cell. The soluble and membrane proteins that are essential for the structure and function of the lysosome are synthesized in the endoplasmic reticulum (ER) and then transit by vesicular transport to the Golgi complex, and further to the trans-Golgi network (TGN), undergoing several post-

translational modifications. Their transport from the TGN to the endolysosomal system may be direct, to the early or late endosome, and/or indirect, via the constitutive secretory pathway with proteins being first transported to the plasma membrane, in the case of membrane proteins, or secreted to the extracellular medium, in the case of soluble proteins, and then taken up by endocytosis (4, 5).

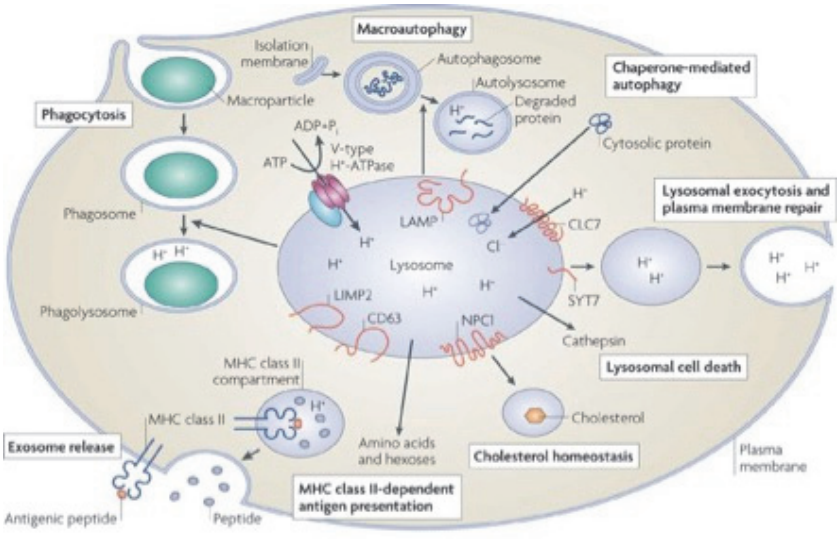


**Figure 1: Main roles of the lysosome**

Besides the degradation and recycling of macromolecules, lysosomes are also involved in the immune response, plasma membrane repair, cell homeostasis and metabolic signaling, among other cell functions, being able to trigger cell death pathways (Reprinted from Saftig *et al.*, 2009 (6)).

Most soluble proteins destined to lysosomes acquire a mannose-6-phosphate (M6P) residue(s) in their N-linked oligosaccharide chains in the TGN, which allows them to be directly targeted to pre-lysosomal compartments by mannose-6-phosphate receptors (M6PR) (Fig. 2). The binding of M6P-tagged hydrolases to M6PR is pH-dependent. At pH 6.7 of the TGN, the M6PR binds the lysosomal cargo proteins, as well as the clathrin adaptors GGA (Golgi-localized, γ-ear-containing, ADP-ribosylation factor (Arf)-binding proteins) and Adaptor Protein 1 (AP-1), enabling the transport of M6PR-cargo complex to early endosomes in clathrin-coated vesicles. The dissociation of the cargo proteins from M6PR occurs in the late endosome (LE) due to the acidic milieu (pH ~6) of its lumen (5). While the soluble lysosomal proteins reach the lysosome by fusion with the LE, M6PRs are recycled back to TGN for further cycles of lysosomal protein transport (6, 7).

Approximately 5-20% of M6P-containing lysosomal soluble enzymes escape M6PR binding in the TGN and are secreted by the cell (7). These enzymes may be internalized by the same or other cells, via plasma membrane M6PRs in clathrin-coated vesicles, reaching their lysosomes (4, 5, 8). In addition to M6PR, other sorting receptors, such as sortilin and the lysosome integral membrane protein 2 (LIMP-2/ SCARB2), participate in the transport of soluble lysosomal proteins (Fig. 2). The GM2 activator protein and cathepsins (CTS) D and H are some of the proteins transported to the lysosome by sortilin (4, 9). However, for most lysosomal hydrolases, alternative pathways cannot compensate the deficiency of the canonical M6P dependent transport such as occurring in mucolipidosis II/III, caused by genetic defects in mannose 6-phosphorylation of proteins (4).

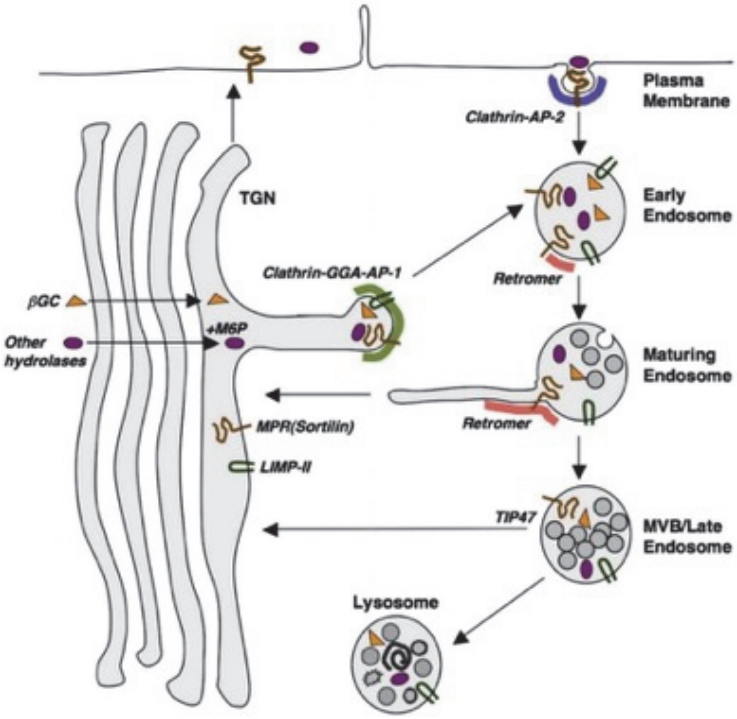


**Figure 2: Sorting pathways of lysosomal proteins**

At the TGN, M6P-tagged acid hydrolases bind to M6PR. Several soluble lysosomal proteins exhibit M6PR-independent lysosomal trafficking being transported by sortilin (Cathepsins D and H), or LIMP-2 (β-glucocerebrosidase, βGC). Most of lysosomal proteins are directly targeted to pre-lysosomal compartments but a smaller fraction is secreted to the extracellular space and may be afterwards re-captured by the same or other cells through sorting receptors at the cell surface. The sorting receptors: M6PR, sortilin and LIMP-2, as well as lysosomal membrane proteins, are trafficked to the endolysosomal system either directly, or indirectly, being first transported to the plasma membrane (Reprinted from Braulke & Bonifacino 2009 (7)).

Some targeting pathways are specific for a single enzyme, which is the case of β-glucocerebrosidase that is targeted to lysosomes by the lysosomal membrane protein, LIMP-2. It is suggested that the two proteins associate at the neutral pH of the ER and dissociate in acidic milieu of the LE/ lysosome (10).

The lysosomal membrane proteins rely on specific signals in their amino acid sequence to be targeted to lysosomes. The consensus sorting signals are tyrosine- ((Fx)NPXY or (G)YXXφ, being φ a bulky hydrophobic residue) or dileucine-containing ([D/E]XXXL[L/I] or DXXLL) sequences, usually present in cytosolic N- or C-terminal domains of lysosomal proteins. These motifs are recognized by GGA or AP (AP-1, -2 and -3) complexes, which also recruit clathrin for formation of the coated endocytic vesicles. Alternative signal sequences and sorting pathways independent of clathrin, have been recently identified (4, 11, 12). Though lysosomal membrane proteins have the ability to reach the lysosome via direct and indirect pathways from the TGN, the fractions of protein trafficked by each route may differ (7).

Sardiello and colleagues discovered in 2009 a gene network (13), which they named CLEAR (Coordinated Lysosomal Expression and Regulation), that controls the coordinated expression of lysosomal genes. The genes encoding proteins involved in lysosomal biogenesis, endocytosis, exocytosis, autophagy and lysosomal degradation have a CLEAR consensus element (GTCACGTGAC) in their promoters. The expression of the genes of the CLEAR network is upregulated by transcription factor EB (TFEB), a member of the microphthalmia-associated transcription factor, in response to cellular stress and nutrient deficit (14). Briefly, in basal conditions, the mammalian target of rapamycin complex 1 (mTORC1) is associated with the lysosomal membrane where it phosphorylates TFEB at serine residues 142 and 211. The phosphorylation of these residues creates a site for 14-3-3 protein binding, which sequesters TFEB in the cytoplasm (15). However, conditions such as nutrient deprivation, lead to mTOR inhibition and translocation of TFEB to the nucleus, where it activates expression of the genes of CLEAR network (16). This results in consequent increase in the number of lysosomes and autophagosomes that generate missing nutrients (14). (For details on lysosomal metabolic signaling see 1.4).

### 1.1.2.2 Lysosomal proteins

The degradation of all types of biological macromolecules (proteins, carbohydrates, lipids and nucleic acids (17) is performed in the lysosome by the action of approximately 60 soluble hydrolases that are active at a pH of 4.5-5 of the lysosomal lumen (18). It also relies on the presence of soluble proteins involved in transport of lipids inside the lysosomes (so called activators), and lysosome membrane proteins including transporters and channels amongst others, essential to the function of the lysosome, its stability and biogenesis (19). Lysosome membrane proteins are also required for the number of physiological processes involving lysosomes, such as lysosomal motility, membrane repair, antigen presentation, phagocytosis, macroautophagy, chaperone-mediated autophagy and lysosomal exocytosis (20).

The lysosome contains in its membrane, transporters of metabolites, ion channels, signaling receptors, Rab GTPases and SNARE (soluble N-ethylmaleimide-sensitive factor attachment protein receptor) proteins that mediate, respectively, the traffic and fusion of lysosomes with other membranes (20). The transmembrane vacuolar-type $H^+$-ATPase protein (v-ATPase) is an active transporter that uses energy from ATP hydrolysis on its cytoplasmatic side to pump protons from the cytosol into the lumen of the lysosome. Besides the formation of an electric potential between the sides of the lysosomal membrane, this assures an acidic pH optimal for hydrolytic activity of the lysosomal lumen enzymes. The acidic milieu also enables the structural changes in the macromolecules for an easier access by the hydrolases (21). Several ion channels, such as the lysosomal membrane $Ca^{2+}$ channel Mucolipin-1 (MCOLN1, TRPML1), seem also to contribute for the maintenance of this luminal lysosomal pH by mechanisms not yet understood (14). The lysosome associated membrane proteins 1 and 2 (LAMP1 and LAMP2), LIMP-2 and CD63 are the most abundant among lysosomal membrane proteins (6). These proteins are highly glycosylated and sialylated at their luminal domains forming a glycocalyx on the inner surface of the lysosomal membrane (6). This layer is thought to protect the lysosomes from self-digestion (22). Though only 25 lysosomal membrane proteins have been identified and studied so far, more than 100 are predicted to exist (17).

The catabolism of membrane-anchored sphingolipids also requires the presence of sphingolipid-activator proteins, the saposins A-D and GM2-activator protein (23).

### 1.1.3 Functions and properties of the lysosome

#### 1.1.3.1 Transport and positioning in the cell

The transport of lysosomes, essential for cell physiology, occurs along microtubules, and is dependent on dynein and kinesins as motor proteins, with contribution of actin filaments and myosin (3).

In non-polarized cells, and under steady-state conditions, the majority of lysosomes concentrate in the 'perinuclear cloud' that surrounds the microtubule-organizing center. These lysosomes are more acidic comparatively to the ones located at the periphery of the cell, However, depending on nutrient availability, the ratio between these two lysosomal populations is changed by transport of organelles towards the microtubule minus-end, driven by dynein motor to the perinuclear area (retrograde transport), or to the microtubule plus-end driven by kinesin motor to the cell periphery (anterograde transport) (24). In polarized cells such as neurons, the fully acidified mature lysosomes are found mainly in the cell bodies and endosomes/lysosomes undergo maturation along their retrograde transport from the axon terminals to the soma (25, 26).

The lysosome localization in the perinuclear area is also essential for the fusion between lysosomes and autophagosomes (27), whereas the motility of lysosomes enables their interaction with the plasma membrane and other organelles as will be described in details further.

#### 1.1.3.2 Interaction with other organelles

The lysosomes are able to fuse with the cell membrane allowing communication between the cells and with the extracellular space, essential for immune response and cellular homeostasis (28). They also fuse with other compartments of the endocytic and autophagic pathways (LE/ MVB, amphisomes and autophagosomes) (18), regulating the turnover of macromolecules and organelles. Moreover, lysosomes (and LE) tether with other intracellular organelles such as the endoplasmic reticulum, mitochondria and peroxisomes (27). This is thought to be essential for exchange of metabolites and lipids (specially cholesterol) at the membrane contact sites which function as signalling microdomains (28), and for regulation of organelle dynamics (27, 29). Through lysosome-mitochondria membrane contact sites, lysosomes are believed to regulate mitochondrial fission, whereas mitochondria control lysosomal motility, tethering and fusion (29).

Recently Cioni and colleagues (30) (2018) identified the association of Rab7-positive late endosomes, ribosomes and mitochondria in neuronal axons. The results of this study suggest that LE act as sites of translation for mRNAs that are important for the maintenance of mitochondria in the axons.

### 1.1.3.3 Degradation and recycling of macromolecules

The turnover of organelles as well as other intra- and extracellular structures and macromolecules is assured by their lysosomal degradation and/or recycling of their components, delivered by the autophagic and endocytic pathways (31). The resulting products are trafficked to the TGN for recycling, released into the cytosol (32), or secreted from the cell through lysosomal exocytosis (33).

The cell has another degradative mechanism, the ubiquitin-proteosome pathway, to catabolize short-lived and misfolded proteins exported from the ER. However, long-lived macromolecular complexes such as protein aggregates, and damaged organelles, are only degraded by the lysosome-autophagy system (34). Endocytosis and autophagy, the major pathways for delivery of extracellular and cytosolic macromolecules to the lysosome, and subsequent degradation, will be described below (Fig. 3).

#### 1.1.3.3.1 Endocytosis

The main function of the endocytic pathway is the uptake and transport of plasma membrane components and macromolecules from the cellular environment for lysosomal degradation/recycling (84). The uptake occurs through different mechanisms depending on the type of the endocytosed cargo. Phagocytosis corresponds to the endocytosis of bulk particles such as pathogens (Fig. 1), while macropinocytosis, to the non-specific uptake of extracellular fluid. The receptor-mediated endocytosis (RME) corresponds to the specific cellular uptake of macromolecules, viruses and exosomes, which bind to plasma membrane receptors mostly inside clathrin- or caveolin-coated pits. There are also clathrin- and caveolin-independent RME mechanisms (35). Furthermore, the endocytosis of several ligands may be lipid raft-mediated, through binding to these plasma membrane domains enriched in sphingolipids and cholesterol (35-37)

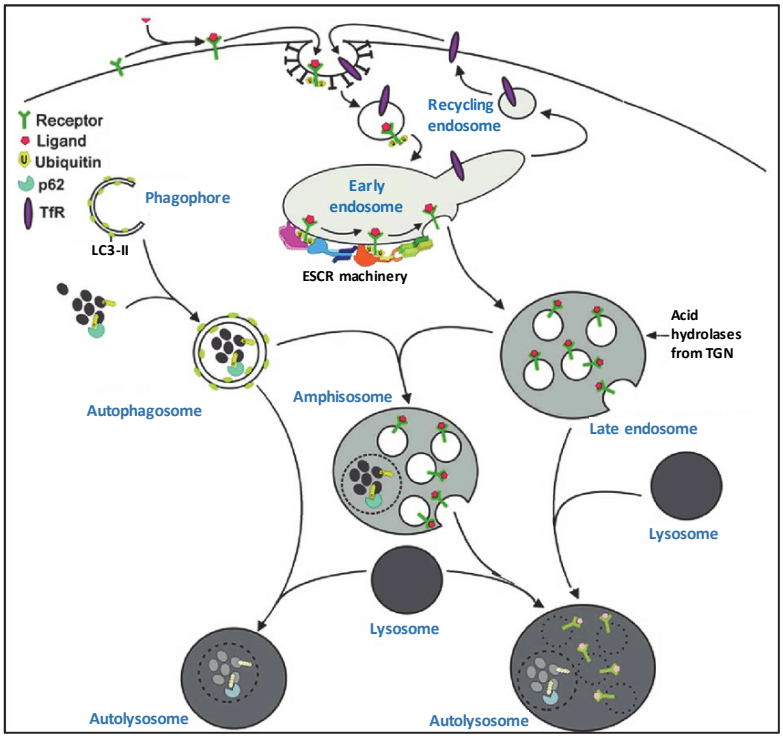


**Figure 3: Endocytosis and autophagy as pathways for transport of materials to be degraded / recycled in the lysosomes**

The diagram shows different endocytic and autophagic compartments. TfR, transferrin receptor. (Adapted from Nixon *et al.*, 2008 (38)).

In the process of endocytosis, the plasma membrane folds around extracellular material to be internalized, creating an endocytic vesicle. The vesicles undergo homotypic fusion forming early endosomes, the organelles where sorting of the cargo occurs. The recycling endosomes receive the material to be recycled back to the plasma membrane (39), while part of the cargo transits from early and late endosomes to the TGN in retrograde transport vesicles, also for recycling (40). The material to be catabolized is retained in the early endosomes that mature into LE, ultimately reaching the lysosomes, where the cargo is degraded by the lysosomal hydrolases (Fig. 3).

The endosomal sorting complex required for transport (ESCRT) machinery regulates the formation of intraluminal vesicles (ILVs) (41). In this process, ubiquitinated cell membrane proteins become exposed to the endosomal lumen through an inward budding of the endosomal membrane (Fig. 3). Besides the formation and progressive accumulation of ILVs, the maturation of early into LE

involves morphological and biochemical changes, including further acidification of their milieu by the transmembrane v-ATPase. The early endosomes have a tubular shape with a pH between 6.8 and 6.1, while late endosomes, also known as multivesicular bodies (MVB), are spherical and more acidic (pH 6.0–4.8). The pH of lysosomes may reach 4.5 (42, 43). This pH gradient is used for sorting cargo to the appropriate organelle of the endosomal system since the dissociation between targeting receptors and their corresponding ligands occurs at specific pH values (44).

The fusion of lysosomes with LE/MVBs, originates hybrid organelles, so-called endolysosomes (EL) (Fig. 3), where pH is optimal for hydrolases to catabolize their specific substrates. The degradation products are then transported to the TGN for re-use via retrograde trafficking, or released outside the cell. In the latter case, the degradation material is secreted by a process named "lysosomal exocytosis" which involves fusion of ELs with the plasma membrane (45) (Fig. 1). Lysosomal exocytosis, is likely present in all cell types (46) but is particularly active in cells of the hematopoietic lineage, osteoclasts and melanocytes (47). In the CNS, it has been detected in the neurons, microglia, astrocytes and oligodendrocytes (48-51). Lysosomal exocytosis is a $Ca^{2+}$-regulated process that is important for plasma membrane reparation, pathogen defense, regulation of intracellular levels of α-synuclein in neurons, myelination, and ATP neurotransmitter release by astrocytes, among others (48, 51-54). Besides the lysosomal membrane $Ca^{2+}$ channel TRPML1, several SNARE (VAMP-7 and synaptotagmin VII on lysosomes, SNAP23 and syntaxin 4 on the plasma membrane) and Rab proteins are essential for the lysosomal exocytosis mechanism (55). The fusion of endolysosomes/lysosomes with the plasma membrane may lead to secretion of M6P-tagged hydrolases that can be taken up by surrounding cells.

Several types of cells secrete exosomes, extracellular vesicles resulting from the fusion of LE/MVBs with the plasma membrane and release of their ILVs outside the cell (35, 40, 56) (Fig. 1). These vesicles can transfer their cargo (proteins, lipids, nucleic acids) into target cells by endocytosis and have an important role in intercellular signaling, particularly in immune response, (57, 58). In immune cells there is a constitutive secretion of exosomes. However, cellular interactions as well as the concentration of specific molecules and ions, such as $Ca^{2+}$, may also stimulate these and other cell types to secrete extracellular vesicles (56-59).

#### 1.1.3.3.2 Autophagy

Autophagy is a conserved catabolic process for elimination of detrimental intracellular material, such as protein aggregates and non-functional organelles, and recycling of cellular constituents. It involves interaction between compartments of the endocytic and autophagic pathways (32).

The autophagy is regulated by mTORC1 and, consequently, activated by depletion of nutrients, and cellular stress, such as caused by hyperthermia, hypoxia (34), oxidative stress and formation of unfolded proteins or aggregates. All these conditions induce translocation of the TFEB to the nucleus of the cell, where it activates the expression of the genes involved in lysosomal biogenesis, acidification and exocytosis, endocytosis, autophagy and degradation of macromolecules (13).

Three subtypes of autophagy have been described: microautophagy, chaperone-mediated autophagy (CMA) and macroautophagy (60).

The microautophagy is a non-selective degradative process where the cytosolic material is directly internalized by random invagination of the lysosomal membrane. This pathway is activated by reduction of intracellular level of glutamine, the amino acid which is specifically sensed by mTOR signalling complex (61).

The CMA, identified so far only in the mammals, is a process by which cytoplasmic proteins harboring specific recognition motifs are recognized by the heat shock cognate 70 (Hsc70) that delivers them to the surface of lysosomes (Fig. 1). Then the substrate-chaperone complex binds to the cytosolic tail of monomeric LAMP-2A, one of the three isoforms of LAMP2, and promotes its multimerization. The cargo proteins are then unfolded and translocated into the lysosomes for degradation, which is followed by disassembly of the LAMP-2A transmembrane multimeric complex (62).

The motives for Hsc70 recognition are KFERQ and KFERQ-like amino acid sequences. Several studies showed that α-synuclein and tau/MAPT (microtubule-associated protein tau) proteins are CMA substrates in the soluble form, but not as aggregates (reviewed by (62)). Misfolding and aggregation of these two neuronal proteins is linked to the pathogenesis of Parkinson's (PD), and Alzheimer's disease (AD) as well as several frontotemporal dementias (63).

Macroautophagy, referred further as autophagy, is a degradative process where a portion of cytoplasm, containing protein aggregates, lipids, carbohydrates, organelles or pathogens is getting

enclosed by a double membrane to form an autophagosome (6, 29, 32) (Fig. 1; Fig 3). The formation of the autophagosome is a highly regulated process, involving the coordinated participation of a high number of autophagy-related (ATG) proteins, SNAREs and ubiquitin-like proteins, besides other membrane components (32).

The autophagy is activated by mTOR inhibition in response to nutrient deprivation, hyperthermia, hypoxia and reactive oxygen species (ROS) production or directly by the 5' Adenosine monophosphate-activated protein kinase (AMPK) leading to the phosphorylation of the components of the autophagy-related 2 (Atg1)–Unc51-like kinase (ULK) complex containing ULK1, ULK2, Atg13, FIP200 and Atg101. The phosphorylation of ULK1 triggers the translocation of this protein complex containing also beclin-1 (or Atg6) and the class III phosphoinositide 3-kinase (PI3K CIII, or Vps34) from the cytoskeleton to the nucleation of a cup-shaped isolation membrane, the phagophore. The phosphatidylinositol 3-phosphate (PI3P) generated by Vps34 binds to its effectors, WD repeat domain phosphoinositide-interacting 1 protein (WIPI1) and WIPI2, catalyzing the two ubiquitination-like reactions that regulate elongation of the isolation membrane around a region of cytoplasm or selected substrate.

The first reaction leads to conjugation of the complex of ubiquitin-like proteins, ATG12-5-16L1 to the phagophore, in the presence of Atg7 and Atg10 proteins. This induces the second reaction which consists of lipidation of the cytosolic microtubule-associated protein light chain 3 (LC3-I), which is also an ubiquitin-like protein. The conjugation of phosphatidylethanolamine to LC3-I leads to its association with the membrane of the phagophore in the form called LC3-II, and results in the closure of the isolation membrane and formation of a double membrane autophagosome (Fig. 3) (32).

The concerted action of SNARE proteins, tethering factors and Rab GTPases promotes the fusion of autophagosome with LE/MVB forming amphisomes (which then fuse with lysosomes) or with lysosomes to form autolysosomes (Fig. 3). These autophagic vesicles have different levels of maturation: the autophagosomes do not have degradation machinery and in the amphisomes, degradation is incipient, while the autolysosomes present full degradative capacity of their content by lysosomal hydrolases (64). The catabolic products of the autophagosomes contents are finally released, via permeases (65), into the cytosol for usage by the cell. LC3-II, which is bound to outer and inner membranes of the newly formed autophagosomes, is degraded upon fusion of these

vesicles with lysosomes. A rise of cellular LC3-II levels thus may indicate an increase of the number of autophagosomes but, also, suppression of the degradation of their content.

Several properties of lysosomes such as the membrane content of LAMP2, $PI_{(3,5)}P_2$ and cholesterol influence their capacity to fuse with autophagosomes and amphisomes. In particular, the increased rigidity of the lysosomal membrane, due to an increment in the cholesterol levels, may impair its fusion with the autophagosomes (64).

The autophagy of damaged organelles and misfolded proteins is highly selective and requires autophagic receptors to bind and present the cargo proteins to the autophagic machinery (32, 64). In particular, the autophagic receptor p62 (or SQSTM1) recognizes and binds misfolded ubiquitinated protein aggregates (Fig. 3). Its interaction with LC3-II in the inner membrane of the autophagosome targets the ubiquitinated proteins to degradation. p62 is degraded along its cargo (32, 66). When mitochondria become dysfunctional and their membrane is depolarized, PINK1, located in the outer membrane, recruits and phosphorylates the E3 ubiquitin ligase, parkin. This protein ubiquitinates then the voltage-dependent channel 1 (VDAC1), and recruits p62 that associates to LC3-II, targeting its cargo, the damaged mitochondria, for degradation, in a process named mitophagy (32). Besides mitochondria, other damaged organelles such as peroxisomes, ER fragments, lipid droplets, and even lysosomes with damaged leaking membrane are also selectively targeted for autophagy (6, 29, 32, 67). Besides *de novo* biosynthesis of lysosomes, autophagic lysosome reformation also ensures lysosome homeostasis during autophagy (68). In this process, tubules extruded from the autolysosome generate proto-lysosomes, which mature into functional lysosomes (68).

The autophagy pathway enables the clearance of molecules potentially harmful for the cell, such as protein aggregates and damaged organelles. This process is important for all cells, but is especially vital for neurons and other long-living non-mitotic cells (47). Neuronal cells also rely on the autophagy to eliminate (or prune) dendritic spines and inappropriate synaptic connections, particularly during the development (69), to regulate turnover of synaptic vesicles and neurotransmitter receptors. In the liver, the autophagic pathway is particularly important for removal of misfolded proteins, lipids and the turnover of organelles, especially the ER and mitochondria.

### 1.1.3.4 Metabolic regulation

In recent years, the role of the lysosomes in regulation of metabolic homeostasis in response to environmental conditions has been unraveled (70). The lysosomes control metabolic signalling by sensing energy, ions and nutrients, such as amino acids, cholesterol and glucose (47, 70) (Fig. 1).

The mTORC is considered to be the master regulator of cellular growth. In nutrient-rich conditions, the lysosomes mediate anabolic signaling. The high level of amino acids and cholesterol inside lysosomes leads to the recruitment of mTORC1 by the complex vATPase-SLC38A9-Ragulator-Rag GTPase complex. Another GTPase, Rheb, also bound to the lysosomal membrane, is activated by cytosolic growth factors via protein kinase B or Akt (71), activating mTORC1 which, by its turn, phosphorylates TFEB that is then retained in the cytoplasm by 14-3-3 proteins. These environmental conditions favor the lysosomal transport to the cell periphery, where mTORC1 may also be activated by growth factors (70) and the inhibition of AMPK, the major sensor of energy stress, which does not activate autophagy (32). (The role of AMPK in autophagy is described in the section 1.3.1.2 Autophagy). Thus, conditions rich in nutrients, energy, growth factors and ions favor mTORC1 activation, which drives the biosynthesis of lipids, nucleotides, ribosomes and stimulates glycolysis and glucose uptake (71, 72). When nutrients are no longer available, mTORC1 is released from vATPase-SLC38A9-Ragulator-Rag GTPase complex, and Rheb GTPase activity is inhibited by the absence of growth factors. Consequently, TFEB is not phosphorylated by mTORC1. The TRPML1 activation mediated by $PI_{(3,5)}P_2$ leads to lysosomal $Ca^{2+}$ release and activation of calcineurin phosphatase, which dephosphorylates TFEB. The non-phosphorylated state of TFEB allows its translocation to the nucleus (70). The low ATP level in the cells drives the activation of AMPK pathway, promoting mitochondrial biogenesis and fission, as well as biogenesis of lysosomes (73) and induction of autophagy (32)). TRPML1 activation also induces the transport of lysosomes to the perinuclear location driven by dynein (70). In summary, in fasting conditions the catabolism is activated, with biogenesis of lysosomes and autophagosomes favoring lysosomal recycling of elements needed by the cell, and generation of ATP by mitochondrial biogenesis.

### 1.1.3.5 Neurotransmission

The communication between neurons occurs by transfer of electric or chemical signals from one neuron to other via synapses.

Synaptic transmission at electric synapses occurs by bidirectional flux of electric current across intercellular gap junctions of adjacent neurons. Besides the ions carrying the electric current, small molecules such as cyclic adenosine monophosphate (cAMP) and inositol trisphosphate ($IP_3$), can also diffuse through these gap junction channels (74).

Chemical synapses are intercellular junctions between a pre-synaptic neuron and post-synaptic cells, mainly neurons, but also glia and oligodendrocyte progenitors (75). At these type of synapses, which are the most frequent, electrical signals (action potential) at presynaptic terminal are converted into chemical signals transmitted to postsynaptic cells. In fact, when an action potential reaches a neuron presynaptic terminal it causes the influx of $Ca^{2+}$ by opening voltage-dependent $Ca^{2+}$ channels. The increased intracellular calcium levels trigger the exocytosis of synaptic vesicles containing neurotransmitters into the synaptic cleft, which fuse with the plasma membrane at the active zone of the presynaptic terminal. This fusion is mediated by SNARE proteins at the vesicle (v-SNAREs, as synaptobrevin) and at the target membrane (t-SNAREs, such as syntaxin and SNAP-25) (76). The binding of neurotransmitters to specific receptors (ionotropic or metabotropic) at the postsynaptic cell membrane may initiate ionic flux towards the post-synaptic neuron, altering the transmembrane electrical potential and the likelihood to evoke an action potential in this cell, and activate signal transduction signaling, modulating protein synthesis, and cell growth, among others (77).

The endolysosomal system is essential for the formation of chemical synapses, synaptic transmission and synaptic plasticity. The pre-synapse protein homeostasis is maintained by exocytosis of synaptic vesicles carrying neurotransmitters and subsequent endocytosis and recycling of the synaptic vesicle proteins at the pre-synaptic terminal. Besides the ubiquitin-proteasome system and chaperone activity, the autophagy assures the control quality of the numerous proteins involved in the synaptic function (78). Though the biogenesis of autophagosomes may be detected in the cell body, dendrites or mid-axons, it is especially frequent at the distal ends of axons (70) (Fig. 4). It is also thought that presynaptic endocytosis is involved in the formation of autophagosomes and their retrograde transport to the cell body (79).

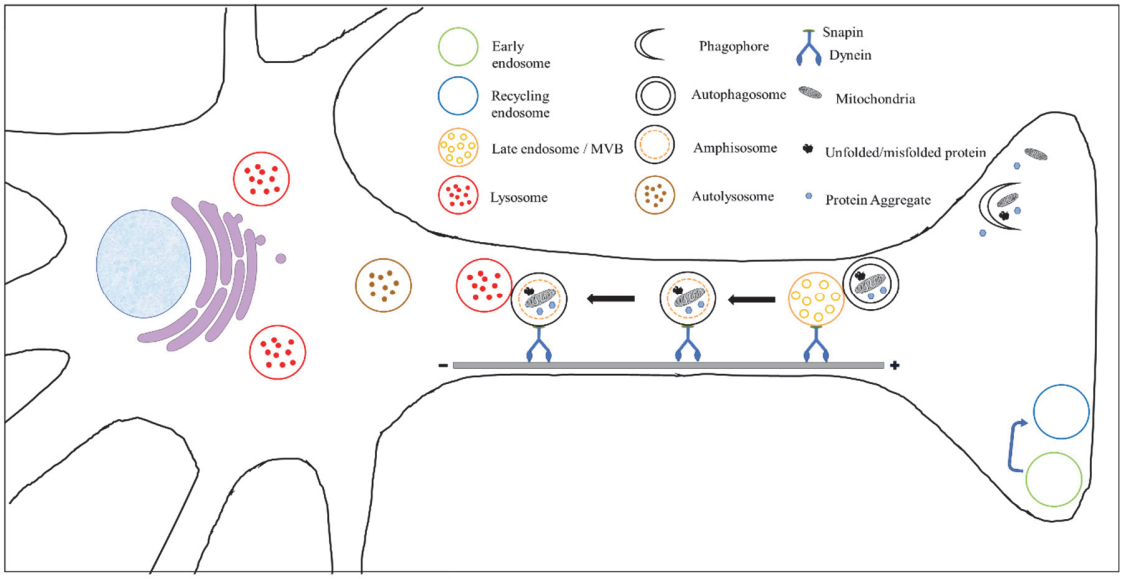


**Figure 4: Maturation of endolysosomal and autophagic compartments through retrograde axonal transport**

The autophagosomes, mainly formed at the axon terminal, are transported retrogradely to the soma by fusion with the LE/MVB, forming amphisomes. The fusion of amphisomes and lysosomes predominantly occurs at a perinuclear location, where most mature lysosomes are located (Adapted from Winckler *et al.*, 2018 (80)).

### 1.1.3.6 Ion storage

The content of free $Ca^{2+}$ in the lysosomes is similar or higher than that in the ER, organelle typically associated with the storage of this cation. The vesicular trafficking in the endolysosomal system and the fusion between the lysosomes and the PM or other organelles are all dependent on $Ca^{2+}$ (21). Stress inducers, such as oxidative stress and lysosome deacidification, lead to an efflux of lysosomal $Ca^{2+}$ to the cytoplasm via TRPLM1, which elicits the cell adaptive response by induction of lysosome biogenesis and autophagy (70).

The lysosome has also an important role in preventing harmful effects in the cells caused by accumulation of iron and copper ions in the cytosol (71).

### 1.1.3.7 Cell death

Lysosomal integrity and function are essential for cellular homeostasis (81). The lysosomal membrane permeabilization (LMP) may be initiated by several internal and external stimuli that compromise the integrity of the lysosomal membrane. Such stimuli include the reactive oxygen species (ROS) and the pro-apoptotic protein Bax (bcl-2-like protein 4), which introduce pores in the membrane. An enlargement of the lysosome and lysis of its membrane may result from disruption of the cytoskeleton or action of lysosomotropic agents. Besides, the sphingolipid composition of the lysosomal membrane, namely the content in sphingosine, sphingomyelin and cholesterol, may alter the stability and permeability of the lysosomal membrane (81-85).

The rupture of the lysosomal membrane leads to acidification of the cytoplasm, prompts the massive release of lysosomal hydrolases, including CTS, into the cytosol causing uncontrolled damage of cellular components and, finally, cell death by necrosis (81, 86). However, partial LMP promotes the leakage of a subset of the lysosomal components to the cytosol, triggering several endolysosomal damage-responses: the activation of the mTORC1-TFEB pathway promotes the formation of functional lysosomes (87), autophagy of dysfunctional lysosomes (lysophagy), repair of small ruptures of the membrane by ESCRT proteins and exocytosis of dysfunctional lysosomes. However, these responses may not be sufficient to ensure cell survival, and several regulated cell death pathways may be induced or amplified by LMP, according with the nature and intensity of stimuli, and the cell type (81, 84, 88).

The selective release of cathepsins into the cytosol due to partial LMP is implicated in the activation of lysosome-dependent cell death (Fig. 1). Several CTS, including B, D and L, maintain proteolytic activity at a neutral pH of the cytoplasm, and, in some instances, activate Bid and the translocation of Bax to form pores across the outer mitochondrial membrane (81, 89, 90). This irreversible process of mitochondrial outer membrane permeabilization (MOMP) leads to the release of apoptogenic factors, including cytochrome c (Cytc), from the mitochondrial intermembrane space to the cytoplasm. Cytosolic Cytc activates the caspase pathway, which involves the initiator caspase Casp9 and the executer caspases Casp3, 6 and 7, resulting in destruction of subcellular structures and cell demise (90). The MOMP leads to the dissipation of the mitochondrial transmembrane potential ($\Delta\psi m$) and, consequently, to mitochondrial dysfunction (90). At this stage, the generation of mitochondrial ROS, amplifies the LMP apoptotic

signaling (84). Besides apoptosis and necrosis, LMP may trigger other regulated cell death pathways, the pyroptosis, necroptosis and ferroptosis (81).

Pyroptosis is a type of cell death specifically related to inflammation and immunity and driven by the activation of the inflammasome (91). Lipopolysaccharide (LPS) is an important trigger of this cell death pathway in the cells of the monocytic lineage (92). LMP was shown to induce the assembly and activation of NLRP3 (Nucleotide-binding oligomerization domain (NOD), leucine rich repeat (LRR) and pyrin domain containing 3) inflammasome in macrophages (84). As a result, activation of inflammatory caspases leads to formation of ion channels or pores in the cell membrane by the pyroptosis effector gasdermin D, eventually leading to plasma membrane destruction (93). In the case of necroptosis, LMP triggers a series of events leading to the activation of RIPK3 and MLKL, MOMP and cell death (92, 94).

Despite the fact that autophagy is a survival mechanism of the cell, due to its role in the removal of potentially toxic intracellular components and generation of nutrients, there are situations when it may also lead to cell demise via autophagy-dependent cell death pathway (65, 81). For example, the selective autophagic degradation of catalase, the major enzymatic ROS scavenger, leads to ROS production and, ultimately, necrosis (95).

## 1.2 Lysosomal storage diseases

### 1.2.1 Definition and classification

Lysosomal storage diseases (LSDs) are a large group of genetic metabolic disorders characterized by the accumulation of macromolecules or monomeric compounds inside organelles of the endosomal-lysosomal-autophagic system (96).

Until now 66 clinical LSDs have been described (97), associated with pathogenic variants in 53 genes (98). Most LSDs results from the impairment of the activity of a lysosomal hydrolase, leading to the storage of its undegraded or partially degraded substrate in the lysosome. Since their discovery, LSDs have been grouped according to the biochemical nature of the products stored in the lysosome, and classified as mucopolysaccharidoses, sphingolipidoses, mucolipidoses, oligosaccharidoses/ glycoproteinoses, lipidoses and glycogen storage diseases. However, not all

LSDs can be easily classified according to these classical categories, since the deficiency in one protein may lead to the lysosomal storage of different types of substrates.

**Table 1: Lysosomal storage disorders classified by the molecular defect**

| Disease/ molecular defect | Affected protein | Gene | Main storage materials |
|---|---|---|---|
| **Sphingolipidoses / Sphingolipid-cleaving enzymes** | | | |
| Fabry | α-Galactosidase A | *GLA* | Globotriasylceramide |
| Farber | Acid ceramidase | *ASAH1* | Ceramide |
| GM1 Gangliosidosis (I, II, III) | GM1-ß-galactosidase | *PSAP* | GM1, keratan sulfate, oligos, glycolipids |
| GM2 gangliosidosis, Tay- | ß-Hexosaminidase A | *HEXA* | GM2, oligos, glycolipids |
| Gangliosidosis GM2, | ß-Hexosaminidase A + B | *HEXB* | GM2, oligos, glycolipids |
| Gaucher (I, II, III) | β-Glucocerebrosidase | *GBA* | Glucosylceramide |
| Krabbe | ß-Galactosylceramidase | *GALC* | Galactosylceramide |
| Metachromatic | Arylsulfatase A | *ARSA* | Sulfatides |
| Niemann-Pick (A, B) | Sphingomyelinase | *SMPD1* | Sphingomyelin |
| **Metabolism of cholesterol** | | | |
| Wolman/ CESD | Acid lipase | *LIPA* | Chol esters, triglycerides |
| Niemann-Pick, Type C1 * | Niemann-Pick type 1 | *NPC1* | Chol and sphingolipids |
| Niemann-Pick, Type C2 | Niemann-Pick type 2 | *NPC2* | Chol and sphingolipids |
| **Mucopolysaccharidoses / GAG-cleaving enzymes** | | | |
| MPS I (Hurler, Scheie, Hurler/Scheie) | α-Iduronidase | *IDUA* | Dermatan sulfate, heparan sulfate |
| MPS II (Hunter) | Iduronate sulfatase | *IDS* | Dermatan sulfate, heparan sulfate |
| MPS IIIA (Sanfilippo A) | Heparan sulfamidase | *SGSH* | Heparan sulfate |
| MPS IIIB (Sanfilippo B) | N-acetyl-α-D-glucosaminidase | *NAGLU* | Heparan sulfate |
| MPS IIIC (Sanfilippo C) * | Heparan sulfate acetyl-CoA: α-glucosaminide N-acetyltransferase | *HGSNAT* | Heparan sulfate |
| MPS IIID (Sanfilippo D) | N-acetyl glucosamine-6-sulfatase | *GNS* | Heparan sulfate |
| MPS IVA (Morquio A) | Acetyl galactosamine-6-sulfatase | *GALNS* | Keratan sulfate, condroitin-6-sulfate |
| MPS IVB (Morquio B) | ß-Galactosidase | *GLB1* | Keratan sulfate |
| MPS VI (Maroteaux-Lamy) | Acetyl galactosamine-4-sulfatase | *ARSB* | Dermatan sulfate |
| MPS VII (Sly) | ß-Glucuronidase | *GUSB* | Dermatan sulfate, heparan sulfate, condroitin-6-sulfate |
| MPS IX (Natowicz) | Hyaluronidase | *HYAL1* | Hyaluronan |
| **Oligosaccharidoses, glycoproteinoses / glycoprotein degradation** | | | |
| Aspartylglicosaminuria | Glycosylasparaginase | *AGA* | Aspartylglucosamine |
| Fucosidosis | α-Fucosidase | *FUCA1* | Fucoside-rich oligos, glycoproteins, glycolipids |
| a-Mannosidosis | α-Mannosidase | *MANSA* | Mannose-rich oligos |
| ß-Mannosidosis | ß-Mannosidase | *MANBA* | Man(ß1→4)GlnNAc |

| | | | |
|---|---|---|---|
| Schindler | N-acetylgalactosaminidase | *NAGA* | Sialylated/ asialo-glycopeptides, glycolipids |
| Sialidosis | Neuraminidase | *NEU1* | Oligos, glycopeptides |
| **Glycogenoses / glycogen degradation** | | | |
| Glycogenosis II/ Pompe | Acid maltase | *GAA* | Glycogen |
| **Non-enzymatic lysosomal proteins** | | | |
| GM2 Gangliosidosis, AB | GM2 activator protein | *GMA2A* | GM2 ganglioside, oligos |
| Metachromatic | Saposin B | *PSAP* | Sulfatides |
| Krabbe | Saposin A | *PSAP* | Galactosylceramide |
| Gaucher | Saposin C | *PSAP* | Glucosylceramide |
| **Transmembrane proteins** | | | |
| Sialic acid storage disease (ISSD, Salla) | Sialin | *SLC17A5* | Sialic acid |
| Cystinosis | Cystinosin | *CTNS* | Cystine |
| **Lysosomal structural proteins** | | | |
| Danon * | Lysosome-associated membrane protein 2 | *LAMP2A* | Cytoplasmatic debris and glycogen |
| Mucolipidosis IV * | Mucolipin | *TRMPL1* | Sulfatides, GSLs, GAGs |
| **Enzyme protective proteins** | | | |
| Galactosialidosis | Protective protein cathepsin A (PPCA) | *CTSA* | Sialyloligosaccharides |
| **Post-translational processing** | | | |
| Multiple sulfatase deficiency | Multiple sulfatase | *SUFM1* | Sulfatides, GSLs, GAGs |
| **Protein trafficking** | | | |
| Mucolipidosis IIα/ß, IIIα/ß | GlcNAc-1-P transferase, α/ß | *GNPTAB* | Oligos, GAGs, lipids |
| Mucolipidosis IIIɣ | GlcNAc-1-P transferase, ɣ | *GNPTG* | Oligos, GAGs, lipids |
| **Polypeptide degradation** | | | |
| Pycnodysostosis | Cathepsin K | *CTSK* | Type I and II collagen |
| **Vesicular fusion** | | | |
| MPS-Plus | Vacuolar protein sorting-associated protein 33A | *VPS33A* | Heparan sulfate, dermatan sulfate, chol |
| **Neuronal ceroid lipofuscinoses / defects causing ceroid lipofuscin CNS storage** | | | |
| NCL 1 | Palmitoyl-protein thioesterase 1 | *PPT1* | Saponins A & D, oligo-PP-dol |
| NCL 2 | Tripeptidyl peptidase 1 | *CLN2* | oligo-PP-dol, SCMAS |
| NCL 3 * | Battenin | *CLN3* | oligo-PP-dol, SCMAS |
| NCL 4B, Parry type | DnaJ homolog subfamily C5 | *DNAJC5* | oligo-PP-dol, SCMAS |
| NCL 5 | CLN5 protein | *CLN5* | oligo-PP-dol, SCMAS |
| NCL 6 * | CLN6 protein | *CLN6* | oligo-PP-dol, SCMAS |
| NCL 7 * | MFS domain-cont. protein 8 | *MFSD8* | oligo-PP-dol, SCMAS |
| NCL 8 * | CLN8 protein | *CLN8* | oligo-PP-dol, SCMAS |
| NCL 10 | Cathepsin D | *CTSD* | oligo-PP-dol, SCMAS |

Oligos, oligossacharides; chol, cholesterol; GAG, glycosaminoglycan; C6S, chondroitin 6-sulfate; Man(ß1→4)GlnNAc, ß-1,4-Mannosyl-N-acetylglucosamine; GSLs, glycosphingolipids; GlcNAc-1-P, N-acetylglucosaminephosphotransferase 1; oligo-PP-dol, dolichyldiphosphoryloligosaccharide; SCMAS, subunit c of mitochondrial ATP synthase; * also due to defects in transmembrane proteins

Another classification system of LDSs is based on the nature of the underlying molecular defect (Table 1) (28, 99, 100). Besides acid hydrolases, the lysosomal storage of materials can also be due to defects in non-enzymatic lysosomal proteins such as activator proteins and membrane proteins (channels, transporters, receptors and structural proteins) required for lysosomal structure and function. Some LSDs are caused by deficit in proteins participating in the biogenesis of lysosomes, post-translational processing, protection and vesicular trafficking of lysosomal proteins (28, 99-101).

### 1.2.2 Clinical manifestations

Lysosomal disorders exhibit a wide range of clinical manifestations. The symptoms, their onset and severity, as well as a nature and amount of material(s) stored in specific cells, tissues and organs, display high variability within each disorder and even subtype.

The majority of patients affected by LSDs are born healthy with onset of symptoms generally occurring during childhood (infantile and juvenile forms). Despite the fact that LSDs are regarded mainly as pediatric disorders, there are also cases with onset during adulthood.

Degeneration of the central nervous system (CNS) was described for approximately 70% of LSDs (102). Its severity varies, ranging from mild cognitive decline to severe and rapidly progressing mental retardation (103, 104). Behavioral changes are generally associated to the onset of cognitive dysfunction (Carol Dillon 2013) and psychiatric symptoms are commonly detected in adult forms of LSDs. (105). These symptoms may be confounded with other pathologies, delaying the diagnosis of patients, especially those with a later onset of symptoms (106).

Signs of somatic pathology, such as facial dysmorphism, skeletal manifestations as, e.g., dysostosis multiplex, hepatomegaly, splenomegaly, as well as the presence of neurologic abnormalities, together with disease onset and severity, may suggest the diagnosis of a specific LSD or group of disorders. However, the variability of clinical signs in LSDs and the fact that they overlap in different disorders can hinder fast and accurate clinical diagnosis of a specific disease (107) .

### 1.2.3 Birth prevalence

Despite being individually rare, collectively, LSDs are relatively common with an estimated birth prevalence of approximately 1 per 5,000 live births (97) ranging from 1 per 2,200 in United Arab Emirates to 1 in each 12,500 live births in British Columbia (108-121). As a consequence, LSDs have a significant impact on the health of populations and healthcare systems (109, 122).

Relatively few data are available on the frequency of most individual LSDs due to their rarity. Gaucher disease type I is the most frequent LSD, with a worldwide prevalence of 1/50,000 to 1/100,000, and 1/850 in the Ashkenazi Jewish population (123). In fact, population groups that have been geographically and/or culturally isolated over long periods of time, such as the Ashkenazi Jewish, Finnish, French Canadian, North African and Middle Eastern, present higher birth prevalence for several LSDs. Multiple factors, such as high consanguinity, founder effects, genetic drift and natural selection may account for high frequency of recessive disorders in these populations (122, 124-128).

### 1.2.4 Molecular genetics

LSDs are autosomal recessive disorders, except MPS II, Fabry and Danon diseases, which have an X-linked inheritance (129). Many LSDs are caused by a high number of pathogenic variants, such MPS II, with 628 reported so far (130). However, the majority of variants associated to LSDs are private, or unique, to specific populations or, even, families.

Most deletions, insertions and splice site variants introduce shifts in the mRNA frame, leading to the introduction of a premature stop codon and degradation of the transcript by the nonsense mediated mRNA decay mechanism (NMD) (131, 132). All these sequence variants, as well as the nonsense mutations, result in the absence of protein and enzyme activity. In contrast, missense variants originate proteins where the WT amino acid is substituted by other residue, often causing a misfolding of the protein. In most cases, mutant misfolded enzymes are retained in the endoplasmic reticulum (ER) and are targeted for degradation by the endoplasmic reticulum-associated degradation pathway (ERAD). The misfolded proteins are dislocated from the ER to the cytoplasm where they are degraded by the ubiquitin proteasome system (UPS) (133). Accumulation of misfolded protein in the ER lumen (ER stress) causes activation of intracellular signal transduction pathways, named collectively as the unfolded protein response (UPR) (134).

A higher residual activity in the patient's cells normally reflects a higher portion of a mutant protein properly folded by cell chaperones and transported to their target destination, the lysosomes (135, 136).

In the case of Tay Sachs and Sandhoff variants of GM2 gangliosidosis, caused by deficiency of β-Hexosaminidases A and B (HexA and B) (see chapter N) the severity and onset of the disease was inversely correlated to the residual enzyme activity and the turnover rate the substrate, GM2 (137). While in infantile cases, HexA residual activity in fibroblasts was <0.5% of the WT protein, in juvenile (or subacute) and adult (or chronic) forms it reaches 2-4% of the activity detected in controls (138). GM2 cleaving rates of 10-20% of the control had been detected in asymptomatic individuals (137, 139). The presence of enzymatic pseudodeficiency, corresponding to low levels of enzyme found in healthy individuals, was also detected in metachromatic leukodystrophy (140) and GM1 gangliosidosis (141), among other lysosomal disorders (99).

Importantly, the phenotype presented by the patient, in general shows only a partial correlation with the type of mutation(s) and enzyme activity level of the mutant protein. Patients carrying the same pathogenic variants, including siblings, may exhibit different phenotypes with distinct ages at onset, symptoms and severity, which suggests the effect of epigenetic factors and/or the existence of modifier genes (28, 142).

## 1.3 Mucopolysaccharidoses

### 1.3.1 Definition and classification

Mucopolysaccharidoses (MPSs) are a group of lysosomal storage disorders characterized by the deficiency of enzymes involved in the catabolism of glycosaminoglycans (GAGs), formerly known as mucopolysaccharides. The seven distinct types of MPS (Table 1) are caused by deficit in one of eleven enzymes affecting the degradation of the five main types of GAGs: heparan sulfate (HS), dermatan sulfate (DS), chondroitin sulfate (CS), keratan sulfate (KS) and hyaluronic acid (HA). Deficiency in one of these enzymes caused by pathogenic variants in the corresponding encoding gene (Table 1), leads to the accumulation of undegraded or partially degraded GAGs within lysosomes causing progressive cellular dysfunction and damage to multiple tissues and

organs (143). All MPSs are autosomal recessive disorders with the exception of MPS II, or Hunter syndrome, which is X-linked.

### 1.3.2 Glycosaminoglycans and the biochemical basis of mucopolysaccharidoses

The glycosaminoglycans (GAGs) are unbranched polysaccharides formed by repetitions of disaccharide units each composed by a hexosamine (galactosamine or glucosamine), and a hexuronic acid (glucuronic or iduronic acid) or a hexose (galactose) in the case of keratan sulfate. GAGs are classified according to the nature of the hexosamine, hexuronic acid or hexose units and the glycosidic link between them in HS, heparin, DS, CS, KS and HA. The heterogeneity of GAG results from the type, number (between 25 and 200), acetylation and sulfation pattern of component disaccharide units (144).

The simplest GAG corresponds to HA, formed by nonsulfated N-acetylglucosamine (GlcNAc) and glucuronic acid (GlcA) sequential units. HA is synthesized by transmembrane proteins and secreted into the extracellular space (145). The biosynthesis of the remaining GAGs, which are highly sulfated, occurs in the Golgi apparatus where they also undergo post-translational modifications (146).

GAGs attach covalently to core proteins forming proteoglycans that locate at the surface and extracellular matrix of, playing an important role in cell growth, attachment, migration and differentiation, neuronal plasticity and immune defense against pathogens (146). Despite presenting a similar structure to HS, heparin has an intracellular localization in cytoplasmic granules of mast cells (147).

The degradation of GAGs occurs in the lysosome by stepwise action of several enzymes that ultimately reduces them to monosaccharides and inorganic sulfate.

### 1.3.3 Clinical manifestations and diagnosis

The MPSs are progressive disorders with different onset and severity of symptoms, which cause significant morbidity and reduced lifespan in the patients (148). They are multisystem disorders, with wide spectrum of symptoms that may include coarse facial features, organomegaly, ear/nose/throat infections, corneal cloudiness, skeletal and cardiovascular dysfunction (149). The

patients affected by neuropathic MPSs (I, II, III and VII) present lysosomal storage of HS whereas those having MPS IVA, IVB, VI and IX, show accumulation of KS, CS, DS or HA and display somatic symptoms.

The initial diagnosis of a MPS is based on the onset and clinical symptoms presented, which is later confirmed by detection of an increased amount of GAGs and partially degraded primary substrate in biologic fluids, absent or reduced enzyme activity essay in the patient's cells and, finally, identification of the pathogenic variants by molecular analysis.

Newborn pilot screening studies have been performed for MPS I in Italy (150, 151), Brazil (152), Mexico (153), several states in the USA (Illinois and Missouri) (154, 155), NY (156) and Washington (157) and in Japan for MPS I, II, III and IVB (158). In Taiwan, newborn screening for MPS I and II is routinely performed since 2015 (159). MPS I has been included in the USA Recommended Uniform Screening Panel in 2018 and is currently being screened in newborns (160). For most studies, the first-tier screen corresponds to enzyme measurement by fluorometric or tandem mass spectrometry (MS/MS) essays in the newborn dried blood spot (DBS) samples, generally in multiplex with other LSDs (161). In Japan, the DBS GAG-derived disaccharides were measured by liquid chromatography tandem mass spectrometry (LC-MS/MS) (158). A second-tier screen is performed in DBS samples with an initial positive result using a different method such as urinary GAG (uGAGs) analysis, enzyme measurement and molecular testing (158, 161).

### 1.3.4 Birth prevalence

The birth prevalence of Mucopolysaccharidoses varies for each disorder, between populations and geographic areas. The estimated combined MPSs birth prevalence ranges from 1.35 in South Korea to 4.8 per 100,000 live births in Portugal (108-113, 115-121, 162-166). In the Eastern province of Saudi Arabia the MPS birth prevalence, estimated as 16.9 per 100,000 live births, is likely due to the high rates of consanguinity in the region (114).

The MPS birth prevalence in Europe was estimated in 3.14 cases per 100,000 live births (120), being more frequent in Portugal and The Netherlands (110, 113) and less prevalent in Sweden, Denmark and Poland (119, 163). East Asia is the region with the lowest birth prevalence of MPSs, estimated as 1.35 in South Korea, 1.53 in Japan and 2.04 per 100,000 live births in Taiwan (120,

167). Overall, MPS III and I are the most frequent, whereas MPS VII and IX are considered the rarest (120).

## 1.4 Mucopolysaccharidosis III

### 1.4.1 Definition and classification

Sanfilippo syndrome or Mucopolysaccharidosis type III (MPS III) was first described in 1963 by the pediatrician Sylvester Sanfilippo (168).

There are four subtypes of MPS III (A, B, C and D) each caused by the deficiency of a specific enzyme involved in the catabolism of heparan sulfate (HS) (143). In 1972, Kresse and Neufeld identified the N-sulphoglucosamine sulphohydrolase, or sulfamidase (SGSH), as the deficient enzyme in Sanfilippo A patients, while Von Figura & Kresse (169) and O'Brien *et al.* detected a deficit in N-acetyl-α-D-glucosaminidase (NAGLU) in MPS IIIB patients (170). The Sanfilippo C patients were found to have a deficient activity in heparan sulfate acetyl-CoA: α-glucosaminide N-acetyltransferase (HGSNAT) enzyme by Klein and colleagues in 1978 (171). Deficient activity of N-acetylglucosamine-6-sulfatase (G6S) in MPS IIID patients was detected in 1980 by Kresse *et al.* (172). All deficiencies lead to a storage of partially degraded HS in the lysosomes causing cell, tissue and organ dysfunction (96).

### 1.4.2 Heparan sulfate and the biochemical basis of Sanfilippo syndrome

#### 1.4.2.1 Generalities and physiological role of heparan sulfate proteoglycans

Heparan sulfate is the commonest and considered the most physiologically important glycosaminoglycan (173). It is formed by repeats of disaccharide units containing D-glucuronic acid (GlcA) or L-iduronic acid (IdoA), some of which are sulfated, and acetylated or sulfated D-glucosamine residues (143). The glycosidic bond between D-glucosamine (GlcN)/ N-Acetyl-D-glucosamine (GlcNAc) and GlcA has a α1→4 configuration while the one established between GlcA and IdoA to the aminosugar is respectively, β1→4 and α1→4 (174) HS chains are

ubiquitously expressed and covalently attached to core proteins in proteoglycans, which are located at cell surface and on the extracellular matrix (basement membranes and interstitial matrix) of animal cells (175, 176) (Fig. 5).

The heparan sulfate proteoglycans (HSPG) are highly diverse differing in the core protein, but especially in the number of HS chains, the respective disaccharides' units in each chain and their sulfation pattern. This diversity, especially the size of HS chains and their sulfation patterning, allows the specific binding of a high number of HS-binding proteins (HSBPs) (177). The main categories of HSBPs are growth factors, morphogens, extracellular structural proteins and cell adhesion proteins involved in cell attachment, migration, invasion, differentiation and tissue repair. HSPGs perform other functions such as blood coagulation, endocytosis mediation (178, 179) and synapse formation and plasticity (180). Chemokines, cytokines and proteins of the complement pathways also bind to HSPG, participating in inflammatory response to injury or infection (181) (Fig. 5).

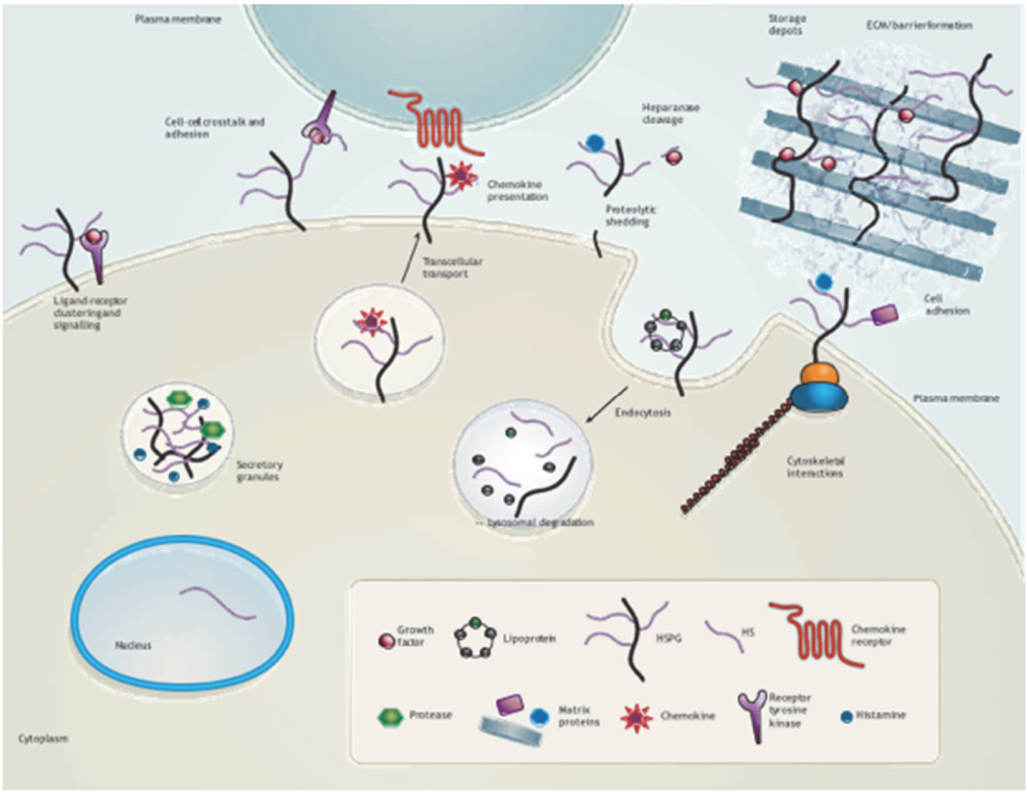


**Figure 5: Physiological role of heparan sulfate proteoglycans**

The figure depicts the main cellular functions of heparan sulfate proteoglycans (HSPG) (Adapted from Bishop *et al.*, 2007 (182)).

In addition, the action of endogenous heparanases and proteases, as well as proteases from several pathogens, may lead to HSPG shedding by HS cleavage, changing the structure of HS chains, and to the down-regulation of HSPG-dependent functions (176, 178).

#### 1.4.2.2 Biosynthesis of heparan sulfate proteoglycans

After the synthesis of the proteoglycan core proteins in the ER, the remaining steps of biosynthesis of HS chains occur in the Golgi apparatus. In this organelle, the HS biosynthesis is initiated by formation of a glucuronic acid-galactose-galactose-xylose tetrasaccharide anchor (GlcAβ1-3Galβ1-3Galβ1-4Xyl) that links the HS chain to the core protein. The first reaction corresponds to the transfer of a xylose residue to a specific serine in the core protein by one of two xylosyltransferases, XYLT1 or XYLT2. Afterwards, two galactose residues followed by a glucuronic acid are successively transferred to the growing tetrasaccharide linker, by the action of, respectively, galactosyltransferase 1, 2, and glucuronyltransferase 1 enzymes. The linkage region may be modified by sulfation of the galactose residues and phosphorylation of xylose.

The elongation step of HS biosynthesis starts with the addition of GlcNAc to the linker by exostosin like-glycoyltransferase 3 (EXTL3), followed by the alternate transfer of GlcA and N-GlcNAc to the growing chain by the action of EXTL1 and EXTL2 enzymes, respectively (183).

Several modifications in the HS chains occur during the last step of its synthesis, starting by the *N*-deacetylation and *N*-sulfatation of some subsets of GlcNAc residues by N-deacetylase/N-sulfotransferase enzymes (NDSTs), being followed by the epimerization of many GlcA units, located next to deacetylated and sulfated glucosamine units (GlcNS), into IdoA by C5-epimerase (183). The majority of IdoA units are subsequently modified by 2-*O*-sulfation and, finally, specific GlcNAc residues undergo 6-*O* and, less frequently, 3-*O* sulfation (Huang et al., 2015). The *O*-sulfation modifications are performed by the action of one 2-*O*-sulfotransferase (2OST), three 6-*O*-sulfotransferases (6OSTs) and seven 3-*O*-sulfotransferases (3OSTs), and are essential for generation of HS ligand binding sites (183).

### 1.4.2.3 Catabolism of heparan sulfate proteoglycans

The first steps of HSPGs degradation occurs at the cell surface and ECM by action of 6-*O*-endosulfatases Sulf1 and Sulf2, and heparanase enzymes. While Sulf enzymes remove 6-*O*-sulfate groups from HS chain, endogenous heparanase and several ECM proteases produce HS fragments by cleavage of HS chains. The resulting partially degraded HSPGs are then internalized and may be recycled back to the cell surface and ECM through further cycles of degradation and biosynthesis of GAG chains, followed by exocytosis (183) or undergo further catabolism in the lysosomes. The degradation of HS chains occurs by sequential action of nine lysosomal enzymes, three exo-glycosidases (α-L-iduronidase (IDUA), β-D-glucuronidase (GUSB) and N-acetyl-α-D-glucosaminidase), five sulfatases (iduronate-2-sulfatase (IDS), arylsulfatase G, glucuronate-2-sulfatase (GDS), N-acetylglucosamine-6-sulfatase, N-sulphoglucosamine sulphohydrolase), and one N-acetyltransferase (Acetyl-CoA: α-glucosaminide N-acetyltransferase) at the non-reducing terminus (Fig. 6). It has been suggested that these enzymes work cooperatively in a complex, as this allows an optimization of the HS degradation, by passing efficiently the substrates from an enzyme to the next one in the pathway (143).

The first step of the pathway is the removal of sulfate groups from IdoA residues by IDS which are then cleaved by IDUA. These enzymes participate in the catabolism of both HS and DS. Consequently, the deficiency of IDS and IDUA leads to the lysosomal storage of both these GAGs causing, respectively, MPS II (Hunter syndrome) and I (Hurler/ Hurler-Scheie and Scheie syndromes).

Arylsulfatase G (ARSG), or glucosamine-3-*O*-sulfatase, catalyzes the hydrolysis of 3-*O* sulfate group from the rare 3-*O*-sulfated *N*-sulfoglucosamine terminal residues. The deficiency in ARSG leads to lysosomal storage of HS (184, 185) in the canine and murine models and was named MPS IIIE despite not being reported in humans until recently. A homozygous missense variant in *Arsg* was detected in Yemenite Jews presenting an atypical, late onset Usher syndrome, with retinal degeneration and hearing loss. The variant p.D45Y abolishes ARSG enzyme activity but uGAG values in these patients are at the upper limit of the normal range in MPS disorders (186). The next reaction in HS catabolism corresponds to the hydrolysis of 6-sulfate groups from terminal glucosamine units, which is catalyzed by SGSH. In order to be cleaved, the HS GlcN terminal residues need to be acetylated by HGSNAT. The acetyl group is transferred from a cytoplasmic

Acetyl-CoA to the amino group of the lysosomal glucosamine at the non-reducing terminal of HS chains. MPS IIIA and MPS IIIC are caused by deficiency of SGHS and HGSNAT activity, respectively, causing lysosomal accumulation of HS.

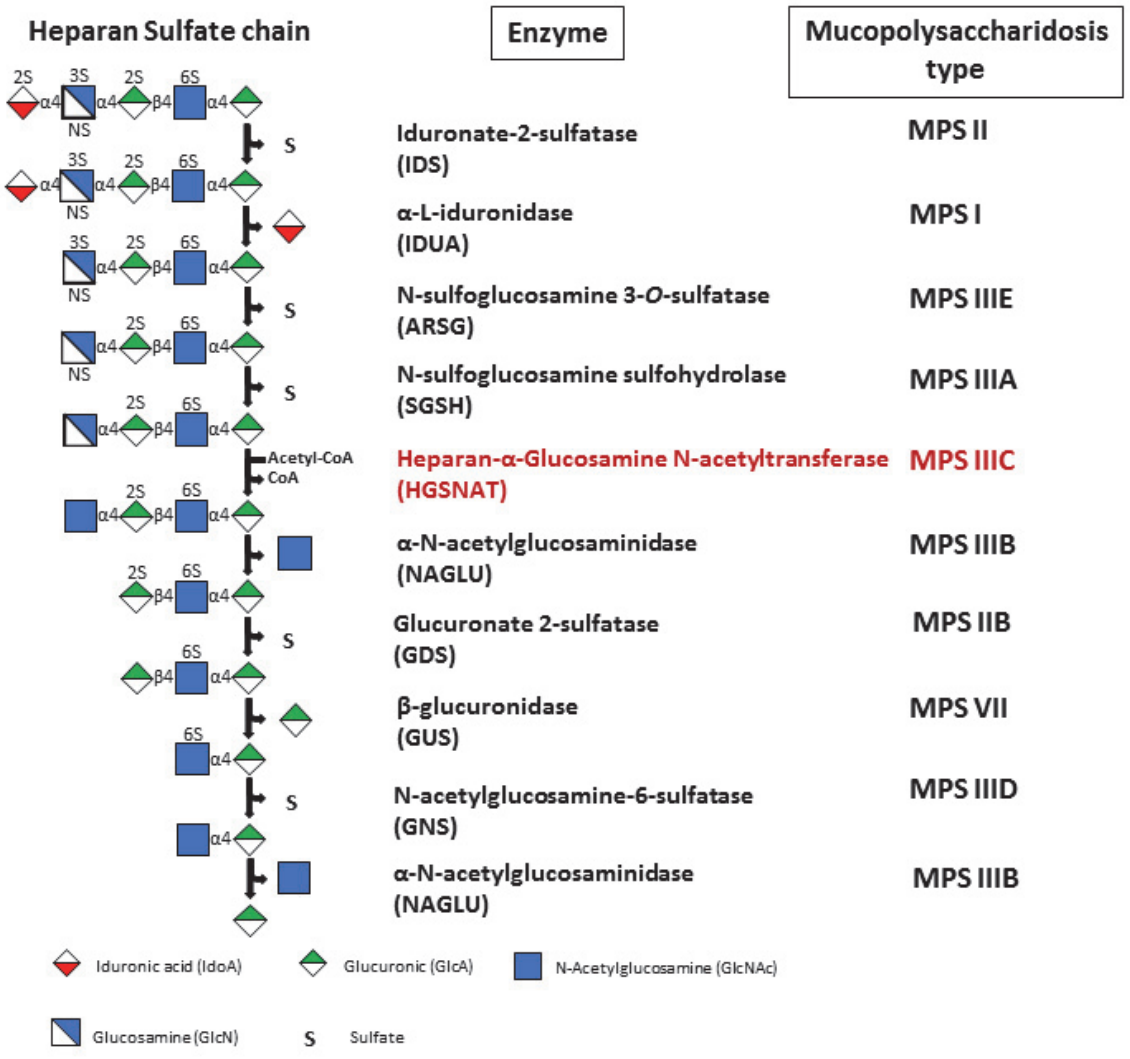


**Figure 6: Heparan sulfate catabolic pathway**

The enzymes involved in the stepwise degradation of heparan sulfate, reactions they catalyze, and mucopolysaccharidoses caused by their deficiency, are shown. (Adapted from Frezze *et al.*, 2009 and Kowalewski *et al.*, 2012 (185, 187)).

The terminal acetylated glucosamine synthetized in the previous reaction can be then removed by the action of NAGLU enzyme, which deficiency causes MPS IIIB. The removal of 2-*O*-sulfate groups from the terminal 2-*O*-sulfo-glucuronic acid residues of HS, as well as CS and DS, is performed by the action of Glucuronate-2-sulfatase (GDS) or arylsulfatase K (ARSK) (188). The rarity of 2-*O*-sulfo-glucuronic acid residues might explain the moderate accumulation of HS and CS in an *Arsk/Gds*-knockout mouse model, recently characterized by Christof Trabszo *et al.* (189). To date, there has been no deficiency in GDS/ARSK reported in humans, suggesting that such defect would lead only to a very mild or no phenotype (tentatively named as MPS IIB) (189, 190).

The cleavage of terminal β-D-GlcA residues from HS, CS and DS chains is performed by GUSB. MPS VII (Sly syndrome) is due to GUSB enzyme deficit causing the accumulation of these GAGs in the lysosome. Finally, GNS is responsible for the removal of 6-sulfate groups from N-acetyl-D-glucosamine 6-sulfate residues at the nonreducing end of HS. MPS IIID patients have deficient GNS activity and show lysosomal storage of HS.

### 1.4.3 Diagnosis

#### 1.4.3.1 Biochemical identification and quantification of GAGs

Lysosomal accumulation of undegraded or partially degraded HS, is the hallmark of all patients affected with MPS III. HS is also secreted by the cells and detected at high levels in body fluids such as urine, blood and cerebrospinal fluid (CSF) (191). The quantification of urinary GAGs is generally the first step in the diagnosis of MPS disorders, including MPS III (192).

Qualitative and semi-quantitative tests, using cationic dyes on filter papers, such as toluidine spot test, have been widely used in the past but are now considered obsolete due to high rate of false negative and high rate of false positive results. The most frequent quantitative test consists in the spectrophotometric measurement of the complex formed by 1,9-dimethylmethylene blue (DMB) and sulfated urinary GAGs. A similar test can be performed using Alcian blue dye, which also forms a complex with GAGs detectable by spectrophotometry, being, however, less sensitive and specific than with DMB (148). However, concentrations of GAGs in the urine of MPS patients with mild clinical phenotypes can overlap with those in healthy controls, are very different between age groups and can be influenced by other metabolic conditions and medications. All these factors

result in high false-negative and false-positive rates (143, 148). Besides, measurement of total urinary GAGs cannot distinguish between individual MPS diseases.

Though two-dimensional electrophoresis and thin-layer chromatography can be used for detection of individual GAGs, more recent methodologies, such as tandem mass spectrometry coupled to high performance liquid chromatography (LC-MS/MS), have higher sensitivity to detect and precisely quantify specific GAGs. This allows to evaluate with higher accuracy the efficacy of a treatment, such as enzyme replacement therapy, in reducing the storage of GAGs (193). Besides urine, tandem mass spectrometry has been also used to quantify GAGs in the blood, serum (194), plasma (195), cerebrospinal fluid (196) and dried blood spots (158, 197). However, these methodologies only allow the confirmation of MPS III diagnosis, while identification and quantification of residues at the nonreducing ends of GAG chains by LC-MS/MS provides a possibility to identify specific Sanfilippo subtypes (198).

#### 1.4.3.2 Enzymatic essays

The gold standard test to confirm the diagnosis of a specific MPS III is the measurement of the activity of the enzyme suspected to be deficient in the patient's leukocytes, lymphocytes, plasma, serum, dried blood spots or cultured fibroblasts. The substrates used in the enzymatic assays can be fluorogenic (4-methylumbelliferyl), chromogenic (p-nitrophenyl) or radioactive (130, 148).

#### 1.4.3.3 Molecular analysis

Genetic analysis is performed to confirm the diagnosis by identifying the pathogenic variant(s) in the corresponding gene, responsible for the MPS III. The diagnosis of a family index case is typically followed by familial genetic counseling to discuss the possible clinical phenotype of the patient, treatment interventions, as well as prenatal diagnosis of future siblings, pre-symptomatic testing of non-affected members and detection of carriers in the family, by genetic screening for the pathogenic variant(s). The prenatal molecular test is performed in cultured amniotic fluid cells and fresh or cultured chorionic villi and, whenever possible, complemented by enzyme assay and GAG quantitation in the same type of samples (130, 199).

Currently, next-generation sequencing (NGS) of complete genomes (Whole genome sequencing, WGS) and exomes (Whole exome sequencing, WES), which uses massive parallel sequencing, is performed to identify genes and pathogenic variants associated with a disease in situations where

other diagnostic approaches have failed. NGS may represent in the future the first-line test for diagnosis of MPS III because it is rapid and becomes more and more affordable (130). For a small number of MPS III pathogenic variants it became possible to provide their correlation with the clinical phenotype. However, the majority of variants associated with these diseases are rare and have unknown significance requiring further characterization by performing *in sillico* predictions of pathogenicity and functional studies.

### 1.4.4 MPS III birth prevalence and molecular genetics

The worldwide birth prevalence of MPS III ranges from 0.17 in Colombia to 1.89 per 100,000 live births in the Netherlands. MPS III seems to be less frequent in East Asia and in the American continent, but several countries in Europe have similar low frequencies (Fig. 7).

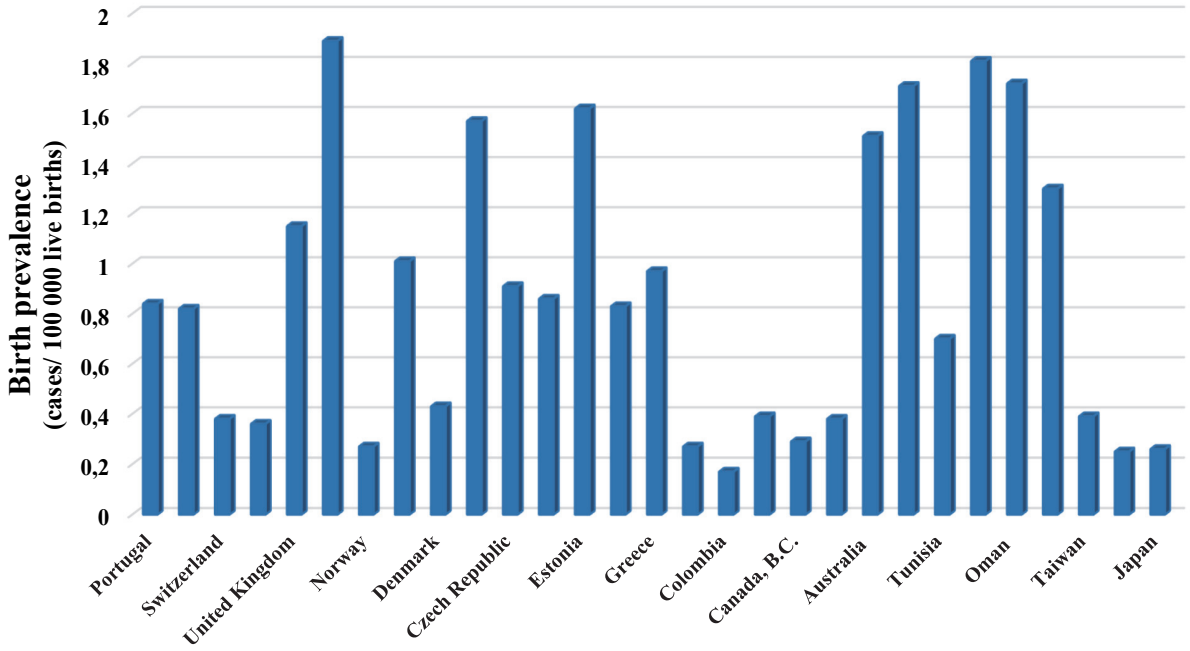


**Figure 7: Birth prevalence of Mucopolysaccharidosis type III per country**

Notes: Other studies estimated MPS III live birth prevalence in Sweden and Oman as 0.67 (163) and 2.35 (116) per 100,000 live births, respectively. The values in the graph correspond to the longest period of study (Oman (199)) or the highest number of patients detected over the same time interval (Sweden (118)). British Columbia; E.P. Eastern province

MPS IIIA and IIIB are more frequent than MPS IIIC and IIID, the last being very rare (108-119, 162-167, 200-205) (Fig. 8).

In Eastern China, among 190 MPS patients diagnosed between 2016 and 2012, 3,7% (seven cases) corresponded to Sanfilippo A and B (206). A study including mostly Indian patients, but also Sri Lankan and Afghanistan, has shown that 11,8% of the 85 MPS patients diagnosed during an 11-year period, from 2002 to 2012, were either MPS IIIA (9,4%) or IIIB (2,4%) (206, 207). There were no cases of MPS IIIC and IIID in both studies (206, 207). Due to the absence of public records on the number of live-births in the respective geographic areas during the time period of these two studies, it is not possible to estimate the corresponding MPS IIIA, IIIB, as well as combined MPS III birth prevalence (120, 206, 207).

#### 1.4.4.1 MPS IIIA

MPS IIIA (MIM 252900) is caused by variants in the *SGSH* gene that encodes the lysosomal hydrolase SGHS (EC 3.10.1.1). The gene is located in 17q25.3 region contains eight exons and has a total size of 11 Kb. Among 159 disease-causing variants described so far in MPS IIIA patients, 108 (67.9%) are missense (HGMD® Professional 2021.2, July 2021).

MPS IIIA is the most frequent type of MPS III. Its estimated birth prevalence (or incidence at birth) ranges from 0 per 100 000 live births in the North of Portugal, Greece and United Arab Emirates, to 1.62 cases per 100 000 live births in Estonia (108-111, 113, 115, 117-119, 162-164, 167, 204, 205) being more prevalent in Northern Europe (Fig 8).

Though detected in different populations, p.R245H is the most commonly found variant among German, Dutch, Australian/American and British patients (101, 208-211). A founder effect of the missense variant, p.R245H, likely introduced in Cayman Islands by British settlers, is responsible for the estimated carrier frequency of 1/7 to 1/10 in the population from the West Bay district of Grand Cayman (212, 213). The p.R74C, p.S66W, c.1079delC and c.1091delC variants are the most frequent in the Polish, Sardinian, French and Spanish patients, respectively (101, 166, 208, 214, 215). The high frequency of certain variants in specific populations or geographic areas may suggest the presence of founder effects, which can be verified by performing haplotype studies. Besides founder effects, haplotype analyses may indicate the occurrence of events such as

migration and natural selection. A haplotype contains alleles that are in genetic linkage and are inherited together. The study of the inheritance of a cluster of polymorphisms (single nucleotide polymorphisms (SNPs), short tandem repeats (STRs), variable number of tandem repeats (VNTRs)) associated with a rare variant in different populations, might be used to infer the evolutionary history of populations (216).

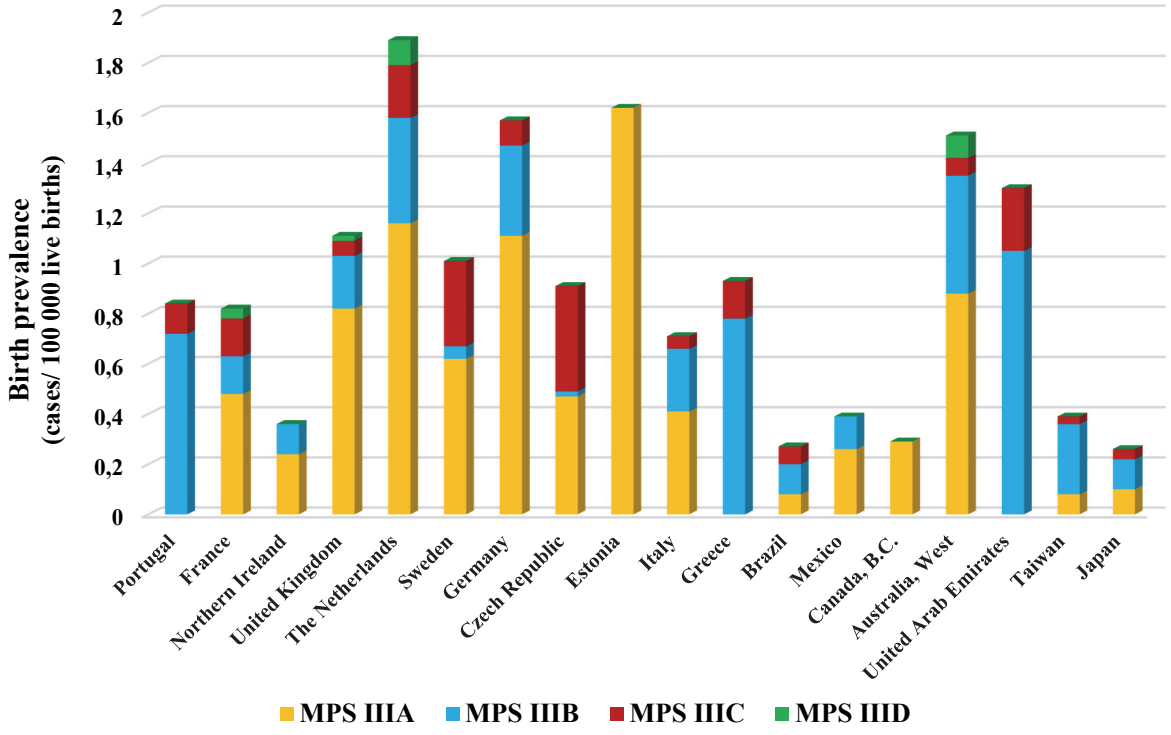


**Figure 8: Birth prevalence of Sanfilippo syndrome subtype A, B, C and D per country**

Notes: In Germany, 32.6% of Sanfilippo B, and 5.7% of Sanfilippo A patients, have Turkish ancestry (162). B.C., British Columbia; E.P. Eastern province.

In the case of MPS IIIA, a haplotype-based study on c.1091delC alleles has shown a common origin for this variant among Spanish patients (215) confirming its hypothesized founder effect. The results of other haplotype study indicated an ancient origin for p.R245H, p.R74C, p.S66W and c.1091delC variants (101).

The relatively high number of reported homozygous and compound heterozygous MPS IIIA patients, allowed to correlate, at least for some of the variants, the genotype with the phenotype (211, 217-220). The patients were separated according with disease progression into rapidly and slowly progressing groups (217). The SGSH variants p.R245H, p.Q380R, p.S66W and c.1080delC are associated with a severe rapidly progressing phenotype (221) while p.G122R, p.R206P, p.E369K and p.I322S, (211, 218, 219, 222) as well as p.T421R, p.P180L, and p.L12Q (221), were linked to an attenuated phenotype. The patients with a milder phenotype show stability of the cognitive and motor functions over many years (211, 219, 223-225). In addition, 10 patients, diagnosed with MPS IIIA between the ages of 3 and 68 years (average age 49 years), were presenting only retinal dystrophy and/or cardiomyopathy but normal cognition (225, 226).

Knottnerus and colleagues showed that the measurement of SGSH activity in MPS IIIA patients' fibroblasts cultured at 30°C may be a useful tool to predict the severity of the patient's phenotype. The fibroblasts of patients with slowly progressing phenotypes, contrarily to those with faster progression, showed an increase in SGHS processing, lysosomal targeting, residual activity and reduction in GAG levels, without a significant increase in protein synthesis, when cultured at 30°C instead of 37. The low temperature likely facilitates the proper folding of mutant proteins associated with SP phenotypes but not those with variants found in the rapidly progressing group (222).

Mild hypothermic conditions have been shown to improve protein folding in cultured cells but the underlying mechanisms are still poorly understood. It is possible that the reduction of 7°C in the physiological temperature leads to an increased expression mRNA and protein levels of specific molecular chaperones (227, 228), the fidelity of the process (229), resulting in improved folding of SP mutant proteins, their escape from ERAD, ultimately enabling their transport to the lysosome.

The study of Knotterus *et al.* suggests that, such as the effect of the reduced temperature, the use of pharmacological and chemical chaperones might improve folding of SP mutant proteins, rescuing, at least partially, enzyme activity and that these variants are good candidates for enzyme enhancement therapy (see chapter 1.4.7.4 Enzyme enhancement therapy).

### 1.4.4.2 MPS IIIB

MPS IIIB (MIM 252920) is caused by pathogenic variants in the *NAGLU* gene encoding the NAGLU enzyme (EC 3.2.1.50). The gene contains six exons, is located on chromosome 17 (17q21.2) and has an approximate size of 83 Kb. So far, 245 sequence variants have been described in *NAGLU*, including 155 missense (63.2%) (230) (HGMD® Professional 2021.2, July 2021) associated with MPS IIIB. The estimated birth prevalence of MPS IIIB ranges from 0 in Estonia and the Canadian province of British Columbia to 1.05/100000 live-births in the United Arab Emirates (UAE) (Fig. 8). Besides UAE, MPS IIIB is particularly frequent in Greece, Portugal and in patients of Turkish descent (113, 162).

The large allelic heterogeneity in MPS IIIB is likely responsible for the wide variety of clinical phenotypes detected in these patients (210). The high birth prevalence of MPS IIIB in Greece is due to the high frequency of p.Y140C, p.H414R, and p.R626* variants that represent 70% of the reported cases (231). The disease-causing variants p.R643C and p.R297* are common in Dutch patients and p.R565P in Japanese MPS IIIB patients (232, 233). Mangas and collaborators (234) have performed the only haplotype study in MPS IIIB alleles. They have shown that p.R234C variant was associated with a common ancestral haplotype in Portuguese and Spanish patients, having thus a single origin in Iberian Peninsula.

As in MPS IIIA, patients with NAGLU deficiency may present a rapidly progressing phenotype or a more attenuated, slowly progressing phenotype (221). The variant p.R297* is associated with a severe MPS IIIB phenotype whereas p.R643C, p.S612G, p.E634K, and p.L497V were detected in patients with a milder clinical course (235, 236). As for SGSH, the residual NAGLU activity in fibroblasts of SP MPS IIIB patients increases significantly when the cells are cultured at 30°C, which does not occur in fibroblasts of RP patients (236), suggesting that this method can be used to predict the severity of the phenotype. In hypothermic conditions, there is an increase in NAGLU mRNA levels, as well as in precursor and mature NAGLU proteins, in slowly progressing MPS IIIB patients' fibroblasts. By blocking the proteasomal breakdown of mutant NAGLU precursor protein, Meijer and collaborators (237) have shown that the increase in the levels of mature protein was partially due to the improved folding and/or processing of the protein variants at lower temperature. The authors concluded that, patients carrying slowly progressing variants might benefit from pharmacological chaperones, small molecule drugs helping mutant protein variants

to adopt a correctly folded conformation.

Such as in MPS IIIA, MPS IIIB SP variants are also therapeutic targets for chemical chaperone therapy. However, the effect of these compounds is nonspecific and require higher concentrations to promote protein folding, whereas pharmacological chaperones are protein- and even missense mutations-specific, acting efficiently at low concentrations (238). Consequently, the use of pharmacological chaperones is considered the most promising as a therapeutic approach.
So far, only one MPS IIIB patient with onset during adulthood has been reported. The patient was diagnosed at 27 years old and presented mild but stable cognitive delay, without visual or cardiac manifestations during a 5-year follow-up period. The patient has been tested after her older sister, presenting progressive cognitive decline since the age of 8 years, was diagnosed with the disease (225).

#### 1.4.4.3 MPS IIIC

MPS III type C (MIM 252930), or Sanfilippo C syndrome, is caused by pathogenic variants in the *HGSNAT* gene leading to deficient activity of heparan sulfate acetyl-CoA: α-glucosaminide N-acetyltransferase or HGSNAT (EC 2.3.1.78) enzyme. The estimated birth prevalence of MPS IIIC ranges from 0 to 0.42 cases per 100 000 live births in Estonia and Czech Republic, respectively (108-111, 113, 115, 117-119, 162-164, 166, 167, 204, 205) (Fig. 8).

Previously, 65 sequence variants in *HGSNAT*, 43.1% of these missense, have been identified in the patients from several countries in Europe, Tunisia and Morocco in North Africa, Turkey, Pakistan, Singapore and Korea in Asia, Canada and USA in North America. Argentina and Colombia are the only countries in South America where MPS IIIC patients were clinically diagnosed and characterized molecularly (239-251). Some of these studies reported a high frequency of certain *HGSNAT* pathogenic variants in specific populations. That is the case of p.S518F and p.R344C, which represent, respectively, 28.6 and 21.4% of the mutant alleles detected in Dutch patients (244), and the c.525dupT variant detected in 83% of Portuguese MPS IIIC alleles (242). In 2007, Fedele *et al.* studied the Italian Sanfilippo C patients and reported high frequency of variants c.852-1G>A and p.R384*, corresponding to 30 and 20% of mutant alleles, respectively, due to potential founder effects in this population (241). More recently, Velasco reported five individuals belonging to a large pedigree in Boyacá region in Colombia, homozygous

for p.Q454*, which also likely corresponds to a founder mutation in this area (249). So far, no follow-up studies have been performed to confirm these hypotheses.

The only haplotype analysis in MPS IIIC patients has been previously performed by Canals *et al*., in 2011. This study suggested a common origin for the splicing variant c.234+1G>A in Spanish and Moroccan patients. For all patients, this variant was present in only one haplotype, associated with the single nuclear polymorphisms (SNPs) c.710C>T/ p.P237Q and c.564-98T>C. Interestingly, the c.234+1G>A variant in Italian and Turkish patients was not associated with p.P237Q substitution (241, 244). The haplotype study performed by Canals also suggested that all c.372-2A>G alleles carried by Spanish patients had the same origin.

#### 1.4.4.4 MPS IIID

MPS IIID (MIM 252940) is caused by mutations in the *GNS* gene, which encodes the GNS enzyme (EC:3.1.6.14). *GNS* comprises 14 exons in approximately 43 Kb, and is located on chromosome 12 (12q14.3). Until now 32 patients from 26 families have been identified, presenting 26 mutations, of which only four (15.4%) are missense (HGMD® Professional 2021.2, July 2021) but four (15.4%) correspond to large deletions. All patients were homozygous with an exception of those from three families. Each family has private pathogenic alleles and no genotype/phenotype correlation has been ever established.

Patients affected by MPS IIID were detected in Europe (Italy, France, Belgium, The Netherlands, Bulgaria and Poland) and Western and Southern Asia (Turkey, Iran, Pakistan, Saudi Arabia and India) (220, 252). However, 30% of patients have Italian, and 22% Turkish ancestry. It is likely that this high frequency in Turkey and the cases of homozygosity detected in Western and Southern Asia are due to high consanguinity levels, which are common in these regions. The high prevalence of disease in Italian patients, and the high homozygosity level found in other European MPS IIID cases may reflect regional founder effects (221). The highest birth prevalence for MPS IIID was estimated in Australia and UAE, with 0.1 and 0.09 cases per 100 000 live births, respectively (Fig. 8).

#### 1.4.4.5 MPS IIIE

Until recently, a fifth subtype of Sanfilippo syndrome, MPS IIIE, caused by ARSG deficiency, had only been described in a naturally occurring dog (184) and a generated knockout mouse (185) models. The first variant reported in ARSG gene, p.D45Y, was detected in homozygosity in five patients of three families of Yemenite Jewish origin, possibly corresponding to a founder mutation (186). These patients presented an atypical, late onset Usher syndrome, generally after 40 years of age, with retinal degeneration and hearing loss. Other neurological or peripheral symptoms typically displayed by MPS III patients were absent. Meanwhile, four other variants were detected in Portuguese (253) and Spanish (254) patients, displaying a similar clinical presentation. The functional study of four of these variants showed that they abolish ARSG enzyme activity by interfering with protein processing and lysosomal targeting (186, 253).

### 1.4.5 Mucopolysaccharidosis IIIC: from *HGSNAT* gene to molecular pathology

#### 1.4.5.1 The *HGSNAT* gene

The MPS IIIC causative gene, *HGSNAT*, was identified in 2006 by two independent research groups (239, 240). It is located in the pericentromeric region of chromosome 8, on 8p11.1, spans a region with approximately 62.5kb, and has 18 exons (239, 240).

Richtrova and colleagues (255) showed that *HGSNAT* transcription is driven by a TATA-less promoter where key elements are located in the 1054 bp region upstream of exon 1, which contains an unmethylated CpG island. TATA-less promoters containing unmethylated CpG islands are a common feature of genes encoding lysosomal proteins, and generally associated with constitutive expression. Besides, high-scoring CLEAR consensus sequences were neither identified in the *HGSNAT* promoter, nor it was confirmed its binding to TFEB, suggesting that *HGSNAT* regulation is TFEB-independent (303). The *HGSNAT* gene has two possible initiation codons at a distance of 84 bp, each preceded by a Kozak sequence (239, 240, 256). The transcription from the upstream ATG would originate a protein with 663 amino acids. The other ATG, with A being at +1 in the transcript, was accepted in terms of nomenclature as the first *HGSNAT* cDNA codon. The translation from this downstream ATG (DS-ATG) would give rise to a protein with 635 amino

acid residues. While Durand and colleagues demonstrated that both ATG initiation sites are used for the synthesis of the protein, other groups suggested that expression from the DS-ATG is predominant (247, 255).

### 1.4.5.2 HGSNAT Biosynthesis

The *HGSNAT* gene encodes the membrane multi-pass HGSNAT protein, with 11 predicted transmembrane domains, an N-terminus located in the lysosomal lumen and a C-terminus in the cytosol (117, 239).

The N-terminal portion of HGSNAT is only conserved among metazoans while the C-terminal is highly conserved across species of different kingdoms, including plants and bacteria (247). HGSNAT has similarity with the uncharacterized conserved protein domain COG4299 (Entrez Gene GeneID 138050) (239, 240) that is present in several bacteria, including some existing in the human gut. The function of COG4299 remains unknows as well as whether it participates in metabolism of HS by these bacteria, although, host HS and heparin are used as high-priority carbohydrate source of energy by the gut *Bacteroides thetaiotaomicron* (174).

Human HGSNAT protein is ubiquitously expressed and, among the tissues analyzed, it has higher expression in the heart, liver, leukocytes, kidney and placenta, and the lowest in the thymus, brain and colon (239, 240). The synthesis of HGSNAT, as well as its post-translation modification by Asn-linked glycosylation at five predicted sites, occurs in the ER (240, 257).

There are two different hypotheses on the proteolytic processing of the enzyme, its sorting and transportation to the lysosome. According to Durand & Felhammer *et al*. (256) the predicted N-terminal signal peptide of HGSNAT is not cleaved in the ER lumen. At the lysosomes, the inactive 77 kDa HGSNAT precursor undergoes proteolytic cleavage into a 29 kDa N-terminal α-chain and a 48 kDa C-terminal β-chain, essential for the activation of the enzyme. The two chains would be held together through disulfide bonds between cysteine residues present at lysosomal luminal domains.In contrast, Fan *et al.*(247) reported that a co-translational cleavage of the signal peptide is essential for the exit of the HGSNAT precursor protein out of the ER. The 62 kDa HGSNAT precursor is catalytically active, and is processed in the lysosome into a 27 kDa N-terminal α-chain (Lys44-Asn144) and a C-terminal β-chain (Gly145-Ile635) with 44 kDa.HGSNAT is targeted to the lysosome by a dileucine-based signal [DE]XXXL[LI], corresponding to the ETDRLI209

sequence, in the first cytosolic loop near the N-terminal region (247, 256). A tyrosine-based sequence at the C-terminal end, YILY627, was also identified as lysosomal sorting signal by Durand and coworkers (256) but believed to be non-functional by Fan and colleagues (247).

### 1.4.5.3 Catalytic mechanism of HGSNAT

HGSNAT is an integral lysosomal membrane protein that transfers an acetyl group from cytoplasmic acetyl-Coenzyme A (acetyl-CoA) to the α-glucosamine residue of intralysosomal HS (171). This transmembrane reaction is critical for the degradation of HS since there is no other enzyme that hydrolyzes unacetylated glucosamine molecule.

According to Bame and Rome (258, 259), HGSNAT has a unique mechanism, acting both as a membrane channel and an enzyme. These authors suggested that it catalyzes the transmembrane acetylation of heparan sulfate through a "ping-pong" mechanism. In the cytosol, the acetyl group from acetyl-CoA, not stable in the lysosomal milieu, is transferred to a histidine residue 269 in the HGSNAT active site (256) This reaction would induce a conformational change in the protein with translocation of the domain containing the acetylated residue into the lysosome, which would be then transferred to the terminal α-glucosamine residue of HS, allowing its further catabolism. The results obtained by Ausseil *et al.* (260), support this mechanism by showing that N-acetyltransferase is acetylated in the absence of the second substrate, glucosamine. Future experiments, including characterization of HGSNAT 3D structure should therefore clarify the mechanism of action of this enzyme.

### 1.4.5.4 Molecular pathology

Twenty eight of the 65 *HGSNAT* variants (42,4%) (239-246, 248-251, 261, 262) previously detected in MPS IIIC patients are missense, likely resulting in unfolded/misfolded proteins degraded by the ERAD pathway. Most of the remaining (nonsense, insertions, deletions and splice-site variants) introduce premature stop codons producing transcripts eliminated by the NMD pathway (239, 242, 429).

Two independent studies were performed to understand the pathology of missense HGSNAT variants (257, 263). The expression, enzyme activity and intracellular targeting of 22 missense

mutant proteins were analyzed in these two publication, together. For 18 of these variants the corresponding enzymatic activity was negligible, and the resulting proteins were not glycosylated, lacked proteolytic processing and were retained in the ER. The authors suggested that mutant proteins were likely misfolded and targeted for degradation by the ERAD system (257, 263).

Three variants, p.P237Q, p.V481L and p.K523Q, originated proteins correctly targeted to the lysosome, proteolytically processed and presenting enzyme activity comparable to the WT. Besides, each was detected in *cis* with a deleterious splice-site mutation. They were suggested to represent neutral SNPs, causing no impact on HGSNAT expression, structure or function (257, 263).

Interestingly, p.A615T HGSNAT mutant was also transported to the lysosome where it undergoes proteolytic cleavage and maturation, but its enzymatic activity was only ~60% of that of the WT enzyme (257, 263). This variant was reported in two patients associated in *cis* with a p.W403C variant. When the construct with both mutant p.A615T and p.W403C variants was expressed, enzyme activity was abolished, and the mutant protein was neither targeted to the lysosome nor processed into mature α- and β-chains (263).

Recent studies have also suggested that p.A615T variant represents a hypomorphic allele. Three siblings from a Dutch non-consanguineous family were reported to present non-syndromic retinitis pigmentosa (RP) with onset at 47-52 years, without other somatic or neurologic manifestations (264). They presented variations in the HGSNAT sequence in both alleles; the missense variants p.G133A and p.A615T were found in *cis* in one allele, and p.A615T was detected in the second. The enzyme activities in the patients' leukocytes were lower than those found in controls but higher than in MPS IIIC patients. Eventually, the allele p.A615T has been detected in six family index patients affected by RP or retinal dystrophy (264-267). One of these patients, affected by late onset sporadic RP, at 47 years was heterozygous for p.A615T allele and a large *HGSNAT* deletion (265). In two others, presenting retinal dystrophy, p.A615T was detected in heterozygosity with variants previously detected in MPS IIIC patients, p.P283L in one patient, and c.1542+4dupA in the other. Finally, two of four patients from different families diagnosed with pericentral RP were homozygous for the p.A615T variant, while one was heterozygous for p.A615T allele and the MPS IIIC variant c.1464+1G>A. The remaining patient was homozygous for p.S318N (266).

Three Israeli patients from two consanguineous families with Ashkenazi Jewish ancestry with adult onset of RP, between the age of 29 and 34 years were homozygous for the p.R124W HGSNAT variant. The enzyme activity measured in their leukocytes was below normal, but superior to that presented by MPS IIIC patients (264).

Besides p.A615T, p.G262R and p.S539C variants, detected in two compound heterozygous sisters with adult onset of RP and dementia, were the only ones associated to a milder form of MPS IIIC (244, 268). These results allowed to conclude that MPS IIIC, similar to MPS IIIA and IIIB, present a wide phenotypic spectrum where a milder phenotype include late onset RP or retinal dystrophy with or without cognitive decline. HGSNAT variants p.A615T, p.S318N, p.R124W, p.G262R and/or p.S539C can be considered as causing such slow progressing phenotypes.

## 1.4.6 Pathophysiology

### 1.4.6.1 MPS III patients

#### 1.4.6.1.1 Clinical manifestations

Despite being multisystem disorders, MPS III clinical phenotypes are dominated by the progressive and severe decline of neurologic function. A range of generally mild manifestations in visceral and skeletal systems may be present, namely hepatomegaly, splenomegaly, coarse facial features, macrocephaly, dysosotosis multiplex, joint stiffness, short stature, hypertrichosis, recurrent ear and nose infections. Hearing and visual impairment may also be detected (166, 195, 200, 239, 249, 269-273).

Clinically, it is difficult to distinguish the different Sanfilippo subtypes. Traditionally, MPS IIIA is considered to be the most severe, with the earliest onset and fastest progression, and lowest life expectancy (200, 221, 274). However, each subtype of Sanfilippo syndrome is clinically heterogeneous due to the high variety of pathogenic variants in the patients.

The onset of symptoms occurs, generally, in early childhood (1-4 years old) with patients presenting a delay in the cognitive development, particularly in language acquisition (166, 200, 270, 271). The second phase of the disease is characterized by a progressive intellectual disability

and manifestation of behavioral problems, namely hyperactivity, aggressiveness, decreased attention, sleep disturbances and autistic behaviors at 3-4 years of age. Several patients present recurrent ear, nose and throat infections. In the last phase, the patients develop severe dementia, progressively losing previously acquired abilities. Dysarthria and gradual loss of speech ability, feeding difficulties due to dysphagia, and presence of extrapyramidal tract signs such as seizures, spasticity and hyperreflexia, are common symptoms of this phase of the disease. The decline in motor function leads to the progressive deficit and eventual loss of the locomotion ability (166, 200, 271, 273). Lifespan is reduced, with death generally occurring during the second or beginning of the third decades of life, most frequently due to respiratory tract infections and cardiorespiratory failure (166, 195, 200) .

As described above, MPS IIIA, IIIB and IIIC patients with adult onset show retinal pathology and/or cardiomyopathy with only mild, or without cognitive decline (264, 268).

#### 1.4.6.1.2 Pathophysiological alterations

Imaging and biochemical findings in MPS III patients during their life as well as postmortem examination, has allowed getting insights into the pathophysiologic events which cause the characteristic mild somatic manifestations and severe cognitive dysfunction (273, 275, 276).

The deficit in either SGSH, NAGLU, HGSNAT or G6S enzyme activity leads to the primary storage of the substrate, HS, in most tissues, but predominantly in the liver, brain, spleen and heart (273, 277). Membrane-bound vacuoles with lysosomal characteristics are found in a large variety of cells including vascular endothelial cells, hepatocytes and macrophages in spleen and thymus, liver Kupffer cells, neurons and glia. The storage material is heterogeneous, forming granular, membranous lamellate concentric or parallel zebra-like inclusions, and lipid inclusions, which have different staining properties. In the neurons, the type and amount of stored material varies within and between cells. Storage vacuoles positively staining for an anti-HS antibody were detected in neuronal cell bodies and axons in cerebral cortex, and dendritic swellings of Purkinje cells in the cerebellum (278).

Few studies have been so far conducted to evaluate the brain lipid profile of MPS III patients. The data obtained shows a marked alteration in the content of glycosphingolipids (GSL) in the patients comparatively to those of controls, with a significant increase of GM2, GM3 and GD3

gangliosides, as well as the neutral glycosphingolipid lactosylceramide (276, 279-281). The secondary storage of these GSL, present in very small amounts in control brain tissues (276), was detected in the neurons, as well as in astrocytes, in the brain of a MPS IIIA patient (279). GM2 was specifically found in the cell bodies and enlarged axons and dendrites of cerebral and cerebellar cortex neuronal cells (278).

The quantitative analysis of GSL in MPS III brains also revealed a marked increase in globotriaosylceramide (Gb3), asialo-GM2 (GA2) (276, 281), asialo-GM1 (GA1) (276) and globotetraosylceramide (Gb4), a reduction in 3-*O*-sulfogalactosylceramide, galactosylceramide (281), and in three of the four major GSL species in the normal brain, GM1a (Monosialoganglioside) GD1a (Disialoganglioside) and GT1b (Trisialoganglioside) (276). The low ratio of 4-eicosasphingenine to 4-sphingenine in gangliosides (inferior to 1) in the brain of an adult Sanfilippo B patient suggested the metabolism of these GSL was altered since an early age (281).

There was no significant difference in the content of total cholesterol content between brain tissues of an MPS IIIA patient and controls (282). The amount of cholesterol in neuron was however higher in the Sanfilippo A patient as compared to controls (279), but further studies are necessary to confirm this result.

Secondary accumulation of lipofuscin and SCMAS (subunit c of mitochondrial ATP synthase) (283) as well as phosphorylated α-synuclein and β-amyloid (1-40) proteins were also detected in the brains of Sanfilippo patients (284). Finally, glial cells were highly vacuolated and gliosis was present throughout the brain (277). These cellular and molecular alterations ultimately lead to neuronal loss (277) and atrophy of the cerebral cortex (285), cerebellum and corpus callosum thinning in MPS III patients (286).

#### 1.4.6.2 MPS III animal models

In the last two decades, naturally occurring and generated animal models for Sanfilippo syndromes have been studied with the aim of understanding the pathogenic mechanisms leading to disease. Despite much effort, the complexity of MPS III pathophysiology is not yet completely understood.

At the time of our study, naturally occurring cases of MPS IIIA have been reported in the wirehaired Dachshund (287) and Huntaway dogs MPS IIIB (288, 289), in the Emu (290),

Schipperke dog (291) and cattle (292). MPS IIID has been identified in the Nubian goat (293), and a missense mutation in *ARSG* gene had been shown to be responsible for the phenotype and pathology presented by American Staffordshire Terrier dogs (184). A spontaneously occurring MPS IIIA mouse was reported and studied in different genetic backgrounds (mix of 129SvJ, C57BL/6, SJL and CD1 strains; C57BL/6 and C57BL/6J) (294-297) while MPS IIIB and IIIE murine models were generated by knockout of genes *Naglu* (298) and *Arsg* (185), respectively. The information on the MPS III animal models is summarized in supplementary table 1.

#### 1.4.6.2.1 Clinical manifestations

The MPS III animals, in general, present the symptoms that recapitulate reasonably well those of human Sanfilippo patients. Like the patients, despite the occurrence of mild, somatic manifestations, the major burden of MPS III animals is progressive cognitive decline and reduced survival.

Progressive locomotor ataxia manifests in large animal models, including juvenile and young adult MPS III dogs, cattle, goats and emus (291, 292, 299). Behavior problems and reduction of cognitive abilities were also detected in these animals and include developmental delay, increased aggressiveness, lethargy, abnormal behavior/ loss of learned behavior and anorexia (291, 292, 299). Loss of menace reaction was exhibit by MPS IIIE canine model (184). Besides ataxia, intention tremor, head tremor and nystagmus was identified at a later phase of disease. Somatic manifestations were not reported, except for the altered hair morphology/coloration in the canine and bovine Sanfillipo B models (291, 292, 299).

MPS IIIA mice display aggressive behavior between the age of 10 and 14 weeks, motor abnormalities starting at 16-18 weeks (295), spatial learning deficits and memory retention difficulties at 20 weeks-old (295). The results of behavioral tests concerning activity pattern and anxiety in mice of different backgrounds and gender were not, however, consensual between studies, which might be due to the use of different test methodologies, housing conditions or genetic backgrounds of mouse strains. Nevertheless, these studies revealed hyperactive behavior of MPS IIIA mice comparatively to WT counterparts, followed by hypoactivity and reduced sense of danger (296, 300-302).

The disease progression in the murine MPS IIIB model is similar to that presented by MPS IIIA mice, though slightly more severe (298, 303, 304). A progressive deterioration of vision and hearing, and alteration of the circadian activity were also reported (304). As for MPS IIIA strain contradictory results also obtained regarding hyperactivity and anxiety/fear in the MPS IIIB mouse by different studies (298, 303, 305).

Besides neurologic signs, MPS IIIA and IIIB mice present other clinical features such as scruffy coat, and enlarged abdomen due to hepatosplenomegaly and distended bladder, at a later stage of disease (296). Death generally occurs due to urinary retention between 8-12 and 9-12 months in MPS IIIA and IIIB mice, respectively (294, 295, 300).

The MPS IIIE murine model has a milder phenotype than those of MPS IIIA and IIIB, presenting reduced exploratory behavior but the same activity level as WT mice, cognitive decline at the age of 12 months, and ataxic gait only at 24 months (185, 306).

#### 1.4.6.2.2 Pathophysiological mechanisms

##### 1.4.6.2.2.1 Cellular storage

Similar pathophysiological alterations are presented by different MPS III animal models. As in Sanfilippo patients, the macrophages and epithelial cells of the liver, kidney, spleen and heart of MPS III animals were the cells with the highest progressive increase in the number and size of storage vacuoles (185, 294, 298, 299, 307-309). Despite these alterations, only mild somatic manifestations occur in these animals, whereas pathology of the nervous system leads to severe neurocognitive impairment.

In the central nervous system, CNS (brain and spinal cord) and peripheral nervous system, PNS (including dorsal root ganglia and retina), storage vacuoles containing granular material, characteristic of HS accumulation, were mainly detected in neurons and microglia, as well as in perivascular macrophages and pericytes (185, 298, 299, 310, 311). The content of storage vacuoles is heterogeneous, especially in the neurons and, besides granular, membranous zebra-type inclusions and concentric swirl-containing vacuoles were observed in cell bodies, dendrites and axons (298). The storage of material was also associated with neuronal swelling and axonal

spheroids (306, 312, 313). Part of the stored material corresponds to gangliosides, mainly GM2 and GM3, unsterified cholesterol and other lipids, which are significantly increased in the brains of Sanfilippo as compared with WT animals. (313-315).

#### 1.4.6.2.2.2 Inflammation

The incomplete catabolism of HS triggers long-term immune responses in the nervous system as well as in peripheral tissues and organs of MPS III animals. Neuroinflammation corresponds to the response of immune cells to the presence of pathogens, traumatic injuries, dead or dying cells, debris, proteins aggregates and other toxic molecules in the CNS. The response to these stimuli by microglia, the resident macrophages in the CNS, and to a lesser extent, by astrocytes and oligodendrocytes, is designated as innate brain immunity (316). These and other innate immune cells have pattern recognition receptors (PRRs) that enables them to detect alterations in CNS homeostasis. Molecular structures, generally on the surface of pathogens, are recognized by glia PRRs as pathogen-associated molecular patterns (PAMPs), while molecules resulting from endogenous stress have "danger" or damage-associated molecular patterns (DAMPs) (317).

Quiescent microglia continuously survey the environment for signs of infection and cellular stress (318). Upon recognition of PAMPs or DAMPs signals, microglia acquire a pro-inflammatory classical activated phenotype, M1. This phenotype is characterized by alteration of the morphology from ramified to amoeboid and the ability to perform a set of functions leading to clearance of pathogens and resolution of other perturbations in the CNS (319). Among them are the secretion of pro-inflammatory cytokines such as tumor necrosis factor-α (TNF-α), interleukin-1β (IL-1β), interleukin-6 (IL-6) and interferon-γ (IFNγ), the production of chemotactic cytokines (chemokines), including macrophage inflammatory protein 1α (MIP-1α or CCL3) and monocyte chemoattractant protein 1 (MCP-1 or CCL2), for recruitment and activation of further microglia and peripheral leukocytes to the inflammation site (320, 321). In addition, an oxidative or respiratory burst with generation of ROS by the action of NADPH oxidase, leads to the lipid peroxidation-dependent release of glutamate (322), while the increased expression of inducible NO synthase (iNOS) induces production of nitric oxide (NO). Other upregulated proteins include divalent metal transporter-1 (DMT-1) and ferritin, responsible for downregulation of transferrin, and increased labile iron ($Fe^{2+}$) concentration (320, 323) as well as several receptors involved in

adaptive immune responses, including major histocompatibility complex II (MHC II) responsible for antigen presentation, the activation and infiltration of T-cells (324, 325). The M2 phenotype of microglia corresponds to an alternative activation state responsible for anti-inflammatory and neuroprotective functions such through secretion of anti-inflammatory cytokines such as IL-4, IL-13, IL-10 and TGF-β, extracellular matrix proteins and glucocorticoids, and expression of neurotrophic factors such as brain-derived neurotrophic factor (BDNF) and nerve growth factor (320, 326). Currently, it is accepted that there is a spectrum between the pro- and anti-inflammatory phenotypes and that molecules expressed by microglia in both M1 and M2 states might overlap. Also, the phagocytic activity of microglia occurs in both pro- and anti-inflammatory situations and is responsible for removal of protein aggregates and other debris, synapses, axons and dendrites, stressed or dying neurons (327).

Similarly to microglia, astrocytes are also involved in a cross-talk with other neural and non-neural cells, either in physiologic or pathologic conditions, via production and recognition of signaling molecules. The astrocytic endfeet wrap around CNS blood vessels assuring blood-brain barrier (BBB) maintenance, function and neurovascular regulation of blood and fluid flow. Astrocytes also associate closely with neuronal synapses, assuring neuronal ion homeostasis and mediation of synaptic transmission by reuptake of neurotransmitters as glutamate, gamma-aminobutyric acid (GABA) and glycine, and release of signals such as ATP and glutamine (328, 329). The astrocytes release anti-oxidant molecules such as glutathione and superoxide dismutase (SOD), lowering ROS and RNS content in the extracellular space as reaction to cellular stress (329). Besides, the astrocytes play also an important role in the CNS innate immunity. Stimuli by PAMP, DAMP signals induce astrocyte activation, driving morphological alterations, namely an increase and hypertrophy of astrocytic processes with upregulation of Glial fibrillary acid protein (GFAP) expression, and functional changes in a process named astrogliosis. Signals such as hypoxia, calcium and cAMP, as well as pro-inflammatory cytokines secreted by microglia are able to trigger astrogliosis (330). The activated astrocytes, on their turn, release antioxidants, upregulate the vascular endothelial growth factor (VEGP) for increased BBB permeability and leukocyte infiltration. Furthermore, they express pro-inflammatory cytokines and chemokines including TNF-α, IL-1β, IL-6, upregulate glutamate transporters leading to an increased uptake of glutamate, promoting also the activation of microglia (329-331). However, a reduction in the pro-

inflammatory phenotype of microglia may also result from secretion of cytokines such as IL-10 and TGF-β by neuroprotective, anti-inflammatory reactive astrocytes (330).

Neuroinflammation is a hallmark of MPS III pathology. Infiltrating macrophages and resident microglia in CNS and PNS of MPS III animals show progressive storage of material, already at an early age, eventually acquiring a foamy appearance at later stages of the disease (308, 332). In MPS IIIA dogs and MPS IIIB mice, microglia containing storage vacuoles were found in perineural positions, suggestive of phagocytic activity (308, 332). Furthermore, activated microglia and astrocytes as well as several proinflammatory cytokines and chemokines expressed by these cells were detected in the brains of MPS IIIB and IIIA mice at 10 days and two months, respectively, and later in life, indicative of chronic neuroinflammation (288, 313, 314).

Ausseil and colleagues (2008) hypothesized that the undegraded HS fragments were responsible for microglia activation in MPS IIIB mice. They showed that partially digested HS-oligosaccharides (HSOs), likely released into the extracellular space by lysosomal exocytosis, caused activation of microglia via TLR4/ adapter protein MyD88 (Myeloid differentiation primary response protein 88)/ NF-κB (Nuclear Factor kappa-light-chain-enhancer of activated B cells) signaling pathway. The activation of NF-kB transcription factor would drive the differentiation and activation of innate and adaptive immune cells, and expression of pro-inflammatory cytokines and chemokines (333). Interestingly, double knockout MPS IIIB mice deficient for the expression of TLR4 or MyD88 presented delayed onset of inflammation but a progression of neuropathology, namely SCMAS accumulation, oxidative stress and *GAP43* mRNA levels, similar to that of MPS IIIB mice (314, 334). The results of this study showed that the neurodegenerative process was independent of inflammation in younger MPS IIIB mice but TLR4/MyD88-independent inflammatory signaling could contribute to neuronal degeneration in older animals.

Foamy macrophages, containing vacuoles with large storage of material, as well as other leukocytes, and lymphocytes, were also found infiltrating several peripheral tissues and organs of MPS III animals (308, 335).

#### 1.4.6.2.2.3 Autophagy

An increase of LC3-II in MPS IIIA murine embryonic fibroblasts (MEFs), as well as a presence of p62-positive inclusions of polyubiquitinated proteins in brain sections of MPS IIIA mice was reported by Settembre and co-workers, reflecting the accumulation of autophagosomes due to the defective fusion of these vesicles with lysosomes (336). Further reports on augmentation in the number of mitochondria and subunit c of mitochondrial ATP synthase (SCMAS) in MPS III mice neurons (336), increased detection of mitochondrial cytochrome c oxidase subunit IV (Cox IV) and reduced $\Delta\psi m$ in mouse embryonic fibroblasts, reinforced the hypothesis of impairment of the autophagy pathway in MPS III cells, causing accumulation of dysfunctional mitochondria (336). A deficient autophagy causing inefficient clearance of toxic misfolded protein molecules may also explain the presence of intracellular phosphorylated tau (Ptau) aggregates in the medial entorhinal cortex (MEC) and dentate gyrus neurons, as well as prion protein deposition in the cerebral cortex, hippocampus and spinal cord dorsal horn neurons of MPS IIIB mice brains (337, 338). Besides, amyloidosis and synucleinopathy were also found in the brains of MPS IIID goats and IIIB mice, respectively (275, 337, 339).

Atrophy of cerebral cortex and cerebellum is reported in MPS III animals (307, 340, 341). Besides, except for MPS IIIA and B mice, all animals display progressive ataxia, consistent with the severe loss of Purkinje cells and neuronal degeneration in the spinal cord detected in these animals (288, 291, 293, 299, 307, 341). In MPS IIIA and IIIB mice, pathologic alterations in the cerebellum are less severe, leading to decline of neuromotor skills but not to ataxia or other cerebellar symptoms.

#### 1.4.6.2.2.4 Other pathophysiological signs

Besides the above mentioned alterations, oxidative stress and synaptic dysfunction have also been implicated in the pathophysiology of Sanfilippo disease. The mRNA expression levels of oxidative stress markers such as iNOS, NADPH oxidase components, SOD2 and glutathione peroxidase 1, were shown to be upregulated in MPS IIIA and IIIB mice brains (342, 343). In contrast, low levels of protein pre-synaptic marker synaptophysin as well as the post-synaptic protein Homer-1, were detected in the cerebral cortex of MPS IIIA (313) and IIIB (344) mice.

### 1.4.7 Therapies for MPS III

Currently, several drugs and medical procedures are used for symptom management in Sanfillipo patients, but no specific therapies are available. During the last years, however, numerous preclinical studies have been performed on the animal models of the different types of Sanfilippo disease, some leading to phase I/ II clinical trials for MPS IIIA and IIIB. The approved treatments for MPS diseases and those being developed for MPS III are summarized in the Table 2 and the Table 3, respectively. The different therapeutic strategies for MPS III aim to restore the activity of the defective enzyme, reduce primary and secondary storage, as well as inflammation, and promote autophagy and lysosomal catabolism.

**Table 2: Approved therapies for the Mucopolysaccharidoses**

| MPS | Type of therapy (administration route) | Drug name | Manufacturer | Reference |
|---|---|---|---|---|
| MPS I (Hurler, Hurler-Scheie or Scheie syndrome) | HSCT Hurler (IV) | n\a | n\a | (345) |
| | ERT Hurler-Scheie or Scheie (IV) | Laronidase® | Biomarin | (346) |
| MPS II (Hunter syndrome) | ERT (IV) | Idursulfase Elaprase® | Shire | (347) |
| MPS IVA (Morquio A syndrome) | ERT (IV) | Elosulfase Vimizim® | Biomarin | (348) |
| MPS VI (Maroteaux-Lamy syndrome) | ERT (IV) | Galsulfase Naglazyme® | Biomarin | (349) |
| | HSCT (IV) | n/a | n\a | (350) |
| MPS VII (Sly syndrome) | ERT (IV) | Vestronidase alfa Mepsevii® | Ultragenyx | (351) |

IV, intravenous; ERT, enzyme replacement therapy; HSCT, hematopoietic stem cell therapy; n/a, not applicable

#### 1.4.7.1 Enzyme replacement therapy

Enzyme replacement therapy (ERT) involves the administration of a recombinant WT human enzyme produced *in vitro* to compensate enzyme deficiency in the patients' tissues. The

effectiveness of ERT relies on receptor-mediated endocytosis of the WT enzyme by deficient cells where storage occurs (352). For most cells, ERT relies on the M6PR mediated uptake of the WT enzyme, whereas in cells of the macrophage lineage the enzyme uptake occurs via the mannose receptor (353).

ERT has been approved by the Food and Drug Administration (FDA) and European Medicines Agency (EMA) for Gaucher, Fabry and Pompe disorders, lysosomal acid lipase deficiency and several MPSs (I, II, IVA, VI and VII). (354). ERT is successfully used in these diseases to treat visceral manifestations, by periodic intravenous (IV) administration of recombinant WT enzyme. It has, nevertheless, limited effect on skeletal, joint and heart valve pathology (355). In the case of neuropathic disorders such as MPS III, it is necessary that the enzymes reach the brain. However, due to their high molecular weight, they are unable to cross the BBB by transmembrane diffusion (356).

The BBB, which function is to tightly regulate CNS homeostasis, is formed around a vascular capillary by a monolayer of endothelial cells connected by tight-junctions, surrounded by pericytes embedded in a basement membrane (BM) and covered by astrocyte end-feet. Interruptions in the astrocytic coverage allow the contact of the neurons and microglia with the BM (357). ). BBB has a selective permeability allowing transcytosis of certain macromolecules, including proteins and peptides, through the endothelial cells into the CNS, mediated by specific receptors. Adsorptive-mediated transcytosis may also occur for polycationic proteins (358).

In the last years, the recombinant enzymes, as well as the protocols of administration used in MPS III ERT, have been modified so that enzymes are able to pass or bypass the BBB, reaching a brain parenchyma to ameliorate storage and pathology.

The first ERT preclinical studies on Sanfillipo disease, performed by IV delivery of recombinant NAGLU and G6S to MPS IIIB mice and IIID goats, respectively, did not increase enzyme activity in the brain of treated animals (352, 359). A long-term therapy, by repeated IV infusions of recombinant human sulfamidase (rhSGSH) into MPS IIIA mice starting from birth, led to normal cognitive function at the age of five months but it did not alter the progressive neurologic impairment in the animals treated starting from the age of 6 weeks. These results can be explained by the M6P-mediated transcytosis of sulfamidase across the BBB during the first weeks of life in mice, but such pathway becomes eventually shut during the development (360).

**Table 3: Clinical trials for Mucopolysaccharidoses III**

| MPS III | Type of therapy (administration route) | Drug name | Developmental status | Sponsors/ colaborators | Clinical trial/ Reference |
|---|---|---|---|---|---|
| MPS IIIA | ERT (IV) | SOBI003 modified-rhSGSH | Phase I/II ongoing | Swedish Orphan Biovitrum (Sobi) | NCT03811028 [1] |
| | ERT (IT) | HGT-1410 rhHNS | Phase I/II complete | Shire | NCT01155778 [1] NCT01299727 [1] 2009-015984-15 [2] (361) |
| | | | Phase IIb complete | Shire | NCT02060526 [1] NCT02350816 [1] 2013-003450-24 [2] (362) |
| | GT (IP) | SAF-301 AAVrh.10-SGSH-IRES-SUMF1 | Phase I/II complete | LYSOGENE | NCT01474343 [1] (363) |
| | GT (IP) | LYS-SAF302 AAVrh.10-SUMF1 | Phase I/II complete | LYSOGENE | NCT03612869 [1] |
| | GT (IV) | ABO-102 scAAV9.U1a. hSGSH | Phase I/II ongoing | Abeona Therapeutics, Inc | NCT02716246 [1] |
| | Autologous CD34+ HSCT *ex vivo* GT (IV) | CD11b.SGSH LV | Phase I/II recruiting | Manchester University/ Orchard Therapeutics, CTI Clinical Trial and Cons. Services, others [4] | NCT04201405 [1] |
| MPS IIIB | ERT (IV) | SBC-103 rhNAGLU | Phase I/II complete | Alexion Pharmaceuticals | NCT02618512 [1] NCT02324049 [1] 2013-003400-39 [2] (357) |
| | ERT (ICV) | BMN 250 AX 250 rhNAGLU-IGF2 (tralesinidase alfa) | Phase I/II complete Phase II extension ongoing | Allievex Corporation | NCT02754076 [1] NCT03784287 [1] |
| | GT (IV) | ABO-101 rAAV9.CMV. hNAGLU | Phase I/II ongoing | Abeona Therapeutics, Inc | NCT03315182 [1] |
| | GT (IP) | rAAV2/5-hNAGLU | Phase I/II complete | Institut Pasteur | 2012-000856-33 [2] ISRCTN 19853672 [3], (364) |
| | | | Phase I/II extension complete | UniQure Biopharma B.V./ Institut Pasteur, Venn Life Sciences | NCT03300453 [1] (365) |
| | SRT (PO) | Genistein | Phase III complete | Manchester University NHS Foundation Trust | 2013-001479-18 [2] |
| MPS III A/B/C/D | SRT (PO) | Miglustat (N-butyl- -deoxynojirimycin) | Phase IIb to III complete | Hospices Civils de Lyon/ Actelion | (300) |

PO, oral; IV, intravenous; IT, intrathecal; ICV, intracerebroventricular; IP, intraparenchymal; ERT, enzyme replacement therapy; GT, gene therapy; HSCT, hematopoietic stem cell therapy; SRT, substrate reduction therapy; [1] ClinicalTrials.gov NC#; [2] EudraCT (European Union Drug Regulating Authorities Clinical Trials Database) #; [3] ISRCTN (International Standard Randomised Controlled Trial Number); [4] University College, London, Great Ormond Street Hospital for Children NHS Foundation Trust and Manchester University NHS Foundation Trust

In two different studies the glycan structure of the rhSGSH was chemically modified to reduce its M6P-mediated cellular uptake, in order to obtain higher concentrations of the enzyme in circulation, enabling it to cross the BBB and clear storage. This strategy had been previously used with a relative success for rhGUSB in the MPS VII mice but the mechanism by which the modified enzyme passes the BBB is still debated. Several hypotheses were proposed including transcytosis mediated by an unknown receptor, and leakage of BBB in MPS III mice, reported in 3 months-old MPS IIIB mice (310) and Sanfilippo patients (360).

Repeated administration of high IV doses of sulfamidase to MPS IIIA mice increased enzyme activity in non-CNS tissues and brain homogenates. However, modified-rhSGSH was found in brain endothelium, meninges and choroid plexus but not in neurons and glia of treated mice (366). However when treatment was performed over a longer period, the enzyme was also detected in the brain parenchyma, and improved neuropathology, behavior problems and learning, as compared with untreated MPS IIIA mice, were reported (367). Due to the encouraging results in preclinical studies a currently phase I/II clinical trial (ClinicalTrials.gov NCT03811028) is currently ongoing to evaluate safety, tolerability and efficacy of long-term IV administration of the chemically modified rh sulfamidase (SOBI003) in MPS IIIA patients between 18 and 78 months-old (Table 3).

A fusion protein of a sulfamidase with an IgG domain of a monoclonal antibody against the human insulin receptor (HIRMAb-SGSH) or the transferrin receptor (cTfRMAb-SGSH) is able to penetrate the BBB in rodents (368) As transferrin and insulin receptors are abundantly expressed on the surface of endothelial cells forming the BBB (369), this strategy relies on the receptor-mediated transcytosis of the therapeutic enzymes through these cells into the brain (370). The systemic administration of chimeric cTfRMAb-SGSH resulted in substantially reduced GAG level in brains and improved motor activity in treated MPS IIIA mice as compared with untreated animals (368).

The IV infusion of the recombinant human NAGLU (SBC-103), produced in hen oviduct cells, resulted in increased enzyme activity and dose-dependent reduction of the heparan sulfate disaccharide content in the brain of MPS IIIB mice (371). However, human phase I/II, dose-escalating, open-label clinical trial involving 11 MPS IIIB patients failed to provide clear evidence of SBC-103 passage through the BBB after intravenous delivery of the enzyme (NCT02618512

and NCT02324049; EudraCT #2013-003400-39; (357), and was, consequently, terminated (Table 3).

Multiple studies opted for direct administration of the therapeutic enzyme to the CNS either by intracerebral administration into the brain parenchyma (IP) or into the CSF by intracerebroventricular (ICV), intracisternal (ICT), or intrathecal lumbar (IT) routes.

Repeated administration or continuous infusion of recombinant enzymes in the CSF via pumps in MPS IIIA mice and dogs enables amelioration of clinical and brain pathology especially when treatments were started at an early age, before the onset of symptoms (311, 314, 369, 370, 371) (372, 373). These studies showed that, despite being the most invasive procedure, delivery via ICV route assured the widest distribution of enzyme in the brain and improvement of pathology in deep layers of the cerebral cortex (372, 374).

The administration of recombinant human HNS (rhHNS) by IT injection, the less invasive among the three routes, to cynomolgus monkeys assured delivery of the enzyme to CNS, especially to the cortical grey matter (375). A phase I/II dose-escalation, open-label clinical trial using a surgically implanted intrathecal drug delivery device (IDDD) for the administration of rhHNS (HGT-1410) to MPS IIIA patients, resulted in the reduction of heparan sulfate levels in CSF, but without a clear impact on cognitive function (NCT01155778; NCT01299727; EudraCT#2009-015984-15). Several adverse events in the patients related to the delivery device were reported but, in general, the administration of rhHNS was deemed safe and well tolerated (361). Most recently a 48-week phase IIb open-label trial using the same recombinant enzyme administered via IDDD at a dosage of 45 mg every two or four weeks and was performed (NCT02060526; NCT02350816; EudraCT#2013-003450-24). Despite the fact that HS level in the CSF was reduced in the treated patients, neurocognitive amelioration was not achieved and the trial was suspended (362) (Table 3).

*In vitro* studies have shown low intracellular uptake of the human recombinant NAGLU by several cell types, due to inadequate mannose-6-phosphorylation (M6P) of the enzyme (352). A recombinant NAGLU enzyme with improved lysosomal targeting was further generated based on the ability of the cation-independent M6PR (CI-MPR), one of the two M6Rs that deliver M6P-tagged proteins to the lysosome, to serve also as the receptor for insulin-like growth factor 2 (IGF2). When a chimeric enzyme, BMN 250 (tralesinidase alfa), generated by the fusion of

NAGLU with IGF2, was delivered by intracerebroventricular (ICV) route, allowed enzyme it was effectively endocytosed by neurons, microglia and astrocytes, reducing lysosomal storage in the CNS and neuroinflammation in the MPS IIIB mouse and dog models (376). Interestingly, a recent study showed that BMN 250, which binds with high affinity to CI-MPR/ IGF2 receptor, has different cellular uptake patterns among neural cells. In normal rodent neurons and astrocytes, the cellular uptake of BMN 250 is CI-MPR-mediated, whereas in the case of microglia, it is receptor independent (377). The encouraging results of the preclinical studies enabled researchers to proceed for the phase I/II open-label dose-escalation study (NCT02754076) to evaluate the tolerability, safety and efficacy of BMN 250, now designated AX 250, in MPS IIIB patients after ICV delivery. The safety and efficacy of long term ICV administration of AX 250 at the maximum tolerated tested dose estimated in the previous study, is currently being evaluated in an extension phase II clinical trial (NCT03784287) (Table 3).

To conclude, the administration of exogenous MPS III hydrolases delays significantly the progression of cognitive decline in MPS III animals but still does not provide an effective correction of the phenotype. Besides, it may also elicit an adverse immune response (312), resulting in lower efficacy of the ERT treatment and is associated with high costs. Furthermore, in the case of MPS IIIC, the uptake of WT enzyme by deficient cells is not possible, as HGSNAT, being a transmembrane lysosomal protein, is not secreted, being transported to the lysosome in a M6P-independent manner, as previously described.

#### 1.4.7.2 Cell therapy

This therapy is based on the fact that, as mentioned previously, a portion of lysosomal hydrolases escape normal sorting in the TGN, are secreted, and can be taken up by the same or other cells via M6PR-mediated endocytosis. The uptake of secreted functional hydrolases by enzyme-deficient cells is referred to as cross-correction (378).

In hematopoietic stem cell (HSC) transplantation, HSC from a compatible donor (allogenic) or genetically modified patient's HSC expressing normal enzyme (autologous), are used to cross-correct the recipient's deficient cells. It requires a myeloablative conditioning regimen to eradicate the hematopoietic stem cell population of the patient (379). The transplant and engraftment of HSC in the bone marrow of the patient, and its differentiation into cells of lymphoid and myeloid

lineages, leads to the presence of normal enzyme in the blood circulation, which can be then internalized via M6PR by cells of peripheral tissues and organs. This therapeutic approach is of particular interest for neuropathic disorders. The hematopoietic stem and progenitors cells (HSPC) transplant-derived monocytes are capable to pass the BBB and engraft the CNS, differentiating into microglia and other resident myeloid populations, and can serve as a long-term source of enzyme for cross-correction of remaining brain cells (380). Nevertheless, the efficacy of the transplantation of allogenic stem cells from bone marrow or umbilical cord blood (UCB) in MPS III patients and animal models has been disputed. Several studies showed that HSCT does not ameliorate neurological disease nor prevents its progression in MPS III murine models (381) and patients (382), suggesting that it should not be considered for treatment of Sanfilippo disorder as the risk of morbidity and mortality of the procedure itself outweighs its potential benefits. Other studies, however, demonstrated that UCB cells transplant might have an effect on halting the progression of the disease when performed at an early age (below two years old) in the Sanfilippo patients (383). Besides, the ICV and IV delivery (311, 384) as well as the repeated IV administration of UCB cells to MPS IIIB mice (385) lead to reduction of brain pathology and neurological symptoms. A therapeutic effect in the CNS of MPS III mice has been achieved by combination of HSCT with *ex vivo* gene therapy, likely due to the higher amounts of functional enzyme expressed by transplantation of gene-corrected stem cells as compared with conventional donor Hematopoietic Stem and Progenitor Cells (HSPCs) (297, 386-388) (see the chapter Gene therapy for further details).

HSCT is the standard treatment for Hurler syndrome (MPS IH), halting the progression of neurologic decline and somatic disease, improving life expectancy, if performed in children under the age of two and a half years with a normal or mildly impaired cognitive development (development quotient >70) (389). Patients affected by Hurler syndrome (MPS IH), the most severe form of MPS I, display severe somatic manifestations such skeletal abnormalities and characteristic coarse facial features, heart disease, respiratory problems, hepatosplenomegaly, motor development and speech delay, already in the first year of life (390). The early onset, the type and severity of clinical signs of MPS IH enable an earlier diagnosis comparatively to Sanfilippo patients, where unspecific signs of cognitive decline, including behavioral problems, between 1-4 years old are the earliest symptoms detected, generally represent an obstacle to an effective and early diagnosis, as previously mentioned.

As the impairment in cognition generally occurs between 12 and 24 months of age, children diagnosed with MPS IH may be treated before the onset, or at the beginning, of cognitive decline (390). In MPS III and other neuropathic disorders, the fact that the first clinical signs are neurologic and there is a long diagnostic delay prevents the treatment of patients at a pre-symptomatic or an early stage of the disease, where HSCT could be most effective. Besides, the use of ERT for MPS IH before HSCT has been shown to improve somatic clinical manifestations before the procedure, reducing transplant-related complications and mortality. Furthermore, the ERT-driven reduction of GAG content in the bone marrow might improve donor engraftment and HSCT efficiency (391). As aforementioned, there are currently no ERT therapies approved for Sanfilippo syndrome.

Human embryonic stem cells (ESC) are pluripotent cells derived from preimplantation embryos while inducible pluripotent stem cells (iPSC) are generated from reprogrammed adult cells. Both ESCs and iPSC are able to generate neural stem cells (NSC), which are multipotent cells that differentiate into neurons, astrocytes and oligodendrocytes. The iPSC-based technology has been used to generate different types of neural cells by reprogramming somatic cells from patients, most often, fibroblasts. So far, human iPSC lines were obtained from skin fibroblasts of two MPS IIIB patients (392, 393) and from two MPS IIIC patients that were further differentiated into mature neurons (394). The generation of patient-specific iPSC is not only very useful to study functional neuron-related phenotypes but can also be used to provide long-term secretion of WT enzymes into the CNS by transplantation and engraftment of corrected autologous NSC into the brain, avoiding the risk of immune rejection (395). Clarke and colleagues used a lentiviral vector for *ex vivo* correction of *Naglu*$^{-/-}$ NSC reprogrammed from iPSC, formerly differentiated from MPS IIIB mice MEFs. The engrafted NSC were able to cross-correct NAGLU-deficient cells, reducing GAG storage and neuroinflammation (395).

### 1.4.7.3 Gene therapy

Gene therapy (GT) is based on the delivery of the wild-type copy of a gene into the cells containing a defective gene sequence (396). The purpose of this therapy is to restore enzyme activity in cells receiving the therapeutic copy of the gene either directly, or by cross-correction in case of soluble proteins. Despite representing an attractive approach for the treatment of genetic disorders, such

as Sanfilippo syndrome, there are still concerns related to the efficacy and safety of this therapy in the patients.

The correct gene copy is most frequently delivered to the cells via viral vectors, but different types of non-viral vectors, such as liposomes, are also used in GT. The desirable viral vector system is that capable of accommodating large DNA/RNA inserts, resulting in high level, long-term expression of missing protein, targeting specific cell types without safety risks or immunogenic response, and producible at high titers (356). For MPS III, the transduction of deficient cells has been performed using retroviral (RV), lentiviral (LV), adenoviral (AV) and adeno-associated virus (AAV)-based vectors, the last being the most widely used in preclinical studies, and clinical trials, due to low safety risks and immunogenic potential. AAV vectors persist in transduced cells as dsDNA circular episomes, with a very low risk of integration in the host chromosome and, consequently, reduced risks of mutagenesis unlike AV, RV and LV that randomly integrate in the host genome. Besides long-term gene expression, there are other advantages of AAV vectors, such as their ability to infect pre- and post-mitotic cells and existence of variants showing tropism for different cell types. The tropism of different AAV serotypes is conferred by protein motifs on the viral capsid that bind to distinct cell surface glycan receptors (356). During the last two decades several AAV serotypes, including AAV2 (303, 397), AAV2/5 (364, 398, 399), AAV2/8 (400), AAV5 (303), AAV8 (305, 401), AAV9 (305, 401-407), AAV rh10 (363, 408) AAV rh74 (409) have been used in the different studies to evaluate their ability to transduce cells in somatic tissues and to cross the BBB and target cells of the CNS.

AAV, as well as LV, vectors have been used in MPS III *in vivo* gene therapy, by direct delivery of the wild-type gene intravenously, by injection into different areas of the brain parenchyma or into the CSF. The systemic delivery via single IV injection of AAV9 vector encoding hSGSH under an ubiquitous promoter allowed sustained long-term expression of the transgene in somatic tissues and the CNS of MPS IIIA mice, with clearance of GAG storage, reduction of inflammation, improvement of behavior, learning and lifespan (401, 407). The same results were obtained in MPS IIIB mice when using rAAV9 expressing hNAGLU (403). Other authors achieved correction of brain pathology and behavior in the murine model of MPS IIIIA using a vector expressing a highly secreted rSGSH engineered to cross the blood-brain barrier. In this study, the authors used an AAV2/8 vector encoding a chimeric SGSH, containing the signal peptide (sp) from the highly

secreted iduronate-2-sulfatase (IDS) and the BBB-binding domain from the Apolipoprotein B (400).

In order to increase the activity of hSGHS and the effectiveness of the therapy, Fraldi and co-workers (398) used AAV2/5 as vehicle to co-deliver *hSGHS* and *SUlfatase Modifying Factor 1* (*SUMF1*) genes to MPS IIIA mice. *SUMF1* encodes Formylglycine-generating enzyme (FGE), required for post-translational activation of all sulfatases. The vector carrying the two genes was administered by intracerebral injection in the lateral ventricules resulting in reduction of storage and inflammation in transduced brain regions and amelioration of cognitive and motor functions (398). These results were proof of concept for the clinical phase I/II trial (NCT01474343) with participation of four MPS IIIA children with an age between 2 years and 8 months and 6 years. The AAVrh10 vector containing both *hSGHS* and *SUMF1* (SAF-301) was administered by bilateral injection into 3 areas of the brain parenchyma. The phase II/ III study if this trial is still ongoing for evaluation of the long-term efficacy of therapy and additional patients have been recruited (SAF-302; NCT03612869), however the preliminary results after one year showed absence of adverse events or toxicity but only a mild improvement in cognitive function behavior, attention, and sleep (363).

In general, GT resulted in amelioration of behavior and lifespan of MPS III animals when performed at pre-symptomatic or early stages of the disease (398, 407, 408, 410-413) (Table 3). However, Fu and colleagues (407) showed that one time IV delivery of a self-complementary AAV9 carrying *SGSH* under control of U1a promoter (scAAV9.U1a.hSGSH) providing high levels of secreted hSGSH leads to normalization of behavior and pathology in MPS IIIA mice treated at an early age. Furthermore, it also drives partial correction of pathology, halting progression of cognitive impairment and increasing lifespan of animals when conducted at intermediate stages of disease. This is an important result as the majority of MPS III patients are diagnosed only after exhibiting neurologic symptoms. This therapeutic vector (ABO-102) is currently being administered via IV infusion in an open label, dose escalating, phase I/II clinical trial (NCT02716246) in MPS IIIA children and adults, being at an initial or intermediary/advanced stages of the disease, to assess safety and efficacy in humans (Table 4).

In the case of MPS IIIB, a single intravenous (IV) injection of rAAV9-CMV-hNAGLU resulted in normal or supraphysiological levels of NAGLU with correction of pathology in the CNS, PNS

and peripheral tissues of MPS IIIB mice, without adverse clinical events and toxicity, but eliciting immunogenic response to both rAAV9 and hNAGLU (403, 406). An open label, dose escalating, phase I/II clinical trial based on one-time IV delivery of rAAV9-CMV-hNAGLU (ABO-101) to MPS IIIB children and adults is currently ongoing (NCT03315182) (356).

Several preclinical studies on MPS IIIB animal models opted for intracerebral delivery of AAV or LV vectors encoding hNAGLU to overcome the passage across the BBB and achieve higher distribution of vector and enzyme in the CNS (303, 305, 381, 397, 399, 414, 415). All studies reported improvement of neuropathology, except for the thalamic administration of AAV8 and AAV9 vectors expressing hNAGLU where only a limited distribution of therapeutic vectors in the brain was detected (305). Studies in MPS IIIB mice and dogs using intraparenchymal delivery of rAAV2/5 encoding hNAGLU combined with immunosuppressive therapy (303, 416) were proof of concept for the clinical trial performed by Tardieu and colleagues in 2017 (364). Four children with an age from 20 to 53 months participated in this uncontrolled phase I/II, open-label clinical trial, where the therapeutic vector was delivered by simultaneous bilateral injection in 16 sites of the brain parenchyma in a single session. The detected NAGLU activity in the CSF in the patients was 10-20% of that in controls leading to an age-dependent improvement of neurocognitive progression in all patients during a period of 30 months after treatment. Despite several adverse reactions and an initial anti-NAGLU immune response with a later immunological tolerance, the treatment was considered well tolerated and, showed efficacy for children under 2 years (364).The extension study for evaluation of long-term safety and efficacy (EudraCT#2012-000856-33; ISRCTN 19853672; NCT03300453) has been recently completed (Table 4) supporting the previous results. In spite of the presence of NAGLU-specific T cells in the peripheral blood, the CNS expression of the therapeutic vector was stable over the 5.5 year period follow-up, not triggering neuroinflammation at least in the first year post-procedure (Gougeon 2021).

Another approach, suggested for treatment of MPS III, is so-called *ex vivo* GT, where cells of the patient are modified *in vitro* to correct the genetic defect and then, infused back into the recipient. As previously mentioned, allogenic and autologous transplant of HSCT transduced with LV vectors encoding human SGSH (297, 387) or NAGLU (386, 388) were able to correct neuropathology and behavior in MPS IIIA and IIIB mice, respectively. The results of a study by Langford-Smith and colleagues (288) showed that transplant of WT donor HSC, transduced *ex vivo* with an LV vector expressing hSGSH, into MPS IIIA mice myeloablated by busulfan

normalized brain HS levels and sulfation pattern, as well as the hyperactive behavior and sense of danger, whereas transplant of LV-hSGHS transduced MPS IIIA HSC or non-transduced WT HSC did not, perhaps due to insufficient level of the enzyme expressed in the brain (297). However, an allogenic transplantation of HSC has higher risks of immune-mediated graft rejection and failure as compared with an autologous one (417). Thus, in order to obtain a higher NAGLU expression in the CNS through an autologous transplant of LV-transduced MPS IIIA HSC, Sergienko and colleagues (387) used a vector encoding a codon-optimized SGSH (coSGSH) under the control of myeloid-specific CD11b promoter. In this case, the level of the SGSH enzyme expressed by transduced monocytes that transmigrated across the BBB and engraft the brain parenchyma was sufficient to normalize lysosomal size, primary and secondary brain storage, neuroinflammation, and correct hyperactivity in MPS IIIA mice. Using the same approach for MPS IIIB mice, Holley et al. (388) showed that autologous transplant of HSC treated with LV-coNAGLU, under the control of CD11b promoter, enabled brain monocytes/microglia to secrete NAGLU at a supraphysiological level and resulted in cross-correction of neighboring enzyme-deficient neurons, astrocytes, and likely microglia. Upon treatment, neuropathological alterations (lysosomal compartment size, HS and GM2 storage, micro- and astrogliosis), as well as behavior of MPS IIIB mice, were corrected. Interestingly, when the authors attempted to limit NAGLU presence to the engrafted donor macrophages, by using LV-coNAGLU-IGF2, encoding for the poorly-secreted chimeric protein of NALGU with IGF2 peptide, the improvement of neuropathological changes were similar to those after the treatment with the unmodified vector. This suggested that correction of brain macrophages/microglia was key for improvement of the brain pathology.

The results of these preclinical studies suggested that this LV-based approach could be successfully transposed to MPS IIIA and B patients. The efficiency and safety concerns related to this therapy were further evaluated in a recent study by Ellison and collaborators (418). The authors performed the autologous transplant of *ex vivo* genetically modified CD34+ haematopoietic stem and progenitor cells into MPS IIIA mice, using a clinical grade self-inactivating LV encoding a codon optimized SGSH, driven by CD11b (CD11b.SGSH LV). The results showed an effective engraftment of peripheral blood mononuclear cells derived from CD34+ cells in the hematopoietic organs of transplanted mice, resulting in a widespread distribution of transduced cells in non-hematopoietic organs, including the brain. In terms of safety, the therapeutic vector showed

reduced risk of insertional mutagenesis in the host genome and genotoxicity, low potential of transmission to germline cells and generation of splice-truncated vector during production was shown to be negligible. Due to the encouraging results of this study, a phase I/II clinical trial (NCT04201405) is currently recruiting MPS IIIA children between the age of three and 24 months for transplant of autologous CD34+ cells transduced *ex vivo* with CD11b.SGSH LV and follow-up for a minimum period of three years (Table 3).

A novel type of gene therapy based on the delivery of *SGSH* by a non-viral gene vector has been also essayed in MPS IIIA mice. The hydrodynamic tail vein delivery of pFAR4 plasmid vector encoding *SGSH*, driven by a ubiquitous or a liver-specific promoter, led to high and prolonged sulfamidase secretion by the liver with correction of pathology in visceral organs, and in the brain when the mice were treated at an early age (419).

Overall, the recent GT approaches for MPS III have shown promising results that suggest that efficient, and safe treatments might be soon used in Sanfilippo patients. In the cause of MPS IIIC, where cross-correction of brain cells is unlikely because the defective enzyme, *HGSNAT* is a transmembrane protein, GT using viral or non-viral vectors seems to be most promising approach to transduce and correct enzyme-deficient cells.

#### 1.4.7.4 Enzyme enhancement therapy

Enzyme enhancement therapy (EET) is an alternative type of treatment for MPS III and other lysosomal disorders. It aims to rescue mutant misfolded proteins from ERAD degradation pathway by increasing its transport to the lysosome and residual activity in the cell to a threshold where patients do not present clinical symptoms. For several LSDs this level corresponds to ~10-20% of the WT control, as described above. EET typically uses low molecular weight compounds, the chemical and phamacological chaperones (PC), which have a potential to be easily transported across membranes and pass the BBB, to stabilize the proper folding of mutant proteins, restoring their correct trafficking and function (420).

The amino sugar glucosamine, which is a competitive inhibitor of HGSNAT, was shown to increase the enzyme activity of mutant HGSNAT proteins resulting from missense variants or an in-frame deletion (243, 257). It has been proposed that glucosamine acts as a PC, by binding reversibly to the HGSNAT active site and facilitating the correct folding of misfolded mutant

proteins in the ER, and their traffic to lysosomes. In the lysosome, the natural substrate would displace glucosamine from the enzyme active site, partially restoring HGSNAT activity. For other MPS III subtypes, hypomorphic alleles, associated with slow progressing phenotypes are also good targets for pharmacological chaperone therapy.

#### 1.4.7.5 Substrate reduction therapy (SRT)

Substrate reduction therapy (SRT) uses small molecules to inhibit the anabolism of primary and/or secondary substrate(s) or to promote their clearance by alternative catabolic pathways, in order to balance the rates of substrate synthesis and degradation (421). The fact that these small molecules may be able to cross the BBB, makes this an alternative therapeutic approach for neuropathic lysosomal disorders, such as Sanfilippo syndrome.

The IV treatment of MPS IIIA animals with the non-specific inhibitor of GAG synthesis Rhodamine B has also led to reduction of GAG content in the brain, liver and in the urine enabling learning and memory improvement in MPS IIIA treated mice (422). High toxicity of Rhodamine B prevented its use in humans.

Genistein, an isoflavone present in soybeans, is a broad spectrum protein tyrosine kinase inhibitor, which halts the signaling of epidermal growth factor (EGF) and Insulin-like growth factor 1 (IGF1) receptors and, consequently, the expression of GAG-cleaving enzymes. It is also a TFEB transcription activator, capable of promoting GAG clearance (423).

Genistein has been used to reduce the GAG content in the cells of patients with Sanfilippo disease, with variable outcomes. Several MPS IIIA and IIIB preclinical studies, as well as studies in patients, supported a therapeutic effect of the drug on CNS pathology and function, especially when used in high doses (424-427). In contrast, other studies, including an open pilot clinical trials, showed that administration of high doses of genistein was safe (428) but the amelioration of clinical signs of the disease was not confirmed or was inconclusive (235, 426, 428). The results of a long-term phase III clinical trial of high dose oral genistein aglycone in two to 15 years old MPS III A, B or C patients (EudraCT 2013-001479-18), presently completed, have been recently reported (Table 3). Despite a significantly lower amount of uGAGs, the treatment did not result in statistically significant reduction of HS in the CSF. The data obtained does not support clinical efficacy of genistein in the treatment of MPS III (429).

The use of small interfering RNA (siRNA) was also successfully applied to reduce the expression of genes involved in GAG synthesis in cultured fibroblasts from MPS IIIA (430, 431) (and IIIC patients (432).

Finally, miglustat (N-butyl-deoxynojirimycin, NB-DNJ) targets the reduction of secondary storage of GM2 and GM3 gangliosides, which is hallmark in the brain pathology of MPS III. NB-DNJ is an imino sugar that blocks glucosylceramide synthase, inhibiting the synthesis of glucosylceramide and, consequently, glycosphingolipid biosynthesis (354). This is a currently approved SRT for reduction of glucosylceramide in Gaucher disease, and glycosphingolipids in Niemann-Pick disease type C (NPC) patients. Preclinical studies in NPC murine and feline models showed that NB-DNJ passes through the BBB, reducing ganglioside storage, delaying onset of neuropathological alterations and cognitive dysfunction. In NPC patients, treatment with NB-DNJ stabilizes or improves the neurological manifestations, particularly in those with later onset of the disease (433). MPS IIIA mice treated with misglutat showed reduced GM2 storage and neuroinflammation, and improved behavior comparatively to those untreated (434, 435). However, Sanfilippo patients participating in a randomized controlled (phase IIb) clinical trial did not show improvement or stabilization in behavior by NB-DNJ treatment comparatively to those treated with placebo (436).

#### 1.4.7.6 Therapeutic strategies targeting splicing and nonsense mutations

A strategy using modified U1 snRNAs to improve recognition of the mutated 5' splice site consensus motif has enabled partial rescue of c.234 + 1G > A normal splicing process in MPS IIIC fibroblasts without, however, an increase of HGSNAT residual activity (243).

Several compounds have also been tested as nonsense mutation read-through therapy in MPS III in order to restore functional protein expression. The aminoglycoside gentamicin is successfully used to increase enzyme activity in MPS I fibroblasts by reading through the PTC in the mRNAs coding for the mutant proteins p.Q70* and p.W402* (437). However, this compound had any effect on cultured fibroblasts of two Sanfilippo patients, one MPS IIIB, heterozygous for the NAGLU nonsense variants p.W168*/p.Q566*, and the other MPS IIIC, carrying the HGSNAT R384* and c.1542+4dupT alleles. Despite the increase in mRNA levels when treating the MPS IIIB cell line with the aminoglycoside geneticin, and the MPS IIIC fibroblasts with non-

aminoglycoside read through compounds PTC124 and RTC14, an augmentation in enzyme activities was not detected (438).

#### 1.4.7.7 Enhancement of lysosomal-autophagy pathway

Other therapeutic approach targets the expression of TFEB and the lysosomal-autophagy pathway. The activation of TFEB induces lysosomal biogenesis, formation of autophagosomes, autophagosome-lysosome fusion, as well as lysosomal exocytosis, reducing substrate storage in LSDs (13, 16, 46). Medina and colleagues (46) showed that overexpression of TFEB reduces GAG storage and vacuolization in MPS IIIA glia-differentiated neuronal stem cells (NSCs) by activation of MCOLN1, leading to increased intracellular $Ca^{2+}$ concentration and the fusion of lysosomes with the PM. More recently, the treatment with the TFEB activator trehalose promoted clearance of neuronal and glial autophagic vacuoles in the brains of MPS IIIB mice. The activation of the autophagic flux resulted in an amelioration of neuropathology and inflammation, behavior and lifespan in treated animals (439).

#### 1.4.7.8 Anti-inflammatory therapy

Neuroinflammation is a hallmark feature of pathology in MPS IIIA, IIIB, IIIE and IIID animal models but activation of resident macrophages as well as recruitment and infiltration of leukocytes, including lymphocytes, also occurs in the peripheral organs and tissues (292, 299, 308, 332, 335). It is detected as well in MPS III patients (364). The use of prednisolone, an anti-inflammatory steroidal agent that does not cross the BBB, improved the spatial memory, learning ability and motor function in MPS IIIB, slowing down the progression of neurologic disease (335). Also, the autologous transplant of LV-NAGLU transduced HSC combined with the use of prednisolone had a synergistic effect on the reduction of inflammation in somatic tissues of treated MPS IIIB mice, driving the correction of hyperactivity and reduced anxiety (388). These results suggest an involvement of the immune response in neurodegeneration and/or the existence of a compromised, permeable BBB.

The long term treatment of MPS IIIA mice with aspirin, a nonsteroidal anti-inflammatory drug (NSAID) reaching the CNS , normalized brain inflammation markers mRNA levels and corrected

oxidative stress in the brain and peripheral organs, without reducing those related to apoptosis (343).

The compound pentosan polysulfate (PPS), due to its inhibitory activity on MAP-kinase and NF-κB pathways (440), has been successfully used to ameliorate or reverse inflammation in *in vitro* and animal models of several LSDs, including MPS I (441) MPS VI (442, 443), Fabry and Gaucher Disease (444).

The clinical studies involving a small number of mucopolysaccharidosis type I (445) and II patients (446) have demonstrated that the weekly subcutaneous administration of 0.5-2 mg/kg PPS for, at least, 12 weeks were well tolerated. A reduction in serum inflammatory cytokines was reported in treated MPS II patients (446). PPS, which is a semi-synthetic heparin-like glycosaminoglycan, has also the capacity to reduce GAG content in the urine and tissues of MPS I (441) and MPS VI (443) animals though mechanisms underlying these effects have not yet been understood.

In MPS IIIA mice, the subcutaneous treatment with PPS, which does not cross the BBB, resulted in decreased level of GAGs in the spleen and brain, and age-dependent reduction of peripheral and CNS inflammation with improvement of hyperactivity, anxiety and learning ability (447).

#### 1.4.7.9 Antioxidant treatment

CoQ10, or ubiquinone, is an endogenously synthesized lipid that is an important component of the mitochondrial respiratory chain, shuttling electrons from complexes I and II to III (448). When reduced, CoQ10 has antioxidant properties by acting as a free radical scavenger, protecting lipids, proteins and mitochondrial DNA from oxidative damage (448). Matalonga and co-workers demonstrated that CoQ10 level in fibroblasts of MPS IIIA and IIIB patients was lower than those from healthy individuals. Upon treatment with CoQ10, several fibroblast cell lines presented increased NAGLU residual activity and exocytosis levels, as well as reduced GAG storage (449). The use of CoQ10 and, eventually, other antioxidant agents might be, then, beneficial in preventing or slowing the progression of MPS III.

In conclusion, the proper function of lysosomes is essential for cell homeostasis. In this thesis we will address the deficiency of the lysosomal enzyme HGSNAT and how it leads to the rare neurodegenerative disorder MPS IIIC.

## 1.5 Rational, hypotheses and aims of the thesis

MPS IIIC is a severe paedriatic disease, causing high morbidity and reduced life expectancy, as no effective treatment is yet available. Although multiple organ systems are involved, the CNS is the most severely affected, and progressive cognitive dysfunction is a hallmark of these disorders. Due to the relative rarity of MPS IIIC, few data were available on the pathology of the disease, particularly neuropathology. Besides, any animal model had been reported.

MPS III subtypes, caused by deficiency in different enzymes involved in HS catabolism, have a similar clinical presentation, but slight differences on disease severity and progression. At the time of our study, the characterization of MPS III animals, including the murine models of MPS IIIA and IIIB, had enabled a better, though still incomplete, knowledge on the biological mechanisms involved in the pathogenesis of these subtypes.

Besides, despite the identification of the MPS IIIC causative gene in 2006, the molecular characterization of clinical and biochemically diagnosed patients is still limited, not allowing the determination of the mutation spectrum for the disease, and in specific geographic locations/populations. In addition, high frequencies of certain pathogenic variants in specific geographic areas rose the hypothesis that they corresponded to founder effects, which can also have an impact on the efficiency and celerity of diagnosis of Sanfilippo C patients and carriers.

The first research hypothesis of this thesis was that inactivation of the *Hgsnat* gene in a mouse would trigger a similar phenotype to those of Sanfilippo C patients and murine models of remaining MPS III and that pathogenic alterations detected would underlie the disease.

To investigate this hypothesis we aimed the generation of an *Hgsnat* knockout mouse to understand the pathophysiology of the disease. The specific goals included:

- The verification if the mouse model recapitulated the clinical manifestations and the disease progression in humans by evaluation of behavior, learning and memory, motor performance and estimation of survival.
- Relatively to the pathology, to study if the expected *HGSNAT* deficit and HS lysosomal storage caused neuroinflammation, dysregulation of autophagy, accumulation of secondary materials, eventually other (unexpected) pathological alteration, and loss of neurons in the brain of the new murine model.

The second hypothesis of this dissertation was that novel *HGSNAT* variants identified in the new MPS IIIC patients could be deleterious and that their study would help to better understand the pathophysiology of the disease; also, that it would be possible to identify or confirm hypothesized founder effects and infer on the common origin for pathogenic variants shared by patients of different populations through a haplotype analysis.

To clarify this hypothesis, the objectives were the following:

- The identification and characterization, through Sanger sequencing, *in silico* and functional studies, the molecular defects in newly clinical and biochemically diagnosed MPS IIIC patients.
- To update the mutation spectrum identified in the new MPS IIIC patient and cases reported in the literature and characterize the distribution and frequency of disease-causing *HGSNAT* variants in different geographic areas or populations.
- The determination of the background haplotypes of the disease-causing variants carried by the novel Sanfilippo C patients and others previously reported; the construction of haplotype networks for the MPS IIIC alleles and those detected in several control populations of 1000 genomes database; the integration of previous results with frequency of variants in different populations in large genomic databases and historical data.

# Chapter II: Neuroinflammation, mitochondrial defects and neurodegeneration in mucopolysaccharidosis III type C mouse model

**(Manuscript published in *Brain*, February 2015)**

## 2.1 Context

This chapter describes the generation and study of the first MPS IIIC animal model, with the aim of understanding the pathophysiology of the disease, most especially that underlying neurodegeneration, largely uncharacterized.

We have shown, for the first time, that in the brain of *Hgsnat*-Knockout mice, lysosomal storage in neurons and microglia trigger downstream pathological reactions ultimately leading to neuronal mitochondrial dysfunction and death. Our findings were reported as a research article, published in the journal Brain (***Brain***. 2015 Feb; 138(2): 336–355. doi: 10.1093/brain/awu355. PMID: 25567323).

## 2.2 Author contributions

Carla Martins is the first co-author of this manuscript and performed most experiments: evaluation of mice survival; performed the water maze experiment and horizontal bar test; studied neuroinflammation (expression of cytokines by RT-qPCR, astrogliosis and microgliosis by immunohistochemistry, IHC); quantified neuronal density in mice brains; evaluated the GM2 and GM3 brain storage and mitochondrial network integrity by IHC; collected and processed most mouse tissues for further analyses; performed data analysis and participated in the writing and final revision of the manuscript.

Helena Hůlková is the second co-author of this manuscript and performed the electron microscopy experiments under supervision of Martin Hrebícek.

Larbi Dridi performed the rotarrod and inverted wire screen tests, the western blot for LC3 I/II quantification, participated in the evaluation of neuronal density, and in the collection and processing of tissues; performed X-ray analysis under supervision of Alain Moreau.

Virginie Dormoy-Raclet quantified mRNA *HGSNAT* expression and measured the activity of lysosomal enzymes in mice tissues.

Lubov Grigoryeva performed the open field test with Alexander Langford-Smith under supervision of Brian W. Bigger, which also provided MPS IIIA mice brain samples.

Yoo Choi performed IHC for HS.

Fiona L. Wilkinson and Graziella DiCristo provided technical advice on confocal microscopy and IHC.

Kazuhiro Ohmi performed IHC for protein neurodegeneration markers under supervision of Elizabeth Neufeld.

Edith Hamel supervised the water maze experiment.

Jerôme Ausseil performed MS/MS for HS quantification and provided MPS IIIB mice brain samples.

David Cheillan performed MS/MS for quantification of gangliosides.

Eva Svobodová, Zuzana Hájková and Markéta Tesařová measured the activity of mitochondrial enzymes and performed coenzyme Q10 quantification assays in mice brains under supervision of Hana Hansíková.

Alexey V. Pshezhetsky conceptualized, designed and supervised the study, wrote and revised the manuscript with participation of all authors.

# Neuroinflammation, mitochondrial defects and neurodegeneration in mucopolysaccharidosis III type C mouse model

Carla Martins,[1,*] Helena Hůlková,[2,*] Larbi Dridi,[1] Virginie Dormoy-Raclet,[1] Lubov Grigoryeva,[1] Yoo Choi,[1] Alexander Langford-Smith,[3] Fiona L. Wilkinson,[3] Kazuhiro Ohmi,[4] Graziella DiCristo,[1] Edith Hamel,[5] Jerôme Ausseil,[6] David Cheillan,[7] Alain Moreau,[1] Eva Svobodová,[2] Zuzana Hájková ,[8] Markéta Tesařová,[8] Hana Hansíková ,[8] Brian W. Bigger,[3] Martin Hrebícek[2] and Alexey V. Pshezhetsky[1]

[1] CHU Ste-Justine, University of Montreal, Montreal, QC, Canada

[2] Institute of Inherited Metabolic Disorders, First Faculty of Medicine and General University Hospital in Prague, Charles University, Prague, Czech Republic

[3] Stem Cell and Neurotherapies, University of Manchester, Manchester, UK

[4] Department of Biological Chemistry, David Geffen School of Medicine, University of California Los Angeles, Los Angeles, California, USA

[5] Montreal Neurological Institute, McGill University, Montréal, QC, Canada

[6] CHU Amiens, and Unité INSERM U1088, UFR de Médecine, Université de Picardie-Jules Verne, Amiens, France

[7] Service des Maladies Héréditaires du Métabolisme et Dépistage Néonatal - Centre de Biologie Est, Hospices Civils de Lyon, Bron, France

[8] Department of Paediatrics, First Faculty of Medicine and General University Hospital in Prague, Charles University, Prague, Czech Republic

Correspondence to: Alexey V. Pshezhetsky,
Service de génétique médicale,
CHU Sainte-Justine,
3175 Côte Ste-Catherine,
Montréal (QC) H3T 1C5,
Canada
E-mail: alexei.pchejetski@umontreal.ca

## 2.3 Abstract

Severe progressive neurological paediatric disease mucopolysaccharidosis III type C is caused by mutations in the *HGSNAT* gene leading to deficiency of acetyl-CoA: α-glucosaminide N-acetyltransferase involved in the lysosomal catabolism of heparan sulphate. To understand the pathophysiology of the disease we generated a mouse model of mucopolysaccharidosis III type C by germline inactivation of the *Hgsnat* gene. At 6–8 months mice showed hyperactivity, and reduced anxiety. Cognitive memory decline was detected at 10 months and at 12–13 months mice showed signs of unbalanced hesitant walk and urinary retention. Lysosomal accumulation of heparan sulphate was observed in hepatocytes, splenic sinus endothelium, cerebral microglia, liver Kupffer cells, fibroblasts and pericytes. Starting from 5 months, brain neurons showed enlarged, structurally abnormal mitochondria, impaired mitochondrial energy metabolism, and storage of densely packed autofluorescent material, gangliosides, lysozyme, phosphorylated tau, and amyloid-β. Taken together, our data demonstrate for the first time that deficiency of acetyl-CoA: α-glucosaminide N-acetyltransferase causes lysosomal accumulation of heparan sulphate in microglial cells followed by their activation and cytokine release. They also show mitochondrial dysfunction in the neurons and neuronal loss explaining why mucopolysaccharidosis III type C manifests primarily as a neurodegenerative disease.

## 2.4 Introduction

Mucopolysaccharidosis III or Sanfilippo syndrome is a metabolic genetic disease caused by lysosomal accumulation of heparan sulphate (Neufeld and Muenzer, 2001; Valstar *et al.*, 2008). The disease includes four allelic subtypes caused by the genetic deficiencies of heparan N-sulphatase (MPS III type A; MIM #252900), N-acetylglucosaminidase (MPS III type B; MIM #252920), heparan sulphate acetyl-CoA: glucosaminide N-acetyltransferase or HGSNAT (MPS III type C; MIM #252930), and N-acetylglucosamine 6-sulphatase (MPS III type D; MIM #252940). The majority of MPS IIIC patients have severe clinical manifestations with onset in early childhood. They rapidly develop progressive and severe neurological deterioration causing hyperactivity, sleep disorders, loss of speech, behavioural abnormalities, neuropsychiatric problems, mental retardation, hearing loss, visceral manifestations, such as mild hepatomegaly,

mild dysostosis multiplex, mild coarse facies, and hypertrichosis (Bartsocas *et al.*, 1979). Most patients die before adulthood but some survive to the fourth decade with progressive dementia and retinitis pigmentosa (Neufeld and Muenzer, 2001; Ruijter *et al.*, 2008; Valstar *et al.*, 2008). The birth prevalence of MPS IIIC in Portugal and The Netherlands is 0.12 and 0.21 per 100 000, respectively (Poorthuis *et al.*, 1999; Pinto *et al.*, 2004). HGSNAT transfers an acetyl group from cytoplasmic acetyl-CoA to terminal N-glucosamine residues of heparan sulphate within the lysosomes (Klein *et al.*, 1978). To date, more than 80 *HGSNAT* mutations have been identified including 18 missenses which all result in misfolding of the mutant enzyme (Feldhammer *et al.*, 2009). Important insights into the physiological mechanism of MPS III have been obtained from studying animal models of the disease. Spontaneous avian (Aronovich *et al.*, 2001) and canine (Aronovich *et al.*, 2000; Ellinwood *et al.*, 2003) models of MPS IIIA and B and a caprine model of MPS IIID (Ginsberg *et al.*, 1999) have been described, but the majority of data have been obtained by studying a knockout mouse model of MPS IIIB (Li *et al.*, 1999) and a spontaneous mouse model of MPS IIIA (Bhaumik *et al.*, 1999). Several mechanisms potentially underlying the neurodegenerative process in MPS III were described. First, in both mouse models microglia cells are activated through interaction of their Toll-like receptor 4 (TLR4) with underdegraded heparan sulphate fragments, as are astrocytes and the entire immune system in the brain (Ohmi *et al.*, 2003; Villani *et al.*, 2007; Ausseil *et al.*, 2008; DiRosario *et al.*, 2009). At the same time, inhibition of the TLR4 signalling pathway in MPS IIIB mouse while delaying brain inflammation did not stop progression of the neurodegenerative process (Ausseil *et al.*, 2008). Second, storage of GM2 and GM3 gangliosides occurring in brain cerebral cortical and cerebellar neurons (McGlynn *et al.*, 2004; Crawley *et al.*, 2006) was previously suggested to cause neuronal apoptosis in Tay-Sachs and Sandhoff diseases where GM2 ganglioside is accumulated due to genetic defects of hexosaminidases A and B, respectively (Huang *et al.*, 1997; Wada *et al.*, 2000). Interestingly, recently described double mutant MPS IIIA and IIIB mice with a knockout GalNAc transferase (Galnt3) crucial for the synthesis of gangliosides have significantly reduced lifespan and increased neurodegeneration as compared to the corresponding single mutant MPS IIIA and MPS IIIB mice, suggesting that absence of gangliosides may also be deleterious in MPS III (Mohammed *et al.*, 2012). Third, neurodegeneration could be caused by protein aggregates (Ginsberg *et al.*, 1999; Hamano *et al.*, 2008; Ohmi *et al.*, 2009) detected in neurons of medial entorhinal cortex and the dentate gyrus and linked to impaired autophagy and/or increased extralysosomal level of heparan

sulphate proteoglycans, glypicans (Ohmi *et al.*, 2011). Fourth, stored heparan sulphate fragments, which are in excess and abnormally sulphated in MPS IIIA and IIIB (Wilkinson *et al.*, 2012), can cause adverse signaling reactions in brain neurons inducing, in particular, overexpression of GM130 protein and subsequent alterations of the Golgi ribbon architecture (Roy *et al.*, 2012), enhanced proliferation and outgrowth of neuritis (Hocquemiller *et al.*, 2010) as well as alteration of neural cell migration (Bruyère *et al.*, 2014) all potentially contributing to neuropathology. However, it still remains to be determined which of the above mechanisms are important for the development of neuronal dysfunction and, therefore should be the target for the pharmaceutical intervention along with finding the ways to restore deficient HGSNAT activity in the patients' cells. It is also not understood whether the pathophysiological mechanism in all four subtypes of MPS III is the same despite different genetic and biochemical defects and severity of the clinical manifestation. In the current work, we report the generation of the first animal model of the MPS IIIC by inactivation of the Hgsnat gene in mice and present new pathological and mechanistic findings explaining the brain disease progression by the neuronal loss associated with mitochondrial dysfunction.

## 2.5 Materials and methods

### Animals

Generation of C57Bl6 mice with targeted disruption of *Hgsnat* gene was performed at the Texas Institute for Genomic Medicine as previously described (Zambrowicz *et al.*, 2003; Hansen *et al.*, 2008). The heterozygous mice were crossed to C57BL/6NCrl strain distributed by Charles River Quebec or bred to each other and the litter genotyped by PCR as described below. The *Hgsnat-Geo* mice were compared with the appropriate age and sex matching wild-type controls. All mice were bred and maintained at the Canadian Council on Animal Care (CCAC) accredited animal facilities of the CHU Ste-Justine Research Centre according to the CCAC guidelines. Mice were housed in an enriched environment with continuous access to food and water, under constant temperature and humidity, on a 12h light/dark cycle. Approval for the animal experimentation was granted by the Animal Care and Use Committee of the CHU Ste Justine. The genotypes of mice were determined using genomic DNA extracted from the clipped tail tip (see Supplementary

material for sequences of primers and PCR conditions). A 463 and 297 bp fragments were amplified separately in wild-type and *Hgsnat-Geo* homozygous mice, respectively, whereas both fragments were amplified in mice heterozygous for the *Hgsnat-Geo* allele. Quantification of mouse Hgsnat mRNA and cytokines in mouse brain tissues was performed using a Stratagene Mx3000PQPCR System (see Supplementary material for sequences of primers and PCR conditions). Total RNA was isolated from cultured cells or mouse tissues using the TRIzol reagent (Invitrogen) according to the manufacturer's protocol and reverse transcribed to cDNA using random primers and SuperScriptIII reverse transcriptase (Invitrogen). *RLP32* mRNA was used as a reference control.

**Neurological and behavioural examination of mice**

The motor performance of mice was evaluated using a simplified neurological examination as previously described (Lema *et al.*, 2004). The rotating rod motor coordination test was performed using an accelerating 5 line Rotarod treadmill for mice (3 cm in diameter). Animals (eight per age per genotype) were briefly trained at 4 rpm and tested using an accelerating mode (from 4 to 40 rpm over 5 min). Three trials separated by 20 min rest intervals were performed on three consecutive days. The open field test was performed by individually placing 2, 4, 6, 8 and 10 month old *Hgsnat-Geo*, or wild-type mice into the centre of an arena (40 cm length 40 cm width  50 cm height, white Plexiglas). Mouse behaviour was recorded for 1 h and analysed using Top Scan software version 2.0 (Clever Sys. Inc). The path length, rapid exploratory behaviour (speed 4 100 mm/s), immobility (speed 5 0.05 mm/s) as well as frequency, path length, duration and speed in the central (25%) area of the cage were analysed. The open field test was performed 1 h into the mouse light cycle (Langford-Smith *et al.*, 2011). A 30 min room adjustment period was implemented before the start of each test. All experiments were performed with a naïve group of 6–10 animals by the same investigator (L.G.).

The 5, 7, 8 and 10 month old mice (six per age per genotype) were subjected to the Morris Water Maze test for spatial learning, essentially as described by Seyrantepe *et al.* (2010). During a 3 day habituation period, mice were required to swim to a visible platform located in a selected quadrant of a circular (1.4 m in diameter and 34 cm high) tank filled with water (18 1C). The escape latencies were measured and visual and motor acuity as well as motivation were tested. On the fourth day, the water was made opaque with an inert paint, the platform was moved to a different quadrant

and submerged (1 cm), the visual wall cues were switched and 5 days of hidden platform testing ensued. Mice were given three trials of 90 s to find the platform (the maximum intertrial interval was 45 min). On Days 1 and 4, mice that could not find the platform in the allotted time were guided to and allowed to stay on it for 10 s. On Day 9, following hidden platform testing, all mice were given a 60 s probe trial in which the percentages of time spent and distance travelled in the target quadrant (no longer containing a platform), as well as the number of crossings over the previous location of the hidden platform were recorded, along with swimming speed. Escape latencies were acquired with the 2020 Plus tracking system and Water 2020 software (Ganz FC62D video camera; HVS Image). All experiments were started at the same time every day and performed by the same investigator (C.M.).

**Analysis of glycosaminoglycans and gangliosides in mouse tissues**

Total glycosaminoglycans and lipids were extracted from brain and liver tissues as previously described (Ausseil *et al.*, 2008). Briefly, frozen tissues were homogenized in water (10% v/w). Lipids were extracted by addition of two volumes of methanol and one volume of chloroform to one volume of the homogenate. After 10 min centrifugation at 1000g the organic phase was collected, evaporated and used to analyse gangliosides. The pellet was resuspended in 100 mM sodium acetate buffer pH 5.5, containing 5 mM cysteine, 5 mM EDTA and 1 mg/ml of papain, digested overnight at 65C and cleared by centrifugation at 2500g for 15 min. For the analysis of total glycosaminoglycans, 100 ml of the supernatant was added to 2.5 ml of dimethylmethylene blue reagent (Whitley *et al.*, 1989) and the absorbance at 535 nm was measured. Glycosaminoglycans concentration (µg per mg of dried pellet) was calculated using purified heparan sulphate standard.

Sphingolipids were extracted from the lipid fraction in the presence of deuterium labelled standards [N-stearoyl (D3)-monosialoganglioside GM2 and N-stearoyl (D3)-monosialoganglioside GM3, Matreya] by saponification (Kyrklund, 1987) and then fractionated and desalted using reverse phase Bond Elut C18 columns. Samples were analysed by direct flow injection at a rate of 200 ml/min on a triple quadrupole mass spectrometer (API 3200 MS/MS; Sciex Applied Biosystems) in the negative ionization mode using the multiple reactions monitoring (MRM) method. GM2 and GM3 species were measured separately. The concentrations of individual molecular species were calculated by comparing with the corresponding internal

standards. Total GM2 and GM3 concentrations (pmol per mg of dried pellet) were calculated as sums of the concentrations of all molecular species.

**Lysosomal enzyme assays**

N-acetyltransferase, β-galactosidase, α-galactosidase and β-hexosaminidase activities in cellular and tissue homogenates were assayed using the corresponding fluorogenic 4-methylum-belliferyl glycoside substrates as previously described (Seyrantepe *et al.*, 2008). Protein concentration was measured using a Bio-Rad Bradford kit.

**Analysis of LC3 in the mouse brain tissues by western blot**

Total brains were homogenized in five volumes of 250 mM sucrose buffer containing 50 mM Tris-HCl pH 7.4, 1 mM EDTA and protease inhibitor cocktail using a Dounce homogenizer. Nuclei were cleared by centrifugation at 500g for 10 min at 4°C. Supernatants were mixed with an equal volume of sucrose buffer containing 1% TritonTM X-100 and incubated for 1 h at 4°C. Resulting lysates were centrifuged for 15 min at 13 000g and supernatants separated by SDS-PAGE on 15% gels. Western blot analyses were performed according to standard protocols using anti-LC3 (Sigma, 1:2000) and 12G10 anti-tubulin antibody (DSHB, 1:15000). Equal protein loading was assured by Ponceau S staining. Signals were quantified using ImageQuant software.

**Tissue processing for morphological studies**

Animals were deeply anaesthetized with sodium pentobarbital and perfused via intracardiac catheter with phosphate buffered saline, pH 7.4 (PBS) followed by 4% paraformaldehyde in PBS. Brains and visceral organs were removed and immersed in 4% paraformaldehyde in PBS overnight. Tissues for light microscopy were trimmed, dehydrated with an ethanol series followed by acetone, acetone-xylene mixture and xylene and then embedded in paraffin. Tissues for fluorescent confocal microscopy were treated sequentially in 10%, 20% and 30% sucrose in PBS overnight at 4°C and embedded in O.C.T. compound before freezing at 80C. Tissues for electron microscopy were trimmed into small cubes, post fixed with 1% osmium tetraoxide, dehydrated with an ethanol series and propylene oxide and embedded in Durcupan-Eponmixture.

**Histopathology and immunohistochemistry**

Paraffin embedded tissues (4-mm thick sections) were rehydrated with isopropyl alcohol, and then with 96%, 70%, and 60% ethanol. The sections were stained with either haematoxylin and eosin, or periodic acid-Shiff technique (PAS), and a set of primary antibodies. In the latter case the sections were treated with 1% NaN3 and 0.3% H2O2 for 10 min to inactivate endogenous peroxidase, blocked with 5% bovine foetal serum in PBS for 30 min (both at room temperature), and incubated with primary antibodies diluted in 5% bovine serum albumin in PBS overnight at 4°C. After staining with primary and secondary antibodies (see Supplementary material for the list of antibodies and their dilutions) sections were analysed and photographed using a Nikon E800 equipped with Olympus digital camera (DP70). Autofluorescence of neurons was analysed in unstained sections using fluorescence filter BV-2 A (Ex 400-440 nm/DM 455/BA 470).

For fluorescent confocal microscopy 40 mm thick sagittal sections were cut from O.C.T. embedded frozen brains using a CM3050 S Microtome (Leica). The sections were treated with 1% TritonTM X-100, blocked with 10% goat serum in PBS and incubated overnight at 4°C with primary antibodies in 3% goat serum, 0.1% TritonTM X-100 in PBS followed by secondary antibodies. The slides were mounted with Vectashield mounting medium and analyzed using a LSM510 Meta Laser inverted confocal microscope (Zeiss, 63 oil objective, N.A. 1.4). Images were processed and quantified using the LSM image browser software (Zeiss) and Photoshop (Adobe).

**Electron microscopy**

Semi thin sections were cut and stained with Toluidine blue and viewed by light microscopy. The regions of interest for electron microscopy were selected and ultrathin sections were cut and mounted on 200 mesh copper grids. Sections were double contrasted with uranyl acetate and lead nitrate and then analyzed using a transmission electron microscope (JEOL 1200 EX).

**Analyses of mitochondrial energy metabolism in mouse brain**

Frozen brain tissues were homogenized at 4°C in 20 volumes of 50 mM Tris-HCl buffer pH 7.4, containing 150 mM KCl, 2 mM EDTA and 0.2 mg/ml aprotinin. Mitochondria were isolated from the homogenate by differential centrifugation as described (Makinen and Lee, 1968). The activities of the mitochondrial enzymes, NADH: ubiquinone oxidoreductase (NQR, complex I),

succinate:CoQ reductase (SQR, complex II), ubiquinol:cytochrome c oxidoreductase (QCCR, complex III), cytochrome c oxidase (COX, complex IV), NADH:cytochrome c reductase (NCCR, complex I + III), succinate:cytochrome c reductase (SCCR, complex II + III) and citrate synthase (CS) were measured as described (Srere, 1969; Rustin *et al.*, 1994). Pyruvate dehydrogenase activity was determined as described (Dudkova *et al.*, 1995). Protein concentration was measured according to Lowry *et al.* (1951).

Total content of coenzyme Q10 in brain homogenate was determined as described (Mosca *et al.*, 2002) with minor modifications. Brain homogenate (100 ml) was diluted with 100 ml Milli-Q H2O. The mixture was supplemented with 50 µl of 1,4-benzoquinone solution (2 mg/ml) and vortexed for 10 s. After 10 min, 1 ml of n-propanol was added. The mixture was vortexed for 10 s and centrifuged at 10 000 rpm for 2 min. The supernatant (50 ml) was analysed by HPLC using the Supelcosil LC 18 column (Supelco) eluted by ethanol/methanol (70/30 v/v) mixture at a flow rate of 1 ml/min. UV detection was performed at 275 nm. Results were expressed as pmol of Q10 per mg of total protein.

**Quantitative analysis of neuronal density in the mouse brain cortex**

Four mice (two male, two female) were studied for each age and genotype. For each brain, three sagittal sections, cut at 1.44, 1.68 and 1.92 mm lateral from bregma, (Paxinos and Franklin, 2013) were simultaneously stained with anti-NeuN antibodies as described above. For each section, two images of the S1 somatosensory cortex (S1Tr and S1HL for 1.44 and S1Tr and S1FL for 1.68 and 1.92 sections, respectively) were acquired using Nikon Eclipse E600 Epifluorescence Microscope (magnification 200), Zeiss Axiocam 506 digital camera with the same settings for all sections. The acquired images were analysed using Adobe Photoshop CS5 (Adobe Systems Inc). In each image, two rectangular fields with the area of 1.92 mm2 were defined, on the right and left extremities of the photographed areas. The numbers of NeuN stained neuronal nuclei for each field (12 fields for each mouse) were counted by two non biased observers blinded for the genotype, age and sex of the animals.

## 2.6 Results

### Mice homozygous for *Hgsnat-Geo* allele show deficient Hgsnat mRNA and activity in tissues

A functional knockout of the *Hgsnat* locus in C57Bl/6N mice was generated using gene trap technology as previously described (Zambrowicz *et al.*, 2003; Hansen *et al.*, 2008). A selectable marker β-geo, a functional fusion between the β-galactosidase-encoding gene and the neo gene from Tn5 encoding an aminoglycoside 3'phosphotransferase, was inserted into the intron 7 of the Hgsnat gene leading to splicing of exon 7 into the β-geo cassette to generate a fusion protein containing Hgsnat amino acid sequence encoded by the exons 1-7 followed by aminoglycoside 3'-phosphotransferase and β -galactosidase (Fig. 1A). The Btk exon in the trap construct contained termination codons in all reading frames to prevent translation of the downstream *Hgsnat* exons (Fig. 1A).

Mice homozygous for *Hgsnat-Geo* allele (*Hgsnat-Geo* mice) were viable and born in the frequency expected from Mendelian inheritance (26 of the first 100) indicating that disruption of the Hgsnat gene did not cause embryonic lethality. Mice showed normal growth, were fertile and indistinguishable from wild-type or heterozygous animals until the age of 11 months.

Both expression of Hgsnat mRNA measured by real time quantitative PCR (Fig. 1B) and the level of HGSNAT activity measured with fluorogenic substrate Muf-β-D-glucosaminide (Fig. 1C) in tissues and primary cultures of skin fibroblasts from the homozygous animals were reduced to 0.6–1.5% of that in wild-type mice (below or close to detection limit of the method) confirming efficiency of the splicing outcome and validating the model biochemically. In the heterozygous mouse tissues HGSNAT activity was reduced to 50% of wild-type (Fig. 1C). In contrast, b-galactosidase activity measured in liver, kidney, brain, muscle and lung tissues of the *Hgsnat-Geo* mice at pH 7.5 was significantly increased as compared to wild-type mice (not shown) indicating that the *Hgsnat-Geo* fusion protein is produced but does not have N-acetyltransferase activity, which was expected because it is missing 60% of the Hgsnat sequence including its predicted active site residue, His269 and 9 of 11 transmembrane domains presumably forming the AcCoA-transporting channel (Durand *et al.*, 2010).

Activities of other lysosomal glycosidases measured in the tissues of homozygous *Hgsnat-Geo* mice were either similar or higher than those in wild-type mice and progressively increased with age of the animals suggesting augmented production of lysosomes previously described for the mouse models of other subtypes of MPS III and linked to lysosomal storage phenotype (Bhaumik *et al.*, 1999; Li *et al.*, 1999). In the *Hgsnat-Geo* mice the highest increase was observed in liver tissues where α-galactosidase activity was induced 5-fold and β-hexosaminidase activity 20-fold by the age of 6 months (Fig. 1D). β-Hexosaminidase activity was also increased 2–3-fold in the brain, lungs and kidney suggesting that lysosomal storage occurs also in these tissues.

## *Hgsnat-Geo* mice show reduced longevity, progressive behavioural changes and learning impairment

No visible signs of illness were observed in the homozygous *Hgsnat-Geo* mice until the age of 11–12 months, when they showed weight loss and abnormal gait. About 30% of animals at this age showed spasticity of hind limbs and loss of coordination in a balance test (Supplementary Video 1). At 65 weeks of age mice presented signs of urinary retention resulting in abdominal distension absent in human patients but present in mouse models of both MPS IIIA and MPS IIIB (Bhaumik *et al.*, 1999; Li *et al.*, 1999) and had to be euthanized (Fig. 2A). At all ages, heterozygous mice were clinically undistinguishable from their wild-type siblings. No signs of skeletal abnormalities such as scoliosis reported previously in human patients or shortened skull with a 'blunt' snout described in several MPS mouse models including those of MPS IIIA (Bhaumik *et al.*, 1999) were detected in the homozygous *Hgsnat-Geo* mice by X-ray analysis (Supplementary Fig. 1). Similarly, we did not detect any signs of femoral head necrosis also reported for human MPS III patients (de Ruijter *et al.*, 2013).

Neurological assessment (gait, posture, avoidance response, righting reflex, horizontal bar test, inverted wire screen test, all conducted on the group of 10 *Hgsnat-Geo* and 10 wild-type mice by the same examiner blinded for the mouse genotype) was performed at 2 months, when MPS IIIA and B mice still show normal behaviour and then repeated every 2 months with a naïve group of animals. Also every 2 months starting from the age of 4 months we studied motor activity using a motor coordination test performed on an accelerating Rotarod treadmill for mice. Neither

neurological assessment nor the accelerating Rotarod test (Supplementary Fig. 2) revealed any signs of neuromuscular pathology in HGSNAT deficient mice up to the age of 10 months.

In contrast, open field test performed 1 h into their light cycle showed definite signs of increased activity and reduced anxiety including higher than average speed and distance travelled, increased frequency of crossing the central field and central distance travelled, as well as decreased frequency and duration of periods of immobility (Fig. 2B and Supplementary Video 2). The same trend was observed for both male and female mice but for female mice the differences with the control group became significant already at the age of 6-months whereas, for male mice, for most studied parameters the significant difference was observed only at 8-months. By the age of 10 months the signs of hyperactive behaviour diminished resembling the trend observed in human MPS III patients (Fig. 2B).

Hippocampal function was assessed at 5, 7, 8 and 10 months using the Morris Water Maze test to measure memory and spatial learning capability. To make sure that HGSNAT deficient mice had no visual or motor deficits that could affect the outcome of the test, we accessed their ability to reach a visible platform in a 3-day pre-training test. We found that there were no differences between the mutant and wild type groups as HGSNAT-deficient and wild type mice of all age groups showed similar escape latencies in the visible platform testing (Fig. 2C). Learning progress of mutant mice at the ages of 5, 7 and 8 months was similar to that of their wild-type counterparts, as shown in Fig. 2C for the 8-month-old group. In contrast, at the age of 10 months, HGSNAT deficient mice needed significantly more time to find the hidden platform com-pared to their wild-type counterparts, and to both wild-type and mutant 8 month-old mice, suggesting impaired spatial learning. Additionally, in the probe trial on Day 9 when the platform was removed, HGSNAT deficient mice spent significantly less time and travelled less distance than wild-type mice in the target quadrant where the platform used to be located, which indicated a decline of spatial memory (Fig. 2C). Moreover, 10 month-old mutant mice displayed lack of precision with fewer platform crossings compared to wild-type counterparts, and to younger wild-type and HGSNAT deficient mice (Fig. 2C).

## Pathological changes in tissues

Pathological examination of homozygous *Hgsnat-Geo* mice performed at the ages of 2, 4, 6, 10 and 11–12 months did not reveal any gross changes in the visceral organs and brains, except for the strikingly reduced abdominal fat detected at 11–12 months. The same animals usually also had a largely distended bladder filled with 1–2 ml of urine, consistent with urinary retention (Supplementary Fig. 3). Microscopic examination however revealed multiple pathological changes in numerous tissues and organs already detectable at 2 months and progressively increasing with age.

Hepatocytes in the centrolobular and intermediate zones showed microvacuolization of cytoplasm, which became more prominent with age (Supplementary Fig. 4A). Immunostaining with antibody against cathepsin D (CTSD) detected expanded lysosomal system in hepatocytes compatible with lysosomal storage starting from 2 months (Supplementary Fig. 4B). Kupffer cells are increased in number starting from 2 months and become enlarged and strongly stained for CTSD at later stages, showing signs of transformation into foam cells (Supplementary Fig. 4A–C). Besides Kupffer cells, liver sinusoids contained a sparse mixed inflammatory infiltrate. High-resolution analysis of liver tissues by electron microscopy revealed massive accumulation of vacuoles, either electron-lucent or containing a fine sparse material characteristic of glycosaminoglycan storage in the cytoplasm of hepatocytes and less prominent storage of this type in Kupffer and Ito cells (Supplementary Fig. 4E–H).

In the spleen, storage dominated in splenic sinus endothelial cells giving them an appearance resembling that of foam cells (Supplementary Fig. 5). Population of macrophages in red pulp represented a mixture of small dendritic macrophages and slightly enlarged round cells containing autofluorescent lipopigment and corresponding to phagocytic phenotype. Macrophages in white pulp revealed mostly an inconspicuous stellate appearance. In general, there was no convincing presence in spleen tissue of macrophages with storage material even at the most advanced stages of disease (surviving 16-month-old mice). CTSD immunostaining was compatible with lysosomal storage in splenic sinus endothelial cells and was increased starting from 2 months (Supplementary Fig. 5A). Electron-lucent storage vacuoles in splenic sinus endothelial cells were also detected by electron microscopy (Supplementary Fig. 5I).

Quantification of NeuN-stained neurons in the two selected areas of somatosensory cortex showed that neuronal loss in homozygous *Hgsnat-Geo* mice actually occurs starting from the age of 6 months and continues throughout life resulting, by the age of 12 months, in the 430% reduction of neuronal density in these areas (Fig. 3A). In the cerebellar cortex, Purkinje cell loss was massive in the anterior lobe with lobules I, II and III most severely affected and lobules IX and X less affected at 12 months of age (Supplementary Fig. 6). The number of GFAP-positive astrocytes and CD68-positive microglia cells became augmented starting from 4 months in all studied brain areas of the *Hgsnat-Geo* mice as compared with wild-type mice and was further increased with age (shown for somatosensory cortex in Fig. 3B).

The most striking phenomenon observed in all parts of the brain was a coarse vacuolization of the cytoplasm of multiple CD68-positive cells giving them foam cell-like appearance (Fig. 3C). These cells dispersed in grey and less so in white matter, were frequently found adjacent to neurons suggesting that they represent perineuronal microglia. Individual macrophage-like CD68-positive cells with cytoplasmic vacuoles were also detected in perivascular areas. Microglia cells containing storage materials were most prominent in caudatoputamen and in brain cortex. They were first detected in 2-month-old mice, thus preceding pathological changes in neurons and become more frequent at later stages. Contrary to microglial cells, neurons were mostly featured by finely granular appearance of their perikarya without marked distension. The granular material accumulated in these neurons with a variable intensity was strongly PAS-positive (Fig. 3D) and displayed intense autofluorescence (Fig. 3E). Immunostaining with antibodies against CTSD (Fig. 3F) revealed increased number and size of lysosomes in neurons of mutant mice. Neurons strongly stained with CTSD were found in brain cortex, thalamus, hypothalamus, amygdala, midbrain, pons and cerebellum (Supplementary Fig. 7). Accumulation of PAS-positive and autofluorescent materials was most prominent in neurons present in deep cortical layers, in hippocampus and in cerebellum. Neurons in caudatoputamen showed little involvement. Incipient neuronal storage was detectable in 5-month-old mice and widespread yet irregular neuronal storage was present in 12-month-old animals. No signs of lysosomal storage were detected in vascular endothelial cells (data not shown).

Electron microscopy performed in brain cortex confirmed that neurons and microglial cells had two distinct types of storage (Fig. 4). Cortical microglia displayed prominent accumulation of electron-lucent storage vacuoles or those with a sparse fine content. In contrast, neuronal pathology

was dominated by progressive lysosomal storage of electron-dense heterogeneous ceroid-like material and early detectable mitochondrial structural abnormalities. Mitochondria were pleomorphic and increased in number with many of them swollen with disorganized or reduced inner membranes. Storage in microglia was not accompanied by any structural mitochondrial changes. Storage compartments in neurons contained heterogeneous, granular and/or lamellar material, occasionally with lipid droplets. At the same time, electron microscopy of neurons did not reveal lysosomes containing classical zebra-bodies, but some storage deposits contained structures resembling degenerated mitochondria. At the most advanced stages of the disease (14–16 months), ultrastructural pattern in neuronal lysosomes was dominated by massive accumulation of closely packed fibrillary deposits often resembling storage material of a rectilinear and/or fingerprint type in neuronal ceroid lipofuscinoses (Fig. 4).

Other studied mouse organs and tissues stayed generally unaffected even at 12 months of age except for urinary bladders, which were markedly distended with thin walls. A sparse presence of cells strongly stained for CTSD and presumably having lysosomal storage was detected in lamina, muscularis propria and adventitia. Normally arranged cardiomyocytes without regressive changes were observed in the heart. There was no fibrosis in the interstitium and interstitial elements did not show signs of lysosomal storage at the optical level. Similarly, lysosomal storage was not detectable in alveolar septa in lungs. Population of septal and alveolar macrophages was rich, with focally increased phagocytic activity and undistinguishable from that seen in wild-type. Respiratory bronchial epithelium displayed increased staining for CTSD suggestive of lysosomal storage. In kidney, increased immunostaining for CTSD was detected in glomeruli and in epithelial cells of distal tubules and collecting ducts (Supplementary Fig. 5E). Storage of electron-lucent vacuoles in fibroblasts, vascular pericytes and rarely in vascular endothelial cells was detectable at the ultrastructural level (Supplementary Fig. 5J–L).

## Lysosomal glycosaminoglycans and ganglioside storage in *Hgsnat-Geo* mice

To investigate if HGSNAT deficiency in mouse tissues resulted in impairment of heparan sulphate catabolism, total glycosaminoglycan in mouse brain and liver tissues were measure at the age of 2,4,6,8,10 and 12 months (Fig. 5A). In both tissues, glycosaminoglycan levels were slightly increasing with age while remaining significantly higher than in the wild-type mice (on average 2-

fold increase in brain and almost 10-fold increase in liver at 12 months). At the same time, total glycosaminoglycan in brain tissues of *Hgsnat-Geo* mice at all ages was significantly lower than in MPS IIIB mice.

Glycosaminoglycan accumulation at the cellular level was studied by immunohistochemistry using monoclonal 10E4 antibody specific against a native heparan sulphate epitope (David *et al.*, 1992), which detected increased staining of cytoplasmic LAMP1-positive organelles in multiple cells throughout the somatosensory cortex and all regions of the hippocampus. The lysosomal heparan sulphate storage was detected in multiple NeuN-positive neurons, but even more intense 10E4 staining was detected in the cells negative for NeuN, but positive for the markers of activated microglia cells: Alexa Fluor 568-labelled isolectin B4 (ILB4), and CD68 (Fig. 5B).

Tandem mass spectrometry demonstrated 2-fold increased levels of GM2 and GM3 gangliosides in the brain tissues of 4-month-old *Hgsnat-Geo* mice as compared to their wild-type siblings (Fig. 5C), consistent with previously reported storage of these lipids in the mouse models of MPS IIIA and B (Bhaumik *et al.*, 1999; Li *et al.*, 1999).

Accumulation of gangliosides in brain tissues was further studied by immunohistochemistry using the human-mouse chimeric monoclonal antibody, KM966 (Nakamura *et al.*, 1994) specific to GM2 ganglioside (Huang *et al.*, 1997) and mouse monoclonal antibody specific to GM3 ganglioside. Both gangliosides, almost undetectable in the brain of wild-type mice (Supplementary Fig. 8), were highly present in the brains of *Hgsnat-Geo* mice (Fig. 5D). The ganglioside storage was observed in most areas of the brain, including the cerebellum, but was more prominent in deep layers of cortex and hippocampus (Fig. 5D and Supplementary Fig. 8).

All ganglioside-accumulating cells were recognized by the anti-NeuN antibody and were not stained with ILB4 indicating that they are neurons but not microglial cells (Fig. 5D). In contrast to glycosaminoglycans accumulation, both the number of ganglioside-positive granules in the hippocampal and cerebellar neurons and their size were dramatically increasing between the ages of 8 and 12 months (Supplementary Fig. 8). Intriguingly, when the tissue sections were co-stained for both GM3 and GM2 gangliosides, we detected only modest level of co-localization indicating that the corresponding storage granules tend to segregate from each other (Fig. 5D). A similar pattern was previously observed in MPS IIIA and B mouse models (McGlynn *et al.*, 2004). Also, we observed only partial co-localization between the stored gangliosides and lysosomal marker

LAMP1 (Fig. 5D), which could indicate that the gangliosides are accumulated in the compartments having both lysosomal and non-lysosomal origin.

When we, however, co-stained the cells for gangliosides and the mitochondrial marker cytochrome c oxidase subunit 4 (COX4I1) we detected a high degree of co-localization (Fig. 5D) suggesting that some of the storage granules could appear in the result of impaired mitophagy also consistent with the results of the electron microscopy analysis of neurons (as described above). COX4I1 staining also revealed that the mitochondrial network is less organized and the ratio between the fused and single mitochondria is reduced in the tissues of the mutant mice (Supplementary Fig. 9).

## Brain tissues of *Hgsnat-Geo* mice show altered autophagy, impaired proteolysis and accumulation of missfolded proteins

Impaired autophagy associated with decreased lysosomal and proteosomal proteolysis was found to be a characteristic feature of cells in many lysosomal disorders (Bifsha *et al.*, 2007; Settembre *et al.*, 2013). To test whether it is also the case for liver and brain tissues of HGSNAT-deficient mice, we have analyzed the relative abundance of the two forms of light chain three protein (LC3, now known as MAP1LC3A). During the formation of the autophagosome a cytosolic form of LC3 (LC3-I) is cleaved and conjugated with phosphatidylethanolamine to form the LC3-phosphatidylethanolamine conjugate (LC3-II) tightly associated with the autophagosomal membranes, so the amount of LC3-II or the presence of LC3-positive punctate in the cytoplasm reflects the existence of autophagosomes. In liver tissues of *Hgsnat-Geo* mice the increased levels of the LC3-II were detected at all ages indicating increased autophagosomal genesis or decreased macroautophagic flux (Supplementary Fig. 10). In the brain, the increase of LC3-II was also detected, but only at the age of 6 months and older (Fig. 6A).

The results of western blot were consistent with the results of immunohistochemistry that showed presence of LC3 in the cytoplasm of medial entorhinal cortex neurons at 10 months of age (Fig. 6B). We also detected drastically increased neuronal levels of SCMAS (subunit C of mitochondrial ATP synthase) aggregates and ubiquitin suggestive of mitophagy and a general impairment of proteolysis. We also detected increased levels of O-GlcNAc-modified proteins, an indication of

the endoplasmic reticulum stress often associated with impaired cellular proteolysis (Chatham and Marchase, 2010) (Fig. 6C).

Recent studies have demonstrated that neurons in certain brain areas of MPS IIIB and MPS IIIA mice, primarily dentate gyrus and medial entorhinal cortex involved in learning and memory have increased levels of protein markers of Alzheimer disease and other tauopathies leading to dementia such as lysozyme, hyperphosphorylated tau, phosphorylated tau kinase, GSK3B, and amyloid- β (Ohmi *et al.*, 2009, 2011). All of these markers are also increased in the brains of HGSNAT-deficient mice (Supplementary Fig. 11) although their levels are somewhat lower than those in the MPS IIIA and MPS IIIB mice of similar age (Ohmi *et al.*, 2011).

## Mitochondrial energy metabolism is compromised in brain tissues of *Hgsnat-Geo* mice

To verify whether mitochondrial energy metabolism is affected in the brain cells of *Hgsnat-Geo* mice we measured activities of several mitochondrial respiratory chain enzymes including NADH:CoQ reductase (NQR, complex I), succinate:CoQ reductase (SQR, complex II), cytochrome c oxidase (COX, complex IV), NADH:cytochrome c reductase (NCCR, complex I + III), succinate:cytochrome c reductase (SCCR, complex II + III) in the isolated brain mitochondria. We also measured activities of pyruvate dehydrogenase complex and citrate synthase.

Activities of complex IV (COX) and complex II (SQR) enzymes were significantly lower in *Hgsnat-Geo* mice than in the corresponding wild-type controls at the ages of 8 and 12 months and 8 months, respectively (Fig. 7A). No significant differences in activities of enzymes of complex I, complex I + III, complex III, and complex II + III of respiratory chain as well as pyruvate dehydrogenase and control mitochondrial enzyme citrate synthase were found between *Hgsnat-Geo* and wild-type mice. However, when we analysed the activities of individual enzymes as a function of mouse age, we found that the activities of complex II (SQR), complex II + III (SCCR) and citrate synthase in *Hgsnat-Geo* mice decreased significantly with age, whereas no dependence was detected for the wild-type animals (Fig. 7B).

Consistent with the gradual reduction of the activities of respiratory chain enzymes was the observed decrease of the total content of coenzyme Q10 in the brain tissues of *Hgsnat-Geo* mice.

At the age of 4 months the levels of Q10 in the wild-type and HGSNAT-deficient mice were the same, but in the wild-type mice of older age Q10 stayed at the same level; in the brains of *Hgsnat-Geo* mice it showed a negative correlation with age and at the age of 12 months became significantly lower than that in wild-type mice (Fig. 7).

## Progressive neuroinflammation in *Hgsnat-Geo* mice

Chronic progressive neuroinflammation is well documented in mouse models of lysosomal neurodegenerative diseases including those of MPS IIIA and B, which are characterized by activation of resident microglia and astrocytes, infiltration of leucocytes from the periphery and production of the inflammatory cytokines (Ohmi *et al.*, 2003; Ausseil *et al.*, 2008; Wilkinson *et al.*, 2012). Two-fold increased expression of inflammation markers, MIP1α (CCL3) and TNFα, in the brains of homozygous *Hgsnat-Geo* mice was detected as early as 10 days after birth. The levels of these cytokines further increased with age reaching the maximum at 8 months of age (Fig. 8A). At the same time, IL1β and TGFβ1 were not significantly increased as compared with wild-type controls. Similarly increased expression of MIP1α (CCL3) and TNFα cytokines was detected also in the brain tissues of MPS IIIA mice, whereas MPS IIIB mice had 2-fold higher levels at all ages.

Consistent with high expression level of cytokines brain tissues of HGSNAT-deficient mice showed increased levels of activated microglia cells detected by isolectin B4 staining (Fig. 8B) or antibodies against CD68 (Fig. 3B), whereas almost no staining was detected in matching controls. Besides, significantly higher amount of astrocytes stained with anti-GFAP antibodies was detected in the somatosensory cortex of mutant mice starting from the age of 4 months (Fig. 3B).

Signs consistent with an immune reaction were detected also in the liver. Early activation of Kupffer cells preceding the substantial storage and increased presence in liver sinusoids of inflammatory cells was detectable in *Hgsnat-Geo* mice but not in wild-type mice (Supplementary Fig. 4).

## 2.7 Discussion

Altogether our data demonstrate that HGSNAT deficiency in mice results in lysosomal accumulation of heparan sulphate, in multiple cell types, including brain neurons and microglia. In brain neurons heparan sulphate accumulation is accompanied by secondary accumulation of gangliosides and increased lysozyme, phosphorylated tau, GSK3B, and amyloid-β levels. Signs of general inflammation in the brain including activation of astrocytes, microglia and cytokine production, previously reported for other MPS mouse models are clearly present from the very early age. At the same time a lower level of glycosaminoglycans storage as compared to the MPS IIIB mouse model results in a reduced level of brain inflammation, later onset and slower progression of the disease.

The main organs affected at the optical and ultrastructural levels are the brain, liver and spleen. Lysosomal storage consistent with accumulation of undegraded glycosaminoglycans developed early in hepatocytes, splenic sinus endothelium, and cerebral microglia, and to a lesser extent in liver Kupffer and Ito cells, in fibroblasts and in perivascular cells. In peripheral tissues, storage in epithelial and mesenchymal cells, except for hepatocytes occurred later and with a lesser intensity as compared to mouse MPS IIIA and MPS IIIB models (Bhaumik *et al.*, 1999; Li *et al.*, 1999). Presence of macrophages with storage materials in visceral organs was limited, except for liver Kupffer cells, which were activated and developed storage phenotype with age.

In the brain, substantial heparan sulphate storage in microglia was found as early as at 2 months and seems to be the initial pathological event more evident at the age of 2–4 months then pathological changes in neurons, and possibly explained by high phagocytic activity of microglia causing an extracellular substrate burden. The storage was further increased with age in all examined brain regions. Foam microglial cells were frequently in close contact with neurons. Storage vacuoles in microglia had a uniform electron-lucent appearance different from ceroid-type accumulation in neurons. The apparently different storage patterns detected in microglia and neurons by electron microscopy could be also attributed to the loss of glycosaminoglycans during fixation of the cells; however, further immunohistochemical analysis confirmed that lysosomal storage of heparan sulphate in microglia exceeded that in neurons, whereas gangliosides accumulated mainly in neurons.

Neuronal pathology was also featured by cytoplasmic accumulation of densely packed material in neuronal perikarya, which was likely a source of strong autofluorescence and positive immunostaining for SCMAS. Storage of granular autofluorescent material restricted to individual neurons at 5 months was detected throughout the whole neuronal population at 12 months, but even at this advanced stage, neurons showed variations in the amount of stored materials between brain regions and between cells within a region. Similar heterogeneous storage character was reported for the other MPS disease mouse models (McGlynn *et al.*, 2004). Neuronal loss was not a dominant feature at the early stage of the disease but it became significant at 10 months and further progressed with age. At the electron microscopy level, neuronal pathology was characterized by a combination of early detectable structural alterations in mitochondria, progressive lysosomal storage of heterogeneous material and massive lysosomal accumulation of deposits resembling those detected in neuronal ceroid lipofuscinoses. Similar 'fingerprint-like' structures were previously detected in MPS IIIB mouse and identified as SCMAS aggregates (Ryazantsev *et al.*, 2007). The mitochondrial network in neurons was disorganized and the partial impairment of OXPHOS enzymes (complex II, II + III and IV) in brain tissues was detected by enzymatic assays and immunohistochemical analysis, while mitochondrial compartment in age-matching controls did not reveal any abnormalities.

Taken together, our data characterize MPS IIIC as a neurodegenerative disorder with dominant lysosomal and mitochondrial alterations in neurons. Furthermore, our findings suggest that autophagy, namely mitophagy, represents a substantial source for accumulation of undegraded materials in the lysosomal system of neurons.

The precise sequence of events that starts with the accumulation of heparan sulphate and leads to a widespread brain pathology and neuronal death is yet to be determined, however, our results allow hypothesizing that the malfunction and loss of neurons can be at least partially mediated by pathological changes in their mitochondrial system. We speculate that the disease starts with accumulation of primary storage materials (mostly heparan sulphate and heparan sulphate-derived oligosaccharides) as documented by electron microscopy analysis and immunohistochemistry with heparan sulphate-specific antibodies. These materials released presumably by exocytosis of lysosomes are known to induce general inflammation reactions in the brain by activating TLR receptors of microglia cells, resulting in release of multifunctional cytokines such as TNFα and MIP1α (CCL3), known to cause mitochondrial damage through formation of reactive oxygen

species and oxidative stress (Baregamian *et al.*, 2009; Chen *et al.*, 2010; Chuang *et al.*, 2012; Vitner *et al.*, 2012) eventually leading to neuronal death observed in the somatosensory cortex. In the cerebellar cortex, Purkinje cell degeneration typically observed in other lysosomal storage disorders (Sarna *et al.*, 2001; Macauley *et al.*, 2008) was also present. Although neurodegenerative disease can develop even without neuronal loss, it is important to mention that neuronal death is observed in MPS III patients (Hamano *et al.*, 2008). Ganglioside accumulation detected in neurons starting from 2 months is probably of non-lysosomal origin. It could be caused by altered Golgi function as described previously for MPS IIIB mouse model (Roy *et al.*, 2012). Stored lipids and gangliosides can also be partially of mitochondrial origin due to mitophagy and impaired catabolism of autophagosomal content. Indeed, our data define accumulation of densely packed material displaying a strong autofluorescence as a determining feature in brain neurons of MPS IIIC mice at the advanced stage of the disease. As these granules are SCMAS-positive and their ultrastructural pattern strongly resembles that in neuronal ceroid lipofuscinoses, we speculate that they are derived from autophagosomes. Impairment of autophagosome-lysosome fusion can also result in accumulation of deformed and misfunctional mitochondria otherwise eliminated through autophagy and lysosomal catabolism (de Pablo-Latorre *et al.*, 2012; Osellame *et al.*, 2013). Our data suggest that autophagic alterations may be involved in the neuropathological changes in *Hgsnat-Geo* mouse, nevertheless it remains to be determined whether autophagy is impaired or in contrast increased, as the detected LC3-II accumulation can reflect both increased autophagy or defective proteolysis following formation of the autophagosome. Together, our data validate *Hgsnat-Geo* mouse as an animal model relatively well matching the phenotype of human MPS IIIC. MPS IIIC stands out among lysosomal diseases as it is the only one caused by a deficiency of not a hydrolase but a transferase. It is also one of rare disorders involving defects of an integral membrane protein untreatable by enzyme replacement or haematopoietic stem cell therapy. This makes the *Hgsnat-Geo* mouse a valuable model for experimental evaluation of the efficacy of novel therapeutic strategies that can be potentially applied for such disorders, including gene therapy, substrate deprivation therapy or novel methods of enzyme delivery. Further, our model can provide an important opportunity to better understand underlying pathogenic mechanisms of the disease, particularly regarding the CNS, given that human material is highly limited due to the relative rarity of MPS IIIC. Finally, the mechanism of brain disease in the MPS IIIC mouse model involving mitochondrial dysfunction and brain inflammation may represent a common

phenomenon for metabolic neurodegenerative diseases. It also justifies future studies to determine if the mitochondrial defects in MPS IIIC cells can be at least partially rescued by known antioxidative drugs.

## Acknowledgements

The authors acknowledge Drs Elizabeth Neufeld, Jakub Sikora and Mila Ashmarina for critical reading of the manuscript and helpful advice. We also thank Dr Nobuo Hanai, Dr Akiko Furuya and Kyowa Hakko Kirin Co., Ltd. for a generous gift of monoclonal antibodies against GM2 ganglioside, Dr Pascal Vachon for the help with neurological examination of mice, Saadallah Bouhanik for the help with X-ray analysis, Dr Volkan Seyrantepe for the help with ganglioside analysis by TLC and Carmen Movila for the help in preparation of the manuscript.

## Funding

This work was supported in part by the operating grant (MOP-111068) from Canadian Institutes of Health Research and from JJB Foundation to A.V.P., the grant NT13122-3/2012 from the Ministry of Health of the Czech Republic to Helena Hůlková and M.H. and by Charles University institutional program PRVOUKP24/LF1/3 to Hana Hansíková, M.T. and Z.H. C.M. acknowledges the Ph.D. POPH/FSE scholarship from the Portuguese Foundation for Science and Technology (FCT).

## References


Aronovich EL, Carmichael KP, Morizono H, Koutlas IG, Deanching M, Hoganson G, *et al.* Canine heparan sulfate sulfamidase and the molecular pathology underlying Sanfilippo syndrome type A in Dachshunds. Genomics 2000; 68: 80–4.

Aronovich EL, Johnston JM, Wang P, Giger U, Whitley CB. Molecular basis of mucopolysaccharidosis type IIIB in emu (Dromaius novae hollandiae): an avian model of Sanfilippo syndrome type B. Genomics 2001; 74: 299–305.

Ausseil J, Desmaris N, Bigou S, Attali R, Corbineau S, Vitry S, *et al.* Early neurodegeneration progresses independently of microglial activation by heparan sulfate in the brain of mucopolysaccharidosis IIIB mice. PLoS One 2008; 3: e2296.

Baregamian N, Song J, Bailey CE, Papaconstantinou J, Evers BM, Chung DH, *et al.* Tumor necrosis factor alpha and apoptosis signal regulating kinase 1 control reactive oxygen species release, mitochondrial autophagy, and c-Jun N-terminal kinase/p38 phosphorylation during necrotizing enterocolitis. Oxid Med Cell Longev 2009; 2: 297–306.

Bartsocas C, Gröbe H, van de Kamp JJ, von Figura K, Kresse H, Klein U, *et al.* Sanfilippo type C disease: clinical findings in four patients with a new variant of mucopolysaccharidosis III. Eur J Pediatr 1979; 130: 251–8.

Bhaumik M, Muller VJ, Rozaklis T, Johnson L, Dobrenis K, Bhattacharyya R, *et al.* A mouse model for mucopolysaccharidosis type III A (Sanfilippo syndrome). Glycobiology 1999; 9: 1389–96.

Bifsha P, Landry K, Ashmarina L, Durand S, Seyrantepe V, Trudel S, *et al.* Altered gene expression in cells from patients with lysosomal storage disorders suggests impairment of the ubiquitin pathway. Cell Death Differ 2007; 14: 511–23.

Bruye`re J, Roy E, Ausseil J, Lemonnier T, Teyre G, Boh D, *et al.* Heparan sulphate saccharides modify focal adhesions: implication in mucopolysaccharidosis neuropathophysiology. J Mol Biol 2014; S0022-2836(14)00511-7.

Chatham JC, Marchase RB. Protein O-GlcNAcylation: a critical regulator of the cellular response to stress. Curr Signal Transduct Ther 2010; 5: 49–59.

Chen XH, Zhao YP, Xue M, Ji CB, Gao CL, Zhu JG, *et al.* TNF-alpha induces mitochondrial dysfunction in 3T3-L1 adipocytes. Mol Cell Endocrinol 2010; 328: 63–9.

Chuang YC, Su WH, Lei HY, Lin YS, Liu HS, Chang CP, *et al.* Macrophage migration inhibitory factor induces autophagy via re active oxygen species generation. PLoS One 2012; 7: e37613.

Crawley AC, Gliddon BL, Auclair D, Brodie SL, Hirte C, King BM, *et al.* Characterization of a C57BL/6 congenic mouse strain of mucopolysaccharidosis type IIIA. Brain Res 2006; 1104: 1–17.

David G, Bai XM, Van der Schueren B, Cassiman JJ, Van den Berghe H. Developmental changes in heparan sulfate expression: in situ detection with mAbs. J Cell Biol 1992; 119: 961–75.

de Pablo-Latorre R, Saide A, Polishhuck EV, Nusco E, Fraldi A, Ballabio A. Impaired parkin-mediated mitochondrial targeting to autophagosomes differentially contributes to tissue pathology in lysosomal storage diseases. Hum Mol Genet 2012; 21: 1770–81.

de Ruijter J, Maas M, Janssen A, Wijburg FA. High prevalence of femoral head necrosis in Mucopolysaccharidosis type III (Sanfilippo disease): a national, observational, cross-sectional study. Mol Genet Metab 2013; 109: 49–53.

DiRosario J, Divers E, Wang C, Etter J, Charrier A, Jukkola P, *et al.* Innate and adaptive immune activation in the brain of MPS IIIB mouse model. J Neurosci Res 2009; 87: 978–90.
Dudkova Z, Cederblad G, Hultman E. Determination of pyruvate dehydrogenase complex activity in muscle tissue. Klin. Biochem. Metab 1995; 3: 178–82.
Durand S, Feldhammer M, Bonneil E, Thibault P, Pshezhetsky AV. Analysis of the biogenesis of heparan sulfate acetyl-CoA:alpha-glucosaminide N-acetyltransferase provides insights into the mechanism underlying its complete deficiency in mucopolysaccharidosis IIIC. J Biol Chem 2010; 285: 31233–42.
Ellinwood NM, Wang P, Skeen T, Sharp NJ, Cesta M, Decker S, *et al.* A model of mucopolysaccharidosis IIIB (Sanfilippo syndrome type IIIB): N-acetyl-alpha-D-glucosaminidase deficiency in Schipperke dogs. J Inherit Metab Dis 2003; 26: 489–504.
Feldhammer M, Durand S, Pshezhetsky AV. Protein misfolding as an underlying molecular defect in mucopolysaccharidosis III type C. PLoS One 2009; 4: e7434.
Ginsberg SD, Galvin JE, Lee VM, Rorke LB, Dickson DW, Wolfe JH, *et al.* Accumulation of intracellular amyloid-beta peptide (A beta 1-40) in mucopolysaccharidosis brains. J Neuropathol Exp Neurol 1999; 58: 815–24.
Hamano K, Hayashi M, Shioda K, Fukatsu R, Mizutani S. Mechanisms of neurodegeneration in mucopolysaccharidoses II and IIIB: analysis of human brain tissue. Acta Neuropathol 2008; 115: 547–59.
Hansen GM, Markesich DC, Burnett MB, Zhu Q, Dionne KM, Richter LJ, *et al.* Large-scale gene trapping in C57BL/6N mouse embryonic stem cells. Genome Res 2008; 18: 1670–9.
Hocquemiller M, Vitry S, Bigou S, Bruye`re J, Ausseil J, Heard JM. GAP43 overexpression and enhanced neurite outgrowth in mucopolysaccharidosis type IIIB cortical neuron cultures. J Neurosci Res 2010; 88: 202–13.
Huang JQ, Trasler JM, Igdoura S, Michaud J, Hanal N, Gravel RA. Apoptotic cell death in mouse models of GM2 gangliosidosis and observations on human Tay-Sachs and Sandhoff diseases. Hum Mol Genet 1997; 6: 1879–85.
Klein U, Kresse H, von Figura K. Sanfilippo syndrome type C: deficiency of acetyl-CoA:alpha-glucosaminide N-acetyltransferase in skin fibroblasts. Proc Natl Acad Sci USA 1978; 75: 5185–9.
Kyrklund T. Two procedures to remove polar contaminants from a crude brain lipid extract by using prepacked reversed-phase columns. Lipids 1987; 22: 274–7.
Langford-Smith A, Langford-Smith K, Jones SA, Wynn RF, Wraith JE, Wilkinson FL, *et al.* Female mucopolysaccharidosis IIIA mice exhibit hyperactivity and a reduced sense of danger in the open field test. PLoS One 2011; 6: e25717.
Lema PP, Girard C, Vachon P. Evaluation of dexamethasone for the treatment of intracerebral hemorrhage using a collagenase-induced intracerebral hematoma model in rats. J Vet Pharmacol Ther 2004; 27: 321–8.
Li HH, Yu WH, Rozengurt N, Zhao HZ, Lyons KM, Anagnostaras S, *et al.* Mouse model of Sanfilippo syndrome type B produced by targeted disruption of the gene encoding alpha-N-acetylglucosaminidase. Proc Natl Acad Sci USA 1999; 96: 14505–10.
Lowry OH, Rosebrough NJ, Farr AL, Randall RJ. Protein measurement with the Folin phenol reagent. J Biol Chem 1951; 193: 265–75.
Macauley SL, Sidman RL, Schuchman EH, Taksir T, Stewart GR. Neuropathology of the acid sphingomyelinase knockout mouse model of Niemann-Pick A disease including structure-

function studies associated with cerebellar Purkinje cell degeneration. Exp Neurol 2008; 214: 181–92.
Makinen MW, Lee CP. Biochemical studies of skeletal muscle mitochondria. I. Microanalysis of cytochrome content, oxidative and phosphorylative activities of mammalian skeletal muscle mitochondria. Arch Biochem Biophys 1968; 126: 75–82.
McGlynn R, Dobrenis K, Walkley SU. Differential subcellular localization of cholesterol, gangliosides, and glycosaminoglycans in murine models of mucopolysaccharide storage disorders. J Comp Neurol 2004; 480: 415–26.
Mohammed EE, Snella EM, Rutz-Mendicino MM, Echevarria FD, Awedikian R, Whitley EM, *et al.* Accelerated clinical disease and pathology in mucopolysaccharidosis type IIIB and GalNAc transferase double knockout mice. Mol Genet Metab 2012; 107: 129–35.
Mosca F, Fattorini D, Bompadre S, Littarru GP. Assay of coenzyme Q(10) in plasma by a single dilution step. Anal Biochem 2002; 305: 49–54.
Nakamura K, Koike M, Shitara K, Kuwana Y, Kiuragi K, Igarashi S, *et al.* Chimeric anti-ganglioside GM2 antibody with antitumor activity. Cancer Res 1994; 54: 1511–6.
Neufeld EF, Muenzer J. The Mucopolysaccharidoses. In: Scriver CR, Beaudet AL, Sly WS, Valle D, editors. The metabolic and molecular basis of inherited disease. New York: McGraw-Hill; 2001. p. 3421–52.
Ohmi, K., *et al.*, 2003. Activated microglia in cortex of mouse models of mucopolysaccharidoses I and IIIB. Proc Natl Acad Sci U S A. 100**,** 1902-7.
Ohmi, K., *et al.*, 2009. Sanfilippo syndrome type B, a lysosomal storage disease, is also a tauopathy. Proc Natl Acad Sci U S A. 106**,** 8332-7.
Ohmi, K., Zhao, H.Z., Neufeld, E.F., 2011. Defects in the medial entorhinal cortex and dentate gyrus in the mouse model of Sanfilippo syndrome type B. PLoS One. 6**,** e27461.
Osellame, L.D., *et al.*, 2013. Mitochondria and quality control defects in a mouse model of Gaucher disease--links to Parkinson's disease. Cell Metab. 17**,** 941-53.
Pinto, R., *et al.*, 2004. Prevalence of lysosomal storage diseases in Portugal. Eur J Hum Genet. 12**,** 87-92.
Poorthuis, B.J., *et al.*, 1999. The frequency of lysosomal storage diseases in The Netherlands. Hum Genet. 105**,** 151-6.
Roy, E., *et al.*, 2012. GM130 gain-of-function induces cell pathology in a model of lysosomal storage disease. Hum Mol Genet. 21**,** 1481-95.
Ruijter, G.J., *et al.*, 2008. Clinical and genetic spectrum of Sanfilippo type C (MPS IIIC) disease in The Netherlands. Mol Genet Metab. 93**,** 104-11.
Rustin, P., *et al.*, 1994. Biochemical and molecular investigations in respiratory chain deficiencies. Clin Chim Acta. 228**,** 35-51.
Ryazantsev, S., *et al.*, 2007. Lysosomal accumulation of SCMAS (subunit c of mitochondrial ATP synthase) in neurons of the mouse model of mucopolysaccharidosis III B. Mol Genet Metab. 90**,** 393-401.
Sarna, J., *et al.*, 2001. Patterned cerebellar Purkinje cell death in a transgenic mouse model of Niemann Pick type A/B disease. Eur J Neurosci. 13**,** 1873-80.
Settembre, C., *et al.*, 2013. Signals from the lysosome: a control centre for cellular clearance and energy metabolism. Nat Rev Mol Cell Biol. 14**,** 283-96.
Seyrantepe, V., *et al.*, 2008. Mice deficient in Neu4 sialidase exhibit abnormal ganglioside catabolism and lysosomal storage. Hum Mol Genet. 17**,** 1556-68.

Seyrantepe, V., *et al.*, 2010. Mice doubly-deficient in lysosomal hexosaminidase A and neuraminidase 4 show epileptic crises and rapid neuronal loss. PLoS Genet. 6.
Srere, P.A., 1969. [1] Citrate synthase: [EC 4.1.3.7. Citrate oxaloacetate-lyase (CoA-acetylating)]. In: Methods Enzymol. Vol. Volume 13, M.L. John, ed.^eds. Academic Press, pp. 3-11.
Valstar, M.J., *et al.*, 2008. Sanfilippo syndrome: a mini-review. J Inherit Metab Dis. 31**,** 240-52.
Villani, G.R., *et al.*, 2007. Cytokines, neurotrophins, and oxidative stress in brain disease from mucopolysaccharidosis IIIB. J Neurosci Res. 85**,** 612-22.
Vitner, E.B., *et al.*, 2012. Contribution of brain inflammation to neuronal cell death in neuronopathic forms of Gaucher's disease. Brain. 135**,** 1724-35.
Wada, R., Tifft, C.J., Proia, R.L., 2000. Microglial activation precedes acute neurodegeneration in Sandhoff disease and is suppressed by bone marrow transplantation. Proc Natl Acad Sci U S A. 97**,** 10954-9.
Whitley, C.B., *et al.*, 1989. Diagnostic test for mucopolysaccharidosis. I. Direct method for quantifying excessive urinary glycosaminoglycan excretion. Clin Chem. 35**,** 374-9.
Wilkinson, F.L., *et al.*, 2012. Neuropathology in mouse models of mucopolysaccharidosis type I, IIIA and IIIB. PLoS One. 7**,** e35787.
Zambrowicz, B.P., *et al.*, 2003. Wnk1 kinase deficiency lowers blood pressure in mice: a gene-trap screen to identify potential targets for therapeutic intervention. Proc Natl Acad Sci U S A. 100**,** 14109-14.

## Figures

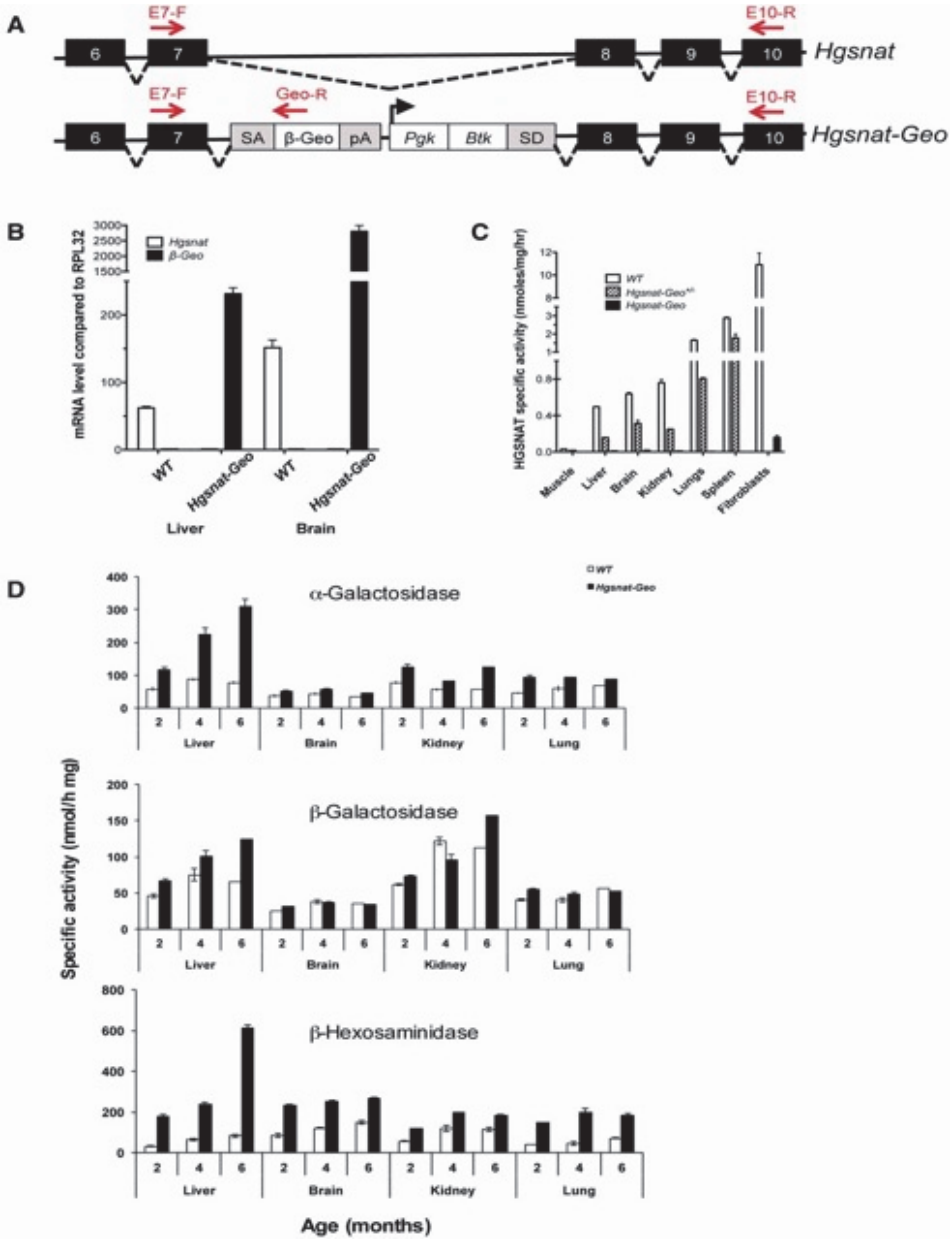


**Figure 1:** Targeting the *Hgsnat* gene in mice. (A) Strategy for producing the targeted disruption of the *Hgsnat* gene. The gene trap vector used by Texas A&M Institute for Genomic Medicine contains a splice acceptor site (SA) upstream of a β-galactosidase/neomycin phosphotransferase (*Geo*) fusion gene followed by polyadenylation sequence (pA), PGK and BTK genes and splice donor site (SD) inserted into intron 7 of the *Hgsnat* gene as confirmed by genomic sequencing. Hence, the downstream exons 8–13 in the gene trap transcript were replaced by the Geo sequence.

Exons in the mouse *Hgsnat* gene are shown as black numbered boxes and *Geo-PGK-BTK* cassette, as white boxes. Primers (E7-R, Geo-R, and E10-F) were used to measure the expression of the wild-type *Hgsnat* and of the targeted *Hgsnat-Geo* alleles by real time quantitative PCR. (B) Real time quantitative PCR shows that expression of the *Hgsnat* mRNA in brain and liver tissues of mice homozygous for the *Hgsnat-Geo* allele is reduced to 0.6 and 1.6% of that in the tissues of their wild-type (WT) siblings. Total RNA was extracted from tissues of 4-month-old wild-type and *Hgsnat-Geo* mice and analysed for *Hgsnat* expression by real time quantitative PCR. The values were normalized for the level of control *RPL32* mRNA. Data are expressed as means (SD) of experiments performed with six mice for each genotype. (C) Deficient HGSNAT activity in tissues of mice homozygous for *Hgsnat-Geo* allele. HGSNAT activity was measured with fluorogenic substrate, Muf-β-D-glucosaminide in the tissues of 4-month-old wild-type, *Hgsnat-Geo*$^{+/-}$ and *Hgsnat-Geo* mice or in cultured skin fibroblasts of wild-type and *Hgsnat-Geo* mice. Data are expressed as means (SD) of independent experiments performed with tissues of six mice for each genotype or with three different cell cultures. (D) Lysosomal hydrolases are increased in tissues of *Hgsnat-Geo* mice. Acidic -galactosidase, β-galactosidase and total β-hexosaminidase activity were measured in the tissues of 1, 4 and 6 month-old *Hgsnat-Geo* mice and their wild-type siblings. Data are expressed as means (SD) of experiments performed with three mice for each genotype.

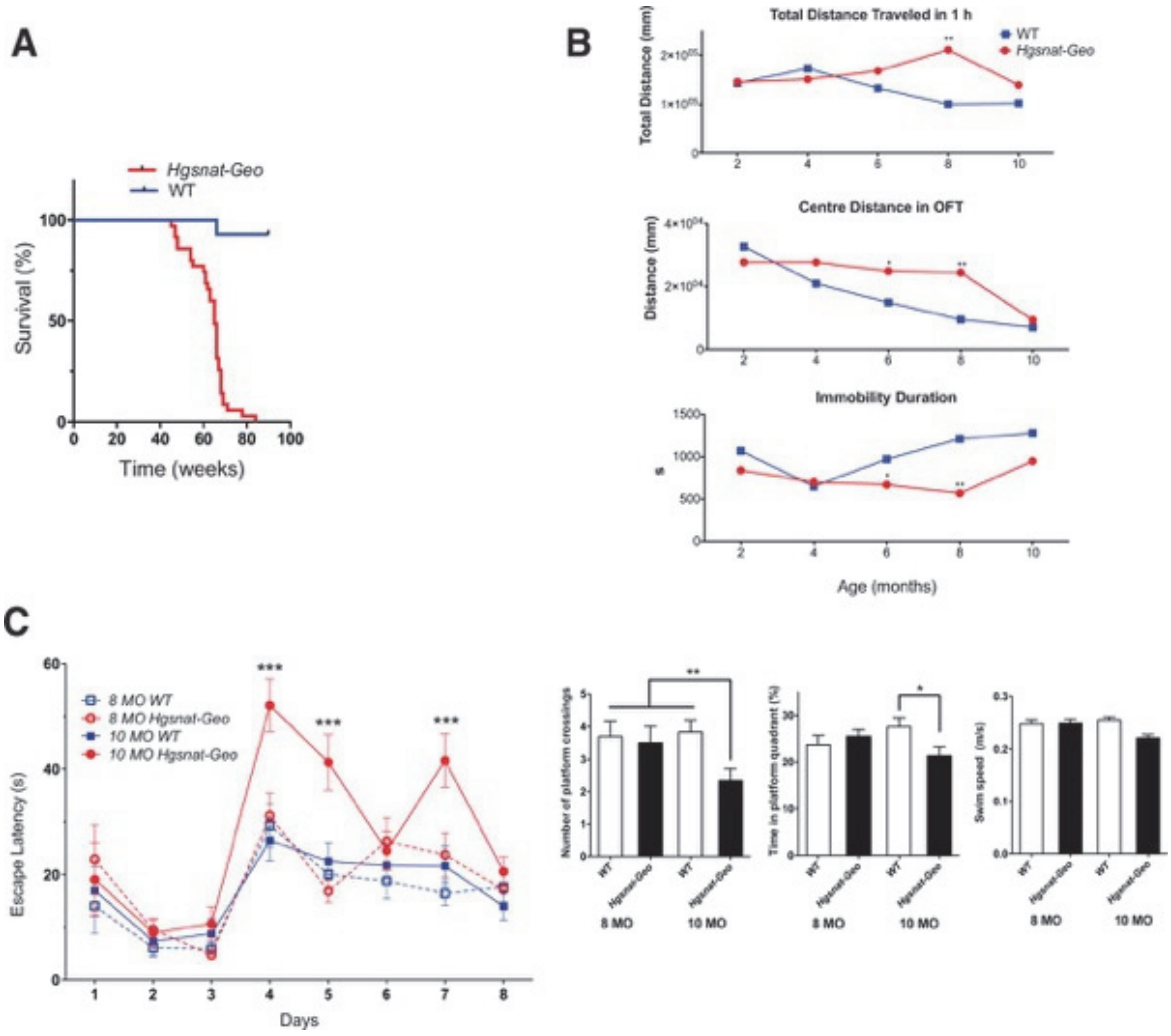


**Figure 2:** *Hgsnat-Geo* mice have shorter life span and show signs of hyperactivity between the ages of 6 and 8 months and learning impairment at the age of 10 months. (A) Kaplan-Meier plot showing survival of *Hgsnat-Geo* mice (n = 50) and their wild-type (WT) counterparts (n = 70). By the age of 70 weeks the vast majority of *Hgsnat-Geo* mice died or had to be euthanized on veterinarian request due to urinary retention. (B) Six and 8-month-old *Hgsnat-Geo* female mice show signs of hyperactivity and reduced anxiety compared to wild-type mice as detected by the open field test (OFT) performed 1 h into their light cycle. Increased activity (total distance travelled) was detected starting from 5 months of age, with significant hyperactivity at 8 months. Reduced anxiety (increased centre activity) was detected starting from 3 months, with significant difference with wild-type at 6 and 8 months. At 6 and 8 months *Hgsnat-Geo* mice also spent significantly less time immobile as compared to wild-type mice. *P*-value was calculated by two-

way ANOVA (*$p < 0.05$, **$p < 0.01$). From six (2, 4 and 6 month-old) to 10 (8 and 10 month-old) naive mice were studied per age/per genotype. (C) *Hgsnat-Geo* mice showed impaired performance in the spatial memory-based Morris Water Maze test at 10 months (MO). All mice showed similar average latencies on Days 1–3 of visible platform testing. Whereas 8-month-old *Hgsnat-Geo* mice had latencies in the hidden platform testing similar to those of their wild-type counterparts (Days 4–8), 10-month-old mutant mice were significantly impaired in this spatial learning test. During the removed platform probe trial on Day 9, *Hgsnat-Geo* mice displayed reduced time in the target quadrant as compared to their wild-type siblings. Numbers of passes over the previous location of the hidden platform were also reduced. Swim speed was comparable among all groups. Six mice were studied for each group. *P*-value for escape latency was calculated by two-way ANOVA (***$p < 0.001$) and for the number of platform crossing and time in platform quadrant, by t-test (*$p < 0.05$, **$p < 0.01$).

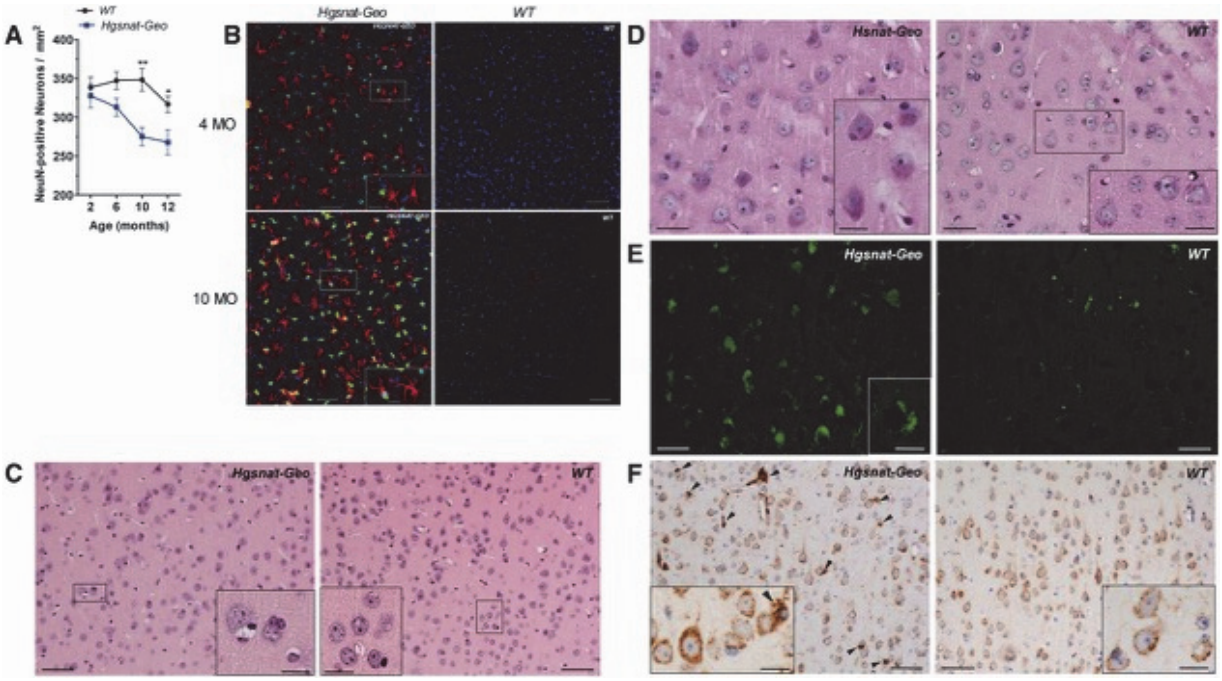


**Figure 3:** Pathological changes in CNS of *Hgsnat-Geo* mice. (A) Progressive loss of neurons in somatosensory cortex. NeuN-positive neurons were counted by two observers blinded for the mouse genotype in two similar fields on three sagittal sections (cut 1.44, 1.68 and 1.92 mm from bregma) of S1 somatosensory cortex of each mouse; four (two male, two female) mice were studied for each age and each genotype. Two-way (age and genotype) ANOVA was used to test differences between the mouse groups: significant differences between the genotypes at a given age in Bonferroni post-test (*$p < 0.05$, **$p < 0.01$) are shown. (B) Increased numbers of GFAP-positive astrocytes and C68-positive microglia are detected in the somatosensory cortex of *Hgsnat-Geo* mice. Somatosensory cortex (layer V) of 4- and 10-month-old *Hgsnat-Geo* mouse and wild-type littermate control (WT); slides stained with chicken polyclonal antibodies against GFAP (AbCam ab4674, 1/600) and rat antibodies against mouse CD68 (MCA 1957, 1/400), followed by DyLightTM 549-conjugated goat anti-chicken IgG (Jackson ImmunoResearch Laboratories 103-505-155, 1/50) and Alexa Fluor488-conjugated goat anti-rat IgG (Invitrogen, 1/400) antibodies. The nuclei were stained with DRAQ5TM (Thermo Scientific 62254, 1/1000). Scale bars = 50 mm; inserts = 20 mm. (C) Presence in cortical grey matter of microglial cells with vacuolized cytoplasm and foam-like appearance. Microglial cells showing storage are either dispersed or adjacent to neurons (shown in details in the insert). Somatosensory cortex (layer V) of 12-month-old *Hgsnat-Geo* mouse and wild-type littermate control (WT); haematoxylin and eosin stain. Scale bars = 100

mm; inserts = 30 mm. (D) Accumulation of PAS-positive granular material is detectable in perikarya of multiple neurons in the brain of *Hgsnat-Geo* mouse. Microglia show presence of storage and foam-like appearance. Brain of wild-type littermate control displays only discrete PAS-positive deposits corresponding with age pigment. Inserts show detailed views of neurons and microglia. Somatosensory cortex (layer V) of 12-month-old *Hgsnat-Geo* and wild-type mice. Scale bars = 50 mm; inserts = 30 mm. (E) A massive accumulation of granular auto-fluorescent ceroid is widely present in cortical neurons of 12-month-old *Hgsnat-Geo* mouse. Insert shows a detailed view of a neuron with ceroid deposits in the perikaryon. Brain of wild-type littermate control contains a small amount of autofluorescent lipofuscin in individual neurons. Somatosensory cortex (layer V) of 12-month-old *Hgsnat-Geo* mouse. Scale bars = 100 mm; insert = 30 mm. (F) Increased CTSD immunostaining comparable with lysosomal storage in microglia and neurons of 12-month-old Hgsnat-Geo mouse. Dispersed, perineuronal or perivascular microglia is strongly positive for cathepsin D (marked by arrowheads). Lysosomal system in neurons is irregularly activated and shows a coarsely granular appearance. Neuronal perikarya are not markedly distended in contrast to microglia. Inserts show detailed views of both cell types. Somatosensory cortex (layer V) of 12-month-old *Hgsnat-Geo* and wild-type mice. Scale bars = 100 mm, insert = 30 mm. Panels show representative images of at least 30 studied for four *Hgsnat-Geo* and four wild-type mice. MO = months.

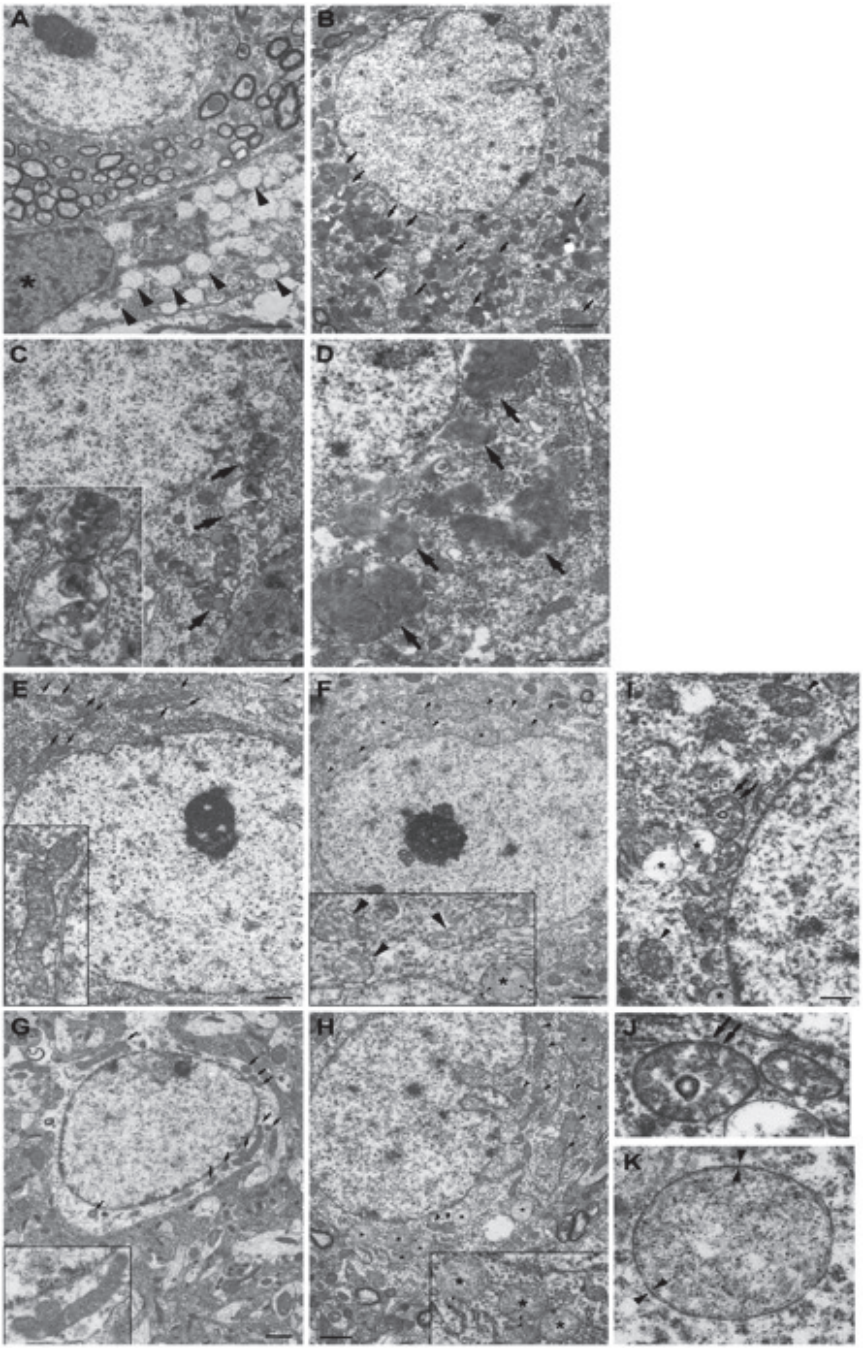


**Figure 4:** Ultrastructural pathology in the brain of *Hgsnat-Geo* mice. (A) Storage pattern in microglia detected at 5 months. Massive accumulation of vacuoles with single limiting membranes and a sparse fine content in the cytoplasm of a cortical microglial cell is compatible with lysosomal glycosaminoglycan storage. Lysosomes containing storage materials are marked by arrowheads. The microglial cell (nucleus is marked by an asterisk) is in a close proximity to a cortical brain

neuron. Scale bar = 2 mm. (B) Lysosomal system in a cortical neuron at 12 months is expanded and massively overloaded by electron dense material (marked by arrows). Scale bar = 2 mm. (C) High magnification micrograph of a cortical neuron at 12 months demonstrates a storage compartment (marked by arrows) containing ceroid-like granular and/or lamellar material packed with a variable density as well as occasional lipid droplets. Insert shows a detailed view of storage deposits. Scale bar = 1 mm. (D) Storage of densely packed fibrillary material (marked by arrows) strongly resembling rectilinear or fingerprint-like ceroid deposits in neuronal lysosomes at advanced stages of the disease. Brain cortex of 16-month-old *Hgsnat-Geo* mouse. Scale bar = 1 mm. Mitochondrial population in neurons of wild-type mice at the age of 5 (E) and 12 months (G) is relatively uniform and is composed of normally shaped mitochondria (marked by arrows) with largely regular cristae (details are shown in the inserts). Scale bar = 1 mm. Mitochondria in a neuron of *Hgsnat-Geo* mouse at the age of 5 months (F) are relatively numerous and pleiomorphic with some of them revealing incipient swelling (marked by arrowheads). Oedematous mitochondria with largely dissolved cristae (marked by asterisks) but with remnants of double membranes (marked by double arrowheads) were detected occasionally. A detailed view of incipient mitochondrial abnormalities is shown in the insert. Scale bar = 1 mm. At the age of 12 months (H), mitochondria in neurons of *Hgsnat-Geo* mice are clearly pleomorphic with many of them displaying swelling and disorganization of their inner membranes (marked by arrowheads). Substantially oedematous mitochondria with largely dissolved cristae are marked by asterisks. Insert shows a detailed view of highly oedematous mitochondria with remnants of double membranes (marked by double arrowheads). Scale bar = 1 mm. (I) A higher magnification demonstrates structural mitochondrial abnormalities in a neuron of *Hgsnat-Geo* mouse at 12 months. Mitochondria are swollen with disorganized (arrowheads) or even dissolved (asterisks) cristae and occasionally contain circular formations (marked by double arrows). Scale bar = 500 nm. (J) A detailed view of a mitochondrion with inner membranes forming circular structures. (K) A detailed view of a highly oedematous mitochondrion with dissolved cristae but with detectable remnants of double membranes (marked by double arrowheads). Panels show representative images of at least 30 studied for 3 *Hgsnat-Geo* and 3 wild-type mice for each age.

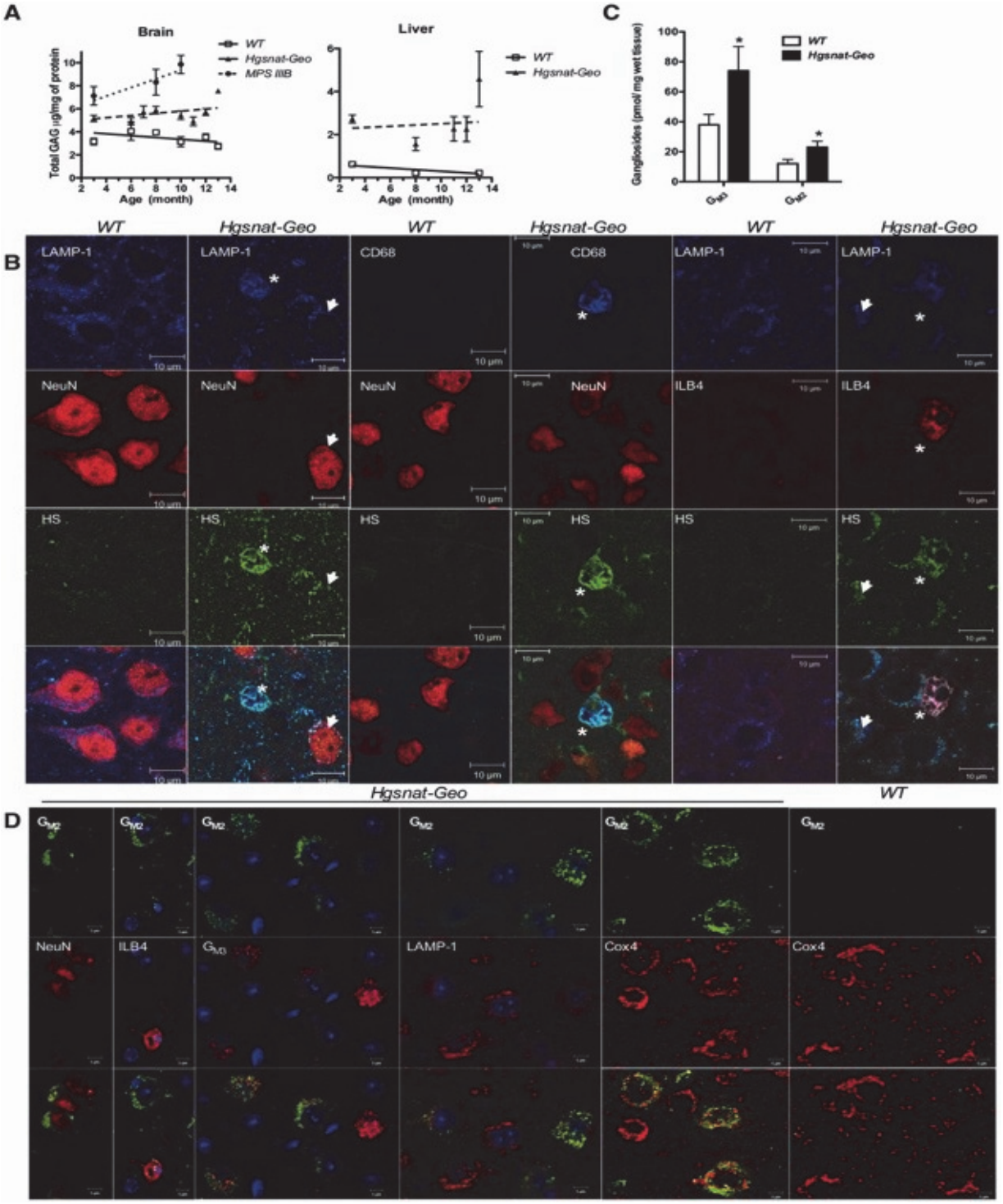


**Figure 5:** Accumulation of primary and secondary storage materials in tissues of *Hgsnat-Geo* mice. (A) Total glycosaminoglycans were measured in the whole brain tissues of *Hgsnat-Geo* mice, α-N-acetylglucosaminidase-deficient (MPS IIIB) mice and their corresponding wild-type

controls as well as in liver tissues of *Hgsnat-Geo* and wild-type mice. The data show means (SD) of individual measurements performed with 15 mice for each age and genotype. (B) Intralysosomal accumulation of heparan sulphate in the brain cells of *Hgsnat-Geo* mice. Sagittal brain sections (40-mm thick) of 4-month-old wild-type and *Hgsnat-Geo* mice were stained with anti-heparan sulphate and anti-LAMP1 antibodies and either antibody against neuronal marker NeuN or microglial marker, isolectin B4 (ILB4) or with antibodies against heparan sulphate, NeuN and CD68. Somatosensory cortex of wild-type mouse does not show heparan sulphate (green) staining while that of *Hgsnat-Geo* mouse contains multiple neurons (arrowheads) or microglia (asterisks) with lysosomal accumulation of heparan sulphate. Foamy microglia (negative for neuronal marker, NeuN, but positive for ILB4 or CD68) show on average an increased staining for heparan sulphate compared to neurons. (C) Levels of GM3 and GM2 gangliosides are increased in the total brain extracts of 4-month-old *Hgsnat-Geo* mice as compared to their wild-type siblings. Total lipids from brain tissue homogenates were extracted with chloroform/methanol 1:1 mixture and analysed by tandem mass spectroscopy. (D) Accumulation of gangliosides in cortical neurons of *Hgsnat-Geo* mice. Forty mm-thick sagittal brain sections of 8-month-old wild-type and *Hgsnat-Geo* mice were stained with anti-GM2 antibodies and either microglial marker, isolectin B4 or antibodies against neuronal marker NeuN, GM3 ganglioside, LAMP1 and mitochondrial marker, cytochrome c oxidase subunit 4 (Cox4, now known as COX4I1). Slides were studied on a Zeiss LSM510 inverted confocal microscope. Panels show representative images of at least 30 studied for three *Hgsnat-Geo* and three wild-type mice for each age.

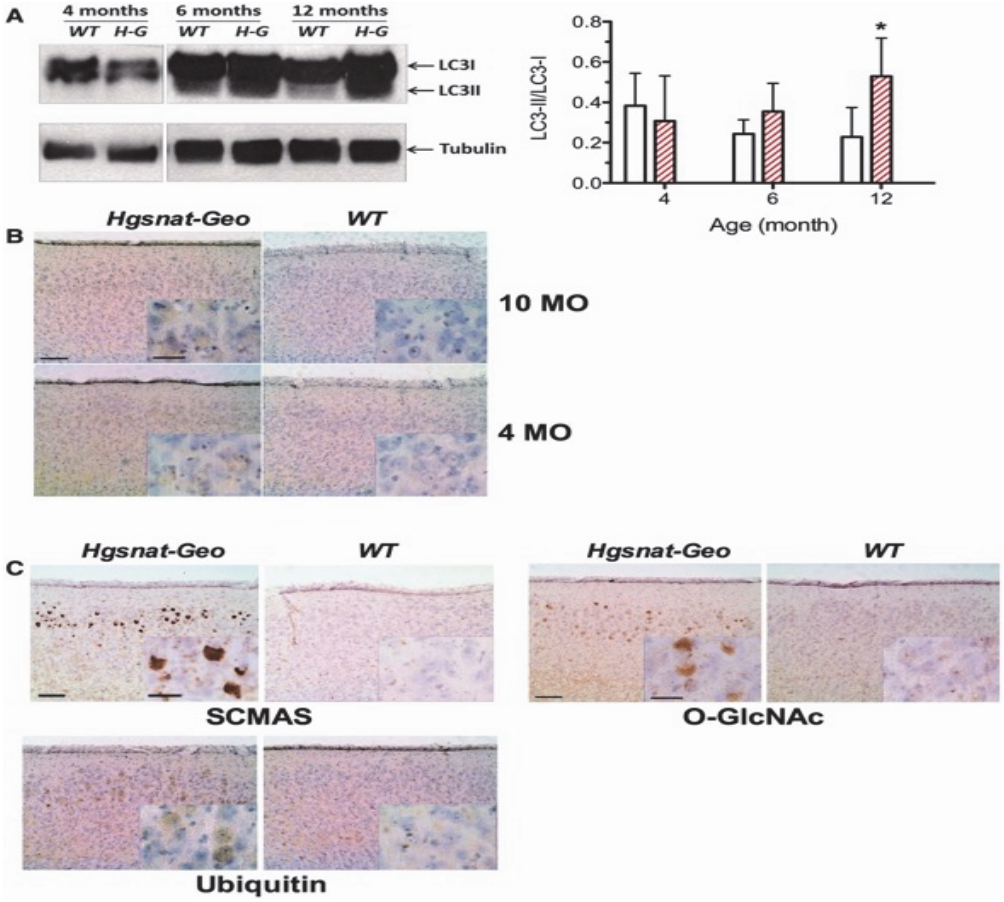


**Figure 6:** Brain tissues of *Hgsnat-Geo* mice show altered autophagy and lysosomal proteolysis. (A) Increased levels of LC3-II were detected in the brain tissues of *Hgsnat-Geo* (H–G) mice at the age of 6 and 10 months but not at the age of 4 months by western blot. Total mouse brains were homogenized in 250 mM sucrose buffer and after removal of nuclei proteins were solubilized with 1% TritonTM X-100. Protein extracts were analysed by western blotting using antibodies specific for mouse LC3 and β-tubulin as a loading control. Panel shows representative data of three independent experiments performed with three *Hgsnat-Geo* and three wild-type mice for each age. Inset graph shows ratios (means and SD) of signal intensities for LC3-II and LC3-I estimated with ImageQuant software. *$p < 0.05$ in unpaired two-tailed t-test. (B) LC3 staining was present in the cytoplasm of medial entorhinal cortex neurons of 10-month-old but not of 4-month-old *Hgsnat-Geo* mice. (C) Signs of impaired lysosomal proteolysis and endoplasmic reticulum stress in the neurons of *Hgsnat-Geo* mice. SCMAS-positive aggregates, *O*-GlcNAc-modified proteins and increased staining for ubiquitin were detected in medial entorhinal cortex neurons of 10-month-old *Hgsnat-Geo* mice. Scale bars = 100 mm; insert = 30 mm.

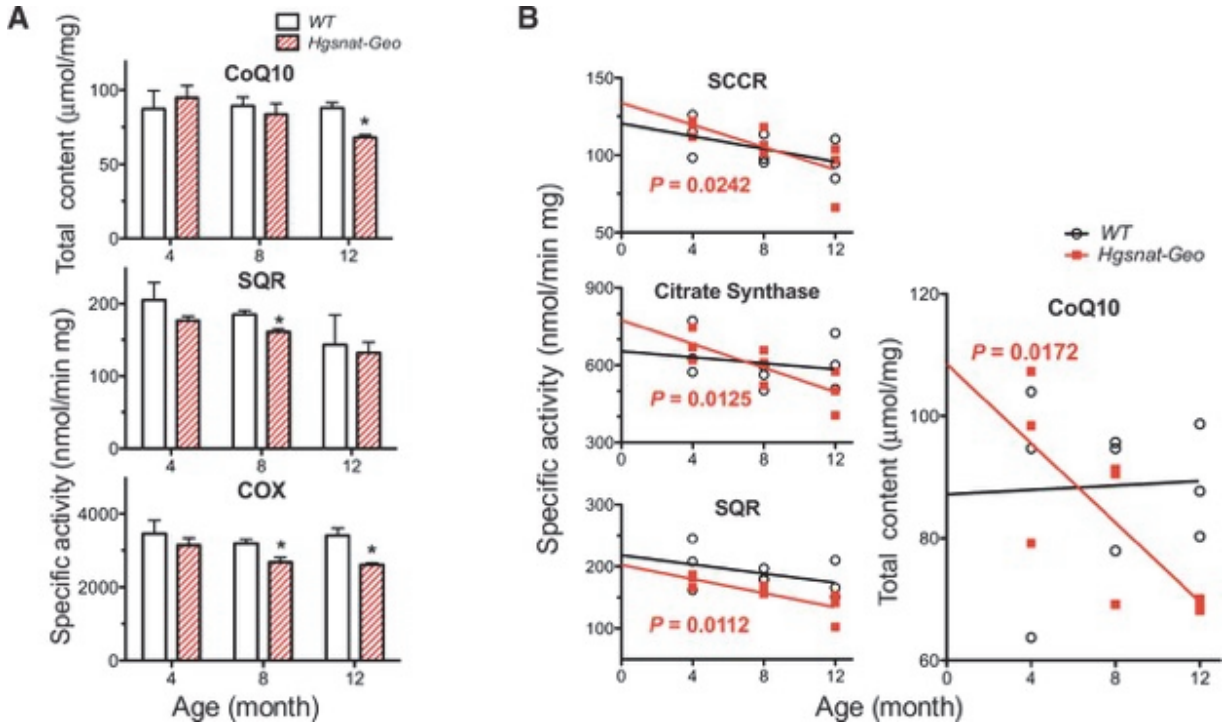


**Figure 7:** Partial impairment of mitochondrial oxidative phosphorylation system in the brains of *Hgsnat-Geo* mice. (A) Activity of succinate: CoQ reductase (SQR, complex II) and cytochrome c oxidase (COX, complex IV) in isolated brain mitochondria of *Hgsnat-Geo* mice are reduced as compared with age-matching wild-type controls. Total content of coenzyme Q10 in brain homogenate of *Hgsnat-Geo* mice is reduced as compared with wild-type controls. The data show means (SD) of individual measurements. Three mice were analysed for each age and each genotype. *$p < 0.05$ in unpaired two-tailed t-test. (B) Correlation between the age and activities of succinate: CoQ reductase (SQR), succinate: cytochrome c reductase (SCCR), citrate synthase (CS), and total coenzyme Q10 content in the brain tissues of *Hgsnat-Geo* and wild-type mice was analysed by the linear regression method. For all parameters in the tissues of *Hgsnat-Geo* but not of wild-type mice the slopes of linear regression lines showed a significant deviation from zero ($p < 0.05$). Three mice were analysed for each age and each genotype.

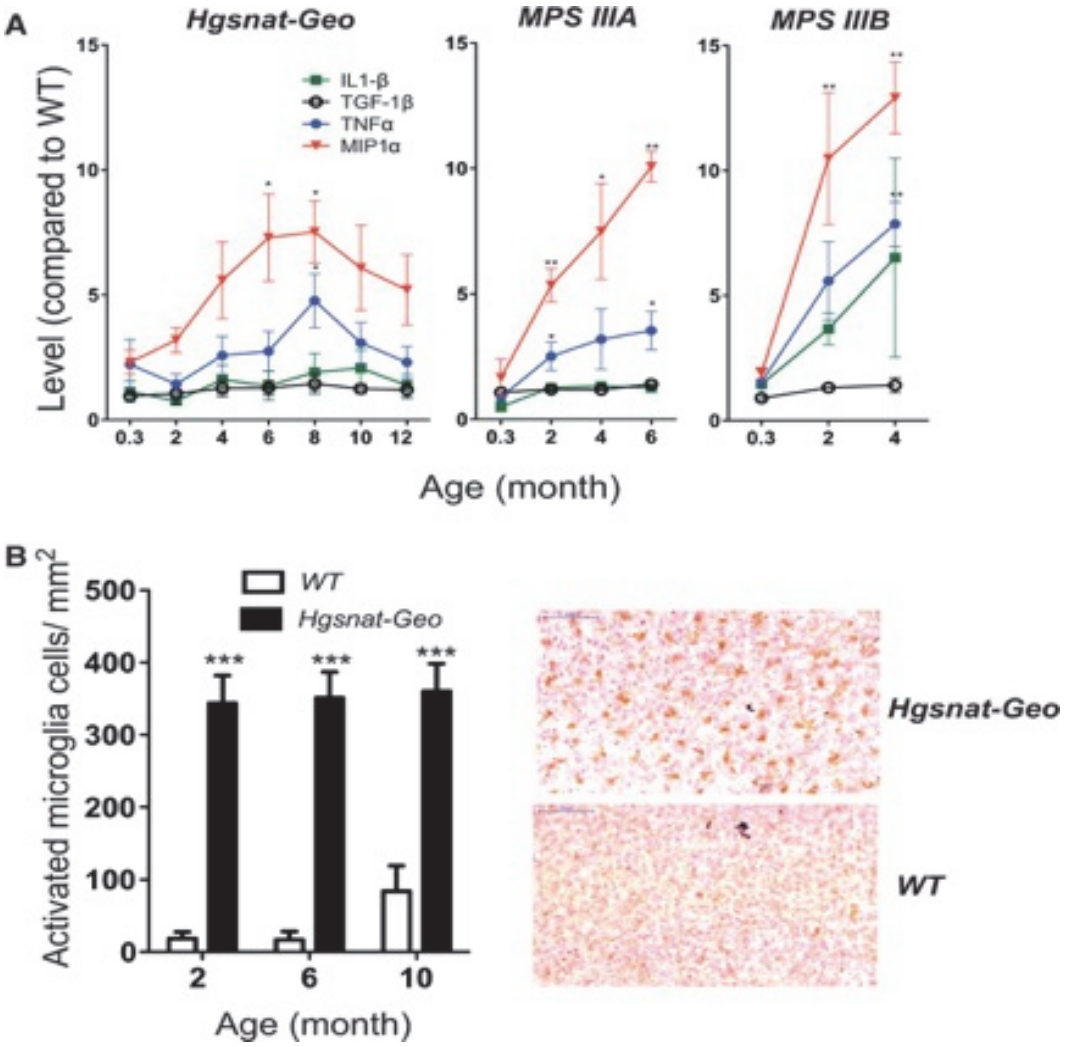


**Figure 8:** Brain inflammation in *Hgsnat-Geo* mice. (A) Total brain tissues of *Hgsnat-Geo* mice show progressively increased expression of inflammation markers, MIP1α (CCL3) and TNFα similar to those in MPS IIIA, but lower than those in MPS IIIB mouse models. Total RNA was isolated from whole mouse brain, reverse-transcribed to cDNA and quantification of cytokines was performed by real time quantitative PCR. The data show ratios of the cytokine levels in *Hgsnat-Geo* mice and those in wild-type (WT) controls (both normalized for the content of RLP32 mRNA). Data show mean values (SD). At least three mice were analysed for each age, sex and genotype. Two-way ANOVA was used to test differences between the mouse groups: significant differences between the mean values in Bonferroni post-test (*$p < 0.05$, **$p < 0.001$) are shown. (B) Increased number of activated microglial cells in brain cortex of *Hgsnat-Geo* mice. Sagittal brain sections (40-mm thick) of wild-type and *Hgsnat-Geo* mice were stained with horseradish

peroxidase-conjugated microglial marker isolectin B4/DAB and counter-stained with haematoxylin, as described (Wilkinson *et al.*, 2012). The total number of microglial cells was counted for three adjacent 0.25 mm2 sections of somatosensory cortex. Data show mean values (SD). Two mice were analysed for each age, sex and genotype. $^{**}p < 0.001$ in unpaired two-tailed t-test.

## Supplementary figures

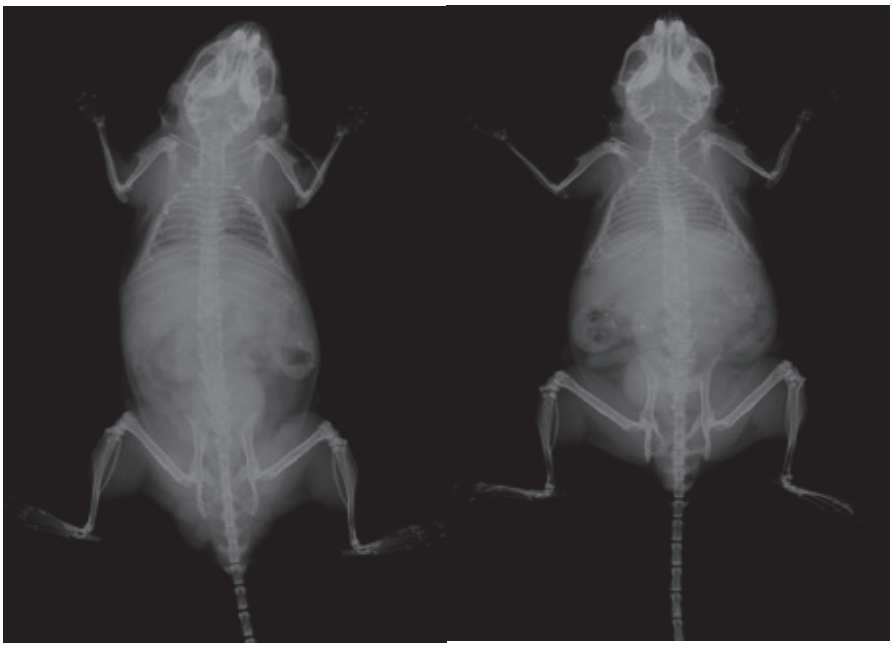

***Hgsnat-Geo*** **WT**

**Figure S1:** No bone deformation was detected by X-ray analysis of *Hgsnat-Geo* mice. Image shows representative radiographs of 2-month-old male *Hgsnat-Geo* (A) and wild type (B) mice taken with Faxitron MX2 instrument. Four mice were analyzed for each genotype.

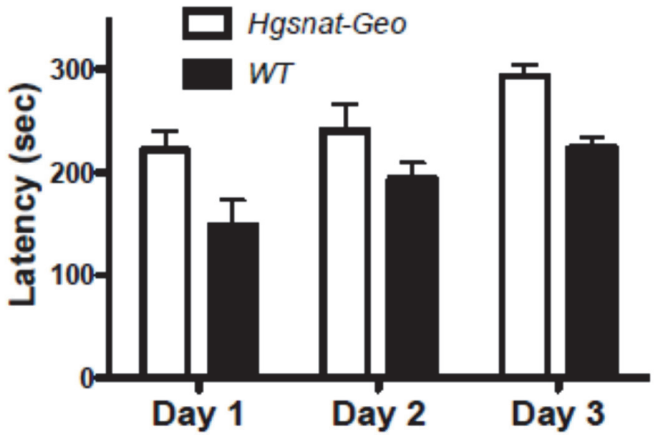


**Figure S2:** No significant difference was observed in accelerating Rotarod performance between 8-month-old wild type and *Hgsnat-Geo* mice. Mice were placed on a rubber-covered rod (3.5 cm in diameter) rotating at 4 rpm. Mice were left for 3 min for adaptation and then the rotation speed was gradually increased from 4 to 40 rpm over the course of 5 min and the latency to fall (in seconds) recorded. The results are shown as means (±SD) of nine tests performed during 3 consecutive days (three tests per day). Four male and four female mice were studied for each sex and genotype. *p* value was calculated by t-test.

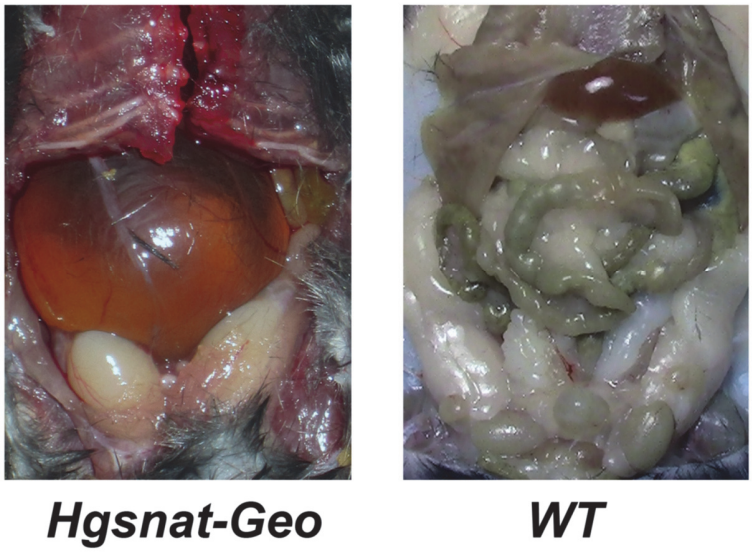


**Figure S3:** Representative dissection of 12-month-old *Hgsnat-Geo* mouse showing signs of urinary retention and a loss of abdominal fat. Both features are not detectable in the age-matching wild type mouse.

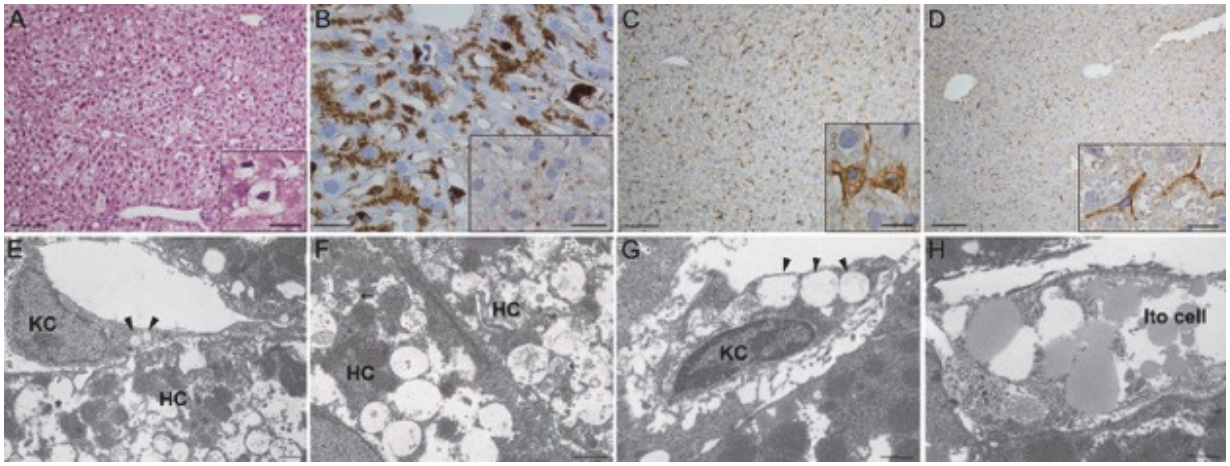


**Figure S4:** Profound lysosomal storage in liver of *Hgsnat-Geo* mice was detected at the optical (A-D) and ultrastructural (E-H) levels.

**(A)** Survey of liver parenchyma of 12-month-old *Hgsnat-Geo* mice showing microvacuolization in hepatocytes mainly in the intermediate zone and increased cellularity in liver sinusoids. Insert shows a detailed view of microvacuolization in the cytoplasm of hepatocytes and a Kupffer cell showing transformation into a foam cell. H&E stain. Bar represents 200 µm, bar in the insert, 30 µm. **(B)** Immunostaining for CathD reveals expanded lysosomal system in hepatocytes and in Kupffer cells in the liver of 12-month-old *Hgsnat-Geo* mice, comparable with lysosomal storage. Insert shows a discrete signal for CathD in hepatocytes of wild type littermate control mouse. Bars represent 50 µm. **(C, D)** Storage within the population of Kupffer cells and their early activation were detected in *Hgsnat-Geo* mice by immunostaining with rat monoclonal antibody (clone BM8) against Mouse Macrophage IgG2a (LS-C139904, LifeSpan Bioscience). Positively stained Kupffer cells in liver sinusoids are enlarged and increased in number in 5-month-old *Hgsnat-Geo* mice **(C)** as compared to age matching wild type mice **(D)**. Individual Kupffer cells display a storage phenotype with rounded vacuolated cytoplasm **(C, insert)**. Kupffer cells in wild type mice are always slim, stellate or needle-shaped **(D, insert)**. Bars represent 200 µm, bars in inserts, 30 µm. **(E)** Intensive lysosomal storage of soluble substances in the cytoplasm of a hepatocyte (HC) contrasting with rarely detectable storage vacuoles (marked by arrowheads) in a Kupffer cell (KC) in the sinusoid of 5-month-old *Hgsnat-Geo* mice. **(F)** Higher magnification of hepatocyte (HC) cytoplasm with accumulation of vacuoles surrounded by a single limiting membrane, either electronlucent or with a sparse fine content. Structures resembling autophagic

vacuoles (marked by arrows) were occasionally detected. **(G, H)** Ultrastructural pattern characteristic for lysosomal storage of GAG (marked by arrowheads) was clearly detectable at 12 months in Kupffer cells (KC) **(G)** and in perisinusoidal Ito cells also containing droplets of neutral lipids in their cytoplasm **(H)**. Bars represent 1 μm.

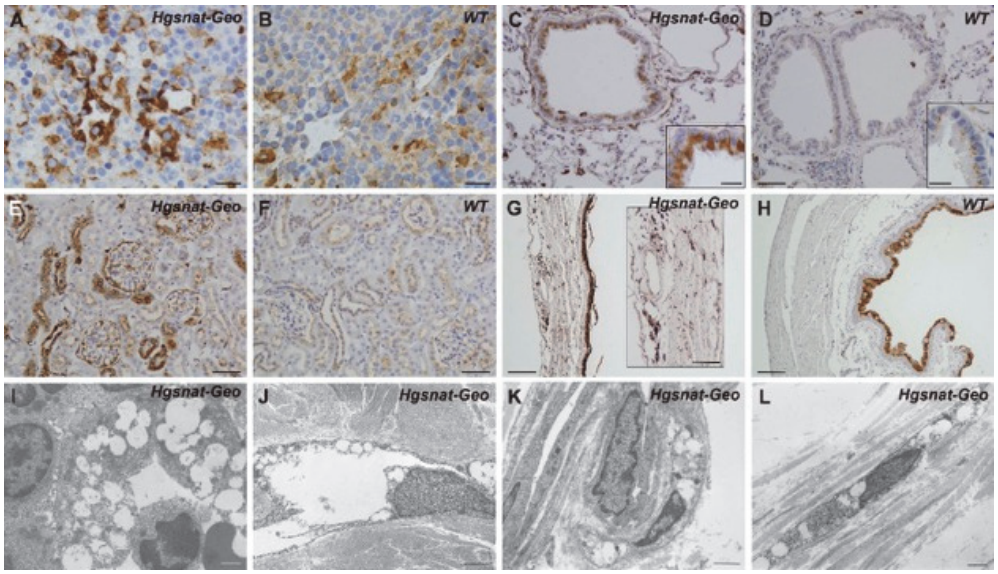


**Figure S5:** Widespread lysosomal storage in epithelial and mesenchymal cells in *Hgsnat-Geo* mice. CathD immunostaining of lysosomal system (A-H) and electron microscopy of selected cell types (I-L). Lysosomal system was expanded and activated in splenic sinus endothelium (A) and less so in bronchial respiratory epithelium (C), as well as in distal tubules, collecting ducts and glomeruli of renal cortex (E) of 12-month-old *Hgsnat-Geo* mice. Tissues of age-matching wild type animals (B, D and F) do not show these features. (G) A thin wall of distended urinary bladder of a 12-month-old *Hgsnat-Geo* mouse with a sparse presence in lamina and muscularis propria and adventitia of cells with expanded cytoplasm strongly positive for CathD. (H) Urinary bladder of age-matching wild type animal has normal wall thickness and structure. Inserts show detailed views of the cells. Electronlucent vacuoles surrounded by single membranes indicative of lysosomal storage of soluble material were detected in splenic sinus endothelium (I), skin vascular endothelial cells (J), perivascular pericytes (K) and fibroblasts (L) of 12-month-old *Hgsnat-Geo* mice. Bars in A, B and Insert C represent 30 μm, bars in C-F and Insert G, 100μm, bars in G and H, 200 μm. Bars in I and L represent 1 μm, bars in J and K, 2 μm.

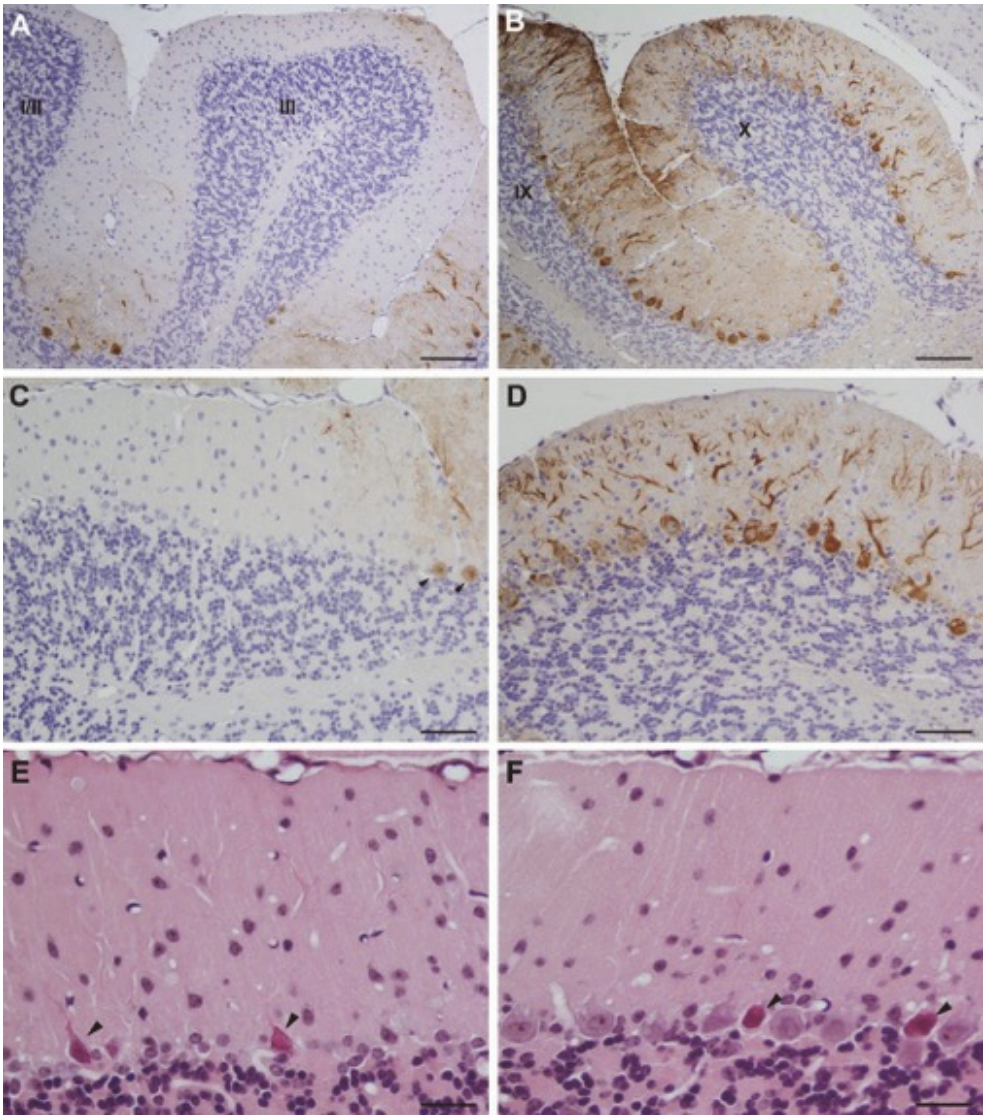


**Figure S6:** Purkinje cell loss in the anterior cerebellar lobe of *Hgsnat-Geo* mouse at the age of 12 months. (A-D) Calbindin immunostaining in the cerebellar cortex. Staining for Purkinje cells is almost absent in lobules I-III (A) when compared to remaining calbindin staining in lobules IX and X (B). Higher magnification of cerebellar cortex shows an exceptional presence of weakly positive Purkinje cells (marked by arrowheads) in the lobule III (C) and a substantially preserved Purkinje cell layer in the lobule X (D). Bars in A and B represent 200 μm, bars in C and D, 100 μm. (E-F) Details of the Purkinje cells layer, H&E staining. Purkinje cells are largely absent in the lobule III (E) in comparison to almost contiguous monolayer of Purkinje cells in the lobule X (F). Degenerating neurons with a shrunken condensed cytoplasm and nuclei are marked by arrowheads. Bars represent 50 μm.

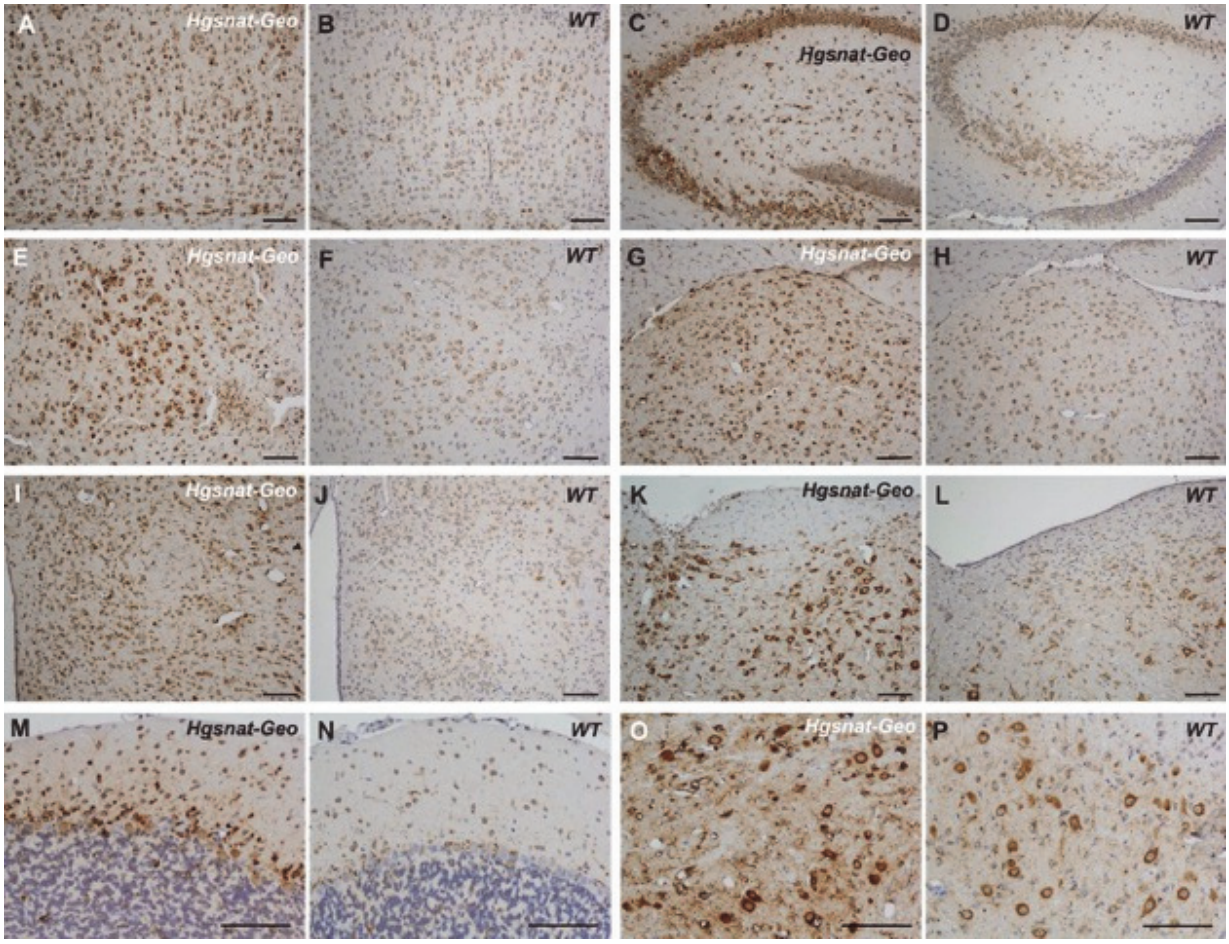


**Figure S7:** Increased CathD immunostaining in neurons compatible with lysosomal storage in *Hgsnat-Geo* mice as compared with relatively weak staining in wild type littermates was observed in in neocortex (A, B), hippocampus (C, D), amygdala (E, F), thalamus (G, H), hypothalamus (I, J), pons (K, L), cerebellar cortex (M, N) and cerebellar nuclei (O, P). Panels A-L show brains of 12-month-old *Hgsnat-Geo* and wild type mice; panels M-P show brains of mice at the age of 5 months before extensive degeneration of Purkinje cells is detected. Bars represent 100 µm.

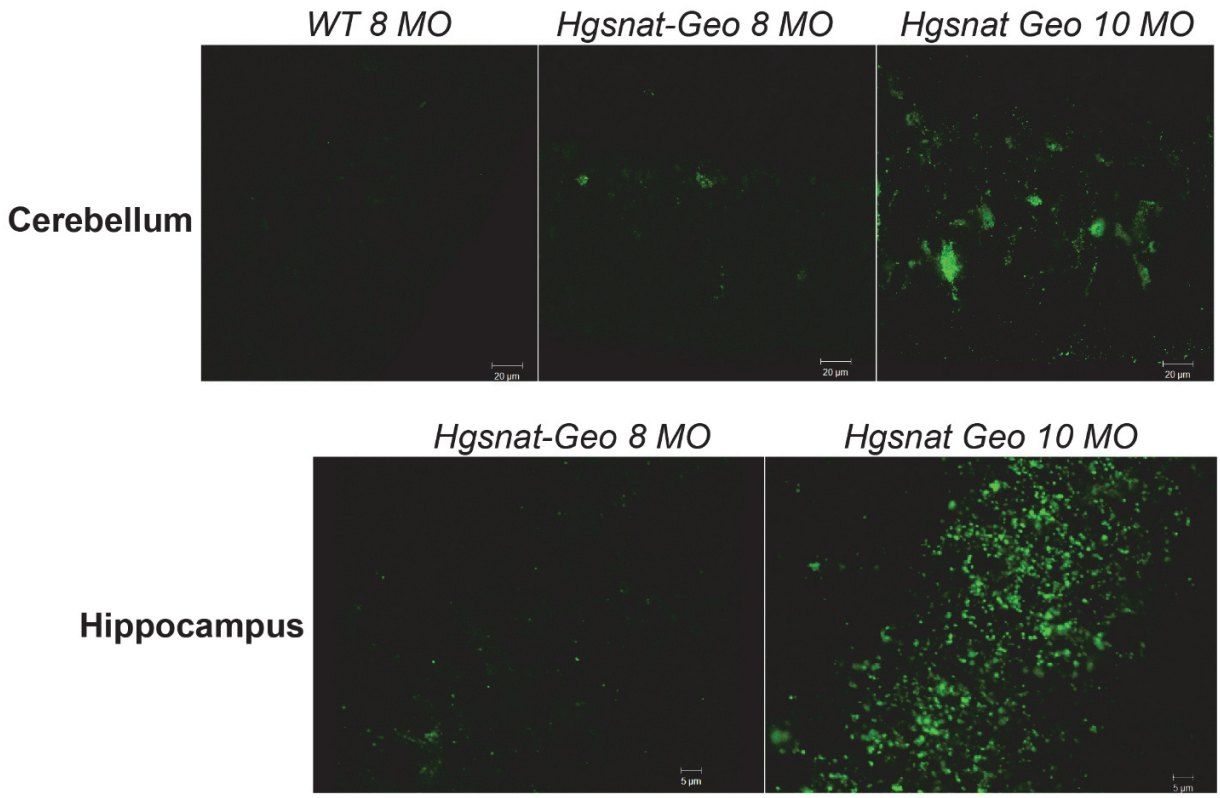


**Figure S8:** Progressive accumulation of GM2 ganglioside was detected in the hippocampus and cerebellum of *Hgsnat-Geo* mice. Bars represent 20 µm (cerebellum) and 5 µm (hippocampus).

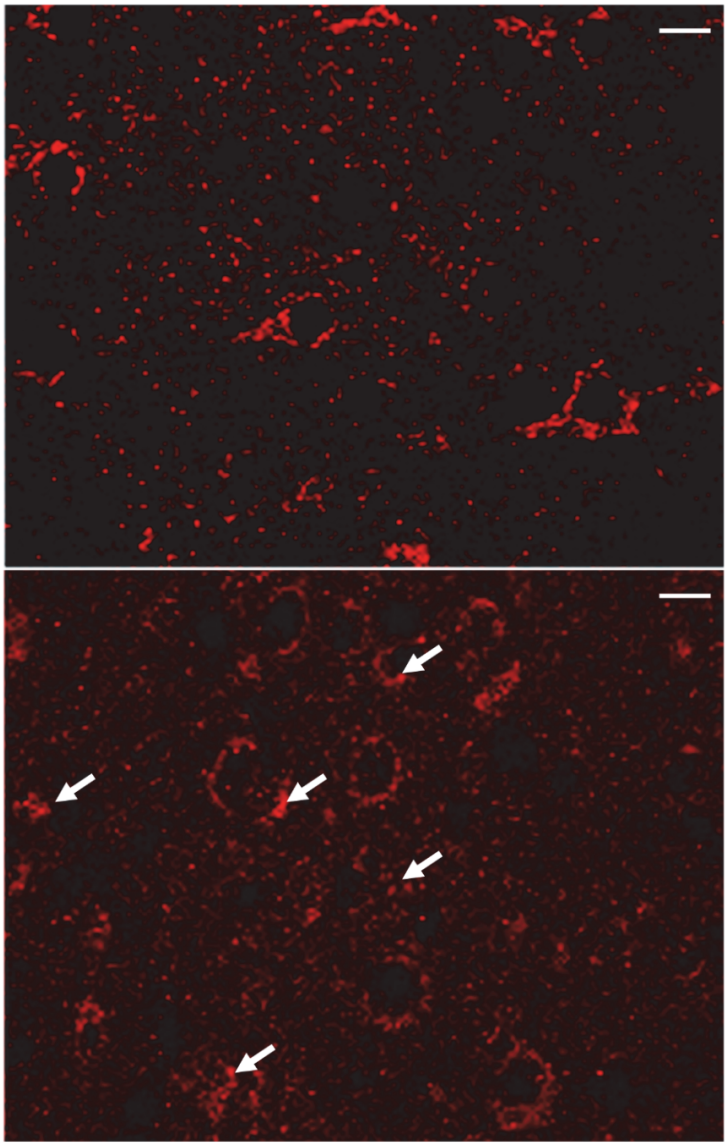

**Figure S9:** Mitochondrial network show signs of disorganization in cortical neurons of *HGSNAT-Geo* mice. Forty µm-thick sagittal brain sections of 8-month-old wild type and *HGSNAT-Geo* mice were stained with mitochondrial marker, cytochrome c oxidase subunit 4 (Cox4). Slides were studied on a Zeiss LSM510 inverted confocal microscope. Arrows show collapsed mitochondria in neurons of *Hgsnat-Geo* mouse.

Panels show representative images of at least 30 studied for 3 *Hgsnat-Geo* and 3 wild type mice for each age. Bars represent 10 µm.

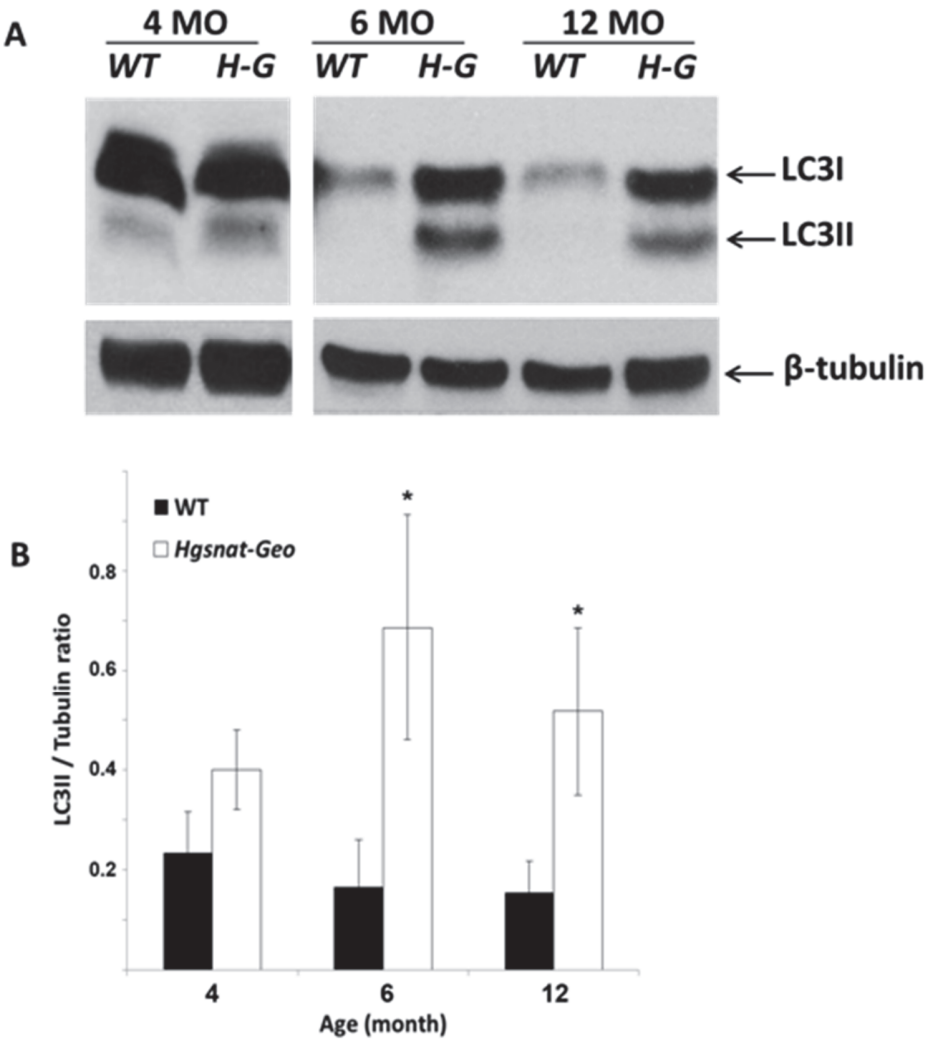


**Figure S10:** Increase of LC3-II in liver tissues of *Hgsnat-Geo* mice suggestive of impaired autophagy. Livers of 4, 6 and 12-month-old Hgsnat-Geo and wild type mice were homogenized in RIPA buffer. Protein extracts were analyzed by Western blot using antibodies specific for mouse LC3 and β-tubulin as a loading control.

A. Panel shows representative data of 3 independent experiments.

B. Graph shows ratios (means and S.D.) of signal intensities for LC3-II and β-tubulin estimated with ImageQuant software. Bars show mean values ±S.D., n=3. *$p$<0.05 in unpaired two-tailed t-test.

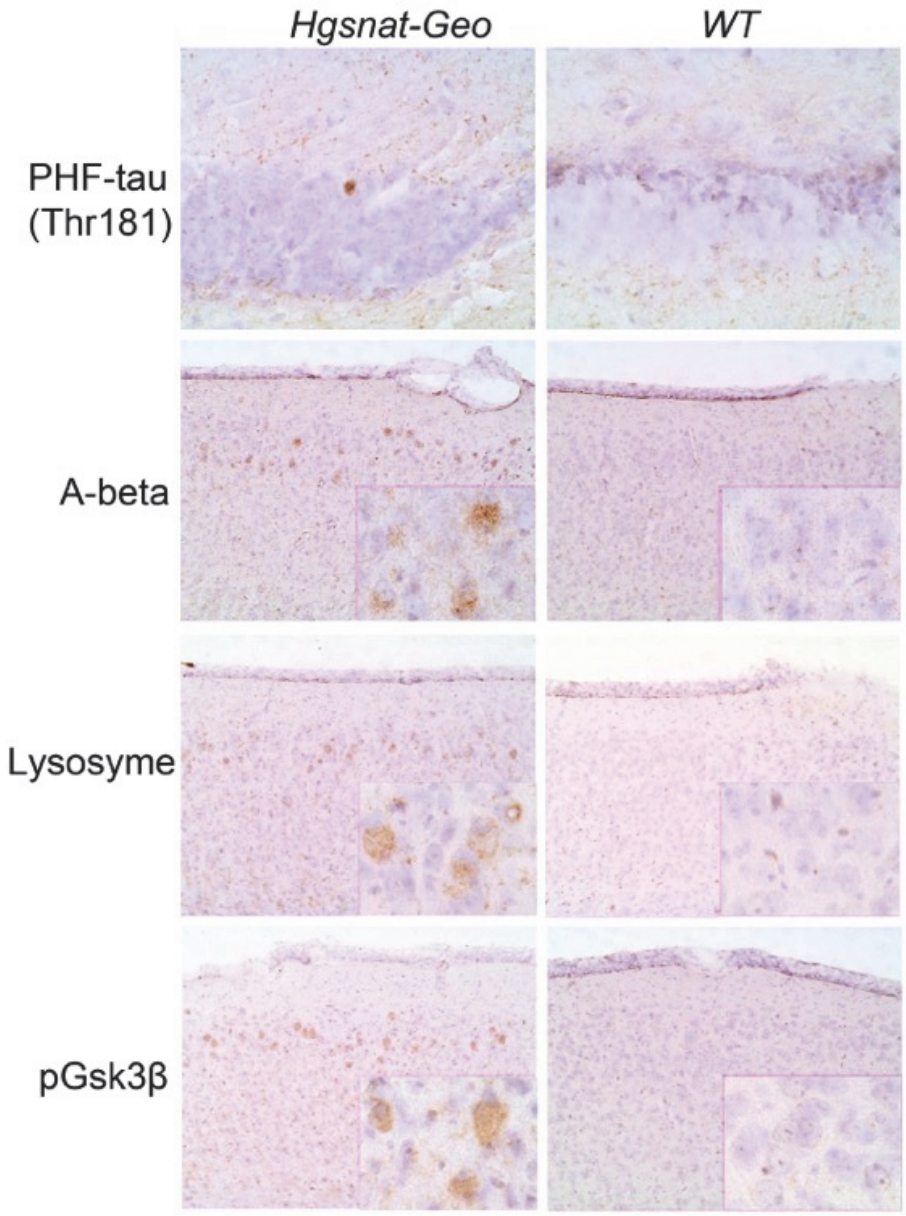


**Figure S11**: Accumulation of brain protein markers of neurodegeneration associated with dementia: lysozyme, beta amyloid (A-beta), and Ptau kinase Gsk3β in MEnt and phosphorylated tau (PHF-tau Thr181) in dentate gyrus of 10-month-old *Hgsnat-Geo* mice. Bars represent 100 µm; bars in the inserts, 30 µm.

The supplementary videos are available at the journal's website.
https://academic.oup.com/brain/article/138/2/336/293428#supplementary-data

# Chapter III: Molecular characterization of a large group of Mucopolysaccharidosis type IIIC patients reveals the evolutionary history of the disease

**(Manuscript published in *Human Mutation*, August 2019)**

## 3.1 Context

Despite the discovery of the causative gene in 2006, the characterization of molecular defects in MPS IIIC patients and the knowledge of the mutation spectrum and frequency in different populations and geographic locations is still limited.

In this chapter, we aimed the molecular characterization of newly clinical and biochemically diagnosed MPS IIIC patients from different geographic origins, confirming the pathogenicity of six novel *HGSNAT* variants through *in sillico* analysis and/or functional studies. The haplotype study of the largest group of Sanfilippo C patients studied so far, including the 27 new and 51 previously reported, enabled getting insights into the origin and evolution of several *HGSNAT* disease-associated variants, including the existence of founder effects. The characterization of the clinical history in the large cohort of new patients contributed to the knowledge of the natural history of the disease and provided a possibility to correlate the genotype with the clinical phenotype. The manuscript with the results of this study was published in the journal Human Mutation in August 2019 (***Hum Mutat.*** 2019 Aug;40(8):1084-1100. doi: 10.1002/humu.23752. Epub 2019 Jun 22. PMID: 31228227), being selected as an Editor's choice research article.

The supplementary tables are available at the journal website:
https://onlinelibrary.wiley.com/doi/10.1002/humu.23752

## 3.2 Author contributions

Carla Martins conceptualized and designed the study. CM performed all experimental procedures except collecting the clinical and biochemical data on the new MPS IIIC patients (uGAGs and HGSNAT activity in patients' fibroblasts and leukocytes) done by Paula Frassinetti V. de Medeiros, Roberto Giugliani, Sandra Leistner-Segal, Nursel Elcioglu, Jill Wood, Mahdiyeh Behnam, Bilge Noyan, Lucia Lacerda and Michael T. Geraghty; the functional study of p.N258I variant performed by Larbi Dridi; and the genotyping of patient Alg1, done by Laboratoire de Biochimie Métabolique, CHU de Rouen, France. CM has analyzed all data, wrote and revised the final version of the manuscript.
Alexey V. Pshezhetsky, Roberto Giuliani and Damian Labuda supervised the study, and revised the manuscript with participation of all authors.

An image, based on this research, was also chosen as back cover of the journal's issue of August 2019 (https://onlinelibrary.wiley.com/doi/10.1002/humu.23893).

Carla Martins conceptualized and designed the image, under supervision of Alexey V. Pshezhetsky. Map adapted from http://d-maps.com.

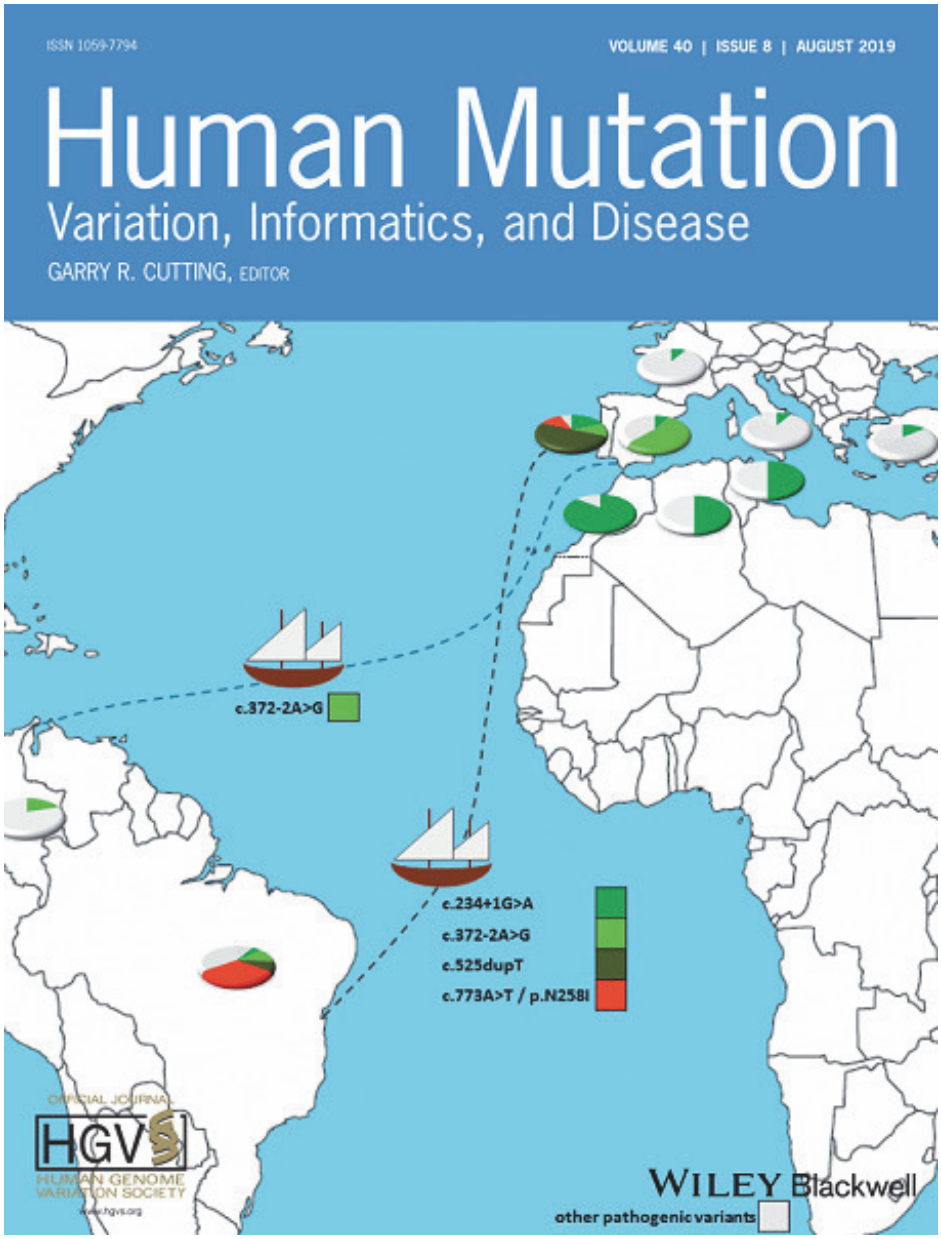


The figure depicts the probable migration routes of the *HGSNAT* pathogenic variants c.234+1G>A, c.372−2G>A, c.525dupT and c.773A>T from the Iberian Peninsula into South America.

# Molecular characterization of a large group of Mucopolysaccharidosis type IIIC patients reveals the evolutionary history of the disease

Carla Martins[1,2], Paula Frassinetti V. de Medeiros[3], Sandra Leistner-Segal[4], Larbi Dridi[2], Nursel Elcioglu[5], Jill Wood[6], Mahdiyeh Behnam[7], Bilge Noyan[5], Lucia Lacerda[8], Michael T. Geraghty[9], Damian Labuda[2], Roberto Giugliani[4] and Alexey V. Pshezhetsky[1,2]

[1]Department of Biochemistry and Molecular Medicine, Université de Montréal, Montreal, Quebec, Canada

[2]Research Center, CHU Sainte-Justine, Université de Montréal, Montreal, Quebec, Canada

[3]Hospital Universitário Alcides Carneiro-HUAC, Federal University of Campina Grande, Campina Grande, Paraiba, Brazil

[4]Department of Genetics, UFRGS, Medical Genetics Service, Hospital de Clínicas de Porto Alegre-HCPA, and Brazilian National Institute of Population Medical Genetics-INAGEMP, Porto Alegre, Brazil

[5]Department of Pediatric Genetics, Marmara University Hospital, Istanbul, Turkey

[6]Jonah's Just Begun-Foundation to Cure Sanfilippo Inc, Brooklyn, New York, USA

[7]Medical Genetics Center of Genome, Isfahan, Islamic Republic of Iran

[8]Biochemical Genetics Unit, Institute of Medical Genetics Jacinto Magalhães, Centro Hospitalar do Porto, Porto, Portugal

[9]Department of Pathology and Laboratory Medicine, Children's Hospital of Eastern Ontario, Ottawa, Canada

## 3.3 Abstract

Mucopolysaccharidosis type IIIC (MPSIIIC) is a severe, rare autosomal recessive disorder caused by variants in the heparan-α-glucosaminide N-acetyltransferase (HGSNAT) gene which result in lysosomal accumulation of heparan sulfate. We analyzed clinical presentation, molecular defects and their haplotype context in 78 (27 novel) MPSIIIC cases from 22 countries, the largest group studied so far. We describe for the first time disease-causing variants in the patients from Brazil, Algeria, Azerbaijan, and Iran, and extend their spectrum within Canada, Colombia, Turkey, and the USA. Six variants are novel: two missense, c.773A>T/p.N258I and c.1267G>T/p.G423W, a nonsense c.164T>A/p.L55*, a splice-site mutation c.494−1G>A/p.[P165_L187delinsQSCYVTQAGVRWHHLGSLQALPPGFTPFSYLSLLSSWNC,P165fs], a deletion c.1348delG/p.(D450fs) and an insertion c.1479dupA/p.(Leu494fs). The missense HGSNAT variants lacked lysosomal targeting, enzymatic activity, and likely the correct folding. The haplotype analysis identified founder mutations, p.N258I, c.525dupT, and p.L55* in the Brazilian state of Paraiba, c.493+1G>A in Eastern Canada/Quebec, p.A489E in the USA, p.R384* in Poland, p.R344C and p.S518F in the Netherlands and suggested that variants c.525dupT, c.372−2G>A, and c.234+1G>A present in *cis* with c.564-98T>C and c.710C>A rare single-nucleotide polymorphisms, have been introduced by Portuguese settlers in Brazil. Altogether, our results provide insights into the origin, migration roots and founder effects of *HGSNAT* disease-causing variants, and reveal the evolutionary history of MPSIIIC.

## 3.4 Introduction

Mucopolysaccharidosis type IIIC or Sanfilippo syndrome type C (MPSIIIC; MIM# 252930) is a rare childhood autosomal recessive disorder caused by mutations in the *HGSNAT* gene, resulting in a deficiency of heparan sulfate acetyl-CoA: α-glucosaminide N-acetyl-transferase (HGSNAT, EC 2.3.1.78) enzyme. HGSNAT is responsible for the transmembrane acetylation of glucosamine residues of lysosomal heparan sulfate (HS) allowing its further catabolism.

The deficiency of HGSNAT causes accumulation of HS in the lysosomes, which leads to progressive neurodegeneration, characteristic behavioral abnormalities and a severe progressive cognitive decline in the patients typically leading to dementia. The disease has an onset in early childhood with death generally occuring before the third decade (Valstar, Ruijter, vanDiggelen, Poorthuis, &Wijburg,2008). Nonspecific treatment is currently available. However, recent advances in understanding the disease pathology (Martins *et al.*, 2015) and preclinical research (Tordo *et al.*, 2018) suggested several promising strategies for development of therapies (Gaffke, Pierzynowska, Piotrowska, & Wegrzyn, 2018; Scarpa *et al.*, 2017).

So far 65 disease-causing variants have been identified in MPSIIIC patients, 28 of them missense. Expression studies showed that resulting amino acid substitutions led to the synthesis of misfolded proteins, unable to escape the endoplasmatic reticulum quality control and reach the lysosomes (Fedele & Hopwood, 2010; Feldhammer, Durand, & Pshezhetsky, 2009). Abnormal RNA splicing, shifts of translation frame and premature termination codons (PTCs) introduced by remaining mutations result in transcripts likely eliminated by the nonsense-mediated messenger RNA (mRNA) decay (NMD) pathway, which explains the negligible enzyme activity detected in patients' cells and functional studies (Feldhammer, Durand, Mrazova, *et al.*, 2009; Feldhammer, Durand, & Pshezhetsky, 2009). Four amino acid substitutions identified in MPSIIIC patients typically in *cis* with splicing or nonsense mutations were considered neutral polymorphisms because the corresponding protein variants showed activity levels comparable to those of the wild-type (WT) enzyme (Feldhammer, Durand, & Pshezhetsky, 2009). Finally, molecular defects in HGSNAT causing partial enzyme deficiency (~30% of healthy control levels) have been recently associated with non-syndromic retinitis pigmentosa (Haer-Wigman *et al.*, 2015).

Mutations in the *HGSNAT* gene have been identified in MPSIIIC patients from several countries in Europe (Belarus, Belgium, Czech Republic, Finland, Germany, Greece, Ireland, Italy, Poland, Portugal, Spain, the Netherlands, and the UK), North Africa (Morocco and Tunisia), Asia (Turkey, Pakistan, Singapore, and South Korea), North (Canada and USA; Ali Pervaiz *et al.*, 2011; Canals *et al.*, 2011; Coutinho *et al.*, 2008; Fan *et al.*, 2006; Fan, Tkachyova, Sinha, Rigat, & Mahuran, 2011; Fedele & Hopwood, 2010; Fedele *et al.*, 2007; Feldhammer, Durand, Mrazova, *et al.*, 2009; Hrebicek *et al.*, 2006; Hu *et al.*, 2017; Huh *et al.*, 2013; Matos *et al.*, 2014; Ouesleti *et al.*, 2011, 2017; Ruijter *et al.*, 2008) and South America (Argentina and Colombia; Canals *et al.*, 2011; Velasco *et al.*, 2017). Approximately 30% of all MPSIIIC variants are shared between different populations suggesting the existence of a common ancestor. Besides, certain mutations are present at a relatively high frequency in some geographic regions of Italy, Portugal, the Netherlands, and Colombia possibly due to founder effects (Coutinho *et al.*, 2008; Fedele *et al.*, 2007; Ruijter *et al.*, 2008; Velasco *et al.*, 2017).

To verify these hypotheses and to investigate the origin and subsequent fate of *HGSNAT* disease-causing variants, we analyzed their background haplotypes in the largest group of MPSIIIC patients studied so far including 25 novel index cases. Our results revealed variants with common ancestor haplotypes and the existence of several founder mutations, which can facilitate targeted screening efforts in the concerned populations.

## 3.5 Patients and methods

### Patients and sample collection

Ethical approval for the study was provided by the institutional review board at Sainte-Justine Hospital Research Center (CHUSJRC). Written informed consent was obtained from the parents of the patients or their legal representatives.

We studied 27 individuals clinically diagnosed with MPSIIIC from 25 families originating from Brazil (n = 14), Turkey (n =5), USA (n =2), Algeria (n =1), Azerbaijan (n =1), Canada (n = 1), Colombia (n =1), Iran (n =1), and Portugal (n = 1). Clinical and laboratory information including the activity levels of lysosomal enzymes in blood leukocytes or cultured skin fibroblasts, as well

the levels of urinary glycosaminoglycans was provided by the referring physicians or the parents of the patients.

Genomic DNA was extracted from the blood of patients and, when possible, of parents using DNeasy Blood & Tissue Handbook kit (Qiagen, Toronto, ON, Canada). The genomic DNA of the Canadian patient (Can1) was extracted from her cultured skin fibroblasts provided by the Genetics Diagnostic Laboratory of Children's Hospital of Eastern Ontario.

**Genotyping**

DNA fragments corresponding to the *HGSNAT* exons and their flanking intronic regions (~40 bp from each side), 3′-untranslated region (3′-UTR) and two extragenic fragments containing the single-nucleotide polymorphisms (SNPs) rs11784974 and rs4737089 were amplified by polymerase chain reaction (PCR) using genomic DNA as a template. Sanger sequencing was performed as previously described (Hrebicek *et al.*, 2006) using the 3730xl DNA Analyzer (Applied Biosystems, Carlsbad, CA) at the McGill University Quebec Innovation Centre. Nineteen fragments spanning a region of 87.1Kb were amplified for each of the new MPSIIIC patients, as well as for the 52 MPSIIIC patients previously reported by our group (Feldhammer, Durand, Mrazova, *et al.*, 2009; Hrebicek *et al.*, 2006; Ruijter *et al.*, 2008). Sequences of additional primers are shown in Table S7.

The Human genome assembly GRCh37/hg19 (Genome Reference Consortium) was used as a reference. Nucleotide (complementary DNA [cDNA]) and protein sequence variations were called according to RefSeq NM_152419.2 and NP_689632.2, respectively, and HGVS recommendation (http://varnomen.hgvs.org/). The novel variants were submitted to the *HGSNAT* gene homepage-Global Variome shared LOVD (https://databases.lovd.nl/shared/genes/HGSNAT).

The variants were identified at CHUSJRC with the exception of those for the Canadian, Portuguese and USA1 patients that were diagnosed by Genetics Diagnostic Laboratory in Children's Hospital of Eastern Ontario (Canada), Centro hospitalar do Porto (Portugal) and Greenwood Genetic Centre (Greenwood, SC), respectively, and further verified in CHUSJRC. Except for the Brazilian and Colombian patients (for which DNA sample of the parents was not available), all variants were

confirmed by analyzing parental DNA. For the Algerian patient, the variants were identified in Laboratoire de Biochimie Métabolique, CHU de Rouen (France).

**RNA extraction and analysis**

Total RNA was isolated from cultured skin fibroblasts using the TRIzol® reagent (Invitrogen, Burlington, ON, Canada) according to the manufacturer's protocol, and reverse-transcribed to cDNA using SuperScript® III reverse transcriptase (Invitrogen). For splicing analysis of *HGSNAT* mutation c.494−1G>A, a fragment encompassing exons 4–6 was amplified by PCR from the cDNA of the patient and a healthy control (Table S7 for the sequences of primers). The amplified fragments were analyzed by Sanger sequencing. *RLP32* cDNA was used as a control.

**Site-directed mutagenesis**

The plasmids expressing missense *HGSNAT* alleles were obtained by site-directed mutagenesis of previously reported pCTAP-*HGSNAT* plasmid (Feldhammer, Durand, & Pshezhetsky, 2009) encoding the WT long splicing variant of the human *HGSNAT* cDNA using QuickChange Lightning kit (Stratagene, La Jolla, CA). The sequences of primers used are shown in Table S7.

**Expression of recombinant HGSNAT and western blot analysis**

COS-7 cells, cultured in Eagle's minimal essential medium (Invitrogen) supplemented with 10% fetal bovine serum (Wisent Inc., St-Bruno, QC, Canada), and 1% antibiotic-antimycotic (Life Technologies, Burlington, ON, Canada) were transfected with the plasmids encoding WT HGSNAT and its variants with amino acid substitutions using Lipofectamine 2000 (Invitrogen) by the manufacturer's protocol. Nontransfected COS-7 cells were used as a control. The cells were harvested 48 hr post-transfection and homogenized by sonication (3 × 10 s) in ddH2O for measurement of N-acetyltransferase activity. Proteins were resolved by sodium dodecyl sulfate polyacrylamide gel electrophoresis (SDS-PAGE) on an 8% gel and transferred to a nitrocellulose membrane. HGSNAT was detected using a primary rabbit polyclonal antibody against an N-terminal epitope (Q52 to N156) of human HGSNAT (HPA029578, 1:1,000; Sigma-Aldrich,

Oakville, ON, Canada) followed by an horseradish peroxidase (HRP)-conjugated secondary anti-rabbit antibody (1:3,000; Invitrogen). Anti-α-tubulin antibody (12G10, 1:800; DSHB, Iowa City, IA, USA) was used as a control. The signal, developed by incubation with Pierce® ECL Western blot analysis Substrate (Thermo Fisher Scientific Inc., Rockford, Il), was detected by X-ray film (Agfa HealthCare NV, Mortsel, Belgium).

**Enzyme assays**

N-acetyltransferase and total β-hexosaminidase enzyme activities in cell homogenates were measured using fluorogenic 4-methylumbelliferyl β-D-glucosaminide (Moscerdam, Rotterdam, The Netherlands) and 4-methy-lumbelliferyl N-acetyl β-D-glucosaminide (Sigma-Aldrich) substrates as described (Ausseil *et al.*, 2004; Feldhammer, Durand, & Pshezhetsky, 2009). Proteins were quantified using the Bradford method.

**Immunocytochemistry**

COS-7 cells cultured on glass slides in six-well plates until ~70%confluency were transfected with plasmids coding for the WT HGSNAT or its mutants, as described above. Forty-eight hours after transfection the cells were incubated with LysoTrackerTM Red DND-99 (Thermo Fisher Scientific, Mississauga, ON, Canada) for 1 hr at 37°C, washed with ice-cold phosphate-buffered saline (PBS) and fixed with 4% paraformaldehyde and 4% sucrose in PBS for 5 min. Cells were then permeabilized by 0.25% (v/v) Triton X-100 in PBS for 10 min and blocked for 1 hr in 3% horse serum and 0.1% Triton X-100 in PBS. HGSNAT localization was assessed by staining with the antibody against an epitope at the N-terminal peptide of HGSNAT (HPA029578; Sigma-Aldrich) followed by anti-rabbit IgG Alexa 488-labeled antibody (Thermo Fisher Scientific). The images were captured by LSM510 Meta Laser (Carl Zeiss MicroImaging GmbH, Jena, Germany) or Leica TCS SPE (Leica Microsystems CMS GmbH, Mannheim, Germany) confocal microscopes (×63 glycerol immersion objectives, N.A. 1.4) and processed using the LSM image browser software (Carl Zeiss) or the ImageJ software (U.S. National Institutes of Health, Bethesda, MD).

**Haplotype analysis**

Haplotypes were obtained by studying common SNPs, with minor allele frequencies (MAF) equal to or above 1% in control populations, which were polymorphic in the group of 78 MPSIIIC patients studied. Haplotypes were either directly inferred from the genotypic data of the patients and their relatives and/or deduced in silico by PHASE 2.1.1 software (www.stat.washington.edu/stephens/software.html). Phylogenetic haplotype networks based on these SNPs were calculated both for the phased data from MPSIIIC patients (in the case of consanguinity, only one allele was considered) and nine control populations of 1000 Genomes project (http://www.internationalgenome.org, Phase 3 data set). The following populations were studied: Utah Residents (CEPH) with Northern and Western European Ancestry/CEU, Finnish in Finland/FIN, British in England and Scotland/GBR, Iberian Population in Spain/IBS, Tuscany in Italy/TSI, Punjabi from Lahore, Pakistan/PJB, Han Chinese in Beijing, China/CHB, Colombians from Medellin, Colombia/CLM and Yoruba in Ibadan, Nigeria/YRI.

The pairwise fixation index (Fst) between patients grouped according to geographic origin and controls was calculated using Arlequin 3.5.2.2 software (Excoffier & Lischer, 2010) as a measure of genetic distance. The resulting matrix of values for 1,000 interpolations was converted to a two-dimensional plot using IBM SPSS Statistics for Windows, Version 25.0 (IBM Corp., Armonk, NY) multidimensional Scaling (MDS).

**Statistical analysis**

The data were analyzed by Student's t test or one-way analysis of variance (ANOVA) followed by Tukey's post-hoc multiple comparison test using the GraphPad Prism software (GraphPad Software, Inc., San Diego, CA). A p value of 0.05 or less was considered significant.

## 3.6 Results and discussion

### Clinical findings in the new MPSIIIC patients

This study reports 27 previously undescribed MPSIIIC patients (25 family index cases) from nine countries: Brazil, Portugal, Colombia, Algeria, Turkey, Azerbaijan, Iran, USA, and Canada (Table 1). The clinical and family histories, as well as the geographic origin of the patients, are described in Table S1A. On average, patients were 3.5 years old at the time of the onset of clinical symptoms and 11.1 years old at the time of clinical diagnosis.

The earliest detected symptoms were hyperactivity (in 50% of the cases), speech problems including delay in acquisition of the first words (30%) and sentences (44.4%), and cognitive problems (25%; Figure 1). Initial motor development was normal, with independent walking milestone achieved on average by 18 months (Table S1B). Over the disease course the most frequent symptoms were hyperactivity (22/23 patients), aggressiveness (17/19), lack of attention (19/19), neurocognitive deficiency (21/21), macrocephaly (19/21), speech (18/19) and motor problems (17/19), lack of sphincter control (16/19), coarse facial features (16/21), and sleep disturbances (15/19). Recurrent ear and nose infections (13/16) and hypertrichosis (11/11) were also frequently detected while hepatomegaly (10/16), dysostosis multiplex (9/17) and diarrhea (9/16) were reported only for several patients. Tonsillectomy and/or adenoidectomy was performed on nine patients of 19. Epilepsy was detected in 8/19 patients. Short stature, hypoacusia, inguinal and umbilical hernias, and heart problems (mitral insufficiency and inter-auricular communication) were also found but at a lower frequency (Table S1A). The loss of speech (on average at 10 years) was followed by a decline of motor abilities, with incapacity to walk without support by 11–27 years (Table S1C and Figure 1c). Three patients were deceased at the time of the study at the age between 15.8 and 22 years.

Consanguinity was reported for 10 families; six of them were from Turkey, Azerbaijan, and Iran consistent with the high rate of consanguineous marriages in Western Asia (Tuncbilek & Koc, 1994).

**Novel *HGSNAT* pathogenic variants in MPSIIIC patients**

Altogether we identified 18 variants affecting HGSNAT, six of them novel: one nonsense (c.164T>A/p.Leu55Ter), a splice-site (c.494−1G>A/p.[Pro165_Leu187delinsGlnSerCysTyrValThrGlnAlaGlyValArgTrpHisHisLeuGlySerLeuGlnAlaLeuProProGlyPheThrProPheSerTyrLeuSerLeuLeuSerSerTrpAsnCys,Pro165Leufs*13]), a deletion, (c.1348delG/p.(Asp450 Ilefs*32)), an insertion (c.1479dupA/p.(Leu494Ilefs*33)), and two mis-sense changes, (c.773A>T/p.Asn258Ile and c.1267G>A/p.Gly423Trp; Table 1). A pathogenic effect was predicted by Mutation Taster software for all variants and by Polyphen2, Provean, and SIFT for the missense changes (Table S2A). Novel nonsense variant c.164T>A/p.Leu55Ter, in *HGSNAT* exon 2, was identified in three Brazilian patients from two families from the state of Paraiba. Two siblings from a consanguineous family are homozygous for the mutation (Br1, Br2; Figure S1A) while the third patient from another family is a compound heterozygote (Br3; Table 1). The substitution of thymidine by adenine at the nucleotide position 164 leads to the introduction of a PTC with probable degradation of the resulting transcript by NMD. The variant is not present in any database including the dbsnp (https://www.ncbi.nlm.nih. gov/projects/SNP/) and Genome Aggregation Database (gnomAD, http://gnomad.broadinstitute.org/), the last containing approximately 123,000 exome and 15,500 genome sequences from Exome Aggregation Consortium (Lek *et al.*, 2016), 1,000 Genomes project (1000 Genomes Project Consortium, 2012) and other sources.

A novel splice-site change, c.494−1G>A/p.[Pro165_Leu187delinsGlnSerCysTyrValThrGlnAlaGlyValArgTrpHisHisLeuGlySerLeuGlnAlaLeuProProGlyPheThrProPheSerTyrLeuSerLeuLeuSerSerTrpAsn-Cys,Pro165Leufs*13] detected in a homozygous Canadian patient (Can1) from a consanguineous family affects the conserved consensus sequence of the splice acceptor site in intron 4 (Figure S2 and Table 1). Both human splicing finder 3.1 and Netgene2 v2.4 software predicted that the substitution of a G by an A at this position was likely to cause loss of the natural acceptor site with skipping of exon five during pre-mRNA splicing (Table S2). To verify this experimentally, we analyzed whether the mutation affects mRNA synthesis. The analysis of a PCR-amplified fragment corresponding to exons 4–6 in the cDNA synthesized from the patient's and control fibroblasts RNA confirmed that the mutation causes exon five skipping during pre-mRNA splicing (182 bp PCR-amplified cDNA fragment in Figure S2B) and

introduces alternative acceptor and donor sites in intron 6 (300 bp PCR-amplified fragment in Figure S2B). The exon five skipping causes frameshift/PTC (p.Pro165Leufs*13), whereas cryptic splicing presumably results in deletion of 23 (from Pro165 to Leu187) amino acids corresponding to the first transmembrane HGSNAT domain, and insertion of 39 new amino acid residues. Such predictions are consistent with a complete absence of HGSNAT enzymatic activity in the patient's cultured skin fibroblasts (Figure S2A).

The deletion of guanine in exon 13, corresponding to the cDNA nucleotide 1348, c.1348delG/p.(Asp450Ilefs*32), was identified in homozygosity in two Brazilian patients (Br8 and Br9) whose families are not aware of consanguinity (Figure S1C and Table 1). This variant (rs771455190) was also detected in 1 of 15,096 African alleles but absent in all other populations of gnomAD, suggesting a frequency of $4.1 \times 10{-}6$ in the total population. The deletion causes a frameshift and introduces a PTC.

The novel *HGSNAT* insertion c.1479dupA/p.(Leu494Ilefs*33) was detected in a homozygous Turkish patient (Trk5) from a consanguineous family and confirmed to be present in both parents (Figure S1F and Table 1). The insertion of adenine in exon 15 at position 1479 of cDNA leads to a frameshift starting from Leu494 and introduction of a PTC 98 nucleotides downstream of the insertion. The mutation is not present in any database including dbsnp and gnomAD.

The missense mutation c.773A>T/p.Asn258Ile was detected in five Brazilian patients (two homozygous, Br6 and Br7, and three compound heterozygous, Br3, Br4, Br5; Table 1 and Figure S1B) and is not present in any sequence database. The transition of adenine to thymine in exon 8 of *HGSNAT* at the position 773 leads to the substitution of the Asn258 by Ile. The Asn258 residue is located in the second predicted transmembrane domain (TM2) of the HGSNAT protein. The amino acid sequence of this domain including Asn258 is highly conserved in HGSNAT homologs throughout the animal kingdom (Figure S3). It is likely that the substitution of the polar glutamine by the hydrophobic isoleucine residue disrupts the structure of the transmembrane α-helix domain and affects overall conformation of the protein.

The second new missense mutation identified in this study is a guanine to adenine transition in exon 13 at position 1267 of the cDNA leading to the substitution of glycine at the position 423 by a tryptophan residue (c.1267G>T/p.Gly423Trp). The mutation was detected in a patient from USA (USA1) in compound heterozygosity (Figure S1D) accompanied by the missense substitution

c.518G>A/Gly173Asp (Table 1). Gly423 is located in the fourth lysosomal luminal domain of HGSNAT protein and is highly conserved across the animal kingdom (Figure S3). While the hydrogen atom confers flexibility and small size to glycine residue, the aromatic side chain of tryptophan is hydrophobic and rigid. Thus, the Gly423Trp substitution most probably affects the conformation and/or position of the luminal loop. The second mutation in the USA1 patient, c.518G>A/p.Gly173Asp, unreported at the time of identification but recently described in two MPSIIIC Turkish siblings (Hu *et al.*, 2017) affects the glycine residue located in the first transmembrane domain. TM1 is not highly conserved in animal species, and glycine at the position 173 is conserved only in mammals (Figure S3). Nevertheless, the substitution of glycine by the positively charged aspartic acid most likely disrupts the structure of the transmembrane α-helix.

**Impact of new missense mutations on HGSNAT protein**

To assess the impact of novel missense variants p.Gly173Asp, p.Asn258Ile, and p.Gly423Trp, we expressed the corresponding HGSNAT proteins in cultured COS-7 cells. The specific HGSNAT activity in all cells expressing mutants was reduced to below 3% of that in cells transfected with the WT plasmid, and was not significantly different from that in untransfected cells (Figure 2a). The homogenates were further analyzed by Western blot using a commercial polyclonal antibody against the N-terminal HGSNAT epitope to evaluate the level and processing of enzyme mutants (Figure 2b). The HGSNAT protein with the mass of 67 kDa (corresponding to the previously reported mass of nonglycosylated HGSNAT precursor with the TAP tag (Feldhammer, Durand, & Pshezhetsky, 2009) was detected in the cells expressing HGSNAT with amino acid substitutions, whereas the 77 kDa band, corresponding to the mass of glycosylated precursor, and the 29 kDa band corresponding to the mature N-terminal α-subunit of the enzyme, were observed in cells transfected with the WT plasmid, suggesting that the mutants lack lysosomal targeting and processing.

To verify if the mutant HGSNAT proteins were targeted to the lysosome, COS-7 cells transfected with plasmids encoding for the WT and mutant enzymes were incubated with the lysosomal marker dye LysoTrackerTM Red DND-99 and fixed. The cell localization of the HGSNAT protein was assessed by immunocytochemistry (Figure 2c). Analysis of cells by confocal microscopy showed that LysoTracker co-localized with WT HGSNAT protein but not with the mutants.

Together with drastically reduced expression levels of mutant proteins and the absence of enzymatic activity, this result is consistent with their misfolding, retention in the endoplasmic reticulum and proteasomal degradation, thus confirming the pathogenic effect of the mutations.

### *HGSNAT* mutation spectrum, allele frequencies and haplotypes

The frequency and worldwide distribution of the *HGSNAT* mutations in 25 new MPSIIIC index patients together with those previously reported (Ali Pervaiz *et al.*, 2011; Canals *et al.*, 2011; Coutinho *et al.*, 2008; Fan *et al.*, 2011, 2006; Fedele & Hopwood, 2010; Feldhammer, Durand, Mrazova, *et al.*, 2009; Hrebicek *et al.*, 2006; Hu *et al.*, 2017; Huh *et al.*, 2013; Matos *et al.*, 2014; Ouesleti *et al.*, 2011, 2017; Ruijter *et al.*, 2008; Velasco *et al.*, 2017) are summarized in Figure 3. The data show that Europe, South America, and Western Asia are so far the regions with the highest number of families reported with molecular diagnosis of MPSIIIC.

About one-third (23/71) of *HGSNAT* mutations are shared by patients from different populations. To investigate if these variants have the same origin and if higher frequencies of specific mutations in certain populations occur due to founder effects, we analyzed haplotypes of the 25 index cases reported in this study as well as of the 52 MPSIIIC patients previously described by our group (78 patients from 75 families in total, Tables S3 and S4). These haplotypes were compared with those of nine control populations reported in the 1000 Genomes Project.

We have analyzed DNA sequence corresponding to the 18 *HGSNAT* exons, their flanking intronic sequences, the 3′-UTR, and two extragenic fragments, representing in total 8.3 Kb and spanning over an 87.1 Kb region (Figure 4a) in all patients and, when possible, in their parents or other relatives. Besides 46 disease-causing mutations, 10 common polymorphic SNPs (MAF≥ 0.01 in control populations) and four rare variants of unknown biological significance were detected in the patients (Tables S3 and S4).

Based on the analysis of the 10 common polymorphic SNPs, we have identified 25 haplotypes (A–Y) in the control populations from the 1000 Genomes project, but only 13 had an overall frequency above 0.5%. The haplotypes L, R, and S were the most frequent and widely distributed in all populations except for the Africans, where L and S haplotypes were absent, and R and C haplotypes had the highest frequency. We observed that only 13 of these 25 haplotypes were present in the MPSIIIC patients along with a novel haplotype (Z) absent in controls (Figure 4a,b).

The ancestral haplotype was determined by sequence comparison with non-human primates (chimpanzee, gorilla, and orangutan). The haplotype A was designated as the most ancestral in the human population. The appearance of the L and S haplotypes (differing each by two SNPs, one in common, from the haplotype A) should have occurred already outside of Africa, as neither is found in modern African populations including Esan from Nigeria (ESN), Gambian (GWD), Luhya from Kenya (LWK), Yoruba from Nigeria (YRI), and Mende from Sierra Leone (MSL) from 1000 Genomes project. While F haplotype is present in the Yoruba at a very low frequency, M is absent not only in Africa but also in East Asia (Figure 4b). The frequency and distribution of haplotypes in present-day control populations suggest that besides A, haplotypes R, S, and L were likely the earliest to arise and spread among modern humans.

### *HGSNAT* mutation spectrum and founder effects in the Brazilian population

Molecular characterization of Brazilian MPSIIIC patients revealed that besides the three novel mutations described above, they also carry four mutant *HGSNAT* variants (c.525dupT/p.(Val176Cysfs*16), c.234+1G>A/p.Asp40Valfs*19, c.372-2A>G/p.[Leu125_Arg128del,Arg124Serfs*27] and c.1622C>T/p.Ser541Leu) previously identified in patients from Portugal (Table 1, Figure 5) and likely introduced by Portuguese either during the three centuries of Brazilian colonization (1500–1822) or by later waves of migration to this country. To verify this hypothesis, we analyzed haplotypes in the corresponding patients from Brazil and Portugal as well as in the patients from other countries carrying the same mutations.

Seven out of 14 Brazilian MPSIIIC patients reported in this study are from the state of Paraiba (Table 1 and Figure 5). In these patients three mutations were identified, two novel (p.Asn258Ile and a nonsense p.Leu55*), as well as the c.525dupT variant, previously detected only in the Portuguese patients (Coutinho *et al.*, 2008; Feldhammer, Durand, Mrazova, *et al.*, 2009). The p.Asn258Ile mutation was found in five families from three small villages (Alagoa Nova, Cabaceiras, and Taperoa), and represents about 64% of all *HGSNAT* mutations in Paraiba, while p.(Leu55Ter) and c.525dupT are responsible for 18% each (Figure 5). The mutation p.(Leu55Ter) was detected in three patients from two families in the nearby villages of Alagoa Nova and Mogeiro, in the East of Paraiba.

Brazil has one of the largest groups of MPSIIIC patients with 52 new cases diagnosed between 1982 and 2015 (Giugliani, Federhen, Michelin-Tirelli, Riegel, & Burin, 2017). The live-birth prevalence of MPSIIIC in Brazil for the period between 2000 and 2013 was estimated to be 0.09 newly diagnosed patients per 100,000 live births, that is, in the range with other countries (Giugliani *et al.*, 2017). However, based on the birth rate and the number of patients born in the villages of Alagoa Nova, Cabeceiras, Mogeiro, and Taperoa (Brazilian Health System Database http://tabnet.datasus. gov.br) we now estimate the live-birth prevalence of MPSIIIC in these villages for the period between 1990 and 2017 as 32.9, the highest reported to date. In the whole state of Paraiba for the same period the estimated live-birth prevalence of MPSIIIC was 0.54 per 100,000 live births.

The villages of Cabaceiras and Taperoa were founded in the XVIII and XIX centuries, respectively, by Portuguese settlers that generally had large families. On average 20.19 ± 9.13% of the marriages in Paraiba are consanguineous (Weller *et al.*, 2012) and likely responsible for the high frequencies of recessive genetic disorders in this region, including MPSIVA (de Almeida-Barros *et al.*, 2018). Our analysis shows that the c.525dupT variant is associated with the haplotype R in all Brazilian and three out of four Portuguese alleles studied (Table S4). In one Portuguese allele the c.525dupT variant is on haplotype S which differs from R by one SNP. The fact that c.525dupT is associated with two different haplotypes among Portuguese alleles reinforces the hypothesis of the antiquity of this variant in Portugal. Similarly, all Brazilian p.Asn258Ile alleles are on the same haplotype R, whereas all p.Leu55Ter alleles are on haplotype L (Table S4). This together with the high frequency of c.525dupT, pAsn258Ile, and pLeu55Ter in Paraiba, suggests that they are founder mutations in this state. Moreover, it is plausible that c.525dupT and p.Asn258Ile, recently detected in a homozygous Portuguese MPSIIIC patient (L. Lacerda, personal communication) have been introduced by Portuguese migrants.

The c.234+1G>A variant, found in this study in two homozygous patients from São Paulo and Rio de Janeiro, has been previously identified in patients from several countries around the Mediterranean basin and in South Korea (Figure 3 and Table 1). According to gnomAD data c.234+1G>A is present in East and South Asians as well as in non-Finnish Europeans (Table S5). Previous data showed that c.234+1G>A is linked to the c.710C>A/p.Pro237Gln and c.564-98T>C SNPs in Moroccan and Spanish but not in Turkish patients and Italian patients from Sicily (Canals

*et al.*, 2011; Fedele *et al.*, 2007; Ruijter *et al.*, 2008). Our analysis of polymorphic SNPs in the Brazilian, Portuguese, Spanish, Moroccan and Algerian patients showed that c.234+1G>A is associated with the p.Pro237Gln and c.564-98T>C variants in the haplotype C (Figure 4d). However, in a patient from France, the allele carrying c.234+1G>A is present on the haplotype S, not associated with these two SNPs. Together, the difference in four SNPs between haplotypes S and C and the haplotype network for c.234+1G>A (Figure 4d), suggest an independent origin for the mutation associated with the two haplotypes. The haplotype C is the most frequent among the African Yoruba population, representing 35.6% of the haplotypes. It is also frequent in East Asia (CHB, 21.8%), less in South Asia (PJL, 8.9%), and is rare in European populations (3.1%). The multidimensional analysis of pairwise fixation index (Fst) between patients and controls suggests that North African patients (with 60% of the derived A allele at c.234+1G>A site) are genetically closer to YRI population than to any other population studied (Figure 6). Indeed, we find 86% of A allele in Moroccan, and 50%in Algerian and Tunisian MPSIIIC patients (Figure 3). The c.234+1G>A, c.564-98T>C, and c.710C>A/p.Pro237Gln variants were not detected among Africans in 1000 Genomes or gnomAD databases. However, this may be explained by the fact that North African populations are underrepresented in these databases. According to gnomAD the highest frequency for both pathogenic c.234+1G>A variant and SNP c.710C>A/p.Pro237Gln, that does not affect the activity of the HGSNAT protein (Fedele & Hopwood, 2010; Feldhammer, Durand, & Pshezhetsky, 2009), is observed in the Latin-American population (Table S3).

We speculate that c.234+1G>A variant was brought to North Africa and Sicily during the Arab invasions. In North Africa c.234+1G>A, through further mutational events and/or recombination, became associated with the variants c.710C>A/p.P237Q and c.564-98T>C in haplotype C. This North African haplotype was introduced to Iberian Peninsula, and subsequently brough to the Latin America by Portuguese and Spanish migrants where its frequency increased likely due to founder effect. Besides being geographically close to North Africa, Sicily and the Iberian Peninsula were under Arab ruling during centuries, facilitating migration of North Africans to these areas (Capelli *et al.*, 2009; Di Gaetano *et al.*, 2009). At the same time, since c.234+1G>A is a C>T transition located in a CpG site and may represent a recurrent variant (Akalin, Zietkiewicz, Makalowski, & Labuda, 1994) we cannot exclude the possibility that the alleles found in North Africa/Iberian Peninsula/South America have an independent origin from those detected in Sicily/Turkey.

The c.372−2G>A variant has been previously found only in the MPSIIIC patients from Portugal and Spain where it represents 13% and 54% of all mutant alleles, respectively (Figure 3). In the gnomAD database, this allele is only present in heterozygous controls from the Latino population (3/31416, 0.019%). We identified this allele in three homozygous South American patients, two from Brazil and one from Colombia. All these patients, as well as the Portuguese patient heterozygous for the c.372−2G>A mutation (Pt1) and a Spanish homozygous patient (Sp2), share the same haplotype, R (Tables S3 and S4). Altogether these data suggest that c.372–2G>A has an Iberian origin, was likely introduced to Brazil and Colombia (a Spanish colony between XV and XIX centuries) by Portuguese and Spanish migrants, and represents a founder mutation in South America with high frequency in the Latin-American population.

The novel deletion c.1348delG was detected in two homozygous patients without known family consanguinity, one from the city of S. Miguel de Campos in the Alagoas state, and the other from the state of Rio de Janeiro (Table1and Figure 5). In both patients this variant occurs on the background of the widely distributed haplotype R. The c.1348delG variant has been identified in 1 of 15096 African control alleles reported in the gnomAD but has not been observed so far in any other population (Lek *et al.*, 2016). The state of Alagoas is adjacent to Bahia which has the highest percent of African ancestry in Brazil (Kehdy *et al.*, 2015; Lima-Costa *et al.*, 2015). Besides, as one of the largest producers of sugar cane in the country, the state of Alagoas was dependent on the work of slaves brought from Africa. It is estimated that Brazil received around 4.3 millions slaves until 1850 with one million brought to the country through the port of Rio de Janeiro (Trans-Atlantic Slave Trade Database http://slavevoyages.org). The c.1348delG variant found in two patients from the states of Alagoas and Rio de Janeiro could have been therefore introduced to Brazil by African slaves, although additional studies are necessary to confirm this hypothesis.

The substitution c.1622C>T (p.Ser541Leu) was found in two homozygous patients from Sapiranga, and the neighboring city of Sao Leopoldo in the state of Rio Grande do Sul (Figure 5). The mutation has been previously detected in patients from Portugal, France, Ireland, Poland, and Greece (Table 1). Our analysis has shown that in the Brazilian patients, as well as in the French patient, p.Ser541Leu is embedded in the haplotype L. Also, in the patient of Irish ancestry, the mutation is associated with haplotype Q that might have originated from L by mutation (Figure 4d). On the contrary, in the patients from Poland and Portugal, p.Ser541Leu is on haplotype S.

Since this variant is a C>T transition in a CpG site, it might represent a mutation hotspot, independently occurring in several haplotype backgrounds.

On the contrary, since whole genome analysis of inhabitants of Pelotas city in the Rio Grande do Sul state showed a predominant (76.1%) European ancestry component (Kehdy *et al.*, 2015), it is also possible that the p.Ser541Leu mutation in the Brazilian patients from the Rio Grande do Sul may have a common ancestry with the one detected in the French population.

**Founder effects in the Dutch population**

Previously we have reported a high frequency of c.1030C>T/p.Arg344Cys and c.1553C>T/p.Ser518Phe variants in the Netherlands and hypothesized that they were founder mutations in the Dutch population (Ruijter *et al.*, 2008). The haplotype analysis conducted in this study allowed to test this directly. For these patients we also used information from the analysis of five short tandem repeats (STRs): D8S1118, D8S268, D8S2329, D8S1051, and D8S1115 upstream of the SNP rs11784974, previously performed in our lab to map and identify the MPSIIIC causative gene (Ausseil *et al.*, 2004; Hrebicek *et al.*, 2006).

The mutation p.Arg344Cys is present in the patients from three unrelated Dutch families. The first is a large extended family with consanguineous branches (Nthr1-Nthr6) with ten MPSIIIC patients identified in eight generations (Figure S4). The affected members of this family have p.Arg344Cys alleles with the same STR pattern but with the SNP haplotypes either C or Z, which differ by one SNP (Figure 4a). In the second Dutch family (Nthr7), two STRs have different alleles on the same SNP haplotype C. In the third family (Nthr8), the allele presents SNP haplotype C and STR pattern similar to those found in patients from the above two families (Table S4).

Both the SNP haplotype network for the p.Arg344Cys mutation (Figure 4c,d) the STR composition suggest that the mutant alleles in the DutchpatientshaveasalikelyoriginSNP haplotypeC.The p.Arg344Cys alleles in SNP haplotype Z most probably originated from C. The STR haplotypic diversity suggests the existence of recombination and/or mutation of these microsatellites (Table S4). Thus, there is a strong indication that all Dutch alleles carrying p.Arg344Cys variant evolved from a single haplotype through further mutation and/or recombination confirming that p.Arg344Cys is indeed a founder mutation in the The Netherlands.

The p.Arg344Cys variant in CpG site has also been found in other populations besides the Dutch. In this study we identified it in homozygosity in a Turkish patient from a consanguineous family, also associated with the haplotype C. In contrast, in three patients from the UK, France, and Singapore, p.Arg344Cys was found on the haplotype S (Tables S3 and S4). STR markers for the British and French patients showed a similar allele composition, only differing in the number of repeats in D8S2329, suggesting a similar ancestry for the variant in these two populations.

Both the SNP haplotype network and the STR composition indicate that the p.Arg344Cys mutation appeared independently in Dutch patients and those from the UK, France, and Singapore (Figure 4c,d). Also, the mutation p.Arg344Cys affects the same residue as the MPSIIIC mutation p.Arg344His, found in patients from Poland, the Czech Republic and Finland (Feldhammer, Durand, Mrazova, *et al.*, 2009), which indirectly confirms that this codon is a mutation hotspot.

The p.Ser518Phe variant has been detected so far only in Dutch patients from four families. Our data show that all alleles carrying the mutation are associated with the haplotypes A or B, which differ by a single SNP variation. Similarly, all patients had the same STR composition (Table S3). We conclude therefore that all alleles containing the p.Ser518Phe have the same origin confirming that it is a founder mutation in the Dutch population.

**p.Arg384Ter is potentially an ancient *HGSNAT* pathogenic variant**

So far, the change c.1150C>T/p.Arg384Ter is the most frequent among MPSIIIC patients. It also has a wide geographic dispersion, being present in several countries in Europe (Poland, France, Czech Republic, the Netherlands, and Italy), Asia (Turkey and Korea) and Canada (Figure 3). Being a CpG change, p.Arg384Ter may be a recurrent variant independently appearing in these populations. At the same time, some alleles can be related.

Poland has the highest frequency of p.Arg384Ter (Figure 3). The alleles carrying this variant in the Polish patients are associated with haplotypes S, L, and O (Figure 4c,d). Five of seven studied Polish p. Arg384Ter alleles are associated with haplotype S and also carry the rare intronic variant c.372-34A>G (rs189601391; Tables S3 and S4).

This association was only detected in two controls of the 1000 Genomes project, one with Northern and Western European ancestry and the other from Finland. These results suggest that the mutation has been in the Polish population long enough for the occurrence of variations in certain SNPs

and/or recombination between them thus confirming the hypothesis of an ancient origin of p.Arg384Ter. On the basis of the haplotype network (Figure 4c,d) we also speculate that Canadian p.Arg384Ter alleles, associated with haplotype M, might have an origin in France, where p.Arg384Ter is embedded in the related haplotype L. In contrast, the p.Arg384Ter alleles in Turkish patients are associated with the haplotype S and could have appeared independently.

**Frequent variants in North America**

In the homozygous French Canadian patient as well as in the compound heterozygous French patient, the CpG p.Glu471Lys variant is associated with haplotype S, whereas the Dutch allele with the same variation is on haplotype I which differs from S by one SNP. These data suggest that the French and French Canadian alleles likely have the same ancestry, potentially also shared by the Dutch mutant allele (Figures 4c, 6d).

The variant c.1250+1G>A identified in the compound heterozygous USA patient (USA2) with British (Wales) and German ancestry is associated with the haplotype S also detected in the patients from the UK and Poland carrying the same variant (Table S3). This suggests a common European origin for c.1250+1G>A. Indirectly this is also supported by the fact that this variant is present in heterozygosity in 2 of 126550 non-Finnish European samples from gnomAD (Table S5). The second allele of the USA2 patient contains the missense mutation p.Ala489Glu, previously detected in another USA patient (USA3). The p.Ala489Glu change represents 33.3% of the mutations reported so far in patients from the USA. This, together with the fact that in both patients studied here p.Ala489Glu is associated with the haplotype R, suggests that it may be a founder mutation in the USA (Tables S3 and S4).

The variant c.493+1G>A found in three patients from Eastern Canada represents currently 37% of mutations detected in this country. One of these patients, from a French Canadian family, participated in this study. We found that the c.493+1G>A change in this patient is associated with the haplotype R, as in the patient from Singapore heterozygous for the same mutation (Tables S3 and S4). In contrast, in the Algerian patient, the variant is associated with the haplotype W, carrying the previously described neutral HGSNAT variant p.Lys523Gln (rs73569592), mainly detected in African controls (Table S6). In the 1000 Genomes database, the p.493+1G>A variant is present in one African control allele (YRI, #18934) also in the W haplotype. In total,

c.493+1G>A was detected in 9 of 23,996 African control alleles (gnomAD), indicating a frequency of 0.00038 in this population.

We believe that being in a CpG site, c.493+1G>A may be a recurrent mutation appearing independently in the African population (Algerian patient/Nigerian controls) and in the patients from Singapore, and Canada. The variant c.493+1G>A was not detected in European controls (Table S5) suggesting that it might have appeared among Eastern Canadian settlers.

**Common pathogenic variants shared by multiple populations**

The mutation p.Trp403Cys was detected in heterozygosity in a patient from the UK and in homozygosity in a patient from a consanguineous French family, in both in *cis* with the SNP p. Ala615Thr. The p.Trp403Cys mutation was found in 4 control alleles of 1000 genomes project, two from Utah with Northern and Western European Ancestry (CEU), and two from the UK. In all samples, p.Ala615Thr was associated with the rare haplotype T (Figure 4d). The French and British alleles carrying the p.[Trp403Cys;Ala615Thr] variants are also associated with the haplotype T (Tables S3 and S4) indicating that they have a common ancestor.

Previous functional studies have demonstrated that p.Ala615Thr variant is a benign polymorphism, and by itself only slightly affects the enzymatic activity of HGSNAT (Feldhammer, Durand, & Pshezhetsky, 2009). This change, however, has been linked to the phenotype of retinitis pigmentosa when present in homozygosity or heterozygosity (either in *cis* or *trans*) with other *HGSNAT* mutations (Comander *et al.*, 2017; Haer-Wigman *et al.*, 2015; Van Cauwenbergh *et al.*, 2017). p.Ala615Thr shows the highest allele frequency (0.01462 in gnomAD) in the Ashkenazi Jewish population (Table S6B). Considering the disease-causing effect of this allele when combined with other *HGSNAT* variants, screening programs for p. Ala615Thr carriers in this population may be considered.

This study reports the first molecular characterization of an Iranian MPSIIIC patient, homozygous for the CpG p.Pro283Leu mutation previously identified in one heterozygous French and one homozygous UK patients. The analysis of the haplotype network for p. Pro283Leu demonstrates that the mutation-carrying haplotypes L and S for the French and British patients, respectively, are related, suggesting a common origin (Figure 4c,d). In contrast, the Iranian allele associated with the haplotype F presumably has a different ancestry.

The variant c.852−1G>A has been previously identified in homozygosity in four patients from three Italian families by Fedele *et al.*(2007) who suggested that it is a founder variant in Italy. Later, however, the change was detected in a patient from Turkey (Feldhammer, Durand, Mrazova, *et al.*, 2009). Here we report another Turkish patient from a consanguineous family, homozygous for c.852–1G>A on an L haplotype. Similarly, we identified the variant c.1271dupG (previously detected in a patient from Greece) in a Turkish patient, also on haplotype L. Further analysis is necessary to clarify if the alleles carrying the changes c.852–1G>A, located in a methylated CG site, and c.1271dupG, appeared independently in the different populations.

The c.739delA mutation first described in a homozygous Italian patient (Fedele *et al.*, 2007) was later identified in a homozygous patient from North Africa as well as in a patient with an Italian/Belgium ancestry (Feldhammer, Durand, Mrazova, *et al.*, 2009). We have studied the mutant alleles and confirmed that they are embedded in haplotype S and likely share the same ancestry (Tables S3 and S4).

**Genotype-phenotype correlations**

Recent clinical history studies of other subtypes of Sanfilippo disease (MPSIIIA and MPSIIIB) documented two groups of patients with earlier and later onset of clinical presentation. Importantly, the patients from the first group also demonstrated a significantly higher rate of neurodegeneration and cognitive decline (Shapiro *et al.*, 2015, 2016; Whitley *et al.*, 2018). In contrast with these studies where an assessment of cognitive status and brain atrophy was conducted for all reported patients by standardized tests and volumetric magnetic resonance imaging, in our analysis, we mostly relied on the available clinical information provided by the referring medical centers. However, we believe that our current data also suggest the existence of early-onset/rapidly progressing and slower progressing groups in the studied cohort of MPSIIIC patients.

The first group included patients that were diagnosed early (in some cases around 1 year of life) and were never able to communicate by sentences or rapidly lost the ability for verbal communication, walking and interaction with the environment. Although the range of symptoms and their severity varied between the patients they, in general, had faster progression of the disease with the loss of speech and walking ability occuring in general within 1–5 years apart. This group

included patients homozygous for variants causing NMD such as frameshifts (Trk4, c.1271dupG/c.1271dupG; Trk5, c.1479dupA/c.1479dupA) splice (Br12, c.234+1G>A/c.234+1G>A), and nonsense mutations (Br2, p.Leu55Ter/p.Leu55Ter), as well as those homozygous or compound heterozygous for the missense substitutions p.Asn258Ile (Br3, Br4, Br5, Br6, and Br7) and p.Ser541Leu (Br10). Current and previous (Feldhammer, Durand, & Pshezhetsky, 2009) data demonstrate that both p.Asn258Ile and p.Ser541Leu mutations completely abolish lysosomal targeting and activity of HGSNAT consistent with our previous conclusion that such mutations are associated with the severe clinical phenotype (Feldhammer, Durand, & Pshezhetsky, 2009).

For the second, less severely affected group the clinical presentation also varied between the patients but all of them showed a relatively later onset and/or somewhat slower progression of the disease. In particular, for the USA2 patient, the loss of speech occurred at 12 years (eight after the onset of the disease). A loss of social interaction occurred at 25 and walking at 29 years, 25 years after the onset of symptoms. The USA1 patient, despite the early onset of the first symptoms at 2 years, lost the speech ability only at 15 years. Irn1, Trk2, and Trk3 did not show cognitive deficiency until 5–6 years old and, as well as Pt1 and Can1, could communicate for ~ 9.5 years after the onset of clinical signs (mean value for the studied group is 6.2 ± 2.8 years). For the USA1 and Trk2 patients who are currently 17 and 15 year-old, motor problems are still not evident. This late-onset/slowly progressing group also included patients affected with different types of mutations: splicing (Can1 c.494−1G>A/c.494−1G>A; Pt1, c.234+1G>A/c.372-2A>G), missense (Irn1, p.Pro283Leu/p.Pro283Leu; Trk2, p.Arg344Cys/p.Arg344Cys; USA1, p.Gly173Asp/p.Gly423Trp) or their combination (USA2, c.1250+1G>A/p.Ala489Glu). The effects of some of these mutations have been previously studied and several of them including Pro283Leu, Arg344Cys, and c.372-2A>G were partially amenable by the active site-specific chaperone glucosamine (Feldhammer, Durand, & Pshezhetsky, 2009; Matos *et al.*, 2014). Thus, even a very small amount of the residual HGSNAT activity can ameliorate the clinical phenotype of MPSIIIC patients suggesting that for those affected with amenable mutations, chaperone therapy can become a feasible treatment option.

Finally, our data also suggest that clinical presentation for the patients with the same genotype can be different. Specifically, Br1 and Trk3 patients, both had less severe phenotypes including later

onset of the disease and delayed loss of verbal and locomotor abilities, as compared with their siblings, Br2 and Trk4, respectively, suggesting the influence of modifier genes or epigenetic factors.

## 3.7 Conclusion

The current study reports molecular analysis defects in the *HGSNAT* gene in the largest group of MPSIIIC patients studied so far increasing the total number of *HGSNAT* variants associated with MPSIIIC to 71 (Figure S5). Twelve years after the gene discovery it has become obvious that the MPSIIIC disease is more frequent than originally believed (Meikle, Hopwood, Clague, & Carey, 1999; Pinto *et al.*, 2004; Poorthuis *et al.*, 1999). The registries of patients, the underlying molecular defects, and their geographic coverage expanded significantly and suggested the existence of genetic clusters of MPSIIIC disease with high frequencies of specific mutations.

The first analysis of the molecular defects in the MPSIIIC patients in the Brazilian population described here demonstrates that this country has one of the largest groups of patients many of whom carry novel mutations. Another three novel *HGSNAT* disease-causing variants were identified in patients from Iran, Turkey, Canada, and the United States. All novel missense mutations affected folding of the enzyme, similarly to all previously reported ones. Future analysis of the tertiary enzyme structure and the effects of the amino acid substitutions caused by mutations are necessary to understand the mechanism underlying this phenomenon.

For patients with available DNA samples, we determined the background haplotypes of the disease-causing alleles and constructed worldwide MPSIIIC haplotype networks. These results combined with the geographic and historical data allowed to get insights into the mutation migration roots and founder effects and helped to reveal the history of the disease. Specifically, we identified several mutations introduced by Portuguese settlers in the Brazilian population, including the c.525dupT, a founder mutation in the Paraiba state, or the c.372−2G>A variant with an Iberian origin which was introduced by Portuguese and Spanish settlers in Brazil and Colombia. We could trace the origin of c.234+1G>A in *cis* with c.564-98T>C and c.710C>A rare SNPs, c.[234+1G>A; 564-98T>C; 710C>A] from North African alleles with further expansion into the Iberian Peninsula and subsequently to Latin America. We also confirmed or reinforced hypotheses

about possible founder effects of several mutations in the other countries including p.Arg344Cys and p.Ser518Phe in the Netherlands.

Besides, our study contributes to the knowledge of the natural history of MPSIIIC, with a clinical description of a large cohort of new patients. Consistent with previous report (Ruijter *et al.*, 2008) our data show that speech delay, cognitive decline and behavioral abnormalities, including hyperactivity, are the earliest symptoms to be detected resulting in some MPSIIIC children initially misdiagnosed with attention deficit, hyperactivity disorder, or autism (Wijburg, Wegrzyn, Burton, & Tylki-Szymanska, 2013).

Recent studies including those from our laboratory revealed the pathophysiological mechanism of MPSIIIC and suggested several potential avenues for therapeutic intervention, including chaperone therapy, stop codon readthrough, U1 snRNAs, and gene therapy (Feldhammer, Durand, & Pshezhetsky, 2009; Martins *et al.*, 2015; Matos *et al.*, 2014; Tordo *et al.*, 2018).

With clinical trials approaching to test these therapies, the consolidation of data on the natural history of the disease and complete patient registries become crucial for their success. The knowledge of distribution and frequency of MPSIIIC mutations in the populations should enable faster detection of carriers and patients and, in the future, lead to more efficient therapeutic approaches.

**ACKNOWLEDGMENTS**

The authors thank the patients and their families for participating in our study. We also thank Dr. Mila Ashmarina for critically reading the manuscript and helpful advice. This study has been partially supported by an operating grant PJT 156345 from the Canadian Institutes of Health Research, and gifts from Jonah Just Began Foundation and Sanfilippo Children's Research Foundation to A. V. P., from the MPS Brazil Network and INAGEMP-Brazilian National Institute of Population Medical Genetics to R.G. and from Fonds de Recherche du Québec-Santé Réseau de Médecine Génétique Appliquée to D. L.. C. M. was supported by the Ph.D. scholarship (SFRH/BD/84929/2012) from the Fundação para a Ciência e a Tecnologia (FCT, Portugal) financed by POPH/FSE. S.L.S. acknowledges a research scholarship from the Brazilian National Research Council—CNPq (http://cnpq.br/in-english-summary).

## REFERENCES


Akalin, N., Zietkiewicz, E., Makalowski, W., & Labuda, D. (1994). Are CpG sites mutation hot spots in the dystrophin gene? Human Molecular Genetics, 3(8), 1425–1426.

Ali Pervaiz, M., Patterson, M. C., Struys, E. A., Salomons, G. S., Jakobs, C., Oglesbee, D., & Kirmani, S. (2011). Co-morbidity of Sanfilippo syndrome type C and D-2-hydroxyglutaric aciduria. Journal of Neurology, 258(8), 1564–1565. https://doi.org/10.1007/s00415-011-5977-1

Ausseil, J., Loredo-Osti, J. C., Verner, A., Darmond-Zwaig, C., Maire, I., Poorthuis, B., & Pshezhetsky, A. V. (2004). Localisation of a gene for mucopolysaccharidosis IIIC to the pericentromeric region of chromosome 8. Journal of Medical Genetics, 41(12), 941–945. https://doi.org/ 10.1136/jmg.2004.021501

Canals, I., Elalaoui, S. C., Pineda, M., Delgadillo, V., Szlago, M., Jaouad, I. C., & Vilageliu, L. (2011). Molecular analysis of Sanfilippo syndrome type C in Spain: Seven novel *HGSNAT* mutations and characterization of the mutant alleles. Clinical Genetics, 80(4), 367–374. https://doi.org/10.1111/j.1399-0004.2010.01525.x

Capelli, C., Onofri, V., Brisighelli, F., Boschi, I., Scarnicci, F., Masullo, M., & Pascali, V. (2009). Moors and Saracens in Europe: Estimating the medieval North African male legacy in southern Europe. European Journal of Human Genetics, 17(6), 848–852. https://doi.org/10.1038/ ejhg.2008.258

Comander, J., Weigel-DiFranco, C., Maher, M., Place, E., Wan, A., Harper, S., & Pierce, E. A. (2017). The genetic basis of pericentral retinitis pigmentosa-A form of mild retinitis pigmentosa. Genes (Basel), 8(10),E256. https://doi.org/10.3390/genes8100256

Coutinho, M. F., Lacerda, L., Prata, M. J., Ribeiro, H., Lopes, L., Ferreira, C., & Alves, S. (2008). Molecular characterization of Portuguese patients with mucopolysaccharidosis IIIC: Two novel mutations in the *HGSNAT* gene. Clinical Genetics, 74(2), 194–195. https://doi.org/10. 1111/j.1399-0004.2008.01040.x

de Almeida-Barros, R. Q., de Medeiros, P. F. V., de Almeida Azevedo, M. Q., de Oliveira Lira Ortega, A., Yamamoto, A. T. A., Dornelas, S. K. L., & Bento, P. M. (2018). Evaluation of oral manifestations of patients with mucopolysaccharidosis IV and VI: Clinical and imaging study. Clinical Oral Investigations, 22(1), 201–208. https://doi.org/10.1007/s00784-017-2100-8

Di Gaetano, C., Cerutti, N., Crobu, F., Robino, C., Inturri, S., Gino, S., & Piazza, A. (2009). Differential Greek and northern African migrations to Sicily are supported by genetic evidence from the Y chromosome. European Journal of Human Genetics, 17(1), 91–99. https://doi.org/10. 1038/ejhg.2008.120

Excoffier, L., & Lischer, H. E. (2010). Arlequin suite ver 3.5: A new series of programs to perform population genetics analyses under Linux and Windows. Molecular Ecology Resources, 10(3), 564–567. https://doi.org/10.1111/j.1755-0998.2010.02847.x

Fan, X., Tkachyova, I., Sinha, A., Rigat, B., & Mahuran, D. (2011). Characterization of the biosynthesis, processing and kinetic mechanism of action of the enzyme deficient in mucopolysaccharidosis IIIC. PLOS One, 6(9), e24951. https://doi.org/10.1371/ journal.pone.0024951

Fan, X., Zhang, H., Zhang, S., Bagshaw, R. D., Tropak, M. B., Callahan, J. W.,& Mahuran, D. J. (2006). Identification of the gene encoding the enzyme deficient in mucopolysaccharidosis

IIIC (Sanfilippo disease type C). American Journal of Human Genetics, 79(4), 738–744. https:// doi.org/10.1086/508068

Fedele, A. O., Filocamo, M., Di Rocco, M., Sersale, G., Lubke, T., di Natale, P., & Ballabio, A. (2007). Mutational analysis of the *HGSNAT* gene in Italian patients with mucopolysaccharidosis IIIC (Sanfilippo C syndrome). Mutation in brief #959. Online. Human Mutation, 28(5), 523. https://doi.org/10.1002/humu.9488

Fedele, A. O., & Hopwood, J. J. (2010). Functional analysis of the *HGSNAT* gene in patients with mucopolysaccharidosis IIIC (Sanfilippo C Syndrome). Human Mutation, 31(7), E1574–E1586. https://doi.org/ 10.1002/humu.21286

Feldhammer, M., Durand, S., Mrazova, L., Boucher, R. M., Laframboise, R., Steinfeld, R., & Pshezhetsky, A. V. (2009). Sanfilippo syndrome type C: Mutation spectrum in the heparan sulfate acetyl-CoA: Alpha- glucosaminide N-acetyltransferase (*HGSNAT*) gene. Human Mutation, 30(6), 918–925. https://doi.org/10.1002/humu.20986

Feldhammer, M., Durand, S., & Pshezhetsky, A. V. (2009). Protein misfolding as an underlying molecular defect in mucopolysaccharidosis III type C. PLOS One, 4(10), e7434. https://doi.org/10.1371/ journal.pone.0007434

Gaffke, L., Pierzynowska, K., Piotrowska, E., & Wegrzyn, G. (2018). How close are we to therapies for Sanfilippo disease? Metabolic Brain Disease, 33(1), 1–10. https://doi.org/10.1007/s11011-017-0111-4

1000 Genomes Project Consortium, Abecasis, G. R., Auton, A., Brooks, L. D., DePristo, M. A., Durbin, R. M., & McVean, G. A. (2012). An integrated map of genetic variation from 1,092 human genomes. Nature, 491(7422), 56–65. https://doi.org/10.1038/nature11632

Giugliani, R., Federhen, A., Michelin-Tirelli, K., Riegel, M., & Burin, M. (2017). Relative frequency and estimated minimal frequency of lysosomal storage diseases in Brazil: Report from a Reference Laboratory. Genetics and Molecular Biology, 40(1), 31–39. https://doi.org/10.1590/1678-4685-GMB-2016−0268

Haer-Wigman, L., Newman, H., Leibu, R., Bax, N. M., Baris, H. N., Rizel, L., & Ben-Yosef, T. (2015). Non-syndromic retinitis pigmentosa due to mutations in the mucopolysaccharidosis type IIIC gene, heparan-alpha-glucosaminide N-acetyltransferase (HGSNAT). Human Molecular Genetics, 24(13), 3742–3751. https://doi.org/10.1093/hmg/ ddv118

Hrebicek, M., Mrazova, L., Seyrantepe, V., Durand, S., Roslin, N. M., Noskova, L., & Pshezhetsky, A. V. (2006). Mutations in TMEM76* cause mucopolysaccharidosis IIIC (Sanfilippo C syndrome). American Journal of Human Genetics, 79(5), 807–819. https://doi.org/10.1086/ 508294

Hu, H., Hubner, C., Lukacs, Z., Musante, L., Gill, E., Wienker, T. F., & Schuelke, M. (2017). Kluver-Bucy syndrome associated with a recessive variant in HGSNAT in two siblings with Mucopolysaccharidosis type IIIC (Sanfilippo C). European Journal of Human Genetics, 25(2), 253–256. https://doi.org/10.1038/ejhg.2016.149

Huh, H. J., Seo, J. Y., Cho, S. Y., Ki, C. S., Lee, S. Y., Kim, J. W., & Jin, D. K. (2013). The first Korean case of mucopolysaccharidosis IIIC (Sanfilippo syndrome type C) confirmed by biochemical and molecular investigation. Annals of Laboratory Medicine, 33(1), 75–79. https://doi. org/10.3343/alm.2013.33.1.75

Kehdy, F. S., Gouveia, M. H., Machado, M., Magalhaes, W. C., Horimoto, A. R., Horta, B. L., & Brazilian, E. P. C. (2015). Origin and dynamics of admixture in Brazilians and its effect on the pattern of deleterious mutations. Proceedings of the National Academy of Sciences of

the United States of America, 112(28), 8696–8701. https://doi.org/10.1073/pnas.1504447112

Lek, M., Karczewski, K. J., Minikel, E. V., Samocha, K. E., Banks, E., Fennell, T., & Exome Aggregation, C. (2016). Analysis of protein-coding genetic variation in 60,706 humans. Nature, 536(7616), 285–291. https://doi. org/10.1038/nature19057

Lima-Costa, M. F., Rodrigues, L. C., Barreto, M. L., Gouveia, M., Horta, B. L., Mambrini, J., & Epigen-Brazil Group, (2015). Genomic ancestry and ethnoracial self-classification based on 5,871 community-dwelling Brazilians (The Epigen Initiative). Scientific Reports, 5, 9812. https:// doi.org/10.1038/srep09812

Martins, C., Hulkova, H., Dridi, L., Dormoy-Raclet, V., Grigoryeva, L., Choi, Y., & Pshezhetsky, A. V. (2015). Neuroinflammation, mitochondrial defects and neurodegeneration in mucopolysaccharidosis III type C mouse model. Brain, 138(Pt 2), 336–355. https://doi.org/10.1093/ brain/awu355

Matos, L., Canals, I., Dridi, L., Choi, Y., Prata, M. J., Jordan, P., & Vilageliu, L. (2014). Therapeutic strategies based on modified U1 snRNAs and chaperones for Sanfilippo C splicing mutations. Orphanet Journal of Rare Diseases, 9, 180. https://doi.org/10.1186/ s13023-014-0180-y

Meikle, P. J., Hopwood, J. J., Clague, A. E., & Carey, W. F. (1999). Prevalence of lysosomal storage disorders. Journal of the American Medical Association, 281(3), 249–254.

Ouesleti, S., Brunel, V., Ben Turkia, H., Dranguet, H., Miled, A., Miladi, N., & Bekri, S. (2011). Molecular characterization of MPS IIIA, MPS IIIB and MPS IIIC in Tunisian patients. Clinica Chimica Acta, 412(23–24), 2326–2331. https://doi.org/10.1016/j.cca.2011.08.032

Ouesleti, S., Coutinho, M. F., Ribeiro, I., Miled, A., Mosbahi, D. S., & Alves, S. (2017). Update of the spectrum of mucopolysaccharidoses type III in Tunisia: Identification of three novel mutations and in silico structural analysis of the missense mutations. World Journal of Pediatrics, 13(4), 374–380. https://doi.org/10.1007/s12519-017-0005-x

Pinto, R., Caseiro, C., Lemos, M., Lopes, L., Fontes, A., Ribeiro, H., & Sa Miranda, M. C. (2004). Prevalence of lysosomal storage diseases in Portugal. European Journal of Human Genetics, 12(2), 87–92. https:// doi.org/10.1038/sj.ejhg.5201044

Poorthuis, B. J., Wevers, R. A., Kleijer, W. J., Groener, J. E., de Jong, J. G., van Weely, S., & van Diggelen, O. P. (1999). The frequency of lysosomal storage diseases in The Netherlands. Human Genetics, 105(1-2), 151–156.

Ruijter, G. J., Valstar, M. J., van de Kamp, J. M., van der Helm, R. M., Durand, S., van Diggelen, O. P., & Wijburg, F. A. (2008). Clinical and genetic spectrum of Sanfilippo type C (MPS IIIC) disease in The Netherlands. Molecular Genetics and Metabolism, 93(2), 104–111. https://doi.org/10.1016/j.ymgme.2007.09.011

Scarpa, M., Orchard, P. J., Schulz, A., Dickson, P. I., Haskins, M. E., Escolar, M. L., & Giugliani, R. (2017). Treatment of brain disease in the mucopolysaccharidoses. Molecular Genetics and Metabolism, 122S, 25–34. https://doi.org/10.1016/j.ymgme.2017.10.007

Shapiro, E. G., Nestrasil, I., Ahmed, A., Wey, A., Rudser, K. R., Delaney, K. A., & Potegal, M. (2015). Quantifying behaviors of children with Sanfilippo syndrome: The Sanfilippo Behavior Rating Scale. Molecular Genetics and Metabolism, 114(4), 594–598. https://doi.org/10.1016/j. ymgme.2015.02.008

Shapiro, E. G., Nestrasil, I., Delaney, K. A., Rudser, K., Kovac, V., Nair, N., & Whitley, C. B. (2016). A Prospective Natural History Study of Mucopolysaccharidosis Type IIIA. Journal of Pediatrics, 170,278-287. e271-274. https://doi.org/10.1016/j.jpeds.2015.11.079

Tordo, J., O'Leary, C., Antunes, A., Palomar, N., Aldrin-Kirk, P., Basche, M., & Henckaerts, E. (2018). A novel adeno-associated virus capsid with enhanced neurotropism corrects a lysosomal transmembrane enzyme deficiency. Brain, 141(7), 2014–2031. https://doi.org/10.1093/brain/ awy126

Tuncbilek, E., & Koc, I. (1994). Consanguineous marriage in Turkey and its impact on fertility and mortality. Annals of Human Genetics, 58(4), 321–329.

Valstar, M. J., Ruijter, G. J., van Diggelen, O. P., Poorthuis, B. J., & Wijburg, F. A. (2008). Sanfilippo syndrome: A mini-review. Journal of Inherited Metabolic Disease, 31(2), 240–252. https://doi.org/10.1007/s10545- 008-0838-5

Velasco, H. M., Sanchez, Y., Martin, A. M., & Umana, L. A. (2017). Natural history of Sanfilippo syndrome type C in Boyaca, Colombia. Journal of Child Neurology, 32(2), 177–183. https://doi.org/10.1177/ 0883073816672391

Van Cauwenbergh, C., Coppieters, F., Roels, D., De Jaegere, S., Flipts, H., De Zaeytijd, J., & De Baere, E. (2017). Mutations in splicing factor genes are a major cause of autosomal dominant retinitis pigmentosa in Belgian families. PLOS One, 12(1), e0170038. https://doi.org/10. 1371/journal.pone.0170038

Weller, M., Tanieri, M., Pereira, J. C., Almeida Edos, S., Kok, F., & Santos, S. (2012). Consanguineous unions and the burden of disability: A population-based study in communities of Northeastern Brazil. American Journal of Human Biology, 24(6), 835–840. https://doi.org/ 10.1002/ajhb.22328

Whitley, C. B., Cleary, M., Eugen Mengel, K., Harmatz, P., Shapiro, E., Nestrasil, I., & Alexanderian, D. (2018). Observational prospective natural history of patients with sanfilippo syndrome type B. Journal of Pediatrics, 197, 198– 206. e192. https://doi.org/10.1016/j.jpeds.2018.01.044

Wijburg, F. A., Wegrzyn, G., Burton, B. K., & Tylki-Szymanska, A. (2013). Mucopolysaccharidosis type III (Sanfilippo syndrome) and misdiagnosis of idiopathic developmental delay, attention deficit/hyperactivity disorder or autism spectrum disorder. Acta Paediatrica, 102(5), 462–470. https://doi.org/10.1111/apa.12169

## TABLE 1. Molecular defects in new MPSIIIC patients

| Family | Patient | Variants | | Origin | Population distribution |
|---|---|---|---|---|---|
| | | Nucleotide change (cDNA)[a] | Effect on protein [b] | | |
| 1 | Br1 | c.[164T>A];[164T>A] | p.[(L55*)];[(L55*)] | Mogeiro, Paraiba, Brazil | **Not yet reported** |
| 1 | Br2 | c.[164T>A];[164T>A] | p.[(L55*)];[(L55*)] | Mogeiro, Paraiba, Brazil | **Not yet reported** |
| 2 | Br3 | c.[164T>A];[773A>T] | p.[(L55*)];[N258I] | Alagoa Nova, Paraiba, Brazil | **Not yet reported/Not yet reported** |
| 3 | Br4 | c.[525dupT];[773A>T] | p.[(V176fs)];[N258I] | Taperoa, Paraiba, Brazil | Portugal/**Not yet reported** |
| 4 | Br5 | c.[525dupT];[773A>T] | p.[(V176fs)];[N258I] | Cabaceiras, Paraiba, Brazil | Portugal/**Not yet reported** |
| 5 | Br6 | c.[773A>T];[773A>T] | p.[N258I];[N258I] | Taperoa, Paraiba, Brazil | **Not yet reported** |
| 6 | Br7 | c.[773A>T];[773A>T] | p.[N258I];[N258I] | Taperoa, Paraiba, Brazil | **Not yet reported** |
| 7 | Br8 | c.[1348delG];[1348delG] | p.[D450fs];[D450fs] | Rio Janeiro, Rio Janeiro, Brazil | **Not yet reported** |
| 8 | Br9 | c.[1348delG];[1348delG] | p.[D450fs];[D450fs] | S. Miguel de Campos, Alagoas, Brazil | **Not yet reported** |
| 9 | Br10 | c.[1622C>T];[1622C>T] | p.[S541L];[S541L] | Sapiranga, Rio Grande Sul, Brazil | France, Ireland, Poland, Greece, Portugal |
| 10 | Br11 | c.[1622C>T];[1622C>T] | p.[S541L];[S541L] | Sao Leopoldo, Rio Grande Sul, Brazil | France, Ireland, Poland, Greece, Portugal |
| 11 | Br12 | c.[234+1G>A;710C>A]; [234+1G>A;710C>A] | p.[D40Valfs;P237Q]; [D40Valfs;P237Q] | Sao Paulo, Sao Paulo, Brazil | Spain, Portugal |
| 12 | Br13 | c.[372−2A>G];[372−2A>G] | p.[R124fs,L125_R128del]; [R124fs,L125_R128del] | Rio Janeiro, Rio Janeiro, Brazil | Spain, Portugal |
| 13 | Br14 | c.[372−2A>G];[372−2A>G] | p.[R124fs,L125_R128del]; [R124fs,L125_R128del] | Sao Paulo, Sao Paulo, Brazil | Morocco, Tunisia, Turkey, Korea, France, Italy, Spain, Portugal |
| 14 | Clb1 | c.[372−2A>G];[372-2A>G] | p.[R124fs,L125_R128del]; [R124fs,L125_R128del] | Colombia | Morocco, Tunisia, Turkey, Korea, France, Italia, Spain, Portugal |
| 15 | Pt1 | c.[234+1G>A;710C>A]; c.[372−2A>G] | p.[D40Valfs;P237Q]; [R124fs,L125_R128del] | Center/North or Center, Portugal | Morocco, Tunisia, Turkey, Korea, France, Italy, Spain, Portugal/Spain, Portugal |
| 16 | Alg1 | c.[234+1G>A;710C>A]; c.[234+1- G>A;710C>A] | p.[D40Valfs;P237Q];[D40-Valfs;P237Q] | Algeria | Spain, Portugal |
| 17 | USA1 | c.[518G>A];[1267G>T] | p.[G173D];[G423W] | Massachusetts, New England, USAd | Turkey/Not yet reported |
| 18 | USA2 | c.[1250+1G>A];[1466C>A] | p.[(G418*)];[A489E] | Minnesota, USA[e]/California, USA[f] | Poland, Turkey, UK/USA |
| 19 | Can1 | c.[494−1G>A];[494−1G>A] | See [g] | Eastern Ontario, Canada | Not yet reported |
| 20 | Trk1 | c.[852−1G>A];[852−1G>A] | p.[(W284*)];[(W284*)] | Turkey | Italy, Turkey |
| 21 | Trk2 | c.[1030C>T];[1030C>T] | p.[R344C];[p.R344C] | Agri, Turkey | France, UK, Netherlands, Germany, Singapore |

Note: The novel *HGSNAT* variants detected in the patients are indicated in bold.

cDNA: complementary DNA.

[a]cDNA is numbered according to GenBank Reference sequence NM_152419.2.

[b]The ATG codon corresponds to the first amino acid in accordance with the GenBank protein reference sequence NP_689632.2.

[c]Besides the c.234+1G>A and c.710C>A variants the allele also presents in *cis* the intronic variant c.594-98T>C.

[d]The parent carrying c.518G>A allele has British and French Canadian ancestry and the parent carrying c.1267G>T, Bristish ancestry.

[e]The parent carrying c.1250+1G>A has British and German ancestry.

[f]The parent carrying the c.1466C>A allele has German, Swedish, Dutch, and British ancestry.

[g]p.[P165_L187delinsQSCYVTQAGVRWHHLGSLQALPPGFTPFSYLSLLSSWNC,P165fs].

[h]The patients Trk3 and Trk4 are siblings and have consanguineous parents. Molecular analysis was not performed for Trk4.

## Figures

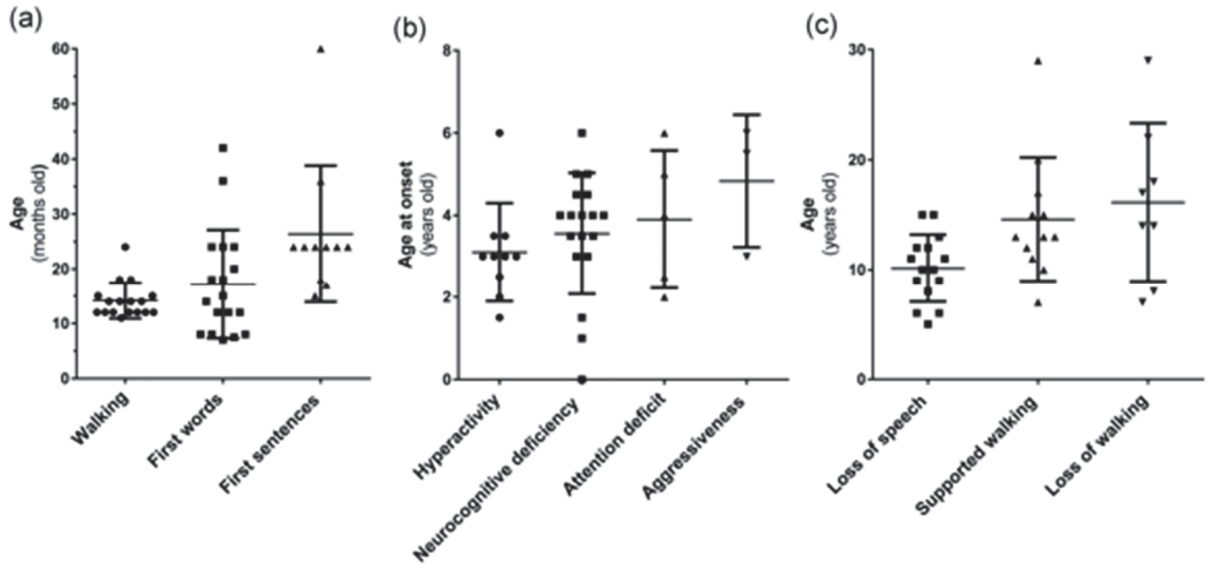


**FIGURE 1: Developmental milestones, onset of symptoms and loss of abilities in new MPSIIIC patients.** (a) Developmental milestones in MPSIIIC patients. The normal age for the children to walk without support, acquire the first words and first sentences is, respectively until, 18 months old, 18 and 30 months old according to WHO Multicenter growth reference study group (2006) and Preston *et al.* (2010). Seven in a total of 18 patients were never able to communicate using sentences. (b) Age at onset of the most frequent symptoms. (c) Age where the abilities of verbal communication and walking are lost among the MPSIIIC patients studied. MPSIIIC: mucopolysaccharidosis type IIIC

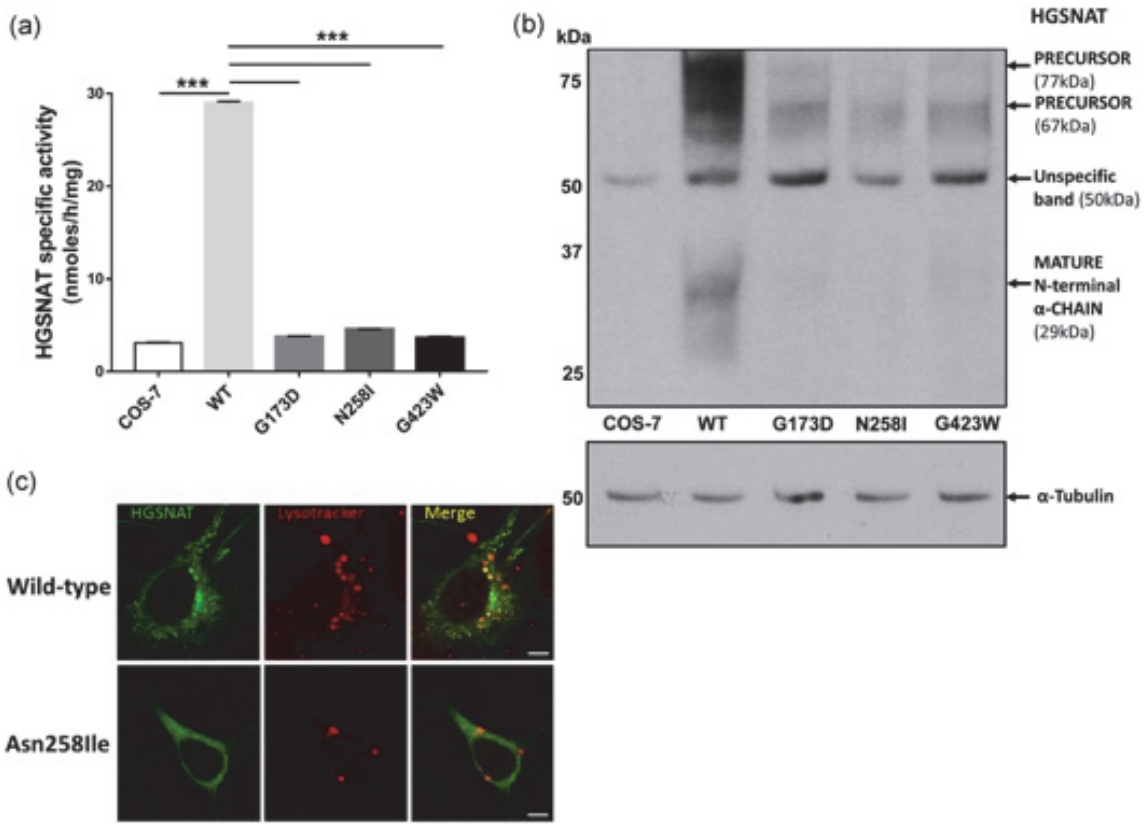


**FIGURE 2: Missense variants Gly173Asp, Asn258Ile, and Gly423Trp affect expression, processing, targeting, and enzymatic activity of corresponding mutant proteins.** (a) Gly173Asp, Asn258Ile, and Gly423Trp HGSNAT mutants lack enzymatic activity. N-acetyltransferase activity was essayed in homogenates of COS-7 cells transfected with pCTAP-tag plasmids encoding for the TAP-tag-labeled WT HGSNAT and its corresponding mutants. The graph shows mean values ± SD of two independent experiments. p values were calculated by one-way ANOVA followed by Tukey's post-hoc multiple comparison test (***$p < 0.001$). (b) The mutant precursor proteins are likely degraded by the ERAD mechanism. The 67 kDa nonglycosylated precursor is the main form detected in the homogenates of cells transfected with the mutant plasmids, while the fully glycosylated 77 kDa precursor and the 29 kDa α-subunit are detected in cells expressing the WT enzyme. The 50 kDa band represents a nonspecific cross-reacting protein also present in untransfected COS-7 cells. Panels show representative blots of two independent experiments yielding similar results. (c) Asn258Ile HGSNAT mutant protein is not targeted to lysosomes. Representative confocal images show COS-7 cells transfected with plasmids encoding for TAP-tagged WT HGSNAT and its Asn258Ile mutant. Similar results were

obtained for Gly173Asp and Gly423Trp HGSNAT mutants (data not shown). Cells grown on glass slides were labeled with Lysotracker Red for one hour before fixation. The localization of HGSNAT was assessed by staining with rabbit polyclonal antibodies against its N-terminal epitope followed by anti-rabbit IgG Alexa 488-labeled antibody (green). The images were captured using an LSM510 Meta Laser confocal microscope (×63 glycerol immersion objectives, NA 1.4). Scale bar = 5 μm. ANOVA: analysis of variance; SD: standard deviation; WT: wild-type

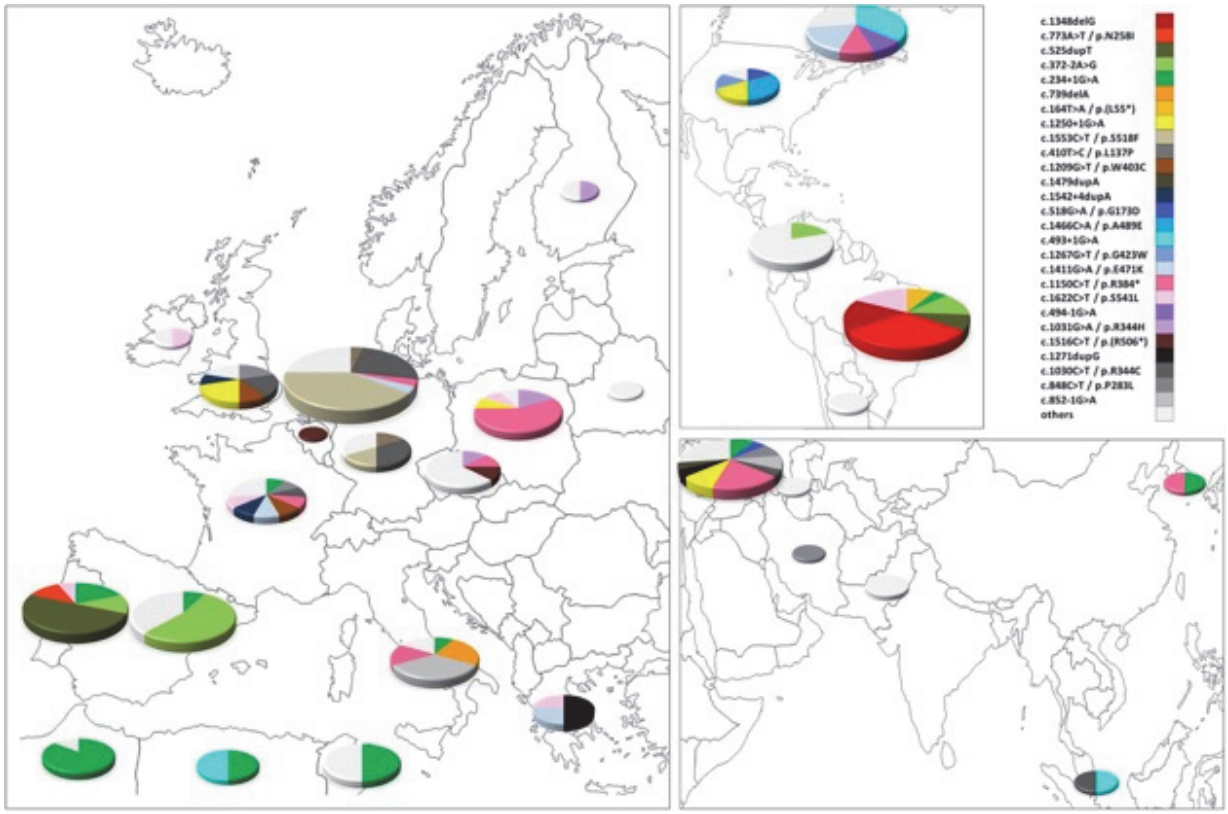


**FIGURE 3: Worldwide distribution of *HGSNAT* pathogenic variants in MPSIIIC patients.** The maps show the frequency and distribution of mutations in *HGSNAT* in all index cases analyzed in this study and reported in the literature. The size of the circles is proportional to the number of alleles detected. In case of consanguinity, only one allele was considered. MPSIIIC: mucopolysaccharidosis type IIIC. (Maps adapted from http://d-maps.com)

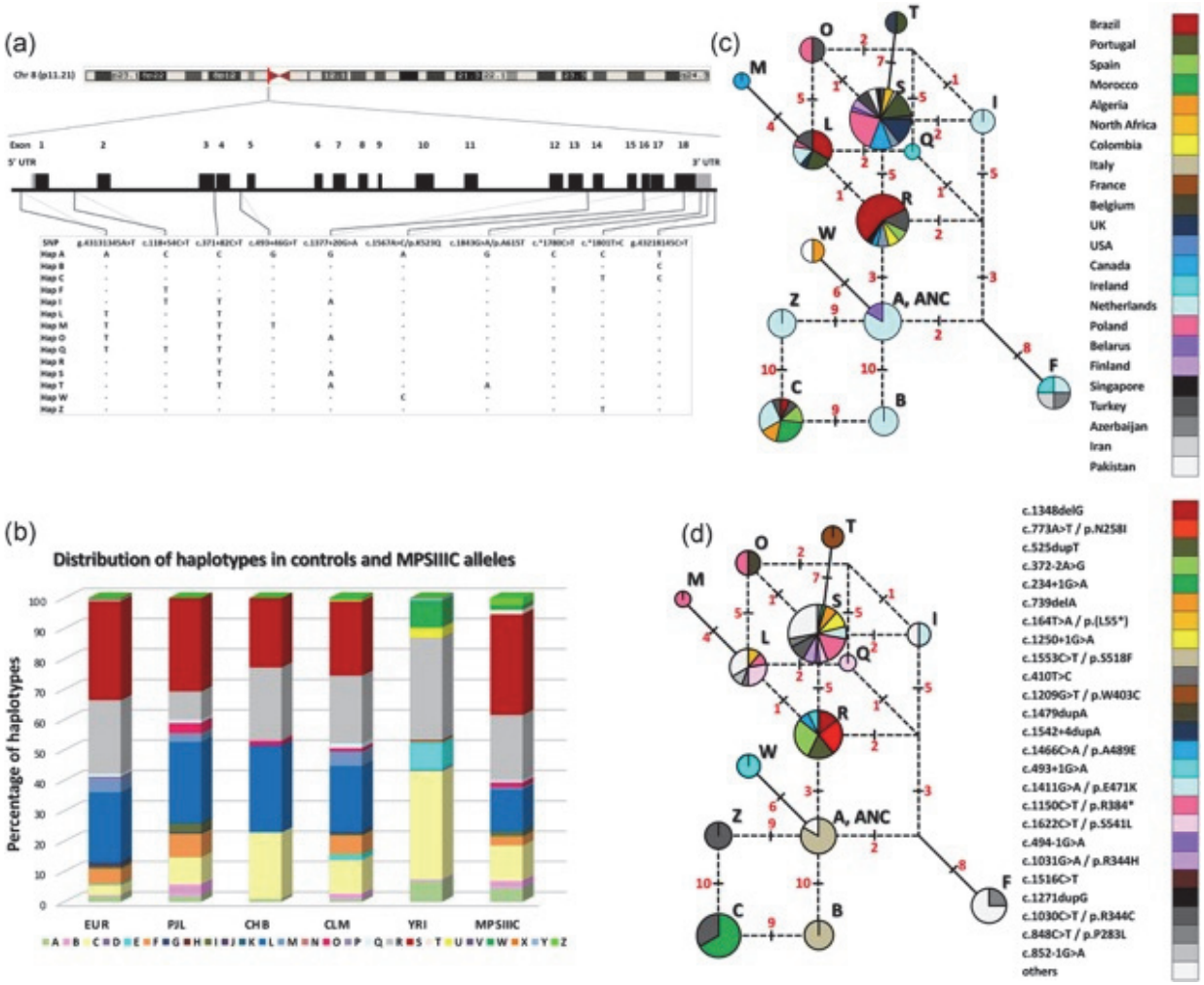


**FIGURE 4: Haplotypes in MPSIIIC patients.** (a) Polymorphic SNPs in MPSIIIC patients. Ten common (MAF ≥ 0.01) polymorphic SNPs were detected in genomic DNA sequences of 78 MPSIIIC patients studied. Haploid genotypes of patients were inferred directly by analyzing parental alleles or, when not possible, in silico by PHASE v2.1 software. Table in the insert shows SNPs and their corresponding positions. *HGSNAT* location (in red) on Human chromosome 8 is as displayed at the UCSC genome browser (http://genome.ucsc.edu). (b) Haplotype distribution in controls and MPSIIIC alleles. The distribution of haplotypes is shown for 72 index family patients where phase was inferred. For comparison, haplotypes were also determined for nine control populations from 1000 Genomes database of Europe (EUR which includes CEU, GBR, FIN, IBS, and TSI), South Asia (PJB), East Asia (CHB), America (CLM), and Africa (YRI). (c,d) A plausible

network of the MPSIIIC haplotypes based on 14 unique haplotypes defined by 10 common polymorphic SNPs in 72 MPSIIIC index patients. Only one allele was considered in families with consanguineous unions. Each circle represents a unique haplotype with the size proportional to its frequency in the sample group. Haplotype A is the ancestral (ANC). Solid lines indicate mutational steps in segments without recombination and dashed lines, reticulations showing the alternative occurrence of mutations and recombinations, with SNP numbers indicated in red (Table S3A for SNP identification and positions). Colors represent specific geographic origins (c) or *HGSNAT* mutations (d) as indicated. SNP: single-nucleotide polymorphism; MPSIIIC: mucopolysaccharidosis type IIIC

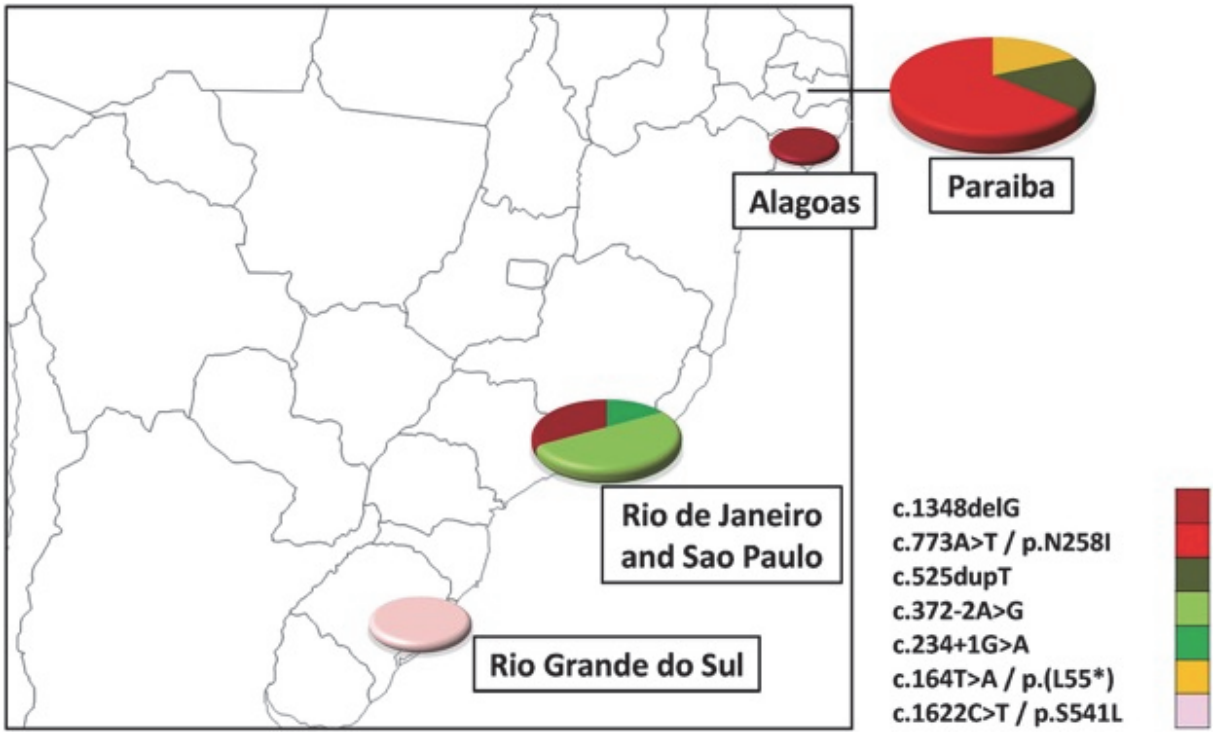


**FIGURE 5: Spectrum and geographic distribution of *HGSNAT* mutations in Brazilian MPSIIIC index patients.** Mutation analysis in 14 patients from 13 Brazilian MPSIIIC families identified seven *HGSNAT* variants including three novel (c.164T>A/p.(Leu55Ter), c.773A>T/p.Asn258Ile, and c.1348delG) and four previously reported (c.234+1G>A, c.372-2A>G, c.525dupT, and c.1622C>T/p.Ser541Leu). The geographic origins of the patients are the state of Paraiba (N = 7, from six families), Alagoas (N = 1), Rio de Janeiro (N = 2), Sao Paulo (N = 2), and the Rio Grande do Sul (N = 2). Only one allele was considered in patients with consanguineous parents. MPSIIIC: mucopolysaccharidosis type IIIC. (Map adapted from https://d-maps.com/carte.php?num_car=4843&lang=en).

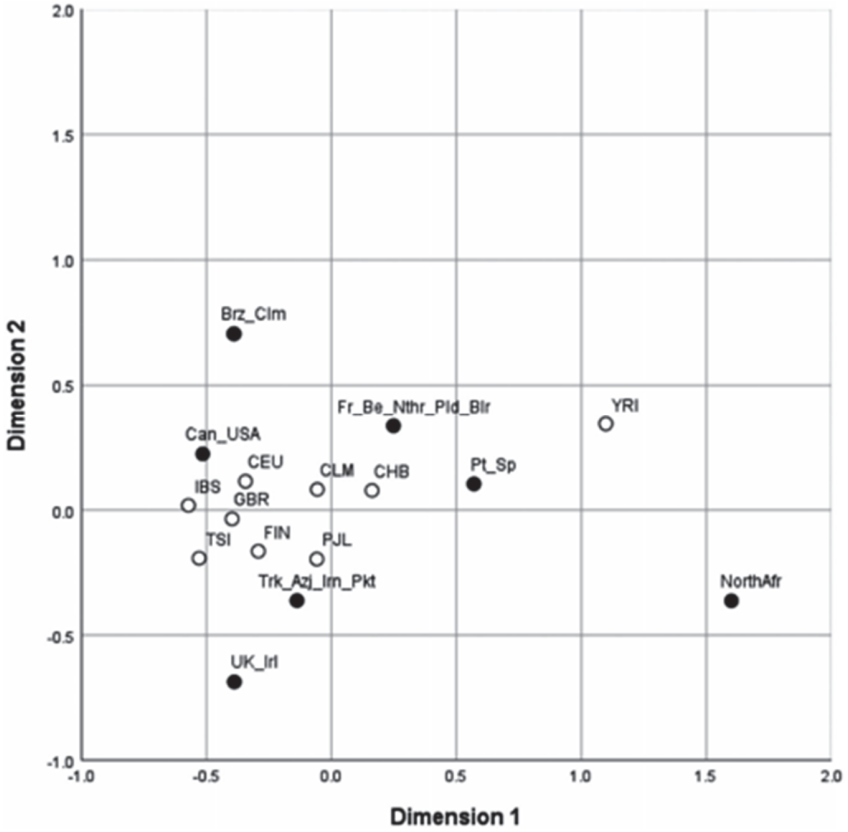


**FIGURE 6: Multidimensional scaling plot obtained from the pairwise Fst genetic distance between haplotypes of controls and MPSIIIC patients.** Pairwise Fst genetic distances were calculated between SNP haplotypes of control European (CEU, GBR, FIN, IBS, and TSI), American (CLM), South Asian (PJL), East Asian (CHB), and African (YRI) populations from 1000 genomes project, and the haplotypes of patients grouped by geographic origin. The European patients were combined in three groups: France/Belgium/Netherlands/Poland/Belarus (Fr_Be_Nthr_Pld_Blr), United Kingdom/Ireland (Uk_Irl), and Portugal/Spain (Pt_Sp). American patients were combined in two groups: United States of America/Canada (USA_Can) and Brazil/Colombia (Brz_Clm). The patients from Turkey/Azerbaijan/Iran/Pakistan formed the Western Asia group (Trk_Azj_Irn_Pkt). The group from North Africa (North Africa) was formed with patients from Morocco, Algeria, and one North African patient of unknown country of origin. Controls are shown in full circles, patients in empty circles. The MDS plot was generated using IBM SPSS Statistics Version 25.0 (raw stress = 0.014). Patients from Italy, Finland, and Singapore were not included in the study due to the small number of haplotypes (N < 10). MDS: multidimensional scaling.

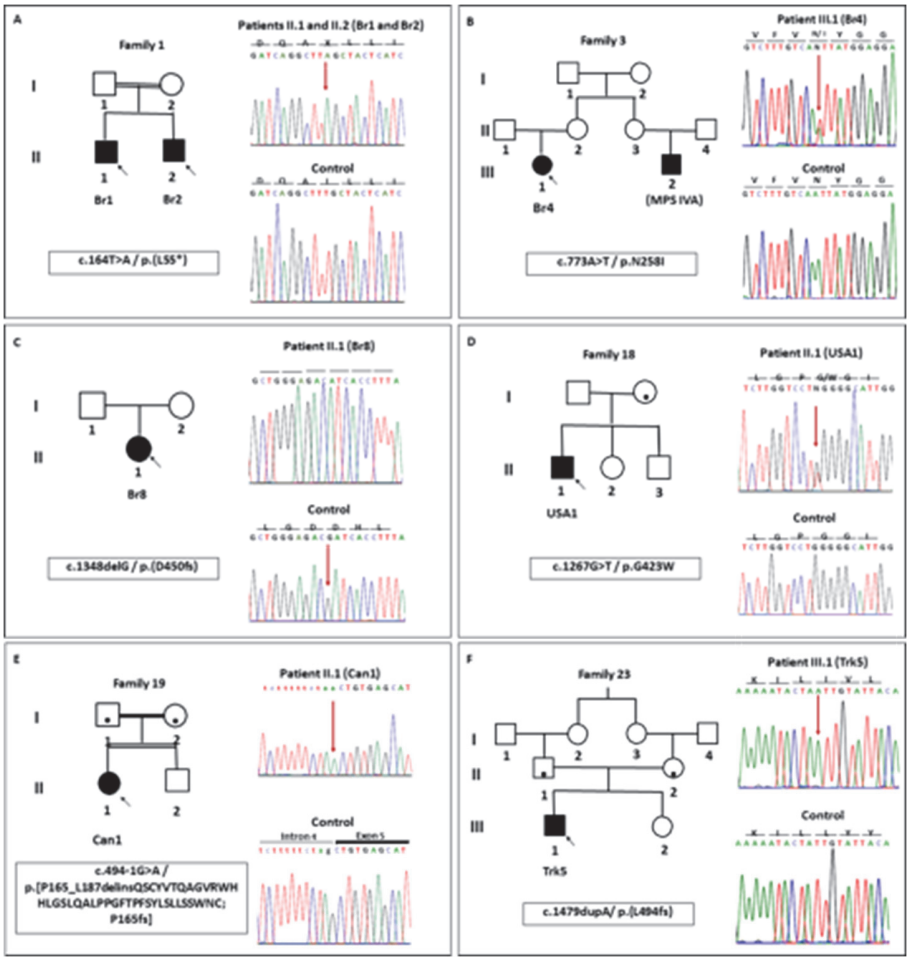


**Supp. Figure S1. Novel *HGSNAT* variants identified in MPSIIIC families**

**(A to F)** The pedigrees of six of the eleven families carrying previously unreported MPSIIIC mutations. Filled symbols show affected patients, clear symbols indicate unaffected individuals and dotted symbols, carriers confirmed by genomic DNA sequencing. Consanguineous marriages are indicated by a double line and probands are marked with an arrow. Electropherogram sequences of patients (top) and normal controls (bottom) show the following mutations: **(A)** c.164T>A/ p.Leu55Ter in homozygosity for Br1 and Br2 patients; **(B)** c.773T>A/ p.Asn258Ile in compound heterozygosity for Br4 patient; **(C)** c.1348delG/ p.(Asp450Ilefs*32) in homozygosity for Br8 patient; **(D)** c.1267G>T/ p.Gly423Trp in the compound heterozygosity for USA patient; **(E)** c.494-1G>A/p.Pro165_Leu187delinsGlnSerCysTyrValThrGlnAlaGly-ValArgTrpHisLeuGlySerLeuGlnAlaLeuProProGlyPheThrProPheSerTyrLeuSerLeuLeuSerSerTrpAsnCys,Pro165LeufsTer13] in homozygosity for Can1 patient; and **(F)** c.1479dupA/ p.(Leu494Ilefs*33) in the homozygosity for Trk5 patient.

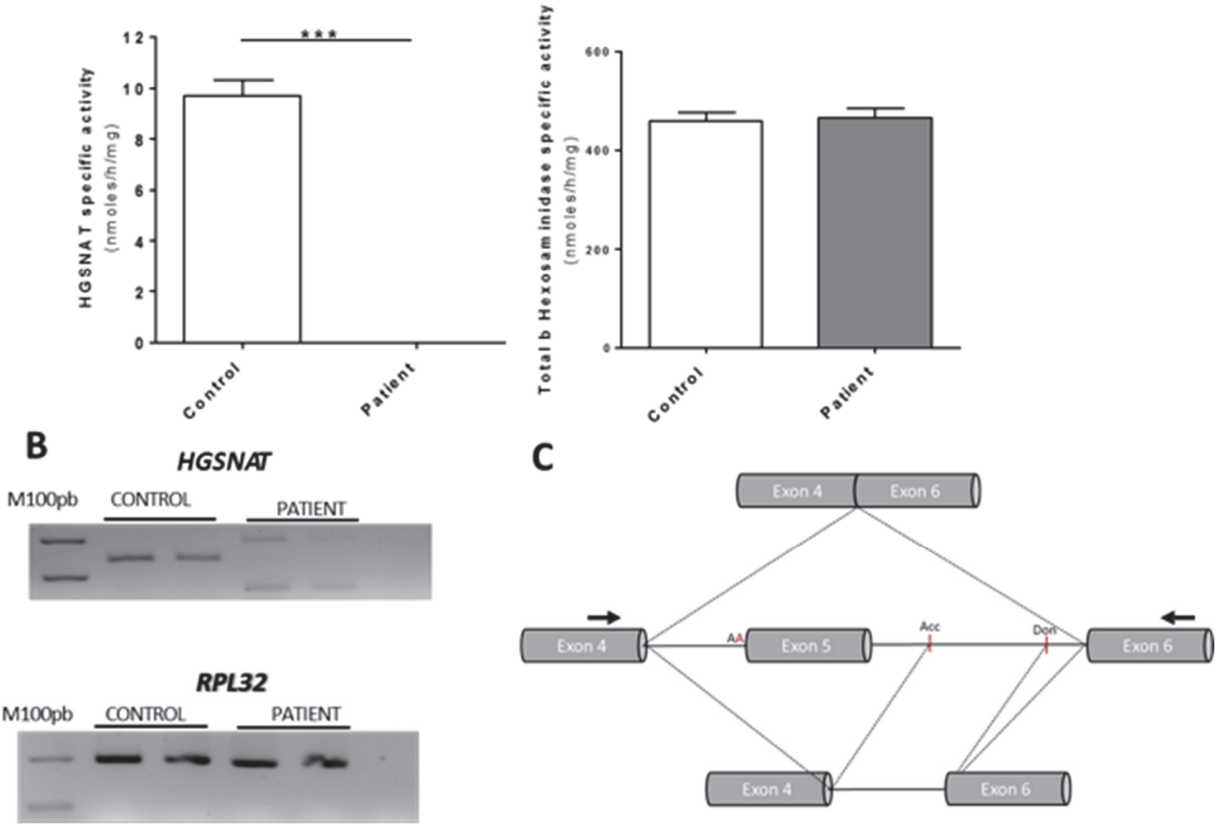


**Supp. Figure S2. Impact of the c.494-1G>A splice-site variant**

**A)** HGSNAT activity was not detected in fibroblasts of the patient homozygous for the c.494-1G>A variant. Activity of N-acetyltransferase and lysosomal control enzyme, β-hexosaminidase was essayed in protein extracts from control and patient's fibroblasts. The bars indicate mean ± SD of two independent experiments. *P*-values were calculated by Student's t-tests (***$P < 0.001$). **B)** PCR amplification using primers in exons 4 and 6 (shown as black arrows) was performed on cDNA synthetized from the RNA extracted from the patient's and control fibroblasts. c.494-1G>A causes exon 5 skipping and a frameshift (182-bp PCR fragment). It also leads to the activation of cryptic acceptor (Acc) and donor (Don) sites in intron 6 leading to insertion of 118 intronic nucleotides (300-bp PCR fragment). This transcript predicts a protein with a deletion of 23 amino acids (Pro164 to Ser187) and an insertion of 39 new residues, QSCYVTQAGVRWHHLGSLQALPPGFTPFSYLSLLSSWNC. *RPL32* was used as control. **C)** Scheme illustrating the effect of c.494-1G>A on *HGSNAT* transcription.

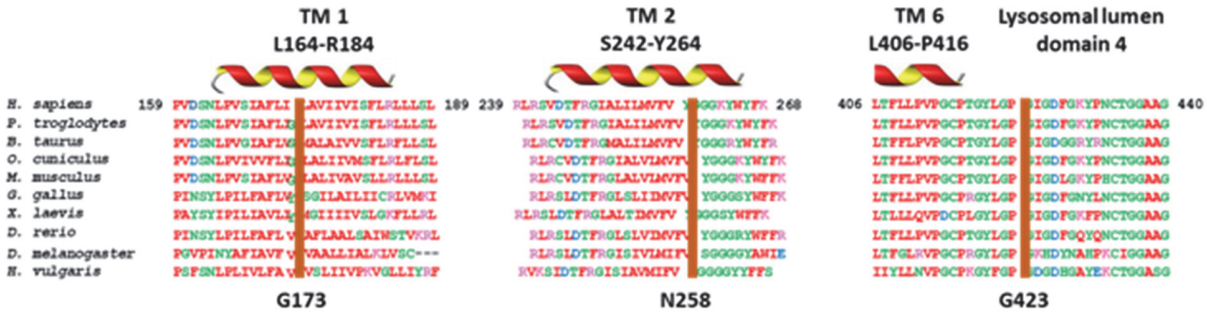


**Supp. Figure S3. Sequence alignment of HGSNAT orthologues show high level of amino acid conservation at the Asn258 and Gly423 positions**

N258 and G423 are located in highly conserved second transmembrane and fourth lysosomal lumen domains of the HGSNAT protein, while G173 located in the first transmembrane domain is conserved only in the mammals. Protein sequences used for alignment are Q68QP4 in the human (*Homo sapiens*), H2QW44 in the chimp (*Pan troglodytes*), F1MF45 in the cow (*Bos Taurus*), G1SUG4 in the rabbit (*Oryctolagus cuniculus*), Q3UDW8 in the mouse (*Mus musculus*), FINBK1 in the chicken (*Gallus gallus*), AOAIL8HW86 in the frog (*Xenopus laevis*), F1Q893 in the zebrafish (*Danio rerio*), Q9W4F7 in the fruit fly (*Drosophila melanogaster*) and T2MBP6 in the fresh-water polyp (*Hydra vulgaris*). The alignment was performed using Clustal Omega software (https://www.ebi.ac.uk/Tools/msa/clustalo/). The colour of the residues indicates their physicochemical properties.

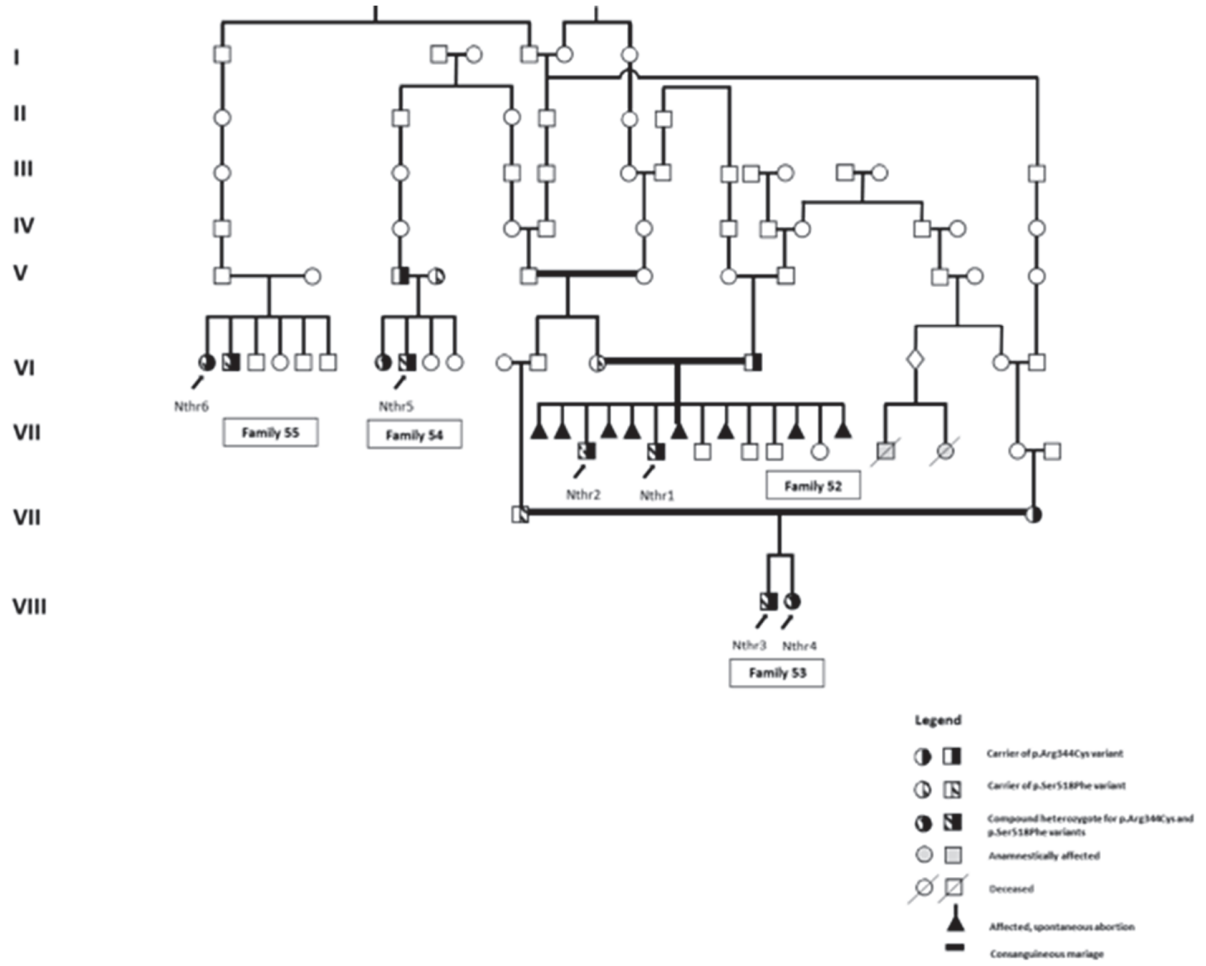


**Supp. Fig. S4 – Pedigree of extended Dutch family with several consanguineous links**

Families 52, 53, 54 and 55 (MPSIIIC patients Nthr1-Nthr6) studied in this work and initially reported by Ruijter *et al.*, 2008.

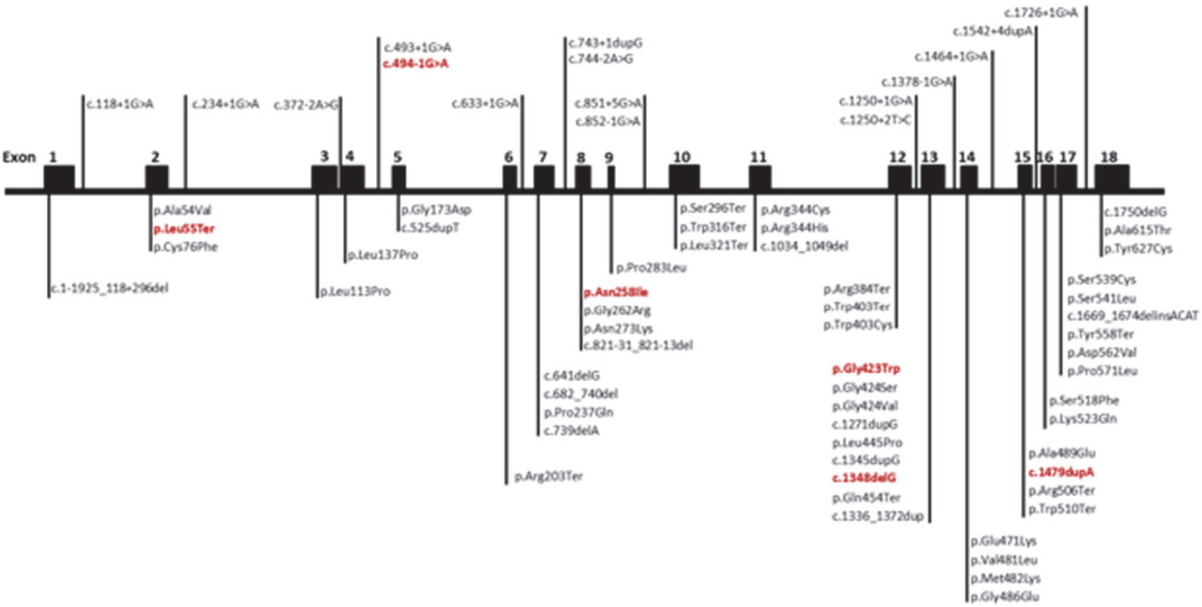


**Supp. Figure S5. Localization of the 71 variants associated with MPSIIIC in the *HGSNAT* gene.**

The novel variants are shown in red. Exons are represented by solid boxes and introns by lines between exons.

The supplementary tables are available at the journal website:
https://onlinelibrary.wiley.com/doi/10.1002/humu.23752

# Chapter IV: General Discussion

In the last decades, research has contributed for the understanding of the etiology and natural history of MPS IIIC. Nevertheless, the pathological mechanisms underlying the disease, especially those implicated in brain disease, have remained elusive due to its rarity and lack of an animal or appropriate cellular model(s).

The overall purpose of this thesis was to gain insights into the pathophysiology of the disease, essential for the development of therapeutic approaches; and contribute to the characterization of the diversity and frequency of *HGSNAT* pathogenic variants in specific populations or geographic locations, which promotes an earlier diagnosis of Sanfilippo C patients. With the prospect of clinical trials and therapies in a near future, the early diagnosis of MPS IIIC patients will likely contribute to the effectiveness of the therapeutic interventions.

## 4.1 Neuropathophysiology in Hgsnat-Geo mice as a complex set of events

Through the generation and study of the first MPS IIIC animal model, a functional *Hgsnat* KO (*Hgsnat-Geo*) mouse, which recapitulates cardinal features of the patients' phenotype, this thesis contributed to the knowledge of pathogenic alterations underlying the disease. Our findings and data on the remaining Sanfilippo subtypes mice models points to shared pathophysiological mechanisms to explain the similar clinical presentation, including the severe progressive cognitive decline, by these disorders (185, 294, 298, 308, 313, 314, 450, 451).

A second *Hgsnat*-knockout MPS IIIC murine model later generated and characterized by Marco and colleagues (450) showed a similar pathology but milder disease progression than the *Hgsnat-Geo* mouse studied in this thesis. This result could be due to different strategies used to functionally knockout the *Hgsnat* gene and/or distinct mice genetic backgrounds, likely leading to slightly different levels of residual HGSNAT activity.

The series of events triggered by the lysosomal HS catabolism impairment and resulting in neurodegeneration in the *Hgsnat-Geo* mice, is yet to be fully characterized. Nevertheless, our findings allow us to suggest that lysosomal storage of HS triggers a chronic neuroinflammatory response and the blockade of endolysosomal and autophagy pathways. These pathological

alterations likely contribute to the malfunction and the death of neurons, at least partially, by dysfunction of mitochondria.

### 4.1.1 Lysosomal HS storage in microglia as initial pathological event?

The work developed in this thesis suggests a main role for microglia on the pathogenesis of MPS IIIC, specifically, by triggering and exacerbating a pro-inflammatory response that likely contributes to the neurodegeneration.

It has been shown that extracellular HS-derived oligosaccharides, specifically containing 2-*O*-sulfated uronic units, likely released by cells through lysosomal exocytosis, are recognized as DAMP by microglia TLR4 receptors, triggering the MyD88/NF-κB pro-inflammatory pathway in MPS III (314, 452). A similar mechanism is proposed for the remaining MPS as other GAGs were shown to bind TLR4 (453).

Data on MPS III patients and animal models (314, 454-456) suggest that HS accumulation might start prenatally in the *Hgsnat-Geo* mice, being likely responsible for the activated cytotoxic phenotype (M1) of microglia since a very early age, detected at 10 days after birth. This result and the fact that lysosomal storage of HS in microglia clearly precedes that of neurons suggests that microglial cells have a dual role in triggering neuroinflammation; by releasing HS fragments to the extracellular space and subsequent recognition of the inflammatory signal with activation of the immune response.

The progressive lysosomal storage of HS in microglia, which becomes prominent with the age, is likely due to their phagocytic ability and further incapacity to degrade this GAG. The increase of neuroinflammation in the *Hgsnat-Geo* murine model might be largely due to the continuous HS storage in microglial lysosomes and consequent extracellular burden. This hypothesis is supported by the results of the first gene therapy study in MPS IIIC using our animal model (Tordo *et al.* 2018, annex sup article 2). The intracerebral injection of a novel, neurotropic AVV vector (AAV-TT) carrying the WT *HGSNAT* gene allowed the effective transduction, and supraphysiological HGSNAT activity, of mice neurons but not of microglia or activated astrocytes. Upon treatment, the brain HS content was approximately 60% of that in untreated mice, and the neuroinflammation

was slighly reduced. Altogether, our work and gene therapy data suggests that microglia and brain macrophages contribute to the exocytosis of HS fragments, eliciting and maintaining neuroinflammation in *Hgsnat-Geo* mice.

### 4.1.2 From chronic neuroinflammation to mitochondrial dysfunction and neurodegeneration?

The characterization of the *Hgsnat-Geo* mice showed that there is a chronic activation of glia and an augmented mRNA expression of pro-inflammatory mediators MIP-1α or TNF-α throughout the life of these animals. DAMPs other than undegraded HS fragments, resulting from the degeneration of neural cells, likely contribute to inflammation at a later stage of the disease, as suggested by studies in MPS IIIA (452) and IIIB mice (314).

The persistent activation of glial cells was detected in the *Hgsnat-Geo* mice and reported in nearly all degenerative disorders, preceding the appearance of symptoms, neuronal pathology and/or loss (185, 343, 451, 457). In fact, the sustained release of pro-inflammatory cytokines and long-term oxidative stress, through ROS and RNS production by activated glia, have been considered the culprit of neurodegeneration in most neuropathic LSDs and age-related disorders (458).

The deletion of MIP-1α or TNF-α expression in a murine model of Sandhoff disease resulted in decreased neuronal death, amelioration of neurologic function and increased lifespan (459, 460). Whereas MIP-1α is mainly associated to the chemotaxis of microglia and recruitment of peripheral leukocytes and lymphocytes to the CNS, TNF-α is not only an important mediator of immune response (330, 461, 462), as it can also trigger neuronal dysfunction or cell death pathways.

High levels of TNF-α, IL-1β, ROS and RNS are known to promote glutamate-induced neuronal excitoxicity and death via mitochondrial $Ca^{2+}$ overload and subsequent dysfunction driven by the mitochondrial Permeability Transition Pore Complex (PTPC) opening (317, 463). Due to the fact that swollen mitochondria with disorganized or collapsed internal cristae are detected in the neurons of *Hgsnat-Geo* mice, we hypothesize that chronic excitoxicity and mitochondrial membrane permeability transition participate in the pathophysiological process in MPS IIIC.

A persistent oxidative stress might also induce mitochondrial outer membrane permeabilization (MOMP), the activation of the caspase cascade and apoptosis. Furthermore, TNF-α can be recognized by the death receptor TNFR1 on the surface of neurons, leading to extrinsic apoptosis or necroptosis, possibly via further mitochondrial structural alterations and dysfunction (92).

Our results showed only a slight, non-significant increase of *IL-1β* mRNA expression after the age of four months, with a peak at 8/10 months. The expression of this cytokine is similar in MPS IIIA and WT mice brains until the age of six months, but shows a trend for an augmentation in MPS IIIB mice since an early age (two months-old). Previous studies have shown an increased *IL-1β* mRNA expression in brains of MPS IIIB (314, 452) and MPS IIIA (343) since an early age, being particularly significant at a later phase of the disease (eight to 10 months). Despite coherent data for MPS IIIB mice, the different *IL-1β* mRNA expression results for MPS IIIA mice in our and previous work might be explained by the use of a different animal model (343) and/or experimental conditions but further analyses should be performed to clarify this question. In the MPS IIIA murine model, the secretion of IL-1β resulted from activation of NRPL3 inflammasome by primary and secondary storage materials (452). It would be also interesting to verify if the *IL-1β* increased expression at 8/10 months in the *Hgsnat-Geo* mice concurs with the inflammasome activation and cell death by pyroptosis. With this purpose, the detection of the mature Casp1 and gasdermin D, as well as the secretion of IL-1β could be analyzed further.

Overall, the peak of neuroinflammation in the *Hgsnat-Geo* mice, at the age of six-eight months, coincides with the detection of hyperactive behavior and reduced anxiety, suggesting these events may be directly linked. The progressive malfunction of neurons might result in neuronal death, which is significant in 10 months-old *Hgsnat-Geo* mice brain cortices.

Interestingly, the rescuing of neuronal HGSNAT activity through AAV-TT-HGSNAT ICV delivery prevents neurodegeneration of *Hgsnta-Geo* mice, even if neuroinflammation is still present, but reduced comparatively to untreated animals (Tordo *et al.* 2018, in annex suplementary article 2). Similar results were obtained in Sandhoff mouse model with conditional HEXB expression in neurons, where GM2 storage in uncorrected microglia elicits a pro-inflammatory response without reducing neuronal viability (464).

Our findings and those of AAV-TT-HGSNAT based gene therapy suggest that neuroinflammation accelerates the neurodegenerative process resulting from neuronal autonomous events in *Hgsnat-Geo* mice.

### 4.1.3 Blockade of the endolysosomal and autophagy-lysosomal pathways leads to neurodegeneration?

In the *Hgsnat-Geo* mice and most LSDs, including MPS IIIA, NPC1 and Fabry disease, the progressive pathological storage of materials in the endolysosomal system eventually leads to structural and functional alterations of late endosomes/ lysosomes and to the impaired fusion between these vesicles and autophagosomes (104, 465, 466). It is possible that oxidative stress due to neuroinflammation and mitochondrial dysfunction might also contribute for the impaired lysosomal integrity and function. As result of the deficient autophagic flux, it occurs accumulation of autophagic substrates such as obsolete mitochondria and other organelles, as well as aggregate-prone proteins in the neuronal cytoplasm, which may induce further inflammation or trigger cell death pathways (452, 467).

Interestingly, the β-amyloid, p-tau and α-synuclein proteins, which are secondary storage materials in the neurons of patients and animal models of different LSDs, including MPS IIIA and IIIB, GM1 gangliosidosis and NPC1 (32, 275, 284, 337, 339, 468), characteristically accumulate in specific age-related disorders. The age-dependent decrease in the function of lysosome and autophagy pathway has been considered the main risk factor to the altered proteostasis in these disorders. Besides, several genes involved in lysosomal structure, function and autophagy have been recently identified as cause or risk factors for these aging induced proteinopathies (469). As example, pathogenic variants in the gene *GBA*, encoding for the lysosomal enzyme glucocerebrosidase and associated to Gaucher disease, are the most common genetic risk factors for PD (470).

The impairment of the autophagic clearance of toxic intracellular materials in the neurons seems, then, to be a common feature of LSDs with neurologic involvement and late-onset neurodegenerative diseases. This point to the main role of the endolysosomal-autophagy network in the maintenance of proper neuronal homeostasis and function.

The mechanism(s) underlying the fusion inhibition between LE/lysosomes and autophagosomes in most LSDs are yet to be understood, but several explanations have been proposed. The first is related to the alteration of the lipid content of endolysosomal membranes. In particular, an increased amount of cholesterol in endolysosomal membranes was shown to sequester and inhibit the recycling of SNARE proteins involved in the formation of autolysososmes in MPS IIIA and MSD mice (104). Indeed, cholesterol, which is enriched in lipid rafts, provides stability to the membrane and is a ligand to several membrane and other proteins. The increased amount of cholesterol in lipid rafts in the endolysosomal membranes may, then, interfere with the normal function of several proteins, including those promoting the vesicular fusion (471).

Other studies support that disruption of axonal transport, either retrograde or anterograde, of endocytic and autophagic vesicles might be responsible for the impaired fusion between LE/lysosomes with autophagosomes in neuropathic LSDs and age-related neurodegenerative disorders (70). The axonal transport deficits might be eventually caused by the enlargement of endolysosomal vesicles (472), inhibition of TRPML1 by stored lipids (473), sustained deacidification of lysosomes (70) resulting from lysosomal membrane permeabilization (LMP) (474), and instability of microtubules by tau protein loss of function due to phosphorylation (475).

Interestingly, the increase of *O*-GlcNAcylation, detected in the brains of *Hgsnat-Geo* mice, has also been shown to inhibit autophagosome maturation through the modification of the SNARE protein SNAP-29 (476). Future research is necessary to confirm and address the causes for the impaired fusion of late endosomes/ lysosomes and autophagosomes in MPS IIIC neurons.

Besides autophagy impairment, the endolysosomal system blockade likely affects other cellular functions in MPS IIIC. In fact, alterations in endocytosis and intracellular trafficking of internalized cargoes to the lysosome were reported in several LSDs (477), as well as the impairment of synaptic vesicle recycling interfering with presynaptic function, and likely neurotransmission, in a mouse model of MPS IIIA (478). The lysosomal dysfunction might directly affect the mitochondrial protein homeostasis (30) and dynamics (29), induce other pathological alterations (463) and signaling (492) leading to dysfunction and eventual death of neurons.

### 4.1.4 Accumulation and alteration of subcellular distribution of GM2 and GM3 gangliosides triggers neuronal dysfunction and apoptosis?

Molecular defects in the hydrolases or lipid-binding protein cofactors involved in the lysosomal catabolism of GM2 and GM3 lead to the primary storage of these glycosphingolipids (GSL). However, such as in *Hgsnat-Geo* mice, these gangliosides also accumulate as secondary storage material in many other LSDs (479) but their role on the neuronal pathology of these disorders has not been clearly established. Also, the mechanisms leading to the secondary accumulation of GM2 and GM3 in these disorders are not yet understood but several hypotheses were so far raised. These include the inhibition of sphingolipid activator proteins (GM2 activator protein, saposin A and B) by stored primary and secondary substrates such as CS, cholesterol, sphingomyelin and lysosphingolipids (479-481); modification in the activity of enzymes involved in the catabolism of GSL due to altered lysosomal pH and inhibition of neuraminidase activities by GAGs (315). However, in the *Hgsnat-Geo*, MPS IIIA and NPC murine models (482, 483) the two ganglioside species were mostly found segregated in different cytosolic vesicular structures in the same neuron, only partially co-localizing with LAMP1. This suggests that they mostly accumulate in compartments other than late endosomes/ lysosomes.

Besides the plasma membrane (PM) and the endolysosomal system, the gangliosides can be found in membranes of different organelles such as the Golgi apparatus, where they are synthesized (484), ER, mitochondria (485), nucleus (486, 487) and in vesicles transported from the endolysosomal system to the Golgi/TGN or PM via salvage pathways (488). The dysfunction and blockade of endolysosomal system seems to alter the intracellular distribution of these GSL, especially those targeting the ER and mitochondria, triggering apoptotic responses via $Ca^{2+}$ dyshomeostasis and mitochondrial dysfunction (489-493). Future studies might be performed to understand the role of the mitochondrial GM2 location in the *Hgsnat-Geo* mice neurons. Endolysosomal network blockage might also cause an impairment of the salvage pathways, leading to the accumulation of gangliosides' carrying vesicles, possibly followed by compensatory synthesis of gangliosides (315). To the different subcellular distribution of GM2 and GM3 gangliosides may contribute the HS-induced alterations of proximal Golgi compartments, as reported in MPS IIIB mice, resulting in sorting defects of GM3 and its consequent vesicular storage

(494). It can also result from the differential expression of genes involved in the biosynthesis and degradation of these and related gangliosides (495).

The partial subcellular co-localization, as well as regional distribution, of GM2 and GM3 in the brain of *Hgsnat-Geo* mice is accompanied by distinct responses to the intrastriatal injection of AAV-WT-HGSNAT (Tordo et al. 2018, annex sup article 2). Whereas GM3 content is significantly reduced upon treatment, the storage of GM2 is only decreased in specific brain areas, despite correction of behavior and memory decline. These data suggest distinct mechanisms not only underlying storage, but also pathology, for these gangliosides in MPS IIIC.

The level of GM2 and GM3 was found augmented in the CSF of MPS IIIA and B patients (496) and is possibly also increased in Sanfilippo C patients but further research is necessary to assess this hypothesis. The *Hgsnat-Geo* mice characterization and gene therapy results suggest these gangliosides, especially GM3, might represent appropriate biomarkers to evaluate treatment efficiency and disease progression in MPS IIIC.

### 4.1.5 Mitochondria damage as the main neuronal death inducer in MPS IIIC

Mitochondrial dysfunction is most likely the key contributing factor to the neurodegeneration in the MPS IIIC, as well as other neuropathic LSD and late-onset neurodegenerative disorders (457, 492, 493).

The etiology of neuronal mitochondria defects in *Hgsnat-Geo* mice seems to be multifactorial, with two main causes, the oxidative stress caused by neuroinflammation and later mitochondrial dysfunction, and the impairment of mitophagy. The accumulation of deformed mitochondria is detected after the age of five months, when neuroinflammation is almost as its peak, and mitophagy likely starts to be deficient. The continuous malfunction and accumulation of mitochondria likely leads to further ROS and RNS generation, organelle and cell damage, eventually compromising the energy availability, particularly demanding in neurons (90, 497, 498).

Despite the striking structural alterations detected in neuronal mitochondria in the brain of *Hgsnat-Geo* mice, the mitochondrial oxidative phosphorylation system presented only a partial impairment after eight months of age. This might be explained by the measurement of respiratory chain

complex activities in isolated brain mitochondria, including those of glial cells, which appear to be morphologically intact and functional. The activity of these and other mitochondrial enzymes, as well as CoQ10 content, would probably be significantly decreased, or found reduced at an earlier age, comparatively to WT animals, if analysis had been performed in neuronal cells only. The mitochondria has a central role on the metabolism and physiology of the cell. Recent studies have shown that, besides the traditional role of energy production, mitochondria are involved in many other cellular functions and mechanisms such as ROS production and signaling, calcium homeostasis in direct interaction with the lysosome and ER, lipid exchange with other organelles, and many others. Besides the above mentioned functions, mitochondria and the lysosome are interdependent in other cell processes including autophagy and organelle dynamics (29, 30, 32). Consequently, the dysfunction in one organelle is likely to exert a negative impact on the function of the other.

Mitochondria is currently viewed as a signaling hub, integrating environmental changes and triggering responses in order to maintain cell homeostasis and survival, or inducing cell death pathways. The signaling from the different pathological events in the studied MPS IIIC mouse are likely responsible for the neuronal defects of mitochondria, leading to dysfunction and ultimately executing the death of the cell.

Mitochondria structural alterations and dysfunction, as well as accumulation of mitochondria due to impaired mitophagy, are also observed in the neurons of many other LSD, such as NPC1, GM1 and GM2 gangliosidosis and late-onset neurodegenerative disorders, including AD, PD and HD (465, 499, 500)

### 4.1.6 Therapeutic approaches for MPS IIIC

Based on our findings we propose that targeting the reduction of HS lysosomal storage in neurons and microglia, which trigger the remaining pathological events, might result in the correction of the neurologic impairment in the *Hgsnat-Geo* mice. Among possible treatments (SRT, enhancement of the endolysosomal and autophagy pathways, and enzyme enhancement therapy), the restoration of the HGSNAT activity in neurons and/or microglia by gene therapy is likely the most efficient therapeutic approach.

As previously mentioned, the MPS IIIC murine model characterized in this thesis was meanwhile used in the first gene therapy study for MPS IIIC, a collaborative research with Dr Bigger at University of Manchester, targeting the HGSNAT deficiency in neuronal cells (Tordo et al. 2018, in annex sup article 2). A single intracerebral administration of the novel neurotropic AAV-TT, vector carrying the missing *HGSNAT* gene enabled the long-term, widespread expression of HGSNAT in the brain of *Hgsnat-Geo* mice. The amelioration of the neuropathology, in particular the reduction of lysosomal storage and neuroinflammation, leads to the correction of behaviour and memory deficits. The encouraging findings of this research are the proof of concept of the future clinical trial on MPS IIIC using this therapeutic vector.

These results are particularly important since MPS IIIC is caused by deficiency of a lysosomal transmembrane protein, which seems to preclude the cross-correction between WT-HGSNAT transduced neurons and remaining deficient cells. The rescue of cognitive function is likely due to an efficient neuronal transduction, combined with high expression of HGSNAT, in *Hgsnat-Geo* treated mice. Congruently, in a NPC1 chimeric mouse, the expression of NPC1, a lysosomal membrane protein, in 15% of neurons lead to a later onset of the disease, and in 30-60% it enabled the near-complete correction of the phenotype (501).

The treatment of the primary defect in microglia will likely also drive major neurologic improvement in the *Hgsnat-Geo* mice, by reducing HS extracellular burden and neuroinflammation. The transplant of hematopoietic cells transduced *ex-vivo* with a LV vector expressing the missing enzyme at supraphysiological levels has enabled the correction of behaviour and neuropathology in MPS IIIA and IIIB mice (387, 388, 418). Due to the limitation of HGSNAT cross-correction, the efficacy of a similar therapeutic approach in the *Hgsnat-Geo* mice might be eventually improved using adjuvant therapies to reduce HS lysosomal storage in neurons, as well as antioxidant and anti-inflammatory compounds.

Several therapeutic approaches targeting reduction of neuroinflammation through down-regulation of pro-inflammatory pathways enabled a slower progression of behavior abnormalities and memory deficit, extending the survival of MPS IIIA and IIIB mice (335, 388, 447). The IL-1 signaling inhibition prevented hyperactivity and memory impairment in 6-month-old MPSIIIA mice (452) but it is possible that cognitive function decline occurs at later ages.

In fact, downstream events resulting from the lysosomal storage of HS in neurons are still likely to promote the dysfunction and/or death of these cells in the absence of inflammation. Studies in 10 days-old mutant MPS IIIB×TLR4$^{-/-}$ and MPS IIIB×MyD88$^{-/-}$ mice (314, 334) and cultured neuronal cells derived from Sanfilippo B and C patients' iPSC lines seem to confirm that inflammation-independent events are also responsible for neuronal pathology (394, 502, 503). Alterations detected in these animal and cellular models, such as the intraneuronal disorganization of the Golgi complex, dysregulation of *GAP43* mRNA levels and neurite growth, as well as accumulation of SCMAS and oxidative stress, are likely a direct or indirect consequence of the lysosomal storage of HS fragments.

Nevertheless, we believe that anti-inflammatory treatments will have a significant neuroprotective effect in MPS IIIC. Therefore, it would be important to explore the impact of drugs associated to an improved pathology and/or delayed onset in different neurodegenerative disorders such as TNFR1-specific antagonist antibodies (458, 504) and specific NSAIDs (505, 506) in the *Hgsnat-Geo* mice. The efficacy of compounds already proven beneficial for other MPS III animal models, such as pentosan polysulfate (447) and the corticosteroid prednisolone (335, 388) could also be evaluated in the MPS IIIC mice, either alone or in combination with other therapies.

Pentosan sulfate (PPS), as well as prednisolone, are unable to cross the BBB either in mice and humans (335, 447, 507), likely contributing to an improvement of brain pathology and clinical symptoms of MPS III animal models through the reduction of peripheral inflammation (335, 388, 447). The consequent decrease in the infiltration of peripheral immune cells into the CNS and neuroinflammation has a neuroprotective effect, driving the amelioration of neurologic function. Indeed, a study led by Killedar *et al*. (508) showed that IV injection of splenic lymphocytes isolated from MPS IIIB mice into naïve WT animals triggered a neuroinflammatory response leading to an increase in the expression of cytokines and other markers of glial activation, lymphocyte infiltration in the CNS and a mild paralytic disease.

Nevertheless, the compromised integrity of the BBB, detected in Sanfilippo patients and murine models (310, 360) might contribute, not only to the infiltration of leukocytes into the brain, augmenting neuroinflammation, but also enable its permeability to therapeutic agents such as PPS and prednisolone, being required further studies to confirm this last hypothesis. Besides the direct

inhibition of anti-inflammatory pathways, PPS has also the capacity to reduce GAG levels making it an interesting therapeutic approach for MPS IIIC.

Therapies targeting pro-inflammatory pathways are likely to achieve a long-term effectiveness treatment of neurologic disease in Sanfilippo C syndrome in combination with other approaches preventing or reducing the HS lysosomal storage in neurons and microglia/ brain macrophages. A possible alternative is the enhancement of endolysosomal and lysosomal-autophagy pathways through pharmacological activation of TFEB or inhibition of the upstream mTORC1 in these target cells. Treatment with trehalose, an mTORC1-independent TFEB activator compound that crosses the BBB, was shown to promote autophagosome clearance in neurons and glial cells, leading to improvement of brain pathology and behavior in MPS IIIB mice, especially at an earlier stage of the disease (439). Trehalose also improved proteostasis and the clearance of α-synuclein and SOD1 aggregates in, respectively, PD (509) and amyotrophic lateral sclerosis ALS (510) animal models, promoting neuronal survival. Nevertheless, the activity of this naturally occurring disaccharide as a chemical chaperone might also contribute to the reduction of misfolded proteins and aggregates in the cells (510).

Promising results in preclinical studies of different late-onset neurodegenerative disorders were achieved by using other autophagy-enhancers such as the mTORC1 inhibitors rapamycin and rapamycin-analog drugs, and lithium, which induces autophagy by reduction of $IP_3$ levels and phosphoinositol signaling (511). In LSDs, treatment of cultured cerebellar cells from a mouse model of Batten disease with lithium, and of human NPC1 iPSC-derived neuronal cells with rapamycin rescues the autophagic defect, promoting neuronal viability (512, 513). However, due to the essential role of mTOR and TFEB in cell metabolism, long-term treatment with mTOR inhibitors and TFEB activators, may cause side effects, being necessary performing studies to evaluate safety of current and prospective drugs (513, 514). Interestingly, treatments targeting the activation of TFEB not only promote lysosomal function and autophagic clearance of dysfunctional mitochondria (515), as previously mentioned, as they can also induce mitochondrial biogenesis and lessen fragmentation (32, 73). Consequently, when used at an early phase, these therapies, targeting both organelles, may likely prevent or delay the onset of neurologic pathology and improve clinical manifestations. The efficiency of trehalose and other inducers of the autophagy pathway in ameliorating brain disease could be, then, tested in the *Hgsnat-Geo* mice.

The functional study of the three *HGSNAT* missense variants in the chapter III of this thesis supported previously results for this type of mutations, where resulting mutant proteins lack proteolytic processing and lysosomal targeting, likely due to misfolding. The development of pharmacological chaperones (PC) able to cross the BBB will likely present a therapeutic benefit for MPS IIIC patients carrying missense variants, by reducing lysosomal HS storage. The future characterization of the HGSNAT tertiary structure will likely enable the development of other active-site PCs besides glucosamine, possibly also mutation-specific.

Despite the indication that use of antioxidant molecules, such as CoQ10, might be potentially beneficial for reducing the disease progression in MPS III (449), preclinical studies may now be undertaken in the studied MPS IIIC murine model.

It is likely that a mitochondrial cocktail, including a high-dose of, not only CoQ10, but also other BBB-crossing antioxidant molecules and metabolic cofactors essential for the activity of mitochondrial enzymes, provides further benefits for MPS IIIC cells neurons than the treatment with individual molecules. Besides, the synergistic effect of specific antioxidants suggests a higher efficacy on the use of a combination of molecules comparatively to their single use (516, 517).

The reduction of oxidative stress, as well as the increased availability of enzyme cofactors, potentially promotes the integrity and function of mitochondrial membranes and proteins, and energy production. Indeed, *In vitro* and preclinical studies support the therapeutic effect of various antioxidant compounds and cofactors, either alone or in combination, in neurologic disease associated to primary or secondary mitochondrial disease (517-520). However, the results of clinical trials suggest only small, or even inexistent, effects of antioxidant therapies in neurodegenerative disorders. This might be explained by the low dose or bioavailability of the different compounds, their or derived metabolites' ability to cross the BBB, the variability in the metabolism in the patients and the stage of the disease (517).

In MPS IIIC, and remaining neurodegenerative disorders, it is expected that the large number of structurally altered, dysfunctional mitochondria present in later stages of the disease significantly limits the efficacy, or even precludes an effect, for this therapeutic approach. Due to the early onset of neuroinflammation, and likely also oxidative stress, it is possible that an appropriate combination of antioxidants could offer a neuroprotective effect when administered at pre-symptomatic or early stages of the disease. Nevertheless, in order to prevent the progression of the

disease, it should be used as an adjuvant to other therapy aiming the reduction of lysosomal storage of HS in neurons.

In spite of the advantages of the *Hgsnat-Geo* model on preclinical research, other cellular or animal models need to be generated to test the efficiency of PCs for missense variants, or drugs that overcome splicing and truncating defects, on increasing the HGSNAT residual activity. This will be likely facilitated by the recent advance of CRISPR/Cas9 and (521) iPSC-based (394) technologies allowing the generation of animal and 2D or 3D neural cellular models, such as the co-culture of brain organoids with microglia and astrocytes (522), carrying different types of *HGSNAT* variants.

### 4.2 Promoting the early diagnosis of MPS IIIC patients

Preclinical studies (398, 407, 408, 410-413) and clinical trials (363, 364) in MPS III have shown that treatment in pre-symptomatic and early stages of the disease is essential for preventing or delaying cognitive decline and extend lifespan. The eminent start of clinical trials and the availability of new therapies urges, then, an early diagnosis of MPS IIIC patients. However, the non-specific symptoms at the onset of the disease are likely responsible for the diagnostic delay detected in our cohort of patients and also reported for other MPS IIIC cases, associated to a psychological and economic burden of patients and their families (166, 244, 249, 523). Consequently, there is a need to reduce the time to diagnosis of the disease.

Interestingly, a tool based in the analysis of facial features by artificial intelligence was able to identify MPS IIIB patients at an early phase of the disease (524). Despite being milder than MPS IIIB, it is possible that a similar analysis of this and other clinical signs, individually or as a group, could enable an efficient and faster diagnosis of Sanfilipo C patients. The early molecular characterization of patients also enables the targeted genetic screening of family members and informed family planning.

Through our research, we have contributed to the knowledge of the spectrum and frequency of HGSNAT disease-causing variants in MPS IIIC patients in different populations or geographic

locations, and confirmed the existence of several hypothesized founder effects, which may enable a more efficient and earlier diagnosis of the disease.

In particular, we have shown that p.L55*, p.N258I, c.525dupT represent HGSNAT founder mutations in four villages (Alagoa Nova, Cabeceiras, Mogeiro and Taperoa) of the Brazilian state of Paraiba, being responsible for the highest live-birth prevalence of MPS IIIC reported so far. In Brazil, the live-birth prevalence estimate is in the range with other countries (205). The identification of this Paraiba's and other geographic clusters of the disease could have an immediate impact on the implementation of regional health policies for preconception carrier screening, prenatal and newborn diagnosis. Our findings suggest that similar measures could be also implemented in populations with a tradition of consanguineous marriages. In these geographic locations or populations, with high frequency of specific pathogenic variants, the targeted screening of variants as the first line of molecular diagnosis could allow a faster diagnosis of patients and carriers.

As linkage disequilibrium decays with the distance, the size of DNA fragment for haplotype analysis, as well as the number of alleles studied, are essential for the correct estimation of the age of genetic variants. Due to the relatively small number of patients carrying alleles for specific pathogenic variants, and the fragment length analysed in our study, the dating of genetic variants present in several Sanfilippo C patients of the same or different populations was not performed. In the future, the identification of other patients and healthy carriers, and the study of extended adjacent genomic regions, or eventually the complete genome, will allow estimating the time to the most recent common ancestor for MPS IIIC variants.

Genomic data from different control populations of 1000 genomes and gnomAD databases enabled us to overcome the absence of specific control populations for the diverse geographic origins of the MPS IIIC patients analysed. The methodology used, based on the analysis of haplotype context IIIC patients, followed by construction of haplotype networks, combined with worldwide distribution and frequency of *HGSNAT* disease-associated variants and historical data, allowed us to get insights into the evolutionary history of MPS IIIC.

Our study has enabled a better characterization of the MPS IIIC natural history, essential for the design of future clinical trials. Furthermore, our results suggest the existence of two groups of patients based on the disease onset, progression and severity, and the genotype presented. To

further confirm our results, prospective studies using standardized tests for evaluation of cognitive function and appropriate statistical analysis should be undertaken. Furthermore, the registries of patients, each time more complete, may provide further information on the clinical history of patients, novel and reported pathogenic variants and contribute to the understanding of genotype/ phenotype correlations. In order to predict or confirm the MPS IIIC phenotype associated to specific *HGSNAT* variants studies in cellular and animal models, as previously mentioned, could be performed. Nevertheless, factors other than *HGSNAT* pathogenic variants seem to influence the different progression and severity of MPS IIIC. It is likely that variation in genes involved in the endolysosomal traffic and degradation, autophagy, inflammatory response, mitochondrial function, metabolism of lipids, $Ca^{2+}$ regulation, UPS and ER-stress response, among others, modify the phenotypic severity of the disease. The study of genomes, transcriptomes and proteomes of siblings, and other patients carrying common HGSNAT variants might unravel disease modifiers, contribute to a deeper understanding of the downstream pathogenic mechanisms and suggest different therapeutic approaches.

## 4.3 Conclusion

Animal models are useful tools to gain insights into the complex pathophysiologic mechanisms underlying human disease, especially in the case of rare neurodegenerative disorders such as MPS IIIC.

In this thesis, through the study *o*f an *Hsgnat* knockout mice, we have demonstrated that HGSNAT deficiency and impaired lysosomal catabolism of HS leads to neuronal death. Further research is necessary to unravel the seemingly intricate set of events driving neurodegeneration in MPS IIIC. Nevertheless, our findings suggest a major contribution of mitochondrial dysfunction, likely resulting from a combination of chronic neuroinflammation and impaired mitophagy. These mechanisms, likely involved in the neuropathogenesis of MPS IIIC, represent potential therapeutic targets of the disease.

The existence of a genuine animal model of MPS IIIC enables future preclinical studies to evaluate safety and effectiveness of therapeutic approaches and further characterization of the pathogenic mechanisms contributing to the disease.

The molecular and clinical characterization of a large cohort of Sanfilippo C patients indicates that the onset and progression of the disease are potentially associated with the type of *HGSNAT* disease-variants carried, but modulated by other genetic or epigenetic variations. Future studies are necessary to define possible *HGSNAT* genotype-phenotype correlations and identify disease-modifying factors.

Our research has also extended the known geographic distribution and mutation spectrum of MPS IIIC, and helped to better characterize the diversity and frequency of *HGSNAT* pathogenic variants in different populations, including the presence of founder effects. This knowledge may contribute to the earlier diagnosis of patients resulting, in a near future, an improved treatment efficiency.

Finally, the haplotype analysis of the largest group of Sanfilippo C patients, in combination with worldwide *HGSNAT* allele frequency and historical data, provided insights into the evolutionary history of MPS IIIC.

# Chapter V: Bibliography


1. De Duve C, Pressman BC, Gianetto R, Wattiaux R, Appelmans F. Tissue fractionation studies. 6. Intracellular distribution patterns of enzymes in rat-liver tissue. Biochem J. 1955;60(4):604-17.
2. Renate L-R. Lysosomes. Springer, Boston, MA; 2005. p. 1-16.
3. Pu J, Guardia CM, Keren-Kaplan T, Bonifacino JS. Mechanisms and functions of lysosome positioning. J Cell Sci. 2016;129(23):4329-39.
4. Staudt C, Puissant E, Boonen M. Subcellular Trafficking of Mammalian Lysosomal Proteins: An Extended View. Int J Mol Sci. 2016;18(1).
5. Alberts B JA, Lewis J, et al. Transport from the Trans Golgi Network to the Cell Exterior: Exocytosis: Garland Science; 2002.
6. Saftig P, Klumperman J. Lysosome biogenesis and lysosomal membrane proteins: trafficking meets function. Nat Rev Mol Cell Biol. 2009;10(9):623-35.
7. Braulke T, Bonifacino JS. Sorting of lysosomal proteins. Biochim Biophys Acta. 2009;1793(4):605-14.
8. Ponder KP, Haskins ME. Gene therapy for mucopolysaccharidosis. Expert Opin Biol Ther. 2007;7(9):1333-45.
9. Canuel M, Libin Y, Morales CR. The interactomics of sortilin: an ancient lysosomal receptor evolving new functions. Histol Histopathol. 2009;24(4):481-92.
10. Reczek D, Schwake M, Schroder J, Hughes H, Blanz J, Jin X, et al. LIMP-2 is a receptor for lysosomal mannose-6-phosphate-independent targeting of beta-glucocerebrosidase. Cell. 2007;131(4):770-83.
11. Bajaj L, Lotfi P, Pal R, Ronza AD, Sharma J, Sardiello M. Lysosome biogenesis in health and disease. J Neurochem. 2019;148(5):573-89.
12. Park SY, Guo X. Adaptor protein complexes and intracellular transport. Biosci Rep. 2014;34(4).
13. Sardiello M, Palmieri M, di Ronza A, Medina DL, Valenza M, Gennarino VA, et al. A gene network regulating lysosomal biogenesis and function. Science. 2009;325(5939):473-7.
14. Fraldi A, Klein AD, Medina DL, Settembre C. Brain Disorders Due to Lysosomal Dysfunction. Annu Rev Neurosci. 2016;39:277-95.
15. Hsu CL, Lee EX, Gordon KL, Paz EA, Shen WC, Ohnishi K, et al. MAP4K3 mediates amino acid-dependent regulation of autophagy via phosphorylation of TFEB. Nat Commun. 2018;9(1):942.
16. Settembre C, Di Malta C, Polito VA, Garcia Arencibia M, Vetrini F, Erdin S, et al. TFEB links autophagy to lysosomal biogenesis. Science. 2011;332(6036):1429-33.
17. Lubke T, Lobel P, Sleat DE. Proteomics of the lysosome. Biochim Biophys Acta. 2009;1793(4):625-35.
18. Luzio JP, Pryor PR, Bright NA. Lysosomes: fusion and function. Nat Rev Mol Cell Biol. 2007;8(8):622-32.
19. Gonzalez A, Valeiras M, Sidransky E, Tayebi N. Lysosomal integral membrane protein-2: a new player in lysosome-related pathology. Mol Genet Metab. 2014;111(2):84-91.
20. Schwake M, Schroder B, Saftig P. Lysosomal membrane proteins and their central role in physiology. Traffic. 2013;14(7):739-48.

21. Appelqvist H, Waster P, Kagedal K, Ollinger K. The lysosome: from waste bag to potential therapeutic target. J Mol Cell Biol. 2013;5(4):214-26.
22. Lloyd-Lewis B, Krueger CC, Sargeant TJ, D'Angelo ME, Deery MJ, Feret R, et al. Stat3-mediated alterations in lysosomal membrane protein composition. J Biol Chem. 2018;293(12):4244-61.
23. Schuette CG, Pierstorff B, Huettler S, Sandhoff K. Sphingolipid activator proteins: proteins with complex functions in lipid degradation and skin biogenesis. Glycobiology. 2001;11(6):81R-90R.
24. Marques ARA, Saftig P. Lysosomal storage disorders - challenges, concepts and avenues for therapy: beyond rare diseases. J Cell Sci. 2019;132(2).
25. Kulkarni VV, Maday S. Neuronal endosomes to lysosomes: A journey to the soma. J Cell Biol. 2018;217(9):2977-9.
26. Ferguson SM. Axonal transport and maturation of lysosomes. Curr Opin Neurobiol. 2018;51:45-51.
27. Oyarzun JE, Lagos J, Vazquez MC, Valls C, De la Fuente C, Yuseff MI, et al. Lysosome motility and distribution: Relevance in health and disease. Biochim Biophys Acta Mol Basis Dis. 2019;1865(6):1076-87.
28. Platt FM, d'Azzo A, Davidson BL, Neufeld EF, Tifft CJ. Lysosomal storage diseases. Nat Rev Dis Primers. 2018;4(1):27.
29. Wong YC, Ysselstein D, Krainc D. Mitochondria-lysosome contacts regulate mitochondrial fission via RAB7 GTP hydrolysis. Nature. 2018;554(7692):382-6.
30. Cioni JM, Lin JQ, Holtermann AV, Koppers M, Jakobs MAH, Azizi A, et al. Late Endosomes Act as mRNA Translation Platforms and Sustain Mitochondria in Axons. Cell. 2019;176(1-2):56-72 e15.
31. De Duve C, Wattiaux R. Functions of lysosomes. Annu Rev Physiol. 1966;28:435-92.
32. Nixon RA. The role of autophagy in neurodegenerative disease. Nat Med. 2013;19(8):983-97.
33. Bonam SR, Wang F, Muller S. Lysosomes as a therapeutic target. Nat Rev Drug Discov. 2019;18(12):923-48.
34. Badadani M. AutophagyMechanism, Regulation, Functions, and Disorders. ISRN Cell Biology. 2012;Volume 2012:11.
35. Gonda A, Kabagwira J, Senthil GN, Wall NR. Internalization of Exosomes through Receptor-Mediated Endocytosis. Mol Cancer Res. 2019;17(2):337-47.
36. Ewers H, Helenius A. Lipid-mediated endocytosis. Cold Spring Harb Perspect Biol. 2011;3(8):a004721.
37. Zuverink M, Barbieri JT. Protein Toxins That Utilize Gangliosides as Host Receptors. Prog Mol Biol Transl Sci. 2018;156:325-54.
38. Nixon RA, Yang DS, Lee JH. Neurodegenerative lysosomal disorders: a continuum from development to late age. Autophagy. 2008;4(5):590-9.
39. Brown MS, Anderson RG, Goldstein JL. Recycling receptors: the round-trip itinerary of migrant membrane proteins. Cell. 1983;32(3):663-7.
40. Cullen PJ, Steinberg F. To degrade or not to degrade: mechanisms and significance of endocytic recycling. Nat Rev Mol Cell Biol. 2018;19(11):679-96.
41. Wenzel EM, Schultz SW, Schink KO, Pedersen NM, Nahse V, Carlson A, et al. Concerted ESCRT and clathrin recruitment waves define the timing and morphology of intraluminal vesicle formation. Nat Commun. 2018;9(1):2932.

42. Maxfield FR, Yamashiro DJ. Endosome acidification and the pathways of receptor-mediated endocytosis. Adv Exp Med Biol. 1987;225:189-98.
43. Langemeyer L, Frohlich F, Ungermann C. Rab GTPase Function in Endosome and Lysosome Biogenesis. Trends Cell Biol. 2018;28(11):957-70.
44. Elkin SR, Lakoduk AM, Schmid SL. Endocytic pathways and endosomal trafficking: a primer. Wien Med Wochenschr. 2016;166(7-8):196-204.
45. Xu H, Ren D. Lysosomal physiology. Annu Rev Physiol. 2015;77:57-80.
46. Medina DL, Fraldi A, Bouche V, Annunziata F, Mansueto G, Spampanato C, et al. Transcriptional activation of lysosomal exocytosis promotes cellular clearance. Dev Cell. 2011;21(3):421-30.
47. Settembre C, Fraldi A, Medina DL, Ballabio A. Signals from the lysosome: a control centre for cellular clearance and energy metabolism. Nat Rev Mol Cell Biol. 2013;14(5):283-96.
48. Shen YT, Gu Y, Su WF, Zhong JF, Jin ZH, Gu XS, et al. Rab27b is Involved in Lysosomal Exocytosis and Proteolipid Protein Trafficking in Oligodendrocytes. Neurosci Bull. 2016;32(4):331-40.
49. Padamsey Z, McGuinness L, Emptage NJ. Inhibition of lysosomal Ca(2+) signalling disrupts dendritic spine structure and impairs wound healing in neurons. Commun Integr Biol. 2017;10(5-6):e1344802.
50. Dou Y, Wu HJ, Li HQ, Qin S, Wang YE, Li J, et al. Microglial migration mediated by ATP-induced ATP release from lysosomes. Cell Res. 2012;22(6):1022-33.
51. Tsunemi T, Perez-Rosello T, Ishiguro Y, Yoroisaka A, Jeon S, Hamada K, et al. Increased Lysosomal Exocytosis Induced by Lysosomal Ca(2+) Channel Agonists Protects Human Dopaminergic Neurons from alpha-Synuclein Toxicity. J Neurosci. 2019;39(29):5760-72.
52. Zhang Z, Chen G, Zhou W, Song A, Xu T, Luo Q, et al. Regulated ATP release from astrocytes through lysosome exocytosis. Nat Cell Biol. 2007;9(8):945-53.
53. Luzio JP, Hackmann Y, Dieckmann NM, Griffiths GM. The biogenesis of lysosomes and lysosome-related organelles. Cold Spring Harb Perspect Biol. 2014;6(9):a016840.
54. Samie MA, Xu H. Lysosomal exocytosis and lipid storage disorders. J Lipid Res. 2014;55(6):995-1009.
55. Ballabio A. The awesome lysosome. EMBO Mol Med. 2016;8(2):73-6.
56. Edgar JR. Q&A: What are exosomes, exactly? BMC Biol. 2016;14:46.
57. Fruhbeis C, Frohlich D, Kuo WP, Kramer-Albers EM. Extracellular vesicles as mediators of neuron-glia communication. Front Cell Neurosci. 2013;7:182.
58. Chivet M, Javalet C, Laulagnier K, Blot B, Hemming FJ, Sadoul R. Exosomes secreted by cortical neurons upon glutamatergic synapse activation specifically interact with neurons. J Extracell Vesicles. 2014;3:24722.
59. Fitzner D, Schnaars M, van Rossum D, Krishnamoorthy G, Dibaj P, Bakhti M, et al. Selective transfer of exosomes from oligodendrocytes to microglia by macropinocytosis. J Cell Sci. 2011;124(Pt 3):447-58.
60. Mizushima N. Autophagy: process and function. Genes Dev. 2007;21(22):2861-73.
61. Li WW, Li J, Bao JK. Microautophagy: lesser-known self-eating. Cell Mol Life Sci. 2012;69(7):1125-36.
62. Kaushik S, Cuervo AM. Chaperone-mediated autophagy: a unique way to enter the lysosome world. Trends Cell Biol. 2012;22(8):407-17.
63. Yan X, Uronen RL, Huttunen HJ. The interaction of alpha-synuclein and Tau: A molecular conspiracy in neurodegeneration? Semin Cell Dev Biol. 2018.

64. Zhao YG, Zhang H. Autophagosome maturation: An epic journey from the ER to lysosomes. J Cell Biol. 2019;218(3):757-70.
65. Yin Z, Pascual C, Klionsky DJ. Autophagy: machinery and regulation. Microb Cell. 2016;3(12):588-96.
66. Hayato Hikita SS, Tetsuo Takehara,. Mechanisms of the autophagosome-lysosome fusion step and its relation to non-alcoholic fatty liver disease. Liver Research. 2018;2( 3):120-4,.
67. Papadopoulos C, Kravic B, Meyer H. Repair or Lysophagy: Dealing with Damaged Lysosomes. J Mol Biol. 2019.
68. Chen Y, Yu L. Recent progress in autophagic lysosome reformation. Traffic. 2017;18(6):358-61.
69. Tang G, Gudsnuk K, Kuo SH, Cotrina ML, Rosoklija G, Sosunov A, et al. Loss of mTOR-dependent macroautophagy causes autistic-like synaptic pruning deficits. Neuron. 2014;83(5):1131-43.
70. Lie PPY, Nixon RA. Lysosome trafficking and signaling in health and neurodegenerative diseases. Neurobiol Dis. 2019;122:94-105.
71. Lawrence RE, Zoncu R. The lysosome as a cellular centre for signalling, metabolism and quality control. Nat Cell Biol. 2019;21(2):133-42.
72. Duvel K, Yecies JL, Menon S, Raman P, Lipovsky AI, Souza AL, et al. Activation of a metabolic gene regulatory network downstream of mTOR complex 1. Mol Cell. 2010;39(2):171-83.
73. Deus CM, Yambire KF, Oliveira PJ, Raimundo N. Mitochondria-Lysosome Crosstalk: From Physiology to Neurodegeneration. Trends Mol Med. 2019.
74. Pereda AE. Electrical synapses and their functional interactions with chemical synapses. Nat Rev Neurosci. 2014;15(4):250-63.
75. Farhy-Tselnicker I, Allen NJ. Astrocytes, neurons, synapses: a tripartite view on cortical circuit development. Neural Dev. 2018;13(1):7.
76. Sudhof TC. Calcium control of neurotransmitter release. Cold Spring Harb Perspect Biol. 2012;4(1):a011353.
77. Glasgow SD, McPhedrain R, Madranges JF, Kennedy TE, Ruthazer ES. Approaches and Limitations in the Investigation of Synaptic Transmission and Plasticity. Front Synaptic Neurosci. 2019;11:20.
78. Vijayan V, Verstreken P. Autophagy in the presynaptic compartment in health and disease. J Cell Biol. 2017;216(7):1895-906.
79. Azarnia Tehran D, Kuijpers M, Haucke V. Presynaptic endocytic factors in autophagy and neurodegeneration. Curr Opin Neurobiol. 2018;48:153-9.
80. Winckler B, Faundez V, Maday S, Cai Q, Guimas Almeida C, Zhang H. The Endolysosomal System and Proteostasis: From Development to Degeneration. J Neurosci. 2018;38(44):9364-74.
81. Wang J, Fedoseienko A, Chen B, Burstein E, Jia D, Billadeau DD. Endosomal receptor trafficking: Retromer and beyond. Traffic. 2018;19(8):578-90.
82. Kroemer G, Jaattela M. Lysosomes and autophagy in cell death control. Nat Rev Cancer. 2005;5(11):886-97.
83. Boya P. Lysosomal function and dysfunction: mechanism and disease. Antioxid Redox Signal. 2012;17(5):766-74.
84. Repnik U, Hafner Cesen M, Turk B. Lysosomal membrane permeabilization in cell death: concepts and challenges. Mitochondrion. 2014;19 Pt A:49-57.

85. Domagala A, Fidyt K, Bobrowicz M, Stachura J, Szczygiel K, Firczuk M. Typical and Atypical Inducers of Lysosomal Cell Death: A Promising Anticancer Strategy. Int J Mol Sci. 2018;19(8).
86. Boya P, Kroemer G. Lysosomal membrane permeabilization in cell death. Oncogene. 2008;27(50):6434-51.
87. Raben N, Puertollano R. TFEB and TFE3: Linking Lysosomes to Cellular Adaptation to Stress. Annu Rev Cell Dev Biol. 2016;32:255-78.
88. Mrschtik M, Ryan KM. Lysosomal proteins in cell death and autophagy. FEBS J. 2015;282(10):1858-70.
89. Oberle C, Huai J, Reinheckel T, Tacke M, Rassner M, Ekert PG, et al. Lysosomal membrane permeabilization and cathepsin release is a Bax/Bak-dependent, amplifying event of apoptosis in fibroblasts and monocytes. Cell Death Differ. 2010;17(7):1167-78.
90. Galluzzi L, Kepp O, Kroemer G. Mitochondrial regulation of cell death: a phylogenetically conserved control. Microb Cell. 2016;3(3):101-8.
91. Tang D, Kang R, Berghe TV, Vandenabeele P, Kroemer G. The molecular machinery of regulated cell death. Cell Res. 2019;29(5):347-64.
92. Galluzzi L, Vitale I, Aaronson SA, Abrams JM, Adam D, Agostinis P, et al. Molecular mechanisms of cell death: recommendations of the Nomenclature Committee on Cell Death 2018. Cell Death Differ. 2018;25(3):486-541.
93. de Vasconcelos NM, Van Opdenbosch N, Van Gorp H, Parthoens E, Lamkanfi M. Single-cell analysis of pyroptosis dynamics reveals conserved GSDMD-mediated subcellular events that precede plasma membrane rupture. Cell Death Differ. 2019;26(1):146-61.
94. Dhuriya YK, Sharma D. Necroptosis: a regulated inflammatory mode of cell death. J Neuroinflammation. 2018;15(1):199.
95. Bialik S, Dasari SK, Kimchi A. Autophagy-dependent cell death - where, how and why a cell eats itself to death. J Cell Sci. 2018;131(18).
96. Neufeld EF. Lysosomal storage diseases. Annu Rev Biochem. 1991;60:257-80.
97. Cox TM, Cachon-Gonzalez MB. The cellular pathology of lysosomal diseases. J Pathol. 2012;226(2):241-54.
98. Poswar FO, Vairo F, Burin M, Michelin-Tirelli K, Brusius-Facchin AC, Kubaski F, et al. Lysosomal diseases: Overview on current diagnosis and treatment. Genet Mol Biol. 2019;42(1 suppl 1):165-77.
99. Filocamo M, Morrone A. Lysosomal storage disorders: molecular basis and laboratory testing. Hum Genomics. 2011;5(3):156-69.
100. Ryan winchester tmc. Lysosomal storage disorders: A practical guide chapter 10 Other lysosomal disorders2012 15 nov 2012.
101. Beesley CE, Young EP, Vellodi A, Winchester BG. Mutational analysis of Sanfilippo syndrome type A (MPS IIIA): identification of 13 novel mutations. J Med Genet. 2000;37(9):704-7.
102. Wraith JE. The clinical presentation of lysosomal storage disorders. Acta Neurol Taiwan. 2004;13(3):101-6.
103. Boustany RM. Lysosomal storage diseases--the horizon expands. Nat Rev Neurol. 2013;9(10):583-98.
104. Ballabio A, Gieselmann V. Lysosomal disorders: from storage to cellular damage. Biochim Biophys Acta. 2009;1793(4):684-96.

105. Staretz-Chacham O, Choi JH, Wakabayashi K, Lopez G, Sidransky E. Psychiatric and behavioral manifestations of lysosomal storage disorders. Am J Med Genet B Neuropsychiatr Genet. 2010;153B(7):1253-65.
106. Pastores GM, Maegawa GH. Clinical neurogenetics: neuropathic lysosomal storage disorders. Neurol Clin. 2013;31(4):1051-71.
107. Kishnani PS, Amartino HM, Lindberg C, Miller TM, Wilson A, Keutzer J, et al. Timing of diagnosis of patients with Pompe disease: data from the Pompe registry. Am J Med Genet A. 2013;161A(10):2431-43.
108. Nelson J. Incidence of the mucopolysaccharidoses in Northern Ireland. Hum Genet. 1997;101(3):355-8.
109. Meikle PJ, Hopwood JJ, Clague AE, Carey WF. Prevalence of lysosomal storage disorders. JAMA. 1999;281(3):249-54.
110. Poorthuis BJ, Wevers RA, Kleijer WJ, Groener JE, de Jong JG, van Weely S, et al. The frequency of lysosomal storage diseases in The Netherlands. Hum Genet. 1999;105(1-2):151-6.
111. Applegarth DA, Toone JR, Lowry RB. Incidence of inborn errors of metabolism in British Columbia, 1969-1996. Pediatrics. 2000;105(1):e10.
112. Dionisi-Vici C, Rizzo C, Burlina AB, Caruso U, Sabetta G, Uziel G, et al. Inborn errors of metabolism in the Italian pediatric population: a national retrospective survey. J Pediatr. 2002;140(3):321-7.
113. Pinto R, Caseiro C, Lemos M, Lopes L, Fontes A, Ribeiro H, et al. Prevalence of lysosomal storage diseases in Portugal. Eur J Hum Genet. 2004;12(2):87-92.
114. Moammar H, Cheriyan G, Mathew R, Al-Sannaa N. Incidence and patterns of inborn errors of metabolism in the Eastern Province of Saudi Arabia, 1983-2008. Ann Saudi Med. 2010;30(4):271-7.
115. Poupetova H, Ledvinova J, Berna L, Dvorakova L, Kozich V, Elleder M. The birth prevalence of lysosomal storage disorders in the Czech Republic: comparison with data in different populations. J Inherit Metab Dis. 2010;33(4):387-96.
116. Al-Maawali AA, Joshi SN, Koul RL, Al-Maawali AA, Al-Sedari HS, Al-Amri BM, et al. Spectrum of paediatric lysosomal storage disorders in oman. Sultan Qaboos Univ Med J. 2012;12(3):295-9.
117. Al-Jasmi FA, Tawfig N, Berniah A, Ali BR, Taleb M, Hertecant JL, et al. Prevalence and Novel Mutations of Lysosomal Storage Disorders in United Arab Emirates : LSD in UAE. JIMD Rep. 2013;10:1-9.
118. Hult M, Darin N, von Dobeln U, Mansson JE. Epidemiology of lysosomal storage diseases in Sweden. Acta Paediatr. 2014;103(12):1258-63.
119. Jurecka A, Lugowska A, Golda A, Czartoryska B, Tylki-Szymanska A. Prevalence rates of mucopolysaccharidoses in Poland. J Appl Genet. 2015;56(2):205-10.
120. Khan SA, Peracha H, Ballhausen D, Wiesbauer A, Rohrbach M, Gautschi M, et al. Epidemiology of mucopolysaccharidoses. Mol Genet Metab. 2017;121(3):227-40.
121. Giugliani R, Federhen A, Michelin-Tirelli K, Riegel M, Burin M. Relative frequency and estimated minimal frequency of Lysosomal Storage Diseases in Brazil: Report from a Reference Laboratory. Genet Mol Biol. 2017;40(1):31-9.
122. Maria Fuller PJM, and John J Hopwood. Epidemiology of lysosomal storage diseases: an overview. In: Pharmagenesis O, editor. Fabry Disease: Perspectives from 5 Years of FOS: Oxford; 2006.

123. Mistry PK, Cappellini MD, Lukina E, Ozsan H, Mach Pascual S, Rosenbaum H, et al. A reappraisal of Gaucher disease-diagnosis and disease management algorithms. Am J Hematol. 2011;86(1):110-5.
124. Scriver CR. Human genetics: lessons from Quebec populations. Annu Rev Genomics Hum Genet. 2001;2:69-101.
125. Risch N, Tang H, Katzenstein H, Ekstein J. Geographic distribution of disease mutations in the Ashkenazi Jewish population supports genetic drift over selection. Am J Hum Genet. 2003;72(4):812-22.
126. Diaz GA, Gelb BD, Risch N, Nygaard TG, Frisch A, Cohen IJ, et al. Gaucher disease: the origins of the Ashkenazi Jewish N370S and 84GG acid beta-glucosidase mutations. Am J Hum Genet. 2000;66(6):1821-32.
127. Anwar WA, Khyatti M, Hemminki K. Consanguinity and genetic diseases in North Africa and immigrants to Europe. Eur J Public Health. 2014;24 Suppl 1:57-63.
128. Maegawa GH, Stockley T, Tropak M, Banwell B, Blaser S, Kok F, et al. The natural history of juvenile or subacute GM2 gangliosidosis: 21 new cases and literature review of 134 previously reported. Pediatrics. 2006;118(5):e1550-62.
129. Staretz-Chacham O, Lang TC, LaMarca ME, Krasnewich D, Sidransky E. Lysosomal storage disorders in the newborn. Pediatrics. 2009;123(4):1191-207.
130. Filocamo M, Tomanin R, Bertola F, Morrone A. Biochemical and molecular analysis in mucopolysaccharidoses: what a paediatrician must know. Ital J Pediatr. 2018;44(Suppl 2):129.
131. Baker KE, Parker R. Nonsense-mediated mRNA decay: terminating erroneous gene expression. Curr Opin Cell Biol. 2004;16(3):293-9.
132. Maquat LE. Nonsense-mediated mRNA decay: splicing, translation and mRNP dynamics. Nat Rev Mol Cell Biol. 2004;5(2):89-99.
133. Vembar SS, Brodsky JL. One step at a time: endoplasmic reticulum-associated degradation. Nat Rev Mol Cell Biol. 2008;9(12):944-57.
134. Walter P, Ron D. The unfolded protein response: from stress pathway to homeostatic regulation. Science. 2011;334(6059):1081-6.
135. Bendikov-Bar I, Horowitz M. Gaucher disease paradigm: from ERAD to comorbidity. Hum Mutat. 2012;33(10):1398-407.
136. Ron I, Horowitz M. ER retention and degradation as the molecular basis underlying Gaucher disease heterogeneity. Hum Mol Genet. 2005;14(16):2387-98.
137. Sandhoff K. My journey into the world of sphingolipids and sphingolipidoses. Proc Jpn Acad Ser B Phys Biol Sci. 2012;88(10):554-82.
138. Clarke JT, Mahuran DJ, Sathe S, Kolodny EH, Rigat BA, Raiman JA, et al. An open-label Phase I/II clinical trial of pyrimethamine for the treatment of patients affected with chronic GM2 gangliosidosis (Tay-Sachs or Sandhoff variants). Mol Genet Metab. 2011;102(1):6-12.
139. Schueler UH, Kolter T, Kaneski CR, Zirzow GC, Sandhoff K, Brady RO. Correlation between enzyme activity and substrate storage in a cell culture model system for Gaucher disease. J Inherit Metab Dis. 2004;27(5):649-58.
140. Gomez-Ospina N. Arylsulfatase A Deficiency. Seattle (WA): University of Washington, Seattle; 1993-2021.: GeneReviews® [Internet]. 2006.
141. Gort L, Santamaria R, Grinberg D, Vilageliu L, Chabas A. Identification of a novel pseudodeficiency allele in the GLB1 gene in a carrier of GM1 gangliosidosis. Clin Genet. 2007;72(2):109-11.

142. Tomanin R, Karageorgos L, Zanetti A, Al-Sayed M, Bailey M, Miller N, et al. Mucopolysaccharidosis type VI (MPS VI) and molecular analysis: Review and classification of published variants in the ARSB gene. Hum Mutat. 2018;39(12):1788-802.
143. Muenzer EFNJ. The Mucopolysaccharidoses 2001.
144. Kreuger J, Spillmann D, Li JP, Lindahl U. Interactions between heparan sulfate and proteins: the concept of specificity. J Cell Biol. 2006;174(3):323-7.
145. Dicker KT, Gurski LA, Pradhan-Bhatt S, Witt RL, Farach-Carson MC, Jia X. Hyaluronan: a simple polysaccharide with diverse biological functions. Acta Biomater. 2014;10(4):1558-70.
146. Ghiselli G, Maccarana M. Drugs affecting glycosaminoglycan metabolism. Drug Discov Today. 2016;21(7):1162-9.
147. Glass CA. Recombinant Heparin-New Opportunities. Front Med (Lausanne). 2018;5:341.
148. Bodamer OA, Giugliani R, Wood T. The laboratory diagnosis of mucopolysaccharidosis III (Sanfilippo syndrome): A changing landscape. Mol Genet Metab. 2014;113(1-2):34-41.
149. Coutinho MF, Lacerda L, Alves S. Glycosaminoglycan storage disorders: a review. Biochem Res Int. 2012;2012:471325.
150. Paciotti S, Persichetti E, Pagliardini S, Deganuto M, Rosano C, Balducci C, et al. First pilot newborn screening for four lysosomal storage diseases in an Italian region: identification and analysis of a putative causative mutation in the GBA gene. Clin Chim Acta. 2012;413(23-24):1827-31.
151. Donati MA, Pasquini E, Spada M, Polo G, Burlina A. Newborn screening in mucopolysaccharidoses. Ital J Pediatr. 2018;44(Suppl 2):126.
152. Bravo H, Neto EC, Schulte J, Pereira J, Filho CS, Bittencourt F, et al. Investigation of newborns with abnormal results in a newborn screening program for four lysosomal storage diseases in Brazil. Mol Genet Metab Rep. 2017;12:92-7.
153. Navarrete-Martinez JI, Limon-Rojas AE, Gaytan-Garcia MJ, Reyna-Figueroa J, Wakida-Kusunoki G, Delgado-Calvillo MDR, et al. Newborn screening for six lysosomal storage disorders in a cohort of Mexican patients: Three-year findings from a screening program in a closed Mexican health system. Mol Genet Metab. 2017;121(1):16-21.
154. Burton BK, Charrow J, Hoganson GE, Waggoner D, Tinkle B, Braddock SR, et al. Newborn Screening for Lysosomal Storage Disorders in Illinois: The Initial 15-Month Experience. J Pediatr. 2017;190:130-5.
155. Hopkins PV, Campbell C, Klug T, Rogers S, Raburn-Miller J, Kiesling J. Lysosomal storage disorder screening implementation: findings from the first six months of full population pilot testing in Missouri. J Pediatr. 2015;166(1):172-7.
156. Wasserstein MP, Caggana M, Bailey SM, Desnick RJ, Edelmann L, Estrella L, et al. The New York pilot newborn screening program for lysosomal storage diseases: Report of the First 65,000 Infants. Genet Med. 2019;21(3):631-40.
157. Scott CR, Elliott S, Hong X, Huang JY, Kumar AB, Yi F, et al. Newborn Screening for Mucopolysaccharidoses: Results of a Pilot Study with 100 000 Dried Blood Spots. J Pediatr. 2020;216:204-7.
158. Kubaski F, Mason RW, Nakatomi A, Shintaku H, Xie L, van Vlies NN, et al. Newborn screening for mucopolysaccharidoses: a pilot study of measurement of glycosaminoglycans by tandem mass spectrometry. J Inherit Metab Dis. 2017;40(1):151-8.
159. Chuang CK, Lin HY, Wang TJ, Huang YH, Chan MJ, Liao HC, et al. Status of newborn screening and follow up investigations for Mucopolysaccharidoses I and II in Taiwan. Orphanet J Rare Dis. 2018;13(1):84.

160. Kanungo S, Patel DR, Neelakantan M, Ryali B. Newborn screening and changing face of inborn errors of metabolism in the United States. Ann Transl Med. 2018;6(24):468.
161. Millington DS, Bali DS. Current State of the Art of Newborn Screening for Lysosomal Storage Disorders. Int J Neonatal Screen. 2018;4(3):24.
162. Baehner F, Schmiedeskamp C, Krummenauer F, Miebach E, Bajbouj M, Whybra C, et al. Cumulative incidence rates of the mucopolysaccharidoses in Germany. J Inherit Metab Dis. 2005;28(6):1011-7.
163. Malm G, Lund AM, Mansson JE, Heiberg A. Mucopolysaccharidoses in the Scandinavian countries: incidence and prevalence. Acta Paediatr. 2008;97(11):1577-81.
164. Krabbi K, Joost K, Zordania R, Talvik I, Rein R, Huijmans JG, et al. The live-birth prevalence of mucopolysaccharidoses in Estonia. Genet Test Mol Biomarkers. 2012;16(8):846-9.
165. Ben Turkia H, Tebib N, Azzouz H, Abdelmoula MS, Ben Chehida A, Chemli J, et al. Incidence of mucopolysaccharidoses in Tunisia. Tunis Med. 2009;87(11):782-5.
166. Heron B, Mikaeloff Y, Froissart R, Caridade G, Maire I, Caillaud C, et al. Incidence and natural history of mucopolysaccharidosis type III in France and comparison with United Kingdom and Greece. Am J Med Genet A. 2011;155A(1):58-68.
167. Lin HY, Lin SP, Chuang CK, Niu DM, Chen MR, Tsai FJ, et al. Incidence of the mucopolysaccharidoses in Taiwan, 1984-2004. Am J Med Genet A. 2009;149A(5):960-4.
168. Sanfilippo S, R. Podosin, L. Langer and R. Good. “Mental retardation associated with acid mucopolysaccharidiuria (heparitin sulfate type).” The Journal of Pediatrics 63 (1963): 837-838. Mental retardation associated with acid mucopolysaccharidiuria (heparitin sulfate type). The Journal of Pediatrics.63(63):837-8.
169. von Figura K, Kresse H. The sanfilippo B corrective factor: a N-acetyl-alpha-D-glucosamindiase. Biochem Biophys Res Commun. 1972;48(2):262-9.
170. O'Brien JS. Sanfilippo syndrome: profound deficiency of alpha-acetylglucosaminidase activity in organs and skin fibroblasts from type-B patients. Proc Natl Acad Sci U S A. 1972;69(7):1720-2.
171. Klein U, Kresse H, von Figura K. Sanfilippo syndrome type C: deficiency of acetyl-CoA:alpha-glucosaminide N-acetyltransferase in skin fibroblasts. Proc Natl Acad Sci U S A. 1978;75(10):5185-9.
172. Kresse H, Paschke E, von Figura K, Gilberg W, Fuchs W. Sanfilippo disease type D: deficiency of N-acetylglucosamine-6-sulfate sulfatase required for heparan sulfate degradation. Proc Natl Acad Sci U S A. 1980;77(11):6822-6.
173. Sugahara K, Kitagawa H. Heparin and heparan sulfate biosynthesis. IUBMB Life. 2002;54(4):163-75.
174. Cartmell A, Lowe EC, Basle A, Firbank SJ, Ndeh DA, Murray H, et al. How members of the human gut microbiota overcome the sulfation problem posed by glycosaminoglycans. Proc Natl Acad Sci U S A. 2017;114(27):7037-42.
175. Sarrazin S, Lamanna WC, Esko JD. Heparan sulfate proteoglycans. Cold Spring Harb Perspect Biol. 2011;3(7).
176. Li JP, Kusche-Gullberg M. Heparan Sulfate: Biosynthesis, Structure, and Function. Int Rev Cell Mol Biol. 2016;325:215-73.
177. Xu D, Esko JD. Demystifying heparan sulfate-protein interactions. Annu Rev Biochem. 2014;83:129-57.
178. Christianson HC, Belting M. Heparan sulfate proteoglycan as a cell-surface endocytosis receptor. Matrix Biol. 2014;35:51-5.

179. Payne CK, Jones SA, Chen C, Zhuang X. Internalization and trafficking of cell surface proteoglycans and proteoglycan-binding ligands. Traffic. 2007;8(4):389-401.
180. Saied-Santiago K, Bulow HE. Diverse roles for glycosaminoglycans in neural patterning. Dev Dyn. 2018;247(1):54-74.
181. Weiss RJ, Esko JD, Tor Y. Targeting heparin and heparan sulfate protein interactions. Org Biomol Chem. 2017;15(27):5656-68.
182. Bishop JR, Schuksz M, Esko JD. Heparan sulphate proteoglycans fine-tune mammalian physiology. Nature. 2007;446(7139):1030-7.
183. Kreuger J, Kjellen L. Heparan sulfate biosynthesis: regulation and variability. J Histochem Cytochem. 2012;60(12):898-907.
184. Abitbol M, Thibaud JL, Olby NJ, Hitte C, Puech JP, Maurer M, et al. A canine Arylsulfatase G (ARSG) mutation leading to a sulfatase deficiency is associated with neuronal ceroid lipofuscinosis. Proc Natl Acad Sci U S A. 2010;107(33):14775-80.
185. Kowalewski B, Lamanna WC, Lawrence R, Damme M, Stroobants S, Padva M, et al. Arylsulfatase G inactivation causes loss of heparan sulfate 3-O-sulfatase activity and mucopolysaccharidosis in mice. Proc Natl Acad Sci U S A. 2012;109(26):10310-5.
186. Khateb S, Kowalewski B, Bedoni N, Damme M, Pollack N, Saada A, et al. A homozygous founder missense variant in arylsulfatase G abolishes its enzymatic activity causing atypical Usher syndrome in humans. Genet Med. 2018;20(9):1004-12.
187. Freeze HH, Kinoshita T, Schnaar RL. Genetic Disorders of Glycan Degradation. In: rd, Varki A, Cummings RD, Esko JD, Stanley P, Hart GW, et al., editors. Essentials of Glycobiology. Cold Spring Harbor (NY)2015. p. 553-68.
188. Dhamale OP, Lawrence R, Wiegmann EM, Shah BA, Al-Mafraji K, Lamanna WC, et al. Arylsulfatase K is the Lysosomal 2-Sulfoglucuronate Sulfatase. ACS Chem Biol. 2017;12(2):367-73.
189. Trabszo C, Ramms B, Chopra P, Lullmann-Rauch R, Stroobants S, Spross J, et al. Arylsulfatase K inactivation causes mucopolysaccharidosis due to deficient glucuronate desulfation of heparan and chondroitin sulfate. Biochem J. 2020;477(17):3433-51.
190. Griffin LS, Gloster TM. The Enzymatic Degradation of Heparan Sulfate. Protein Pept Lett. 2017;24(8):710-22.
191. Lehman TJ, Miller N, Norquist B, Underhill L, Keutzer J. Diagnosis of the mucopolysaccharidoses. Rheumatology (Oxford). 2011;50 Suppl 5:v41-8.
192. Kubaski F, de Oliveira Poswar F, Michelin-Tirelli K, Burin MG, Rojas-Malaga D, Brusius-Facchin AC, et al. Diagnosis of Mucopolysaccharidoses. Diagnostics (Basel). 2020;10(3).
193. Auray-Blais C, Bherer P, Gagnon R, Young SP, Zhang HH, An Y, et al. Efficient analysis of urinary glycosaminoglycans by LC-MS/MS in mucopolysaccharidoses type I, II and VI. Mol Genet Metab. 2011;102(1):49-56.
194. Tomatsu S, Montano AM, Oikawa H, Smith M, Barrera L, Chinen Y, et al. Mucopolysaccharidosis type IVA (Morquio A disease): clinical review and current treatment. Curr Pharm Biotechnol. 2011;12(6):931-45.
195. Lin HY, Chuang CK, Chen MR, Lin SJ, Chiu PC, Niu DM, et al. Clinical characteristics and surgical history of Taiwanese patients with mucopolysaccharidosis type II: data from the hunter outcome survey (HOS). Orphanet J Rare Dis. 2018;13(1):89.
196. Zhang H, Young SP, Auray-Blais C, Orchard PJ, Tolar J, Millington DS. Analysis of glycosaminoglycans in cerebrospinal fluid from patients with mucopolysaccharidoses by isotope-

dilution ultra-performance liquid chromatography-tandem mass spectrometry. Clin Chem. 2011;57(7):1005-12.
197. Yi F, Hong X, Kumar AB, Zong C, Boons GJ, Scott CR, et al. Detection of mucopolysaccharidosis III-A (Sanfilippo Syndrome-A) in dried blood spots (DBS) by tandem mass spectrometry. Mol Genet Metab. 2018;125(1-2):59-63.
198. Lawrence R, Brown JR, Lorey F, Dickson PI, Crawford BE, Esko JD. WITHDRAWN: Glycan-based biomarkers for mucopolysaccharidoses. Dis Markers. 2013.
199. Minelli A, Danesino C, Lo Curto F, Tenti P, Zampatti C, Simoni G, et al. First trimester prenatal diagnosis of Sanfilippo disease (MPSIII) type B. Prenat Diagn. 1988;8(1):47-52.
200. Delgadillo V, O'Callaghan Mdel M, Gort L, Coll MJ, Pineda M. Natural history of Sanfilippo syndrome in Spain. Orphanet J Rare Dis. 2013;8:189.
201. Joshi SN, Hashim J, Venugopalan P. Pattern of inborn errors of metabolism in an Omani population of the Arabian Peninsula. Ann Trop Paediatr. 2002;22(1):93-6.
202. Nelson J, Crowhurst J, Carey B, Greed L. Incidence of the mucopolysaccharidoses in Western Australia. Am J Med Genet A. 2003;123A(3):310-3.
203. Cho SY, Sohn YB, Jin DK. An overview of Korean patients with mucopolysaccharidosis and collaboration through the Asia Pacific MPS Network. Intractable Rare Dis Res. 2014;3(3):79-86.
204. Mendoza-Ruvalcaba SDC, Brambila-Tapia AJL, Juarez-Osuna JA, Silva-Jose TDD, Garcia-Ortiz JE. Biochemical diagnosis of mucopolysaccharidosis in a Mexican reference center. Genet Mol Biol. 2020;43(1):e20180347.
205. Josahkian JA, Trapp FB, Burin MG, Michelin-Tirelli K, Magalhaes A, Sebastiao FM, et al. Updated birth prevalence and relative frequency of mucopolysaccharidoses across Brazilian regions. Genet Mol Biol. 2021;44(1):e20200138.
206. Chen X, Qiu W, Ye J, Han L, Gu X, Zhang H. Demographic characteristics and distribution of lysosomal storage disorder subtypes in Eastern China. J Hum Genet. 2016;61(4):345-9.
207. Sheth J, Mistri M, Sheth F, Shah R, Bavdekar A, Godbole K, et al. Burden of lysosomal storage disorders in India: experience of 387 affected children from a single diagnostic facility. JIMD Rep. 2014;12:51-63.
208. Bunge S, Ince H, Steglich C, Kleijer WJ, Beck M, Zaremba J, et al. Identification of 16 sulfamidase gene mutations including the common R74C in patients with mucopolysaccharidosis type IIIA (Sanfilippo A). Hum Mutat. 1997;10(6):479-85.
209. Blanch L, Weber B, Guo XH, Scott HS, Hopwood JJ. Molecular defects in Sanfilippo syndrome type A. Hum Mol Genet. 1997;6(5):787-91.
210. Weber B, van de Kamp JJ, Kleijer WJ, Guo XH, Blanch L, van Diggelen OP, et al. Identification of a common mutation (R245H) in Sanfilippo A patients from The Netherlands. J Inherit Metab Dis. 1998;21(4):416-22.
211. Meyer A, Kossow K, Gal A, Steglich C, Muhlhausen C, Ullrich K, et al. The mutation p.Ser298Pro in the sulphamidase gene (SGSH) is associated with a slowly progressive clinical phenotype in mucopolysaccharidosis type IIIA (Sanfilippo A syndrome). Hum Mutat. 2008;29(5):770.
212. Matalon R, Deanching M, Marback R, Michals K. Carrier detection for Sanfilippo A syndrome. J Inherit Metab Dis. 1988;11(2):158-60.
213. Rady PL, Surendran S, Vu AT, Hawkins JC, Michals-Matalon K, Tyring SK, et al. Founder mutation R245H of Sanfilippo syndrome type A in the Cayman Islands. Genet Test. 2002;6(3):211-5.

214. Di Natale P, Balzano N, Esposito S, Villani GR. Identification of molecular defects in Italian Sanfilippo A patients including 13 novel mutations. Hum Mutat. 1998;11(4):313-20.
215. Chabas A, Montfort M, Martinez-Campos M, Diaz A, Coll MJ, Grinberg D, et al. Mutation and haplotype analyses in 26 Spanish Sanfilippo syndrome type A patients: possible single origin for 1091delC mutation. Am J Med Genet. 2001;100(3):223-8.
216. Zhao H, Pfeiffer R, Gail MH. Haplotype analysis in population genetics and association studies. Pharmacogenomics. 2003;4(2):171-8.
217. Meyer A, Kossow K, Gal A, Muhlhausen C, Ullrich K, Braulke T, et al. Scoring evaluation of the natural course of mucopolysaccharidosis type IIIA (Sanfilippo syndrome type A). Pediatrics. 2007;120(5):e1255-61.
218. Yogalingam G, Hopwood JJ. Molecular genetics of mucopolysaccharidosis type IIIA and IIIB: Diagnostic, clinical, and biological implications. Hum Mutat. 2001;18(4):264-81.
219. Gabrielli O, Coppa GV, Bruni S, Villani GR, Pontarelli G, Di Natale P. An adult Sanfilippo type A patient with homozygous mutation R206P in the sulfamidase gene. Am J Med Genet A. 2005;133A(1):85-9.
220. Valstar MJ, Bertoli-Avella AM, Wessels MW, Ruijter GJ, de Graaf B, Olmer R, et al. Mucopolysaccharidosis type IIID: 12 new patients and 15 novel mutations. Hum Mutat. 2010;31(5):E1348-60.
221. Valstar MJ, Neijs S, Bruggenwirth HT, Olmer R, Ruijter GJ, Wevers RA, et al. Mucopolysaccharidosis type IIIA: clinical spectrum and genotype-phenotype correlations. Ann Neurol. 2010;68(6):876-87.
222. Knottnerus SJG, Nijmeijer SCM, L IJ, Te Brinke H, van Vlies N, Wijburg FA. Prediction of phenotypic severity in mucopolysaccharidosis type IIIA. Ann Neurol. 2017;82(5):686-96.
223. Muschol N, Pohl S, Meyer A, Gal A, Ullrich K, Braulke T. Residual activity and proteasomal degradation of p.Ser298Pro sulfamidase identified in patients with a mild clinical phenotype of Sanfilippo A syndrome. Am J Med Genet A. 2011;155A(7):1634-9.
224. Coppa GV, Galeotti F, Zampini L, Galeazzi T, Padella L, Santoro L, et al. Mild mental retardation and low levels of urinary heparan sulfate in a patient with the attenuated phenotype of mucopolysaccharidosis type IIIA. Clin Biochem. 2013;46(7-8):688-90.
225. Nijmeijer SCM, van den Born LI, Kievit AJA, Stepien KM, Langendonk J, Marchal JP, et al. The attenuated end of the phenotypic spectrum in MPS III: from late-onset stable cognitive impairment to a non-neuronopathic phenotype. Orphanet J Rare Dis. 2019;14(1):249.
226. Van Hove JL, Wevers RA, Van Cleemput J, Moerman P, Sciot R, Matthijs G, et al. Late-Onset visceral presentation with cardiomyopathy and without neurological symptoms of adult Sanfilippo A syndrome. Am J Med Genet A. 2003;118A(4):382-7.
227. Baik JY, Lee MS, An SR, Yoon SK, Joo EJ, Kim YH, et al. Initial transcriptome and proteome analyses of low culture temperature-induced expression in CHO cells producing erythropoietin. Biotechnol Bioeng. 2006;93(2):361-71.
228. Bedoya-Lopez A, Estrada K, Sanchez-Flores A, Ramirez OT, Altamirano C, Segovia L, et al. Effect of Temperature Downshift on the Transcriptomic Responses of Chinese Hamster Ovary Cells Using Recombinant Human Tissue Plasminogen Activator Production Culture. PLoS One. 2016;11(3):e0151529.
229. Mason M, Sweeney B, Cain K, Stephens P, Sharfstein ST. Reduced Culture Temperature Differentially Affects Expression and Biophysical Properties of Monoclonal Antibody Variants. Antibodies (Basel). 2014;3(3):253-71.

230. Ozkinay F, Emecen DA, Kose M, Isik E, Bozaci AE, Canda E, et al. Clinical and genetic features of 13 patients with mucopolysaccarhidosis type IIIB: Description of two novel NAGLU gene mutations. Mol Genet Metab Rep. 2021;27:100732.
231. Beesley C, Moraitou M, Winchester B, Schulpis K, Dimitriou E, Michelakakis H. Sanfilippo B syndrome: molecular defects in Greek patients. Clin Genet. 2004;65(2):143-9.
232. Weber B, Guo XH, Kleijer WJ, van de Kamp JJ, Poorthuis BJ, Hopwood JJ. Sanfilippo type B syndrome (mucopolysaccharidosis III B): allelic heterogeneity corresponds to the wide spectrum of clinical phenotypes. Eur J Hum Genet. 1999;7(1):34-44.
233. Chinen Y, Tohma T, Izumikawa Y, Uehara H, Ohta T. Sanfilippo type B syndrome: five patients with an R565P homozygous mutation in the alpha-N-acetylglucosaminidase gene from the Okinawa islands in Japan. J Hum Genet. 2005;50(7):357-9.
234. Mangas M, Nogueira C, Prata MJ, Lacerda L, Coll MJ, Soares G, et al. Molecular analysis of mucopolysaccharidosis type IIIB in Portugal: evidence of a single origin for a common mutation (R234C) in the Iberian Peninsula. Clin Genet. 2008;73(3):251-6.
235. de Ruijter J, Valstar MJ, Narajczyk M, Wegrzyn G, Kulik W, Ijlst L, et al. Genistein in Sanfilippo disease: a randomized controlled crossover trial. Ann Neurol. 2012;71(1):110-20.
236. Meijer OLM, Welling L, Valstar MJ, Hoefsloot LH, Bruggenwirth HT, van der Ploeg AT, et al. Residual N-acetyl-alpha-glucosaminidase activity in fibroblasts correlates with disease severity in patients with mucopolysaccharidosis type IIIB. J Inherit Metab Dis. 2016;39(3):437-45.
237. Meijer OLM, Te Brinke H, Ofman R, L IJ, Wijburg FA, van Vlies N. Processing of mutant N-acetyl-alpha-glucosaminidase in mucopolysaccharidosis type IIIB fibroblasts cultured at low temperature. Mol Genet Metab. 2017;122(1-2):100-6.
238. Haneef SA, Doss CG. Personalized Pharmacoperones for Lysosomal Storage Disorder: Approach for Next-Generation Treatment. Adv Protein Chem Struct Biol. 2016;102:225-65.
239. Hrebicek M, Mrazova L, Seyrantepe V, Durand S, Roslin NM, Noskova L, et al. Mutations in TMEM76* cause mucopolysaccharidosis IIIC (Sanfilippo C syndrome). Am J Hum Genet. 2006;79(5):807-19.
240. Fan X, Zhang H, Zhang S, Bagshaw RD, Tropak MB, Callahan JW, et al. Identification of the gene encoding the enzyme deficient in mucopolysaccharidosis IIIC (Sanfilippo disease type C). Am J Hum Genet. 2006;79(4):738-44.
241. Fedele AO, Filocamo M, Di Rocco M, Sersale G, Lubke T, di Natale P, et al. Mutational analysis of the HGSNAT gene in Italian patients with mucopolysaccharidosis IIIC (Sanfilippo C syndrome). Mutation in brief #959. Online. Hum Mutat. 2007;28(5):523.
242. Coutinho MF, Lacerda L, Prata MJ, Ribeiro H, Lopes L, Ferreira C, et al. Molecular characterization of Portuguese patients with mucopolysaccharidosis IIIC: two novel mutations in the HGSNAT gene. Clin Genet. 2008;74(2):194-5.
243. Matos L, Canals I, Dridi L, Choi Y, Prata MJ, Jordan P, et al. Therapeutic strategies based on modified U1 snRNAs and chaperones for Sanfilippo C splicing mutations. Orphanet J Rare Dis. 2014;9:180.
244. Ruijter GJ, Valstar MJ, van de Kamp JM, van der Helm RM, Durand S, van Diggelen OP, et al. Clinical and genetic spectrum of Sanfilippo type C (MPS IIIC) disease in The Netherlands. Mol Genet Metab. 2008;93(2):104-11.
245. Feldhammer M, Durand S, Mrazova L, Boucher RM, Laframboise R, Steinfeld R, et al. Sanfilippo syndrome type C: mutation spectrum in the heparan sulfate acetyl-CoA: alpha-glucosaminide N-acetyltransferase (HGSNAT) gene. Hum Mutat. 2009;30(6):918-25.

246. Canals I, Elalaoui SC, Pineda M, Delgadillo V, Szlago M, Jaouad IC, et al. Molecular analysis of Sanfilippo syndrome type C in Spain: seven novel HGSNAT mutations and characterization of the mutant alleles. Clin Genet. 2011;80(4):367-74.
247. Fan X, Tkachyova I, Sinha A, Rigat B, Mahuran D. Characterization of the biosynthesis, processing and kinetic mechanism of action of the enzyme deficient in mucopolysaccharidosis IIIC. PLoS One. 2011;6(9):e24951.
248. Huh HJ, Seo JY, Cho SY, Ki CS, Lee SY, Kim JW, et al. The first Korean case of mucopolysaccharidosis IIIC (Sanfilippo syndrome type C) confirmed by biochemical and molecular investigation. Ann Lab Med. 2013;33(1):75-9.
249. Velasco HM, Sanchez Y, Martin AM, Umana LA. Natural History of Sanfilippo Syndrome Type C in Boyaca, Colombia. J Child Neurol. 2017;32(2):177-83.
250. Ouesleti S, Coutinho MF, Ribeiro I, Miled A, Mosbahi DS, Alves S. Update of the spectrum of mucopolysaccharidoses type III in Tunisia: identification of three novel mutations and in silico structural analysis of the missense mutations. World J Pediatr. 2017;13(4):374-80.
251. Hu H, Hubner C, Lukacs Z, Musante L, Gill E, Wienker TF, et al. Kluver-Bucy syndrome associated with a recessive variant in HGSNAT in two siblings with Mucopolysaccharidosis type IIIC (Sanfilippo C). Eur J Hum Genet. 2017;25(2):253-6.
252. Elcioglu NH, Pawlik B, Colak B, Beck M, Wollnik B. A novel loss-of-function mutation in the GNS gene causes Sanfilippo syndrome type D. Genet Couns. 2009;20(2):133-9.
253. Peter VG, Quinodoz M, Sadio S, Held S, Rodrigues M, Soares M, et al. New clinical and molecular evidence linking mutations in ARSG to Usher syndrome type IV. Hum Mutat. 2021;42(3):261-71.
254. Abad-Morales V, Navarro R, Bures-Jelstrup A, Pomares E. Identification of a novel homozygous ARSG mutation as the second cause of Usher syndrome type 4. Am J Ophthalmol Case Rep. 2020;19:100736.
255. Richtrova E, Mrazova LS, Musalkova D, Luksan O, Stolnaya L, Minks J, et al. HGSNAT has a TATA-less promoter with multiple starts of transcription. Gene. 2016;592(1):36-42.
256. Durand S, Feldhammer M, Bonneil E, Thibault P, Pshezhetsky AV. Analysis of the biogenesis of heparan sulfate acetyl-CoA:alpha-glucosaminide N-acetyltransferase provides insights into the mechanism underlying its complete deficiency in mucopolysaccharidosis IIIC. J Biol Chem. 2010;285(41):31233-42.
257. Feldhammer M, Durand S, Pshezhetsky AV. Protein misfolding as an underlying molecular defect in mucopolysaccharidosis III type C. PLoS One. 2009;4(10):e7434.
258. Bame KJ, Rome LH. Genetic evidence for transmembrane acetylation by lysosomes. Science. 1986;233(4768):1087-9.
259. Bame KJ, Rome LH. Acetyl-coenzyme A:alpha-glucosaminide N-acetyltransferase. Evidence for an active site histidine residue. J Biol Chem. 1986;261(22):10127-32.
260. Ausseil J, Landry K, Seyrantepe V, Trudel S, Mazur A, Lapointe F, et al. An acetylated 120-kDa lysosomal transmembrane protein is absent from mucopolysaccharidosis IIIC fibroblasts: a candidate molecule for MPS IIIC. Mol Genet Metab. 2006;87(1):22-31.
261. Ouesleti S, Brunel V, Ben Turkia H, Dranguet H, Miled A, Miladi N, et al. Molecular characterization of MPS IIIA, MPS IIIB and MPS IIIC in Tunisian patients. Clin Chim Acta. 2011;412(23-24):2326-31.
262. Ali Pervaiz M, Patterson MC, Struys EA, Salomons GS, Jakobs C, Oglesbee D, et al. Co-morbidity of Sanfilippo syndrome type C and D-2-hydroxyglutaric aciduria. J Neurol. 2011;258(8):1564-5.

263. Fedele AO, Hopwood JJ. Functional analysis of the HGSNAT gene in patients with mucopolysaccharidosis IIIC (Sanfilippo C Syndrome). Hum Mutat. 2010;31(7):E1574-86.
264. Haer-Wigman L, Newman H, Leibu R, Bax NM, Baris HN, Rizel L, et al. Non-syndromic retinitis pigmentosa due to mutations in the mucopolysaccharidosis type IIIC gene, heparan-alpha-glucosaminide N-acetyltransferase (HGSNAT). Hum Mol Genet. 2015;24(13):3742-51.
265. Van Cauwenbergh C, Van Schil K, Cannoodt R, Bauwens M, Van Laethem T, De Jaegere S, et al. arrEYE: a customized platform for high-resolution copy number analysis of coding and noncoding regions of known and candidate retinal dystrophy genes and retinal noncoding RNAs. Genet Med. 2017;19(4):457-66.
266. Comander J, Weigel-DiFranco C, Maher M, Place E, Wan A, Harper S, et al. The Genetic Basis of Pericentral Retinitis Pigmentosa-A Form of Mild Retinitis Pigmentosa. Genes (Basel). 2017;8(10).
267. Carss KJ, Arno G, Erwood M, Stephens J, Sanchis-Juan A, Hull S, et al. Comprehensive Rare Variant Analysis via Whole-Genome Sequencing to Determine the Molecular Pathology of Inherited Retinal Disease. Am J Hum Genet. 2017;100(1):75-90.
268. Berger-Plantinga EG, Vanneste JA, Groener JE, van Schooneveld MJ. Adult-onset dementia and retinitis pigmentosa due to mucopolysaccharidosis III-C in two sisters. J Neurol. 2004;251(4):479-81.
269. Bartsocas C, Grobe H, van de Kamp JJ, von Figura K, Kresse H, Klein U, et al. Sanfilippo type C disease: clinical findings in four patients with a new variant of mucopolysaccharidosis III. Eur J Pediatr. 1979;130(4):251-8.
270. Valstar MJ, Ruijter GJ, van Diggelen OP, Poorthuis BJ, Wijburg FA. Sanfilippo syndrome: a mini-review. J Inherit Metab Dis. 2008;31(2):240-52.
271. Cleary MA, Wraith JE. Management of mucopolysaccharidosis type III. Arch Dis Child. 1993;69(3):403-6.
272. Fedele AO. Sanfilippo syndrome: causes, consequences, and treatments. Appl Clin Genet. 2015;8:269-81.
273. Truxal KV, Fu H, McCarty DM, McNally KA, Kunkler KL, Zumberge NA, et al. A prospective one-year natural history study of mucopolysaccharidosis types IIIA and IIIB: Implications for clinical trial design. Mol Genet Metab. 2016;119(3):239-48.
274. van de Kamp JJ, Niermeijer MF, von Figura K, Giesberts MA. Genetic heterogeneity and clinical variability in the Sanfilippo syndrome (types A, B, and C). Clin Genet. 1981;20(2):152-60.
275. Ginsberg SD, Galvin JE, Lee VM, Rorke LB, Dickson DW, Wolfe JH, et al. Accumulation of intracellular amyloid-beta peptide (A beta 1-40) in mucopolysaccharidosis brains. J Neuropathol Exp Neurol. 1999;58(8):815-24.
276. Viana GM, Priestman DA, Platt FM, Khan S, Tomatsu S, Pshezhetsky AV. Brain Pathology in Mucopolysaccharidoses (MPS) Patients with Neurological Forms. J Clin Med. 2020;9(2).
277. Kurihara M, Kumagai K, Yagishita S. Sanfilippo syndrome type C: a clinicopathological autopsy study of a long-term survivor. Pediatr Neurol. 1996;14(4):317-21.
278. Jones MZ, Alroy J, Rutledge JC, Taylor JW, Alvord EC, Jr., Toone J, et al. Human mucopolysaccharidosis IIID: clinical, biochemical, morphological and immunohistochemical characteristics. J Neuropathol Exp Neurol. 1997;56(10):1158-67.

279. Constantopoulos G, Iqbal K, Dekaban AS. Mucopolysaccharidosis types IH, IS, II, and IIIA: glycosaminoglycans and lipids of isolated brain cells and other fractions from autopsied tissues. J Neurochem. 1980;34(6):1399-411.
280. Hadfield MG, Ghatak NR, Nakoneczna I, Lippman HR, Myer EC, Constantopoulos G, et al. Pathologic findings in mucopolysaccharidosis type IIIB (Sanfilippo's sydnrome B). Arch Neurol. 1980;37(10):645-50.
281. Hara A, Kitazawa N, Taketomi T. Abnormalities of glycosphingolipids in mucopolysaccharidosis type III B. J Lipid Res. 1984;25(2):175-84.
282. Constantopoulos G, Dekaban AS. Neurochemistry of the mucopolysaccharidoses: brain lipids and lysosomal enzymes in patients with four types of mucopolysaccharidosis and in normal controls. J Neurochem. 1978;30(5):965-73.
283. Oldfors A, Sourander P. Storage of lipofuscin in neurons in mucopolysaccharidosis. Report on a case of Sanfilippo's syndrome with histochemical and electron-microscopic findings. Acta Neuropathol. 1981;54(4):287-92.
284. Hamano K, Hayashi M, Shioda K, Fukatsu R, Mizutani S. Mechanisms of neurodegeneration in mucopolysaccharidoses II and IIIB: analysis of human brain tissue. Acta Neuropathol. 2008;115(5):547-59.
285. Bigger BW, Begley DJ, Virgintino D, Pshezhetsky AV. Anatomical changes and pathophysiology of the brain in mucopolysaccharidosis disorders. Mol Genet Metab. 2018;125(4):322-31.
286. Zafeiriou DI, Batzios SP. Brain and spinal MR imaging findings in mucopolysaccharidoses: a review. AJNR Am J Neuroradiol. 2013;34(1):5-13.
287. Aronovich EL, Carmichael KP, Morizono H, Koutlas IG, Deanching M, Hoganson G, et al. Canine heparan sulfate sulfamidase and the molecular pathology underlying Sanfilippo syndrome type A in Dachshunds. Genomics. 2000;68(1):80-4.
288. Jolly RD, Allan FJ, Collett MG, Rozaklis T, Muller VJ, Hopwood JJ. Mucopolysaccharidosis IIIA (Sanfilippo syndrome) in a New Zealand Huntaway dog with ataxia. N Z Vet J. 2000;48(5):144-8.
289. Yogalingam G, Pollard T, Gliddon B, Jolly RD, Hopwood JJ. Identification of a mutation causing mucopolysaccharidosis type IIIA in New Zealand Huntaway dogs. Genomics. 2002;79(2):150-3.
290. Genger SC, Mizukami K, Martin MP, Applegate JR, Jr., Barnes HJ, Giger U. Mucopolysaccharidosis IIIB (Sanfilippo syndrome B) in a commercial emu (Dromaius novaehollandiae) flock. Avian Pathol. 2018;47(1):100-7.
291. Ellinwood NM, Wang P, Skeen T, Sharp NJ, Cesta M, Decker S, et al. A model of mucopolysaccharidosis IIIB (Sanfilippo syndrome type IIIB): N-acetyl-alpha-D-glucosaminidase deficiency in Schipperke dogs. J Inherit Metab Dis. 2003;26(5):489-504.
292. Karageorgos L, Brooks DA, Harmatz P, Ketteridge D, Pollard A, Melville EL, et al. Mutational analysis of mucopolysaccharidosis type VI patients undergoing a phase II trial of enzyme replacement therapy. Mol Genet Metab. 2007;90(2):164-70.
293. Jones MZ, Alroy J, Boyer PJ, Cavanagh KT, Johnson K, Gage D, et al. Caprine mucopolysaccharidosis-IIID: clinical, biochemical, morphological and immunohistochemical characteristics. J Neuropathol Exp Neurol. 1998;57(2):148-57.
294. Bhaumik M, Muller VJ, Rozaklis T, Johnson L, Dobrenis K, Bhattacharyya R, et al. A mouse model for mucopolysaccharidosis type III A (Sanfilippo syndrome). Glycobiology. 1999;9(12):1389-96.

295. Gliddon BL, Hopwood JJ. Enzyme-replacement therapy from birth delays the development of behavior and learning problems in mucopolysaccharidosis type IIIA mice. Pediatr Res. 2004;56(1):65-72.
296. Hemsley KM, Hopwood JJ. Development of motor deficits in a murine model of mucopolysaccharidosis type IIIA (MPS-IIIA). Behav Brain Res. 2005;158(2):191-9.
297. Langford-Smith A, Wilkinson FL, Langford-Smith KJ, Holley RJ, Sergijenko A, Howe SJ, et al. Hematopoietic stem cell and gene therapy corrects primary neuropathology and behavior in mucopolysaccharidosis IIIA mice. Mol Ther. 2012;20(8):1610-21.
298. Li HH, Yu WH, Rozengurt N, Zhao HZ, Lyons KM, Anagnostaras S, et al. Mouse model of Sanfilippo syndrome type B produced by targeted disruption of the gene encoding alpha-N-acetylglucosaminidase. Proc Natl Acad Sci U S A. 1999;96(25):14505-10.
299. Palmieri C, Giger U, Wang P, Pizarro M, Shivaprasad HL. Pathological and biochemical studies of mucopolysaccharidosis type IIIB (Sanfilippo syndrome type B) in juvenile emus (Dromaius novaehollandiae). Vet Pathol. 2015;52(1):160-9.
300. Langford-Smith A, Malinowska M, Langford-Smith KJ, Wegrzyn G, Jones S, Wynn R, et al. Hyperactive behaviour in the mouse model of mucopolysaccharidosis IIIB in the open field and home cage environments. Genes Brain Behav. 2011;10(6):673-82.
301. Lau AA, Crawley AC, Hopwood JJ, Hemsley KM. Open field locomotor activity and anxiety-related behaviors in mucopolysaccharidosis type IIIA mice. Behav Brain Res. 2008;191(1):130-6.
302. Lau AA, Hannouche H, Rozaklis T, Hassiotis S, Hopwood JJ, Hemsley KM. Allogeneic stem cell transplantation does not improve neurological deficits in mucopolysaccharidosis type IIIA mice. Exp Neurol. 2010;225(2):445-54.
303. Cressant A, Desmaris N, Verot L, Brejot T, Froissart R, Vanier MT, et al. Improved behavior and neuropathology in the mouse model of Sanfilippo type IIIB disease after adeno-associated virus-mediated gene transfer in the striatum. J Neurosci. 2004;24(45):10229-39.
304. Heldermon CD, Hennig AK, Ohlemiller KK, Ogilvie JM, Herzog ED, Breidenbach A, et al. Development of sensory, motor and behavioral deficits in the murine model of Sanfilippo syndrome type B. PLoS One. 2007;2(8):e772.
305. Gilkes JA, Bloom MD, Heldermon CD. Preferred transduction with AAV8 and AAV9 via thalamic administration in the MPS IIIB model: A comparison of four rAAV serotypes. Mol Genet Metab Rep. 2016;6:48-54.
306. Kowalewski B, Heimann P, Ortkras T, Lullmann-Rauch R, Sawada T, Walkley SU, et al. Ataxia is the major neuropathological finding in arylsulfatase G-deficient mice: similarities and dissimilarities to Sanfilippo disease (mucopolysaccharidosis type III). Hum Mol Genet. 2015;24(7):1856-68.
307. Fischer A, Carmichael KP, Munnell JF, Jhabvala P, Thompson JN, Matalon R, et al. Sulfamidase deficiency in a family of Dachshunds: a canine model of mucopolysaccharidosis IIIA (Sanfilippo A). Pediatr Res. 1998;44(1):74-82.
308. Ohmi K, Greenberg DS, Rajavel KS, Ryazantsev S, Li HH, Neufeld EF. Activated microglia in cortex of mouse models of mucopolysaccharidoses I and IIIB. Proc Natl Acad Sci U S A. 2003;100(4):1902-7.
309. Mader KM, Beard H, King BM, Hopwood JJ. Effect of high dose, repeated intra-cerebrospinal fluid injection of sulphamidase on neuropathology in mucopolysaccharidosis type IIIA mice. Genes Brain Behav. 2008;7(7):740-53.

310. Garbuzova-Davis S, Louis MK, Haller EM, Derasari HM, Rawls AE, Sanberg PR. Blood-brain barrier impairment in an animal model of MPS III B. PLoS One. 2011;6(3):e16601.
311. Garbuzova-Davis S, Klasko SK, Sanberg PR. Intravenous administration of human umbilical cord blood cells in an animal model of MPS III B. J Comp Neurol. 2009;515(1):93-101.
312. Hemsley KM, King B, Hopwood JJ. Injection of recombinant human sulfamidase into the CSF via the cerebellomedullary cistern in MPS IIIA mice. Mol Genet Metab. 2007;90(3):313-28.
313. Wilkinson FL, Holley RJ, Langford-Smith KJ, Badrinath S, Liao A, Langford-Smith A, et al. Neuropathology in mouse models of mucopolysaccharidosis type I, IIIA and IIIB. PLoS One. 2012;7(4):e35787.
314. Ausseil J, Desmaris N, Bigou S, Attali R, Corbineau S, Vitry S, et al. Early neurodegeneration progresses independently of microglial activation by heparan sulfate in the brain of mucopolysaccharidosis IIIB mice. PLoS One. 2008;3(5):e2296.
315. Walkley SU, Vanier MT. Secondary lipid accumulation in lysosomal disease. Biochim Biophys Acta. 2009;1793(4):726-36.
316. Rivest S. Regulation of innate immune responses in the brain. Nat Rev Immunol. 2009;9(6):429-39.
317. Olmos G, Llado J. Tumor necrosis factor alpha: a link between neuroinflammation and excitotoxicity. Mediators Inflamm. 2014;2014:861231.
318. Reu P, Khosravi A, Bernard S, Mold JE, Salehpour M, Alkass K, et al. The Lifespan and Turnover of Microglia in the Human Brain. Cell Rep. 2017;20(4):779-84.
319. Yauger YJ, Bermudez S, Moritz KE, Glaser E, Stoica B, Byrnes KR. Iron accentuated reactive oxygen species release by NADPH oxidase in activated microglia contributes to oxidative stress in vitro. J Neuroinflammation. 2019;16(1):41.
320. Nnah IC, Wessling-Resnick M. Brain Iron Homeostasis: A Focus on Microglial Iron. Pharmaceuticals (Basel). 2018;11(4).
321. DiSabato DJ, Quan N, Godbout JP. Neuroinflammation: the devil is in the details. J Neurochem. 2016;139 Suppl 2:136-53.
322. Barger SW, Goodwin ME, Porter MM, Beggs ML. Glutamate release from activated microglia requires the oxidative burst and lipid peroxidation. J Neurochem. 2007;101(5):1205-13.
323. Tan HY, Wang N, Li S, Hong M, Wang X, Feng Y. The Reactive Oxygen Species in Macrophage Polarization: Reflecting Its Dual Role in Progression and Treatment of Human Diseases. Oxid Med Cell Longev. 2016;2016:2795090.
324. Cherry JD, Olschowka JA, O'Banion MK. Neuroinflammation and M2 microglia: the good, the bad, and the inflamed. J Neuroinflammation. 2014;11:98.
325. Schetters STT, Gomez-Nicola D, Garcia-Vallejo JJ, Van Kooyk Y. Neuroinflammation: Microglia and T Cells Get Ready to Tango. Front Immunol. 2017;8:1905.
326. Subramaniam SR, Federoff HJ. Targeting Microglial Activation States as a Therapeutic Avenue in Parkinson's Disease. Front Aging Neurosci. 2017;9:176.
327. Janda E, Boi L, Carta AR. Microglial Phagocytosis and Its Regulation: A Therapeutic Target in Parkinson's Disease? Front Mol Neurosci. 2018;11:144.
328. Cvetanovic M, Ingram M, Orr H, Opal P. Early activation of microglia and astrocytes in mouse models of spinocerebellar ataxia type 1. Neuroscience. 2015;289:289-99.
329. Rizor A, Pajarillo E, Johnson J, Aschner M, Lee E. Astrocytic Oxidative/Nitrosative Stress Contributes to Parkinson's Disease Pathogenesis: The Dual Role of Reactive Astrocytes. Antioxidants (Basel). 2019;8(8).
330. Klein ASRS. Astrocytes: Initiators of and Responders to Inflammation2019.

331. Devinsky O, Vezzani A, Najjar S, De Lanerolle NC, Rogawski MA. Glia and epilepsy: excitability and inflammation. Trends Neurosci. 2013;36(3):174-84.
332. Jolly RD, Johnstone AC, Norman EJ, Hopwood JJ, Walkley SU. Pathology of mucopolysaccharidosis IIIA in Huntaway dogs. Vet Pathol. 2007;44(5):569-78.
333. Liu T, Zhang L, Joo D, Sun SC. NF-kappaB signaling in inflammation. Signal Transduct Target Ther. 2017;2.
334. Trudel S, Trecherel E, Gomila C, Peltier M, Aubignat M, Gubler B, et al. Oxidative stress is independent of inflammation in the neurodegenerative Sanfilippo syndrome type B. J Neurosci Res. 2015;93(3):424-32.
335. DiRosario J, Divers E, Wang C, Etter J, Charrier A, Jukkola P, et al. Innate and adaptive immune activation in the brain of MPS IIIB mouse model. J Neurosci Res. 2009;87(4):978-90.
336. Settembre C, Fraldi A, Jahreiss L, Spampanato C, Venturi C, Medina D, et al. A block of autophagy in lysosomal storage disorders. Hum Mol Genet. 2008;17(1):119-29.
337. Naughton BJ, Duncan FJ, Murrey D, Ware T, Meadows A, McCarty DM, et al. Amyloidosis, synucleinopathy, and prion encephalopathy in a neuropathic lysosomal storage disease: the CNS-biomarker potential of peripheral blood. PLoS One. 2013;8(11):e80142.
338. Ohmi K, Kudo LC, Ryazantsev S, Zhao HZ, Karsten SL, Neufeld EF. Sanfilippo syndrome type B, a lysosomal storage disease, is also a tauopathy. Proc Natl Acad Sci U S A. 2009;106(20):8332-7.
339. Ohmi K, Zhao HZ, Neufeld EF. Defects in the medial entorhinal cortex and dentate gyrus in the mouse model of Sanfilippo syndrome type B. PLoS One. 2011;6(11):e27461.
340. Jolly RD, Ehrlich PC, Franklin RJ, Macdougall DF, Palmer AC. Histological diagnosis of mucopolysaccharidosis IIIA in a wire-haired dachshund. Vet Rec. 2001;148(18):564-7.
341. Karageorgos L, Hill B, Bawden MJ, Hopwood JJ. Bovine mucopolysaccharidosis type IIIB. J Inherit Metab Dis. 2007;30(3):358-64.
342. Villani GR, Gargiulo N, Faraonio R, Castaldo S, Gonzalez YRE, Di Natale P. Cytokines, neurotrophins, and oxidative stress in brain disease from mucopolysaccharidosis IIIB. J Neurosci Res. 2007;85(3):612-22.
343. Arfi A, Richard M, Gandolphe C, Bonnefont-Rousselot D, Therond P, Scherman D. Neuroinflammatory and oxidative stress phenomena in MPS IIIA mouse model: the positive effect of long-term aspirin treatment. Mol Genet Metab. 2011;103(1):18-25.
344. Vitry S, Ausseil J, Hocquemiller M, Bigou S, Dos Santos Coura R, Heard JM. Enhanced degradation of synaptophysin by the proteasome in mucopolysaccharidosis type IIIB. Mol Cell Neurosci. 2009;41(1):8-18.
345. Braunlin E, Miettunen K, Lund T, Luquette M, Orchard P. Hematopoietic cell transplantation for severe MPS I in the first six months of life: The heart of the matter. Mol Genet Metab. 2019;126(2):117-20.
346. Jameson E, Jones S, Remmington T. Enzyme replacement therapy with laronidase (Aldurazyme((R))) for treating mucopolysaccharidosis type I. Cochrane Database Syst Rev. 2019;6:CD009354.
347. Whiteman DA, Kimura A. Development of idursulfase therapy for mucopolysaccharidosis type II (Hunter syndrome): the past, the present and the future. Drug Des Devel Ther. 2017;11:2467-80.
348. Regier DS, Tanpaiboon P. Role of elosulfase alfa in mucopolysaccharidosis IVA. Appl Clin Genet. 2016;9:67-74.

349. Gomes DF, Gallo LG, Leite BF, Silva RB, da Silva EN. Clinical effectiveness of enzyme replacement therapy with galsulfase in mucopolysaccharidosis type VI treatment: Systematic review. J Inherit Metab Dis. 2019;42(1):66-76.
350. Harmatz P, Shediac R. Mucopolysaccharidosis VI: pathophysiology, diagnosis and treatment. Front Biosci (Landmark Ed). 2017;22:385-406.
351. McCafferty EH, Scott LJ. Vestronidase Alfa: A Review in Mucopolysaccharidosis VII. BioDrugs. 2019;33(2):233-40.
352. Yu WH, Zhao KW, Ryazantsev S, Rozengurt N, Neufeld EF. Short-term enzyme replacement in the murine model of Sanfilippo syndrome type B. Mol Genet Metab. 2000;71(4):573-80.
353. Kan SH, Troitskaya LA, Sinow CS, Haitz K, Todd AK, Di Stefano A, et al. Insulin-like growth factor II peptide fusion enables uptake and lysosomal delivery of alpha-N-acetylglucosaminidase to mucopolysaccharidosis type IIIB fibroblasts. Biochem J. 2014;458(2):281-9.
354. Platt FM. Emptying the stores: lysosomal diseases and therapeutic strategies. Nat Rev Drug Discov. 2018;17(2):133-50.
355. Muenzer J. Early initiation of enzyme replacement therapy for the mucopolysaccharidoses. Mol Genet Metab. 2014;111(2):63-72.
356. Sawamoto K, Chen HH, Almeciga-Diaz CJ, Mason RW, Tomatsu S. Gene therapy for Mucopolysaccharidoses. Mol Genet Metab. 2018;123(2):59-68.
357. Whitley CB, Vijay S, Yao B, Pineda M, Parker GJM, Rojas-Caro S, et al. Final results of the phase 1/2, open-label clinical study of intravenous recombinant human N-acetyl-alpha-d-glucosaminidase (SBC-103) in children with mucopolysaccharidosis IIIB. Mol Genet Metab. 2019;126(2):131-8.
358. John Laterra RK, Lorris A Betz, and Gary W Goldstein. Blood—Brain—Cerebrospinal Fluid Barriers. Siegel GJ AB, Albers RW, et al.,, editor. Michigan1999 199.
359. Downs-Kelly E, Jones MZ, Alroy J, Cavanagh KT, King B, Lucas RE, et al. Caprine mucopolysaccharidosis IIID: a preliminary trial of enzyme replacement therapy. J Mol Neurosci. 2000;15(3):251-62.
360. Garbuzova-Davis S, Mirtyl S, Sallot SA, Hernandez-Ontiveros DG, Haller E, Sanberg PR. Blood-brain barrier impairment in MPS III patients. BMC Neurol. 2013;13:174.
361. Jones SA, Breen C, Heap F, Rust S, de Ruijter J, Tump E, et al. A phase 1/2 study of intrathecal heparan-N-sulfatase in patients with mucopolysaccharidosis IIIA. Mol Genet Metab. 2016;118(3):198-205.
362. Wijburg FA, Whitley CB, Muenzer J, Gasperini S, Del Toro M, Muschol N, et al. Intrathecal heparan-N-sulfatase in patients with Sanfilippo syndrome type A: A phase IIb randomized trial. Mol Genet Metab. 2019;126(2):121-30.
363. Tardieu M, Zerah M, Husson B, de Bournonville S, Deiva K, Adamsbaum C, et al. Intracerebral administration of adeno-associated viral vector serotype rh.10 carrying human SGSH and SUMF1 cDNAs in children with mucopolysaccharidosis type IIIA disease: results of a phase I/II trial. Hum Gene Ther. 2014;25(6):506-16.
364. Tardieu M, Zerah M, Gougeon ML, Ausseil J, de Bournonville S, Husson B, et al. Intracerebral gene therapy in children with mucopolysaccharidosis type IIIB syndrome: an uncontrolled phase 1/2 clinical trial. Lancet Neurol. 2017;16(9):712-20.

365. Gougeon ML, Poirier-Beaudouin B, Ausseil J, Zerah M, Artaud C, Heard JM, et al. Cell-Mediated Immunity to NAGLU Transgene Following Intracerebral Gene Therapy in Children With Mucopolysaccharidosis Type IIIB Syndrome. Front Immunol. 2021;12:655478.
366. Rozaklis T, Beard H, Hassiotis S, Garcia AR, Tonini M, Luck A, et al. Impact of high-dose, chemically modified sulfamidase on pathology in a murine model of MPS IIIA. Exp Neurol. 2011;230(1):123-30.
367. Gustavsson S, Ohlin Sjostrom E, Tjernberg A, Janson J, Westermark U, Andersson T, et al. Intravenous delivery of a chemically modified sulfamidase efficiently reduces heparan sulfate storage and brain pathology in mucopolysaccharidosis IIIA mice. Mol Genet Metab Rep. 2019;21:100510.
368. Boado RJ, Lu JZ, Hui EK, Pardridge WM. Reduction in Brain Heparan Sulfate with Systemic Administration of an IgG Trojan Horse-Sulfamidase Fusion Protein in the Mucopolysaccharidosis Type IIIA Mouse. Mol Pharm. 2018;15(2):602-8.
369. Bourassa P, Alata W, Tremblay C, Paris-Robidas S, Calon F. Transferrin Receptor-Mediated Uptake at the Blood-Brain Barrier Is Not Impaired by Alzheimer's Disease Neuropathology. Mol Pharm. 2019;16(2):583-94.
370. Pulgar VM. Transcytosis to Cross the Blood Brain Barrier, New Advancements and Challenges. Front Neurosci. 2018;12:1019.
371. Joseph V. Rutkowski KH, Hao Xu, Wei Hu, Matthew Renninger, Mark C.C. Leavitt, Qinming Chen, Sandra Rojas-Caro, Anthony G. Quinn. Intravenous SBC-103, a recombinant human alpha-N-acetylglucosaminidase reduces CNS heparan sulfate content in a mucopolysaccharidosis type IIIB mouse model. Molecular genetics and metabolism. 2014;111( 2):S92.
372. Marshall NR, Hassiotis S, King B, Rozaklis T, Trim PJ, Duplock SK, et al. Delivery of therapeutic protein for prevention of neurodegenerative changes: comparison of different CSF-delivery methods. Exp Neurol. 2015;263:79-90.
373. King B, Marshall NR, Hassiotis S, Trim PJ, Tucker J, Hattersley K, et al. Slow, continuous enzyme replacement via spinal CSF in dogs with the paediatric-onset neurodegenerative disease, MPS IIIA. J Inherit Metab Dis. 2017;40(3):443-53.
374. Beard H, Luck AJ, Hassiotis S, King B, Trim PJ, Snel MF, et al. Determination of the role of injection site on the efficacy of intra-CSF enzyme replacement therapy in MPS IIIA mice. Mol Genet Metab. 2015;115(1):33-40.
375. Chung JK, Pan L, Palmieri K, Youssef AS, McCauley TG. Whole Body and CNS Biodistribution of rhHNS in Cynomolgus Monkeys after Intrathecal Lumbar Administration: Treatment Implications for Patients with MPS IIIA. Int J Mol Sci. 2017;18(12).
376. Aoyagi-Scharber M, Crippen-Harmon D, Lawrence R, Vincelette J, Yogalingam G, Prill H, et al. Clearance of Heparan Sulfate and Attenuation of CNS Pathology by Intracerebroventricular BMN 250 in Sanfilippo Type B Mice. Mol Ther Methods Clin Dev. 2017;6:43-53.
377. Yogalingam G, Luu AR, Prill H, Lo MJ, Yip B, Holtzinger J, et al. BMN 250, a fusion of lysosomal alpha-N-acetylglucosaminidase with IGF2, exhibits different patterns of cellular uptake into critical cell types of Sanfilippo syndrome B disease pathogenesis. PLoS One. 2019;14(1):e0207836.
378. Biffi A. Hematopoietic Stem Cell Gene Therapy for Storage Disease: Current and New Indications. Mol Ther. 2017;25(5):1155-62.

379. Valayannopoulos V, Wijburg FA. Therapy for the mucopolysaccharidoses. Rheumatology (Oxford). 2011;50 Suppl 5:v49-59.
380. Capotondo A, Milazzo R, Garcia-Manteiga JM, Cavalca E, Montepeloso A, Garrison BS, et al. Intracerebroventricular delivery of hematopoietic progenitors results in rapid and robust engraftment of microglia-like cells. Sci Adv. 2017;3(12):e1701211.
381. Heldermon CD, Ohlemiller KK, Herzog ED, Vogler C, Qin E, Wozniak DF, et al. Therapeutic efficacy of bone marrow transplant, intracranial AAV-mediated gene therapy, or both in the mouse model of MPS IIIB. Mol Ther. 2010;18(5):873-80.
382. Shapiro EG, Lockman LA, Balthazor M, Krivit W. Neuropsychological outcomes of several storage diseases with and without bone marrow transplantation. J Inherit Metab Dis. 1995;18(4):413-29.
383. Prasad VK, Kurtzberg J. Transplant outcomes in mucopolysaccharidoses. Semin Hematol. 2010;47(1):59-69.
384. Garbuzova-Davis S, Willing AE, Desjarlais T, Davis Sanberg C, Sanberg PR. Transplantation of human umbilical cord blood cells benefits an animal model of Sanfilippo syndrome type B. Stem Cells Dev. 2005;14(4):384-94.
385. Willing AE, Garbuzova-Davis SN, Zayko O, Derasari HM, Rawls AE, James CR, et al. Repeated administrations of human umbilical cord blood cells improve disease outcomes in a mouse model of Sanfilippo syndrome type III B. Cell Transplant. 2014;23(12):1613-30.
386. Zheng Y, Ryazantsev S, Ohmi K, Zhao HZ, Rozengurt N, Kohn DB, et al. Retrovirally transduced bone marrow has a therapeutic effect on brain in the mouse model of mucopolysaccharidosis IIIB. Mol Genet Metab. 2004;82(4):286-95.
387. Sergijenko A, Langford-Smith A, Liao AY, Pickford CE, McDermott J, Nowinski G, et al. Myeloid/Microglial driven autologous hematopoietic stem cell gene therapy corrects a neuronopathic lysosomal disease. Mol Ther. 2013;21(10):1938-49.
388. Holley RJ, Ellison SM, Fil D, O'Leary C, McDermott J, Senthivel N, et al. Macrophage enzyme and reduced inflammation drive brain correction of mucopolysaccharidosis IIIB by stem cell gene therapy. Brain. 2018;141(1):99-116.
389. Parini R, Deodato F, Di Rocco M, Lanino E, Locatelli F, Messina C, et al. Open issues in Mucopolysaccharidosis type I-Hurler. Orphanet J Rare Dis. 2017;12(1):112.
390. Kiely BT, Kohler JL, Coletti HY, Poe MD, Escolar ML. Early disease progression of Hurler syndrome. Orphanet J Rare Dis. 2017;12(1):32.
391. Cox-Brinkman J, Boelens JJ, Wraith JE, O'Meara A, Veys P, Wijburg FA, et al. Haematopoietic cell transplantation (HCT) in combination with enzyme replacement therapy (ERT) in patients with Hurler syndrome. Bone Marrow Transplant. 2006;38(1):17-21.
392. Vallejo-Diez S, Fleischer A, Martin-Fernandez JM, Sanchez-Gilabert A, Bachiller D. Generation of two induced pluripotent stem cells lines from a Mucopolysaccharydosis IIIB (MPSIIIB) patient. Stem Cell Res. 2018;33:180-4.
393. Huang W, Xu M, Li R, Baskfield A, Kouznetsova J, Beers J, et al. An induced pluripotent stem cell line (TRNDi006-A) from a MPS IIIB patient carrying homozygous mutation of p.Glu153Lys in the NAGLU gene. Stem Cell Res. 2019;37:101427.
394. Canals I, Soriano J, Orlandi JG, Torrent R, Richaud-Patin Y, Jimenez-Delgado S, et al. Activity and High-Order Effective Connectivity Alterations in Sanfilippo C Patient-Specific Neuronal Networks. Stem Cell Reports. 2015;5(4):546-57.

395. Clarke D, Pearse Y, Kan SH, Le SQ, Sanghez V, Cooper JD, et al. Genetically Corrected iPSC-Derived Neural Stem Cell Grafts Deliver Enzyme Replacement to Affect CNS Disease in Sanfilippo B Mice. Mol Ther Methods Clin Dev. 2018;10:113-27.
396. Collins M, Thrasher A. Gene therapy: progress and predictions. Proc Biol Sci. 2015;282(1821):20143003.
397. Fu H, DiRosario J, Kang L, Muenzer J, McCarty DM. Restoration of central nervous system alpha-N-acetylglucosaminidase activity and therapeutic benefits in mucopolysaccharidosis IIIB mice by a single intracisternal recombinant adeno-associated viral type 2 vector delivery. J Gene Med. 2010;12(7):624-33.
398. Fraldi A, Hemsley K, Crawley A, Lombardi A, Lau A, Sutherland L, et al. Functional correction of CNS lesions in an MPS-IIIA mouse model by intracerebral AAV-mediated delivery of sulfamidase and SUMF1 genes. Hum Mol Genet. 2007;16(22):2693-702.
399. Heldermon CD, Qin EY, Ohlemiller KK, Herzog ED, Brown JR, Vogler C, et al. Disease correction by combined neonatal intracranial AAV and systemic lentiviral gene therapy in Sanfilippo Syndrome type B mice. Gene Ther. 2013;20(9):913-21.
400. Sorrentino NC, D'Orsi L, Sambri I, Nusco E, Monaco C, Spampanato C, et al. A highly secreted sulphamidase engineered to cross the blood-brain barrier corrects brain lesions of mice with mucopolysaccharidoses type IIIA. EMBO Mol Med. 2013;5(5):675-90.
401. Ruzo A, Marco S, Garcia M, Villacampa P, Ribera A, Ayuso E, et al. Correction of pathological accumulation of glycosaminoglycans in central nervous system and peripheral tissues of MPSIIIA mice through systemic AAV9 gene transfer. Hum Gene Ther. 2012;23(12):1237-46.
402. Sorrentino NC, Cacace V, De Risi M, Maffia V, Strollo S, Tedesco N, et al. Enhancing the Therapeutic Potential of Sulfamidase for the Treatment of Mucopolysaccharidosis IIIA. Mol Ther Methods Clin Dev. 2019;15:333-42.
403. Fu H, Dirosario J, Killedar S, Zaraspe K, McCarty DM. Correction of neurological disease of mucopolysaccharidosis IIIB in adult mice by rAAV9 trans-blood-brain barrier gene delivery. Mol Ther. 2011;19(6):1025-33.
404. Murrey DA, Naughton BJ, Duncan FJ, Meadows AS, Ware TA, Campbell KJ, et al. Feasibility and safety of systemic rAAV9-hNAGLU delivery for treating mucopolysaccharidosis IIIB: toxicology, biodistribution, and immunological assessments in primates. Hum Gene Ther Clin Dev. 2014;25(2):72-84.
405. Ribera A, Haurigot V, Garcia M, Marco S, Motas S, Villacampa P, et al. Biochemical, histological and functional correction of mucopolysaccharidosis type IIIB by intra-cerebrospinal fluid gene therapy. Hum Mol Genet. 2015;24(7):2078-95.
406. Meadows AS, Duncan FJ, Camboni M, Waligura K, Montgomery C, Zaraspe K, et al. A GLP-Compliant Toxicology and Biodistribution Study: Systemic Delivery of an rAAV9 Vector for the Treatment of Mucopolysaccharidosis IIIB. Hum Gene Ther Clin Dev. 2015;26(4):228-42.
407. Fu H, Cataldi MP, Ware TA, Zaraspe K, Meadows AS, Murrey DA, et al. Functional correction of neurological and somatic disorders at later stages of disease in MPS IIIA mice by systemic scAAV9-hSGSH gene delivery. Mol Ther Methods Clin Dev. 2016;3:16036.
408. Winner LK, Beard H, Hassiotis S, Lau AA, Luck AJ, Hopwood JJ, et al. A Preclinical Study Evaluating AAVrh10-Based Gene Therapy for Sanfilippo Syndrome. Hum Gene Ther. 2016;27(5):363-75.
409. Duncan FJ, Naughton BJ, Zaraspe K, Murrey DA, Meadows AS, Clark KR, et al. Broad functional correction of molecular impairments by systemic delivery of scAAVrh74-hSGSH gene delivery in MPS IIIA mice. Mol Ther. 2015;23(4):638-47.

410. Fu H, Kang L, Jennings JS, Moy SS, Perez A, Dirosario J, et al. Significantly increased lifespan and improved behavioral performances by rAAV gene delivery in adult mucopolysaccharidosis IIIB mice. Gene Ther. 2007;14(14):1065-77.
411. McIntyre C, Derrick Roberts AL, Ranieri E, Clements PR, Byers S, Anson DS. Lentiviral-mediated gene therapy for murine mucopolysaccharidosis type IIIA. Mol Genet Metab. 2008;93(4):411-8.
412. McIntyre C, Byers S, Anson DS. Correction of mucopolysaccharidosis type IIIA somatic and central nervous system pathology by lentiviral-mediated gene transfer. J Gene Med. 2010;12(9):717-28.
413. Lau AA, Rozaklis T, Ibanes S, Luck AJ, Beard H, Hassiotis S, et al. Helper-dependent canine adenovirus vector-mediated transgene expression in a neurodegenerative lysosomal storage disorder. Gene. 2012;491(1):53-7.
414. Fu H, Samulski RJ, McCown TJ, Picornell YJ, Fletcher D, Muenzer J. Neurological correction of lysosomal storage in a mucopolysaccharidosis IIIB mouse model by adeno-associated virus-mediated gene delivery. Mol Ther. 2002;5(1):42-9.
415. Di Domenico C, Villani GR, Di Napoli D, Nusco E, Cali G, Nitsch L, et al. Intracranial gene delivery of LV-NAGLU vector corrects neuropathology in murine MPS IIIB. Am J Med Genet A. 2009;149A(6):1209-18.
416. Ellinwood NM, Ausseil J, Desmaris N, Bigou S, Liu S, Jens JK, et al. Safe, efficient, and reproducible gene therapy of the brain in the dog models of Sanfilippo and Hurler syndromes. Mol Ther. 2011;19(2):251-9.
417. R. C. Selection of Autologous or Allogeneic Transplantation. 6th edition ed. Hamilton (ON)2003.
418. Ellison SM, Liao A, Wood S, Taylor J, Youshani AS, Rowlston S, et al. Pre-clinical Safety and Efficacy of Lentiviral Vector-Mediated Ex Vivo Stem Cell Gene Therapy for the Treatment of Mucopolysaccharidosis IIIA. Mol Ther Methods Clin Dev. 2019;13:399-413.
419. Quiviger M, Arfi A, Mansard D, Delacotte L, Pastor M, Scherman D, et al. High and prolonged sulfamidase secretion by the liver of MPS-IIIA mice following hydrodynamic tail vein delivery of antibiotic-free pFAR4 plasmid vector. Gene Ther. 2014;21(12):1001-7.
420. Cortez L, Sim V. The therapeutic potential of chemical chaperones in protein folding diseases. Prion. 2014;8(2).
421. Malinowska M, Wilkinson FL, Langford-Smith KJ, Langford-Smith A, Brown JR, Crawford BE, et al. Genistein improves neuropathology and corrects behaviour in a mouse model of neurodegenerative metabolic disease. PLoS One. 2010;5(12):e14192.
422. Roberts AL, Thomas BJ, Wilkinson AS, Fletcher JM, Byers S. Inhibition of glycosaminoglycan synthesis using rhodamine B in a mouse model of mucopolysaccharidosis type IIIA. Pediatr Res. 2006;60(3):309-14.
423. Moskot M, Montefusco S, Jakobkiewicz-Banecka J, Mozolewski P, Wegrzyn A, Di Bernardo D, et al. The phytoestrogen genistein modulates lysosomal metabolism and transcription factor EB (TFEB) activation. J Biol Chem. 2014;289(24):17054-69.
424. Piotrowska E, Jakobkiewicz-Banecka J, Tylki-Szymanska A, Liberek A, Maryniak A, Malinowska M, et al. Genistin-rich soy isoflavone extract in substrate reduction therapy for Sanfilippo syndrome: An open-label, pilot study in 10 pediatric patients. Curr Ther Res Clin Exp. 2008;69(2):166-79.
425. Piotrowska E, Jakobkiewicz-Banecka J, Maryniak A, Tylki-Szymanska A, Puk E, Liberek A, et al. Two-year follow-up of Sanfilippo Disease patients treated with a genistein-rich isoflavone

extract: assessment of effects on cognitive functions and general status of patients. Med Sci Monit. 2011;17(4):CR196-202.
426. Malinowska M, Wilkinson FL, Bennett W, Langford-Smith KJ, O'Leary HA, Jakobkiewicz-Banecka J, et al. Genistein reduces lysosomal storage in peripheral tissues of mucopolysaccharide IIIB mice. Mol Genet Metab. 2009;98(3):235-42.
427. Malinova V, Wegrzyn G, Narajczyk M. The use of elevated doses of genistein-rich soy extract in the gene expression-targeted isoflavone therapy for Sanfilippo disease patients. JIMD Rep. 2012;5:21-5.
428. Kim KH, Dodsworth C, Paras A, Burton BK. High dose genistein aglycone therapy is safe in patients with mucopolysaccharidoses involving the central nervous system. Mol Genet Metab. 2013;109(4):382-5.
429. Ghosh A, Rust S, Langford-Smith K, Weisberg D, Canal M, Breen C, et al. High dose genistein in Sanfilippo syndrome: A randomised controlled trial. J Inherit Metab Dis. 2021.
430. Kaidonis X, Liaw WC, Roberts AD, Ly M, Anson D, Byers S. Gene silencing of EXTL2 and EXTL3 as a substrate deprivation therapy for heparan sulphate storing mucopolysaccharidoses. Eur J Hum Genet. 2010;18(2):194-9.
431. Dziedzic D, Wegrzyn G, Jakobkiewicz-Banecka J. Impairment of glycosaminoglycan synthesis in mucopolysaccharidosis type IIIA cells by using siRNA: a potential therapeutic approach for Sanfilippo disease. Eur J Hum Genet. 2010;18(2):200-5.
432. Canals I, Beneto N, Cozar M, Vilageliu L, Grinberg D. EXTL2 and EXTL3 inhibition with siRNAs as a promising substrate reduction therapy for Sanfilippo C syndrome. Sci Rep. 2015;5:13654.
433. Coutinho MF, Santos JI, Alves S. Less Is More: Substrate Reduction Therapy for Lysosomal Storage Disorders. Int J Mol Sci. 2016;17(7).
434. Kaidonis X, Byers S, Ranieri E, Sharp P, Fletcher J, Derrick-Roberts A. N-butyldeoxynojirimycin treatment restores the innate fear response and improves learning in mucopolysaccharidosis IIIA mice. Mol Genet Metab. 2016;118(2):100-10.
435. Fecarotta S, Gasperini S, Parenti G. New treatments for the mucopolysaccharidoses: from pathophysiology to therapy. Ital J Pediatr. 2018;44(Suppl 2):124.
436. Guffon N, Bin-Dorel S, Decullier E, Paillet C, Guitton J, Fouilhoux A. Evaluation of miglustat treatment in patients with type III mucopolysaccharidosis: a randomized, double-blind, placebo-controlled study. J Pediatr. 2011;159(5):838-44 e1.
437. Hein LK, Bawden M, Muller VJ, Sillence D, Hopwood JJ, Brooks DA. alpha-L-iduronidase premature stop codons and potential read-through in mucopolysaccharidosis type I patients. J Mol Biol. 2004;338(3):453-62.
438. Gomez-Grau M, Garrido E, Cozar M, Rodriguez-Sureda V, Dominguez C, Arenas C, et al. Evaluation of Aminoglycoside and Non-Aminoglycoside Compounds for Stop-Codon Readthrough Therapy in Four Lysosomal Storage Diseases. PLoS One. 2015;10(8):e0135873.
439. Lotfi P, Tse DY, Di Ronza A, Seymour ML, Martano G, Cooper JD, et al. Trehalose reduces retinal degeneration, neuroinflammation and storage burden caused by a lysosomal hydrolase deficiency. Autophagy. 2018;14(8):1419-34.
440. Sunaga T, Oh N, Hosoya K, Takagi S, Okumura M. Inhibitory effects of pentosan polysulfate sodium on MAP-kinase pathway and NF-kappaB nuclear translocation in canine chondrocytes in vitro. J Vet Med Sci. 2012;74(6):707-11.

441. Simonaro CM, Tomatsu S, Sikora T, Kubaski F, Frohbergh M, Guevara JM, et al. Pentosan Polysulfate: Oral Versus Subcutaneous Injection in Mucopolysaccharidosis Type I Dogs. PLoS One. 2016;11(4):e0153136.
442. Schuchman EH, Ge Y, Lai A, Borisov Y, Faillace M, Eliyahu E, et al. Pentosan polysulfate: a novel therapy for the mucopolysaccharidoses. PLoS One. 2013;8(1):e54459.
443. Frohbergh M, Ge Y, Meng F, Karabul N, Solyom A, Lai A, et al. Dose responsive effects of subcutaneous pentosan polysulfate injection in mucopolysaccharidosis type VI rats and comparison to oral treatment. PLoS One. 2014;9(6):e100882.
444. Crivaro AN, Mucci JM, Bondar CM, Ormazabal ME, Ceci R, Simonaro C, et al. Efficacy of pentosan polysulfate in in vitro models of lysosomal storage disorders: Fabry and Gaucher Disease. PLoS One. 2019;14(5):e0217780.
445. Hennermann JB, Gokce S, Solyom A, Mengel E, Schuchman EH, Simonaro CM. Treatment with pentosan polysulphate in patients with MPS I: results from an open label, randomized, monocentric phase II study. J Inherit Metab Dis. 2016;39(6):831-7.
446. Orii K, Lim A, Tomatsu S, Stapleton M, Suzuki Y, Simonaro CM, et al. Safety Study of Sodium Pentosan Polysulfate for Adult Patients with Mucopolysaccharidosis Type II. Diagnostics (Basel). 2019;9(4).
447. Guo N, DeAngelis V, Zhu C, Schuchman EH, Simonaro CM. Pentosan Polysulfate Treatment of Mucopolysaccharidosis Type IIIA Mice. JIMD Rep. 2019;43:37-52.
448. Mancuso M, Orsucci D, Calsolaro V, Choub A, Siciliano G. Coenzyme Q10 and Neurological Diseases. Pharmaceuticals (Basel). 2009;2(3):134-49.
449. Matalonga L, Arias A, Coll MJ, Garcia-Villoria J, Gort L, Ribes A. Treatment effect of coenzyme Q(10) and an antioxidant cocktail in fibroblasts of patients with Sanfilippo disease. J Inherit Metab Dis. 2014;37(3):439-46.
450. Marco S, Pujol A, Roca C, Motas S, Ribera A, Garcia M, et al. Progressive neurologic and somatic disease in a novel mouse model of human mucopolysaccharidosis type IIIC. Dis Model Mech. 2016;9(9):999-1013.
451. Roca C, Motas S, Marco S, Ribera A, Sanchez V, Sanchez X, et al. Disease correction by AAV-mediated gene therapy in a new mouse model of mucopolysaccharidosis type IIID. Hum Mol Genet. 2017;26(8):1535-51.
452. Parker H, Ellison SM, Holley RJ, O'Leary C, Liao A, Asadi J, et al. Haematopoietic stem cell gene therapy with IL-1Ra rescues cognitive loss in mucopolysaccharidosis IIIA. EMBO Mol Med. 2020;12(3):e11185.
453. Simonaro CM. Lysosomes, Lysosomal Storage Diseases, and Inflammation. Journal of Inborn Errors of Metabolism and Screening. 2016;4.
454. Martin JJ, Ceuterick C. Prenatal pathology in mucopolysaccharidoses: a comparison with postnatal cases. Clin Neuropathol. 1983;2(3):122-7.
455. Liour SS, Jones MZ, Suzuki M, Bieberich E, Yu RK. Metabolic studies of glycosphingolipid accumulation in mucopolysaccharidosis IIID. Mol Genet Metab. 2001;72(3):239-47.
456. Dwyer CA, Scudder SL, Lin Y, Dozier LE, Phan D, Allen NJ, et al. Neurodevelopmental Changes in Excitatory Synaptic Structure and Function in the Cerebral Cortex of Sanfilippo Syndrome IIIA Mice. Sci Rep. 2017;7:46576.
457. Bosch ME, Kielian T. Neuroinflammatory paradigms in lysosomal storage diseases. Front Neurosci. 2015;9:417.

458. Yun Dong DWD, Peter Paul De Deyn, Petrus J. W. Naudé andUlrich L. M. Eisel Targeting of Tumor Necrosis Factor Alpha Receptors as a Therapeutic Strategy for Neurodegenerative Disorders Antibodies. 2015;4(4):369-408.
459. Wu D, Li Z, Zhong M, Kowalewski T, Matyjaszewski K. Templated synthesis of nitrogen-enriched nanoporous carbon materials from porogenic organic precursors prepared by ATRP. Angew Chem Int Ed Engl. 2014;53(15):3957-60.
460. Abo-Ouf H, Hooper AW, White EJ, Janse van Rensburg HJ, Trigatti BL, Igdoura SA. Deletion of tumor necrosis factor-alpha ameliorates neurodegeneration in Sandhoff disease mice. Hum Mol Genet. 2013;22(19):3960-75.
461. Ren M, Guo Q, Guo L, Lenz M, Qian F, Koenen RR, et al. Polymerization of MIP-1 chemokine (CCL3 and CCL4) and clearance of MIP-1 by insulin-degrading enzyme. EMBO J. 2010;29(23):3952-66.
462. Ishita Bhavsar CSM, and Mohanad Al-Sabbagh. Macrophage Inflammatory Protein-1 Alpha (MIP-1 alpha)/CCL3: As a Biomarker. Dordrech: Springer Science+Business Media 2015 2015.
463. Haroon E, Miller AH, Sanacora G. Inflammation, Glutamate, and Glia: A Trio of Trouble in Mood Disorders. Neuropsychopharmacology. 2017;42(1):193-215.
464. Kyrkanides S, Brouxhon SM, Tallents RH, Miller JN, Olschowka JA, O'Banion MK. Conditional expression of human beta-hexosaminidase in the neurons of Sandhoff disease rescues mice from neurodegeneration but not neuroinflammation. J Neuroinflammation. 2012;9:186.
465. Lieberman AP, Puertollano R, Raben N, Slaugenhaupt S, Walkley SU, Ballabio A. Autophagy in lysosomal storage disorders. Autophagy. 2012;8(5):719-30.
466. Seranova E, Connolly KJ, Zatyka M, Rosenstock TR, Barrett T, Tuxworth RI, et al. Dysregulation of autophagy as a common mechanism in lysosomal storage diseases. Essays Biochem. 2017;61(6):733-49.
467. Settembre C, Fraldi A, Rubinsztein DC, Ballabio A. Lysosomal storage diseases as disorders of autophagy. Autophagy. 2008;4(1):113-4.
468. Winder-Rhodes SE, Garcia-Reitbock P, Ban M, Evans JR, Jacques TS, Kemppinen A, et al. Genetic and pathological links between Parkinson's disease and the lysosomal disorder Sanfilippo syndrome. Mov Disord. 2012;27(2):312-5.
469. Nixon RA. Amyloid precursor protein and endosomal-lysosomal dysfunction in Alzheimer's disease: inseparable partners in a multifactorial disease. FASEB J. 2017;31(7):2729-43.
470. Riboldi GM, Di Fonzo AB. GBA, Gaucher Disease, and Parkinson's Disease: From Genetic to Clinic to New Therapeutic Approaches. Cells. 2019;8(4).
471. Song Y, Kenworthy AK, Sanders CR. Cholesterol as a co-solvent and a ligand for membrane proteins. Protein Sci. 2014;23(1):1-22.
472. Vitry S, Bruyere J, Hocquemiller M, Bigou S, Ausseil J, Colle MA, et al. Storage vesicles in neurons are related to Golgi complex alterations in mucopolysaccharidosis IIIB. Am J Pathol. 2010;177(6):2984-99.
473. Shen D, Wang X, Li X, Zhang X, Yao Z, Dibble S, et al. Lipid storage disorders block lysosomal trafficking by inhibiting a TRP channel and lysosomal calcium release. Nat Commun. 2012;3:731.
474. Pereira VG, Gazarini ML, Rodrigues LC, da Silva FH, Han SW, Martins AM, et al. Evidence of lysosomal membrane permeabilization in mucopolysaccharidosis type I: rupture of calcium and proton homeostasis. J Cell Physiol. 2010;223(2):335-42.

475. Barbier P, Zejneli O, Martinho M, Lasorsa A, Belle V, Smet-Nocca C, et al. Role of Tau as a Microtubule-Associated Protein: Structural and Functional Aspects. Front Aging Neurosci. 2019;11.
476. Guo B, Liang Q, Li L, Hu Z, Wu F, Zhang P, et al. O-GlcNAc-modification of SNAP-29 regulates autophagosome maturation. Nat Cell Biol. 2014;16(12):1215-26.
477. Rappaport J, Manthe RL, Solomon M, Garnacho C, Muro S. A Comparative Study on the Alterations of Endocytic Pathways in Multiple Lysosomal Storage Disorders. Mol Pharm. 2016;13(2):357-68.
478. Sambri I, D'Alessio R, Ezhova Y, Giuliano T, Sorrentino NC, Cacace V, et al. Lysosomal dysfunction disrupts presynaptic maintenance and restoration of presynaptic function prevents neurodegeneration in lysosomal storage diseases. EMBO Mol Med. 2017;9(1):112-32.
479. Breiden B, Sandhoff K. Mechanism of Secondary Ganglioside and Lipid Accumulation in Lysosomal Disease. Int J Mol Sci. 2020;21(7).
480. Anheuser S, Breiden B, Sandhoff K. Membrane lipids and their degradation compounds control GM2 catabolism at intralysosomal luminal vesicles. J Lipid Res. 2019;60(6):1099-111.
481. Anheuser S, Breiden B, Sandhoff K. Ganglioside GM2 catabolism is inhibited by storage compounds of mucopolysaccharidoses and by cationic amphiphilic drugs. Mol Genet Metab. 2019;128(1-2):75-83.
482. McGlynn R, Dobrenis K, Walkley SU. Differential subcellular localization of cholesterol, gangliosides, and glycosaminoglycans in murine models of mucopolysaccharide storage disorders. J Comp Neurol. 2004;480(4):415-26.
483. Walkley SU. Secondary accumulation of gangliosides in lysosomal storage disorders. Semin Cell Dev Biol. 2004;15(4):433-44.
484. Schnaar RL. The Biology of Gangliosides. Adv Carbohydr Chem Biochem. 2019;76:113-48.
485. d'Azzo A, Tessitore A, Sano R. Gangliosides as apoptotic signals in ER stress response. Cell Death Differ. 2006;13(3):404-14.
486. Ledeen R, Wu G. New findings on nuclear gangliosides: overview on metabolism and function. J Neurochem. 2011;116(5):714-20.
487. Tsai YT, Itokazu Y, Yu RK. GM1 Ganglioside is Involved in Epigenetic Activation Loci of Neuronal Cells. Neurochem Res. 2016;41(1-2):107-15.
488. Tettamanti G. Ganglioside/glycosphingolipid turnover: new concepts. Glycoconj J. 2004;20(5):301-17.
489. Virgolini MJ, Feliziani C, Cambiasso MJ, Lopez PH, Bollo M. Neurite atrophy and apoptosis mediated by PERK signaling after accumulation of GM2-ganglioside. Biochim Biophys Acta Mol Cell Res. 2019;1866(2):225-39.
490. Ciarlo L, Manganelli V, Garofalo T, Matarrese P, Tinari A, Misasi R, et al. Association of fission proteins with mitochondrial raft-like domains. Cell Death Differ. 2010;17(6):1047-58.
491. Garcia-Ruiz C, Colell A, Morales A, Calvo M, Enrich C, Fernandez-Checa JC. Trafficking of ganglioside GD3 to mitochondria by tumor necrosis factor-alpha. J Biol Chem. 2002;277(39):36443-8.
492. Sano R, Annunziata I, Patterson A, Moshiach S, Gomero E, Opferman J, et al. GM1-ganglioside accumulation at the mitochondria-associated ER membranes links ER stress to Ca(2+)-dependent mitochondrial apoptosis. Mol Cell. 2009;36(3):500-11.

493. Saito M, Chakraborty G, Shah R, Mao RF, Kumar A, Yang DS, et al. Elevation of GM2 ganglioside during ethanol-induced apoptotic neurodegeneration in the developing mouse brain. J Neurochem. 2012;121(4):649-61.
494. Roy E, Bruyere J, Flamant P, Bigou S, Ausseil J, Vitry S, et al. GM130 gain-of-function induces cell pathology in a model of lysosomal storage disease. Hum Mol Genet. 2012;21(7):1481-95.
495. Kreutz F, dos Santos Petry F, Camassola M, Schein V, Guma FC, Nardi NB, et al. Alterations of membrane lipids and in gene expression of ganglioside metabolism in different brain structures in a mouse model of mucopolysaccharidosis type I (MPS I). Gene. 2013;527(1):109-14.
496. Saville JT, Flanigan KM, Truxal KV, McBride KL, Fuller M. Evaluation of biomarkers for Sanfilippo syndrome. Mol Genet Metab. 2019;128(1-2):68-74.
497. Sobieski C, Fitzpatrick MJ, Mennerick SJ. Differential Presynaptic ATP Supply for Basal and High-Demand Transmission. J Neurosci. 2017;37(7):1888-99.
498. Piña-Crespo J.C. S-BS, Lipton S.A. Concept of Excitotoxicity via Glutamate Receptors. New York, NY: Springer,; 2014.
499. Plotegher N, Duchen MR. Mitochondrial Dysfunction and Neurodegeneration in Lysosomal Storage Disorders. Trends Mol Med. 2017;23(2):116-34.
500. Wang Y, Xu E, Musich PR, Lin F. Mitochondrial dysfunction in neurodegenerative diseases and the potential countermeasure. CNS Neurosci Ther. 2019;25(7):816-24.
501. Ko DC, Milenkovic L, Beier SM, Manuel H, Buchanan J, Scott MP. Cell-autonomous death of cerebellar purkinje neurons with autophagy in Niemann-Pick type C disease. PLoS Genet. 2005;1(1):81-95.
502. Lemonnier T, Blanchard S, Toli D, Roy E, Bigou S, Froissart R, et al. Modeling neuronal defects associated with a lysosomal disorder using patient-derived induced pluripotent stem cells. Hum Mol Genet. 2011;20(18):3653-66.
503. Hocquemiller M, Vitry S, Bigou S, Bruyere J, Ausseil J, Heard JM. GAP43 overexpression and enhanced neurite outgrowth in mucopolysaccharidosis type IIIB cortical neuron cultures. J Neurosci Res. 2010;88(1):202-13.
504. Dong Y, Fischer R, Naude PJ, Maier O, Nyakas C, Duffey M, et al. Essential protective role of tumor necrosis factor receptor 2 in neurodegeneration. Proc Natl Acad Sci U S A. 2016;113(43):12304-9.
505. Jeyakumar M, Smith DA, Williams IM, Borja MC, Neville DC, Butters TD, et al. NSAIDs increase survival in the Sandhoff disease mouse: synergy with N-butyldeoxynojirimycin. Ann Neurol. 2004;56(5):642-9.
506. Benito-Leon J, Contador I, Vega S, Villarejo-Galende A, Bermejo-Pareja F. Non-steroidal anti-inflammatory drugs use in older adults decreases risk of Alzheimer's disease mortality. PLoS One. 2019;14(9):e0222505.
507. Dealler S, Rainov NG. Pentosan polysulfate as a prophylactic and therapeutic agent against prion disease. IDrugs. 2003;6(5):470-8.
508. Killedar S, Dirosario J, Divers E, Popovich PG, McCarty DM, Fu H. Mucopolysaccharidosis IIIB, a lysosomal storage disease, triggers a pathogenic CNS autoimmune response. J Neuroinflammation. 2010;7:39.
509. He Q, Koprich JB, Wang Y, Yu WB, Xiao BG, Brotchie JM, et al. Treatment with Trehalose Prevents Behavioral and Neurochemical Deficits Produced in an AAV alpha-Synuclein Rat Model of Parkinson's Disease. Mol Neurobiol. 2016;53(4):2258-68.

510. Castillo K, Nassif M, Valenzuela V, Rojas F, Matus S, Mercado G, et al. Trehalose delays the progression of amyotrophic lateral sclerosis by enhancing autophagy in motoneurons. Autophagy. 2013;9(9):1308-20.
511. Rahman MA, Rhim H. Therapeutic implication of autophagy in neurodegenerative diseases. BMB Rep. 2017;50(7):345-54.
512. Chang JW, Choi H, Cotman SL, Jung YK. Lithium rescues the impaired autophagy process in CbCln3(Deltaex7/8/Deltaex7/8) cerebellar cells and reduces neuronal vulnerability to cell death via IMPase inhibition. J Neurochem. 2011;116(4):659-68.
513. Maetzel D, Sarkar S, Wang H, Abi-Mosleh L, Xu P, Cheng AW, et al. Genetic and chemical correction of cholesterol accumulation and impaired autophagy in hepatic and neural cells derived from Niemann-Pick Type C patient-specific iPS cells. Stem Cell Reports. 2014;2(6):866-80.
514. Sardiello M. Transcription factor EB: from master coordinator of lysosomal pathways to candidate therapeutic target in degenerative storage diseases. Ann N Y Acad Sci. 2016;1371(1):3-14.
515. Rodriguez-Navarro JA, Rodriguez L, Casarejos MJ, Solano RM, Gomez A, Perucho J, et al. Trehalose ameliorates dopaminergic and tau pathology in parkin deleted/tau overexpressing mice through autophagy activation. Neurobiol Dis. 2010;39(3):423-38.
516. Donghong Liu JS, Alejandra Colina Ibarra, Yukio Kakuda, Sophia Jun Xue,. The scavenging capacity and synergistic effects of lycopene, vitamin E, vitamin C, and β-carotene mixtures on the DPPH free radical. LWT - Food Science and Technology,. 2008;41(7):1344-9.
517. Di Domenico F, Barone E, Perluigi M, Butterfield DA. Strategy to reduce free radical species in Alzheimer's disease: an update of selected antioxidants. Expert Rev Neurother. 2015;15(1):19-40.
518. Delanty N, Dichter MA. Antioxidant therapy in neurologic disease. Arch Neurol. 2000;57(9):1265-70.
519. Kamat CD, Gadal S, Mhatre M, Williamson KS, Pye QN, Hensley K. Antioxidants in central nervous system diseases: preclinical promise and translational challenges. J Alzheimers Dis. 2008;15(3):473-93.
520. Omata T, Fujii K, Takanashi J, Murayama K, Takayanagi M, Muta K, et al. Drugs indicated for mitochondrial dysfunction as treatments for acute encephalopathy with onset of febrile convulsive status epileptics. J Neurol Sci. 2016;360:57-60.
521. Jinek M, Chylinski K, Fonfara I, Hauer M, Doudna JA, Charpentier E. A programmable dual-RNA-guided DNA endonuclease in adaptive bacterial immunity. Science. 2012;337(6096):816-21.
522. Penney J, Ralvenius WT, Tsai LH. Modeling Alzheimer's disease with iPSC-derived brain cells. Mol Psychiatry. 2020;25(1):148-67.
523. Kuiper GA, Meijer OLM, Langereis EJ, Wijburg FA. Failure to shorten the diagnostic delay in two ultra-orphan diseases (mucopolysaccharidosis types I and III): potential causes and implications. Orphanet J Rare Dis. 2018;13(1):2.
524. Cara O'Neill NF, Jill Wood,. The natural history of facial features observed in Sanfilippo syndrome (MPS IIIB) using a next generation phenotyping tool,. Molecular Genetics and Metabolism,. 2019;126(2):5112.
525. Bhattacharyya R, Gliddon B, Beccari T, Hopwood JJ, Stanley P. A novel missense mutation in lysosomal sulfamidase is the basis of MPS III A in a spontaneous mouse mutant. Glycobiology. 2001;11(1):99-103.

526. Lau AA, King BM, Thorsen CL, Hassiotis S, Beard H, Trim PJ, et al. A novel conditional Sgsh knockout mouse model recapitulates phenotypic and neuropathic deficits of Sanfilippo syndrome. J Inherit Metab Dis. 2017;40(5):715-24.
527. Webber DL, Choo A, Hewson LJ, Trim PJ, Snel MF, Hopwood JJ, et al. Neuronal-specific impairment of heparan sulfate degradation in Drosophila reveals pathogenic mechanisms for Mucopolysaccharidosis type IIIA. Exp Neurol. 2018;303:38-47.
528. Aronovich EL, Johnston JM, Wang P, Giger U, Whitley CB. Molecular basis of mucopolysaccharidosis type IIIB in emu (Dromaius novaehollandiae): an avian model of Sanfilippo syndrome type B. Genomics. 2001;74(3):299-305.
529. Raj K, Ellinwood NM, Giger U. An exonic insertion in the NAGLU gene causing Mucopolysaccharidosis IIIB in Schipperke dogs. Sci Rep. 2020;10(1):3170.
530. Yang Q, Zhao X, Xing Y, Jiang C, Jiang K, Xu P, et al. A model of mucopolysaccharidosis type IIIB in pigs. Biol Open. 2018;7(10).
531. Clavijo A, Sun F, Sneed L. Diagnosis of caprine mucopolysaccharidosis type IIID by real-time polymerase chain reaction-based genotyping. J Vet Diagn Invest. 2010;22(4):622-7.
532. Thompson JN, Jones MZ, Dawson G, Huffman PS. N-acetylglucosamine 6-sulphatase deficiency in a Nubian goat: a model of Sanfilippo syndrome type D (mucopolysaccharidosis IIID). J Inherit Metab Dis. 1992;15(5):760-8.
533. Cavanagh KT, Leipprandt JR, Jones MZ, Friderici K. Molecular defect of caprine N-acetylglucosamine-6-sulphatase deficiency. A single base substitution creates a stop codon in the 5'-region of the coding sequence. J Inherit Metab Dis. 1995;18(1):96.

# Chapter VI: Annex

## 6.1 Supplementary table 1: MPS III Animal models

| Disease | Enzyme | Animal model | Naturally occurring | Observations | Reference |
|---|---|---|---|---|---|
| MPS IIIA | SGSH | Wirehaired dachshund dog | Yes | c.737-739delCCA /p.Thr246del | (287, 307) |
| | | Mouse | Yes | c.91G>A/ p.D31N | (294) (525) |
| | | Huntaway dog | Yes | c.708-709insA/ p.P228* | (288), (289) |
| | | Mouse* | No | Conditional *SGSH*-knockout | (526) |
| | | Fruit fly* | No | *SGSH-Knockdown/ CG14291* | (527) |
| MPS IIIB | NAGLU | Mouse | No | *Naglu*-Knockout | (298) |
| | | Emu | Yes | c.1098-1099delGG | (528), (290) |
| | | Schipperke dog | Yes | c.2110_2111ins[A(40_70); 2100_2110] | (291, 529) |
| | | Bovine | Yes | c.1354G>A/ p.E452K | (341) |
| | | Pig* | No | *NAGLU* $^{+/-}$ | (530) |
| **MPS IIIC** | **HGSNAT** | **Mouse** | **No** | ***Hgsnat*-Knockout (*Hgsnat-Geo*)** | **This thesis** |
| | | Mouse * | No | *Hgsnat*-Knockout | (450) |
| MPS IIID | GNS | Nubian goat | Yes | c.322C>T/ p.R102* | (531-533) |
| | | Mouse | No | *Knockout* | (451) |
| MPS IIIE | ARSG | American Staffordshire Terrier (AST) dog | Yes | c.296G>A/ p.R99H | (184) |
| | | Mouse | No | *Arsg*-Knockout | (185) |

*Not yet reported at the time of our study

## Additional studies

Besides the research presented in this dissertation, I have participated in other projects and contributed to the following publications during my doctoral studies:

**Carla Martins**, Catherine Brunel-Guitton, Anne Lortie, France Gauvin, Carlos R. Morales, Grant A. Mitchell and Alexey V. Pshezhetsky. Atypical juvenile presentation of GM2 gangliosidosis AB in a patient compound-heterozygote for c.259G>T and c.164C>T mutations in the *GM2A* gene. ***Mol Genet Metab Rep.*** 2017 Apr 7;11:24-29. **(Supplementary article 1)**

Julie Tordo, Claire O'Leary, André S. L. M. Antunes, Nuria Palomar, Patrick Aldrin-Kirk, Mark Basche, Antonette Bennett, Zelpha D'Souza, Hélène Gleitz, Annie Godwin, Rebecca J. Holley, Helen Parker, Ai Yin Liao, Paul Rouse, Amir Saam Youshani, Larbi Dridi, **Carla Martins**, Thierry Levade, Kevin B. Stacey, Daniel M. Davis, Adam Dyer, Nathalie Clément, Tomas Björklund, Robin R. Ali, Mavis Agbandje-McKenna, Ahad A. Rahim, Alexey Pshezhetsky, Simon N. Waddington, R. Michael Linden, Brian W. Bigger, Els Henckaerts. A novel adeno-associated virus capsid with enhanced neurotropism corrects a lysosomal transmembrane enzyme deficiency. ***Brain.*** 2018 Jul 1;141(7):2014-2031. **(Supplementary article 2)**

Alexey V. Pshezhetsky, **Carla Martins C** and Mila Ashamarina. Sanfilippo type C disease: pathogenic mechanism and potential therapeutic applications. ***Expert Opinion on Orphan Drugs.*** 2018 Oct;6(11):635-646.

## 6.2 Supplementary article 1

# Atypical juvenile presentation of GM2 gangliosidosis AB in a patient compound-heterozygote for c.259G>T and c.164C>T mutations in the *GM2A* gene.

(Manuscript published in Molecular Genetics and Metabolism Reports, April 2017)

### Context

The rarity of GM2-gangliosidosis, AB variant, and the absence of artificial substrates detecting the GM2AP deficiency in the routine laboratory investigation, is a challenge for the diagnosis of the disease. In this project, we studied a patient with an atypical presentation of GM2-gangliosidosis, AB variant, carrying two variants in the *GM2A* gene. The absence of GM2AP in the patient's cultured fibroblasts and the impairment of GM2 degradation shown by the metabolic labeling with GM1, allowed the confirmation the disease.

Our findings were published in Molecular Genetics and Metabolism Reports, in April 2017. (Mol Genet Metab Rep. 2017 Apr 7;11:24-29).

### Contributions

Carla Martins participated in the design of the study, performed all experiments and analyzed the corresponding results, wrote the manuscript and revised the final version.

Catherine Brunel-Guitton, Anne Lortie, France Gauvin and Grant A. Mitchell performed the clinical examination of the patient, reported by GAM.

Carlos R. Morales provided the plasmid encoding wild-type *GM2A*.

Alexey V. Pshezhetsky conceptualized, designed and supervised the study. AVP wrote the manuscript and revised the final version with participation of the remaining authors.

# Atypical juvenile presentation of GM2 gangliosidosis AB in a patient compound-heterozygote for c.259G > T and c.164C > T mutations in the *GM2A* gene

Carla Martins[a], Catherine Brunel-Guitton[a], Anne Lortie[a], France Gauvin[a], Carlos R. Morales[b], Grant A. Mitchell[a,1], Alexey V. Pshezhetsky[a,b,1]

[a] CHU Ste-Justine, University of Montreal, Montreal, QC, Canada

[b] Department of Anatomy and Cell Biology, McGill University, Montreal, QC, Canada

[1] Equally contributed as senior authors.

## ABSTRACT

GM2-gangliosidosis, AB variant is an extremely rare autosomal recessive inherited disorder caused by mutations in the *GM2A* gene that encodes GM2 ganglioside activator protein (GM2AP). GM2AP is necessary for solubilisation of GM2 ganglioside in endolysosomes and its presentation to β-hexosaminidase A. Conversely GM2AP deficiency impairs lysosomal catabolism of GM2 ganglioside, leading to its storage in cells and tissues. We describe a 9-year-old child with an unusual juvenile clinical onset of GM2-gangliosidosis AB. At the age of 3 years he presented with global developmental delay, progressive epilepsy, intellectual disability, axial hypertonia, spasticity, seizures and ataxia, but without the macular cherry-red spots typical for GM2 gangliosidosis. Brain MRI detected a rapid onset of diffuse atrophy, whereas whole exome sequencing showed that the patient is a compound heterozygote for two mutations in *GM2A*: a novel nonsense mutation, c.259G > T (p.E87X) and a missense mutation c.164C > T (p.P55L) that was recently identified in homozygosity in patients of a Saudi family with a progressive chorea-dementia syndrome. Western blot analysis showed an absence of GM2AP in cultured fibroblasts from the patient, suggesting that both mutations interfere with the synthesis and/or folding of the protein. Finally, impaired catabolism of GM2 ganglioside in the patient's fibroblasts was demonstrated by metabolic labeling with fluorescently labeled GM1 ganglioside and by immunohistochemistry with anti-GM2 and anti-GM3 antibodies. Our observation expands the molecular and clinical spectrum of molecular defects linked to GM2-gangliosidosis and suggests novel diagnostic approach by whole exome sequencing and perhaps ganglioside analysis in cultured patient's cells.

## 1. Introduction

GM2-gangliosidosis, AB variant (MIM#272750) is an autosomal recessive disorder of lysosomal ganglioside catabolism caused by mutations in the *GM2A* gene (reviewed in [1]). GM2A encodes the GM2 ganglioside activator protein (GM2AP, MIM #613109). A small (~25 kDa) amphiphilic protein GM2AP facilitates hydrolysis of GM2 ganglioside at the surfaces of the intra-endosomal membranes (IMs) generated during endocytosis [2,3]. At the acidic pH of the endosome, GM2AP is protonated and binds to IMs rich in the anionic lipid, bis (monoacylglycero)phosphate [4,5]. Once bound to the IM surface, GM2AP forms a specific 1:1 complex with GM2 ganglioside, extracts a ganglioside molecule from the membrane and presents it to β-hexosaminidase A (HexA) for the hydrolytic cleavage of β-N-acetylglucosamine residue from the glycan chain, producing GM3 ganglioside for further conversion into lactosylceramide by the ganglioside neurami-nidases Neu3 and Neu4 [6].

All previously described patients with GM2-gangliosidosis AB presented with clinical phenotypes similar to those of acute infantile Tay-Sachs or Sandhoff diseases, though perhaps slightly milder [7,8]. Cherry red macular spots have been reported in all cases. Recently however, three members of a Saudi family homozygous for the c.164C > T (p.P55L) mutation in GM2A have been reported. The patients presented at 7–13 years with a progressive chorea-dementia syndrome characterised by spastic quadriparesis, limb dystonia, generalized chorea and generalized cerebral atrophy [9]. The patients lacked the macular cherry red spots characteristic of GM2 gangliosidosis AB, and there was no report on whether GM2 ganglioside has been stored in their tissues. Here we describe a 9–year-old boy with an atypical delayed clinical phenotype of GM2-gangliosidosis AB. He presented with global developmental delay, progressive epilepsy, intellectual disability, axial hypertonia, spasticity, seizures and ataxia, but similarly to recently described Saudi patients without retinal cherry spots. Molecular and biochemical analysis showed that the patient is a compound-heterozygote for 2 mutations in *GM2A*, one similar to that described by Salih *et al.* [9] and a novel nonsense mutation c.259G > T (p.E87X). These mutations result in drastically reduced levels of GM2AP and impaired GM2 catabolism in the patient's cells.

## 2. Subject/materials and methods

### 2.1. Patient, biochemical and molecular analyses

The patient is followed at Sainte-Justine university hospital center (CHU Ste-Justine) in Montreal. Activities of lysosomal enzymes in blood leucocytes and cultured skin fibroblasts, the levels of urinary glycosaminoglycans and other biochemical tests were performed in the Biochemical Medical Genetics Laboratory of CHU Ste-Justine. Whole exome sequencing was performed on the leucocyte DNA samples using an Illumina HiSeq 2000 sequencer at the Whole Genome Laboratory in Baylor College of Medicine, in Houston, TX.

### 2.2. Immunocytochemistry

Cultured skin fibroblasts of the patient obtained from skin biopsies of the patient and of three normal health controls from the cell repository of the Medical Genetics Division of CHU Ste-Justine were cultured in DMEM containing 10% FBS (Wisent BioProducts) and 1%antibiotic-antimycotic (Life Technologies) on glass slides in 6-well plates until 70% confluency, fixed with 4% PFA, permeabilized with 0.25% (v/v) Triton X-100, and stained with the antibodies against GM2 (KM966, 1:500), GM3 (M2590, Cosmo Bio Co., Ltd., 1:100) or LAMP-2 (mouse anti-human H4B4, DSHB, 1:100) followed by appropriate secondary antibodies (Alexa fluor 488 goat anti-human IgG, 1:500; Alexa fluor 555 goat anti-mouse IgG, 1:400) and Draq5™ solution (all ThermoFisher Scientific). For quantification, images of 40 randomly selected cells were acquired with the LSM510 Zeiss or Leica TCS SPE confocal microscopes (×63 glycerol immersion objectives, N.A. 1.4) and analysed using the ImageJ software. The percentage of GM2-positive cells was measured by manually counting the cells in randomly selected field images acquired with a Nikon Eclipse E800 fluorescence microscope (×40 objective).

### 2.3. Analysis of the GM2AP expression by Western blot

Human fibroblasts or Cos7 cells transfected with the pcDNA3.1-TOPO plasmid expressing human GM2AP [12] were cultured in 10 cm dishes until 80-90% confluency, harvested, and homogenized

in H2O by sonication (3 × 10 s). The protein was quantified using the Bradford reagent (Bio-Rad). After separation by SDS PAGE on a 15% gel, the proteins were transferred to a nitrocellulose membrane and hybridized with antibodies against GM2AP [10] (1:1000) or α-tubulin (12G10, DSHB, 1:15,000) followed by the appropriate secondary antibodies (sc-2020, Santa Cruz Biotechnology, 1:4000 or 7076S, Cell Signaling, 1:10,000). The membrane was developed with Pierce® ECL Western Blotting substrate (Thermo Scientific) and the signal detected using G:Box Chemi XQR system (Syngene).

### 2.4. Analysis of ganglioside catabolism in cultured fibroblasts

Fibroblasts were plated at a density of 2 × 104 cells/cm2 in 10 cm dishes. After 18 h the medium was supplemented with BODIPY® FL C5-Ganglioside GM1 (Life Technologies) at a final concentration of 1.45 μM and the cells were further cultured for 72 h. Gangliosides were purified from the cell pellets and analysed by thin layer chromatography (TLC) on silica plates (Merck) as previously described [11]. The plates were analysed under UV light and images acquired using G:Box Chemi XQR system. The intensity of GM1 and GM2 ganglioside band was quantified using ImageJ software.

## 3. Results

### 3.1. Clinical course

The patient is a nine-year-old boy. He came to medical attention because of seizures at 3 years of age. He is the second child of unrelated French Canadian parents with a negative family history for neurodegenerative problems. Following a normal term pregnancy and spontaneous vaginal delivery he was born weighing 3.5 kg with a head circumference of 33.0 cm. Apgar scores were 9 at one, five and 10 min and he was discharged after 48 h.

His initial development was felt to be normal although in retrospect, signs of motor dysfunction were present before 12 months of age. He sat at 6 months, walked without support at 1 year, but tended to walk in a tiptoe fashion. He climbed stairs in alternating fashion at 2 years. He was toilet

trained by 2 years of age. He was never able to run. He had poor fine motor skills, although he succeeded in feeding himself. He pronounced single words with difficulty by 12 months of age and spoke in sentences by 3 years. A speech therapist diagnosed marked verbal dyspraxia at the age of three years. He had limited interests and disliked changes in his routine. He was suspected clinically to have absence seizures from about 3 years of age but electroencephalographic studies were normal on four occasions. His first proven seizure, at 5 years of age, was a prolonged focal convulsion with secondary generalization lasting about 3 min with a postictal state lasting several minutes. Focal seizures then recurred about once a week, accompanied by loss of contact with his environment and facial twitching. They were treated initially with valproic acid. Soon thereafter the patient was noted to have ataxia and treatment was empirically switched to levetiracetam. Between 5 and 6 years of age he progressively deteriorated, with progressive ataxia, mild spasticity and loss of previous abilities like dressing himself and fecal continence. There was progressive loss of expressive speech, decreased understanding of simple sentences and interest in activities. He developed marked sialorrhea. Swallowing difficulties required thickening of oral fluids. Convulsions increased in frequency to 3–4 per day.

Cerebral magnetic resonance imaging at 5 years of age was normal, but at the age of 5 years 11 months re-examination of the brain and spinal cord revealed diffuse cortical and subcortical atrophy of supra-tentorial and infratentorial structures and ventricular enlargement. No abnormalities of signal were identified. The spinal cord was normal. Electroencephalography at 7.5 years of age showed abnormal diffuse slow wave activity and independent bifrontal, parieto-occipital and temporal epileptic foci. Ophthalmology evaluations at the ages of 5 years 9 months and 8 years 9 months were normal, with normal fundoscopic findings and absence of cherry red spots.

Diagnostic investigations initially focused on lysosomal storage diseases and the levels of glycosaminoglycans in the urine and activities of lysosomal hydrolases in the blood white cells were tested. All tests were normal including the levels of total β-hexosaminidase (3180 nmol/h/mg of protein, normal 1687–4509), HexA measured by thermoinactivation (1246 nmol/h/mg of protein (61%), normal 719–1942 (56–80%)), and HexA measured with specific sulfated substrate (366 nmol/h/mg of protein, normal 154–545). These negative results lead to extensive further investigations. Positive findings are noted here, although their relationship if any with the primary

condition is not obvious. They include mild persistentelevation of plasma aspartate aminotransferase (79-113 units/L, normal 11-43), and recently of alanine aminotransferase (65-160 units/L, normal 5-25) and mild hypercholesterolemia (5.81 mmol/L, normal 3.20-4.40) with normal glucose and triglyceride levels. Normal results were obtained for plasma amino acids, total homocystine, acylcarni-tines, lactate, pyruvate, uric acid, creatine kinase, folate, vitamin B12, very long chain fatty acids, phytanic acid, pipecolic acid, copper and ceruloplasmin. Transferrin isoelectric focusing was normal. Urine glycosaminoglycans, organic acids, creatine, guanidinoacetoacetate, purine and pyrimidine metabolites, α-aminoadipic semialdehyde and copper were normal. Cerebrospinal fluid revealed normal levels of proteins (0.32 g/L, normal 0.15 to 0.40), glucose, lactate, 5-hydroxyindoleacetic acid, homovanillic acid, 3-O-methyldopa, neopterin, tetrahydrobiopterin, 5-methyltetrahydrofolate, amino acids and pyridoxal-5-phosphate.

Treatment with thiamine, biotin and riboflavin was started empirically, without noticeable effect. A trial of ketogenic diet for refractory seizures was stopped after six weeks due to lack of improvement, and worsening feeding difficulties with severe dysphagia. After exome sequencing revealed the mutations in *GM2A* as described below, vitamin therapy was stopped and a trial of corticotherapy (prednisone 2 mg/kg/day) was given over 3 months, because of its potential anticonvulsant and antiinflammatory effects. Corticotherapy reduced seizure frequency and severity, increased awake periods and increased appetite, but had no effect on the other aspects of the disease and progression. Due to the development of complications, prednisone was tapered and stopped over 3 months. Because of severe dysphagia and feeding difficulties, frequent aspiration and suboptimal hydration, a feeding gastrostomy was accepted by the family shortly before nine years of age. The patient had severe multifactorial sleep disturbances related to seizures, neuropathic pain and possibly to feeding difficulties and insufficient caloric intake. After gastrostomy and treatment with melatonin (6 mg po hs), his sleep pattern almost normalized. He is currently also followed by palliative care. He stopped walking at 7.5 years. He has severe spasticity and contractures in all limbs despite a daily program of stretching exercises. He has no visual contact. His ophthalmological exam remains normal without cherry red spots. Addition of phenytoin, substantially decreased the seizure frequency. He has focal right motor seizures, once or twice daily, usually in the morning. The major problem remains spasticity and neuropathic pain, for which different treatments have been tried without any major improvement.

### 3.2. Discovery and investigation of GM2AP deficiency

Whole exome sequencing was performed on leucocyte DNA from the patient. A novel heterozygous nonsense mutation c.259G > T (p.E87X) in exon 3 of *GM2A* gene was detected and confirmed by Sanger sequencing. The father was heterozygous for the c.259G > T change. This variant was not present in the Exome Aggregation Consortium (ExAC) or 1000 Genomes databases. Additionally, the missense mutation c.164C > T (p.P55L), recently reported in homozygosity in patients with progressive chorea-dementia [9], was identified in exon 2 of *GM2A*. By Sanger sequencing, the patient and his mother were both heterozygous. The sequences of other genes potentially implicated in neurological diseases including that of GLB1 were normal.

In order to study GM2AP production in the patient's cells we have established fibroblast cultures from patient's skin biopsy and analysed total protein extract by Western blot using goat polyclonal anti-GM2AP antibodies [10]. Our experiments (Fig. 1) showed that the patient's fibroblasts lacked the ~20 kDa protein band corresponding to the size of mature GM2AP [12,13]. This band was present in fibroblast lines from 3 healthy controls, while the same antibodies detected 2 bands of ~22 and ~20 kDa (most likely GM2AP precursor and mature form, respectively [13]) in the total protein extract of Cos7 cells transfected with a plasmid encoding human GM2AP [12]. These results demonstrate that the GM2AP is reduced in the patient's cells to below detection level and suggest that both p.E87X and p.P55L mutations interfere with the synthesis and/or stability of GM2AP. We further tried to increase the level of GM2AP by treating cells in culture with ambroxol, which previously has been shown to increase *GM2A* expression at least 3 fold, presumably by activating TFEB transcription factor [14]. We also tried to rescue the folding of the mutant GM2AP by culturing fibroblasts at 30 °C [15]. In both cases, however the amount of GM2AP remained below the detection level of Western blot (data not shown).

The catabolism of GM2 ganglioside in the patient's and normal healthy control fibroblasts was analysed by metabolic labeling with fluorescently (BODIPY)-labeled GM1 ganglioside for 48 h. Analysis by TLC of the fluorescently labeled gangliosides extracted from the cell pellets (Fig. 2A) showed that control cells converted the fluorophore-labeled GM1 to GM2 and further, to lactosylceramide (LacCer). Patient's cells also generated GM2 but failed to produce LacCer. In contrast, the amount of GM2 was significantly increased indicating that this ganglio-side is stored in the patient's cells. The results of TLC analysis of the neutral lipid fraction (Supplemental Fig.

1) are also consistent with the above hypothesis indicating that the cells from normal controls contained multiple fluorescently labeled lipid bands (presumably BODIPY-labeled LacCer, glucosylceramide, and ceramide) undetectable in the patient's cells.

To determine if GM2 was stored in lysosomes of cultured fibroblasts from the patient, we analysed them by immunohistochemistry using monoclonal antibodies specific to GM2 ganglioside or its catabolic product GM3 ganglioside (Fig. 3). The cells were stained either with anti-GM2 or anti-GM3 monoclonal antibodies and the antibodies against the lysosomal marker protein, LAMP-2. The intensity of GM2 and GM3 staining was quantified using ImageJ software in randomly selected isolated fibroblasts and the percent of cells with strong staining against GM2 was counted in randomly selected fields by a person who was unaware of the cell genotype. Our results (Fig. 3A and B) indicate that the patient's cells show significantly increased staining for GM2 and decreased staining for GM3 ganglioside consistent with compromised conversion of GM2 into GM3. In the patient's (but not in the control cells) GM2 staining co-localized with the lysosomal marker LAMP-2 (Fig. 3A).

## 4. Discussion

We report the clinical course of a unique patient with GM2 gangliosidosis AB with a juvenile onset and without ocular features such as progressive blindness and macular cherry-red spots. The patient illustrates several points of clinical importance. First, the diagnosis of GM2 gangliosidosis AB must be suspected in the presence of neurodegenerative signs if β-hexosaminidase values in leucocytes or cultured fibroblasts are normal. Second, gene sequencing is therefore likely to be the first line diagnostic technique for atypical cases of GM2 gangliosidosis AB. This patient received an extensive metabolic workup that was otherwise negative. GM2 gangliosidosis AB was suspected only after *GM2A* mutations were identified by exome sequencing. Biochemical diagnosis of GM2 gangliosidosis AB is essential for confirming the biological activity of DNA sequence variants but it requires a high level of expertise and will likely remain confined to a small number of specialized laboratories. This suggests that *GM2A* sequencing should be included in broad panels for neurodegenerative conditions.

The phenotypic spectrum of GM2 gangliosidosis AB may be broader than previously thought. Macular cherry red spots were absent in this patient. Cherry red spots are characteristic of infantile

Tay-Sachs and Sandhoff diseases, but are rarely present in juvenile or subacute cases [16–23]. The lack of cherry red spots may also apply to later-onset cases of GM2 gangliosidosis AB. However, patients with neurodegenerative conditions with normal β-hexosaminidase activity and without cherry red spots would probably not have been submitted for detailed biochemical testing for the possibility of GM2 gangliosidosis. Therefore, it is possible that higher clinical suspicion or unbiased genomic testing will identify new patients and reveal the complete phenotypic spectrum of GM2 gangliosidosis AB. Technically, our results also show that the accumulation of GM2 ganglioside in the cultured fibroblasts from the patients affected with GM2 gangliosidosis AB can be demonstrated by immunohistochemistry even without supplementing the cell medium with an excess of GM1 or GM2 ganglioside. This method may therefore be useful for confirmation of diagnosis in some particular cases.

The reported patient is a compound heterozygote for two mutations in the *GM2A* gene: a novel nonsense mutation c.259G > T (p.E87X) and a missense mutation c.164C > T (p.P55L) recently reported by Salih *et al.* [9] and according to our analysis classified as potentially damaging by both SIFT and Polyphen-2 software. The novel point mutation c.259G > T results in a transcript containing a premature termination codon. The GM2A mRNA containing c.259G > T will likely undergo mRNA nonsense-mediated decay [24,25]. In turn, Pro55 conserved among at least 17 mammalian species is important for supporting the conformation of the turn between two β-strands of GM2AP [26], suggesting that its replacement with the bulky hydrophobic Leu interferes with the tertiary structure of the protein. A misfolded mutant GM2AP may be then targeted for degradation by the Endoplasmatic Reticulum-Associated Degradation pathway (ERAD). This interpretation is consistent with the results of the Western blot analysis, which did not detect GM2AP cross-reactive band in cultured patient's fibroblasts.

Until recently seven *GM2A* mutations have been described in the AB-variant of GM2 gangliosidosis [8,27,28]. Only two of them were missense: p.Cys138Arg was identified in a female patient who died at the age of 14 months and was diagnosed after death [29,30] and p.Arg169Pro, also identified in infantile-onset patient [10]. Both patients were homozygous for the corresponding mutations. Further biochemical studies in patient fibroblasts identified that both of these mutations caused retention and degradation of the mutant proteins in the endoplasmic reticulum [10,31].

In contrast, the later onset and milder symptoms of the patient reported here might be due to the presence of residual levels of active or partially active GM2AP carrying P55L substitution. As it is the case in many lysosomal diseases, the severity and onset of GM2 gangliosidosis inversely correlates with the residual rate of GM2 catabolism. Specifically, in infantile Tay-Sachs and Sandhoff patients the residual GM2 conversion rate does not exceed 0.5%, in juvenile and adult forms it reaches 2–4% of normal, while the residual rates above about 10% of normal seem to be compatible with the healthy state [32,33]. Interestingly, the three recently reported patients homozygous for p.P55L in GM2AP presented with a neurological movement disease without ocular features and an onset at the age of 7–8 years [9]. Although this study did not describe if the patients had GM2 storage it is tempting to speculate that our patient had milder phenotype due to the presence of the Leu55 allele. The amount of the GM2AP protein in the cultured fibroblasts from the patient remained however below detection level even when we tried to increase its synthesis by treating cells with ambroxol to activate its expression [14] or by culturing them at 30 °C, to rescue the fold of the GM2AP mutant [15]. A precise quantification of the GM2 conversion rate is necessary therefore to prove this hypothesis. Alternatively, relatively milder phenotype of our patient can be related to the effects of other genes, which remain to be investigated.

**Funding**

Supported in part by the operating grant (111068) from Canadian Institutes of Health Research to A.V.P. and the Ph.D. scholarship (SFRH/BD/84929/2012) from the Fundação para a Ciência e a Tecnologia (FCT, Portugal) financed by POPH/FSE to C.M.

**Acknowledgements**

We thank the patient and his parents for their support and participation in this study, Dr. Nobuo Hanai, Dr. Akiko Furuya and Kyowa Hakko Kirin Co., Ltd. for a generous gift of monoclonal antibodies against GM2 ganglioside, Dr. Xuefang Pan for the help with studying gangliosides by TLC and Dr. Gaziella Di Christo for providing access to confocal microscopy facilities. We are also grateful to Dr. Thierry Levade (Institut de Médecine Moléculaire de Rangueil, Université Toulouse III Paul-Sabatier, Equipe 14, IFR31, Toulouse) and Dr. Mila Ashmarina (CHU Ste-Justine) for helpful advice.

**References**

[1] K. Sandhoff, K. Harzer, Gangliosides and gangliosidoses: principles of molecular and metabolic pathogenesis, J. Neurosci. 33 (2013) 10195–10208.

[2] J.K. Burkhardt, S. Huttler, A. Klein, W. Mobius, A. Habermann, G. Griffiths,

K. Sandhoff, Accumulation of sphingolipids in SAP-precursor (prosaposin)-deficient fibroblasts occurs as intralysosomal membrane structures and can be completely reversed by treatment with human SAP-precursor, Eur. J. Cell Biol. 73 (1997) 10–18.

[3] W. Mobius, V. Herzog, K. Sandhoff, G. Schwarzmann, Intracellular distribution of a biotin-labeled ganglioside, GM1, by immunoelectron microscopy after endocytosis in fibroblasts, J. Histochem. Cytochem. 47 (1999) 1005–1014.

[4] H.D. Gallala, K. Sandhoff, Biological function of the cellular lipid BMP-BMP as a key activator for cholesterol sorting and membrane digestion, Neurochem. Res. 36 (2011) 1594-1600.

[5] H.D. Gallala, B. Breiden, K. Sandhoff, Regulation of the NPC2 protein-mediated cholesterol trafficking by membrane lipids, J. Neurochem. 116 (2011) 702–707.

[6] V. Smutova, A. Albohy, X. Pan, E. Korchagina, N. Bovin, C.W. Cairo, A.V. Pshezhetsky, Structural basis for substrate specificity of mammalian neuraminidases, PLoS One 9 (2014) e106320.

[7] R. Gravel, M.M. Kaback, R.L. Proia, K. Sandhoff, K. Suzuki, The GM2 gangliosidoses, in: C.R. Scriver, A.L. Beaudet, W.S. Sly, D. Valle (Eds.), The Metabolic and Molecular Bases of Inherited Diseases, McGraw-Hill New York, NY (USA), 2001, pp. 3827–3876.

[8] J. Sheth, C. Datar, M. Mistri, R. Bhavsar, F. Sheth, Shah K GM2 gangliosidosis AB variant: novel mutation from India - a case report with a review, BMC Pediatr. 16 (2016) 88.

[9] M.A. Salih, M.Z. Seidahmed, H.Y. El Khashab, *et al.*, Mutation in GM2A leads to a progressive chorea-dementia syndrome, Tremor Other Hyperkinet. Mov. (N Y) 5 (2015) 306.

[10] M. Schroder, D. Schnabel, R. Hurwitz, E. Young, K. Suzuki, K. Sandhoff, Molecular genetics of GM2-gangliosidosis AB variant: a novel mutation and expression in BHK cells, Hum. Genet. 92 (1993) 437–440.

[11] V. Seyrantepe, M. Canuel, S. Carpentier, *et al.*, Mice deficient in Neu4 sialidase exhibit abnormal ganglioside catabolism and lysosomal storage, Hum. Mol. Genet. 17 (2008) 1556–1568.

[12] U. Schepers, G. Glombitza, T. Lemm, A. Hoffmann, A. Chabas, P. Ozand,

K. Sandhoff, Molecular analysis of a GM2-activator deficiency in two patients with GM2-gangliosidosis AB variant, Am. J. Hum. Genet. 59 (1996) 1048–1056.

[13] G.J. Glombitza, E. Becker, H.W. Kaiser, K. Sandhoff, Biosynthesis, processing, and intracellular transport of GM2 activator protein in human epidermal keratinocytes. The lysosomal targeting of the GM2 activator is independent of a mannose-6- phosphate signal, J. Biol. Chem. 272 (1997) 5199–5207.

[14] A. McNeill, J. Magalhaes, C. Shen, *et al.*, Ambroxol improves lysosomal biochem- istry in glucocerebrosidase mutation-linked Parkinson disease cells, Brain 137 (2014) 1481–1495.

[15] O.L. Meijer, L. Welling, M.J. Valstar, *et al.*, Residual N-acetyl-alpha-glucosamini- dase activity in fibroblasts correlates with disease severity in patients with mucopolysaccharidosis type IIIB, J. Inherit. Metab. Dis. 39 (2016) 437–445.

[16] N. Nardocci, B. Bertagnolio, V. Rumi, L. Angelini, Progressive dystonia symptomatic of juvenile GM2 gangliosidosis, Mov. Disord. 7 (1992) 64–67.

[17] A. Nalini, R. Christopher, Cerebral glycolipidoses: clinical characteristics of 41 pediatric patients, J. Child Neurol. 19 (2004) 447–452.

[18] G.H. Maegawa, T. Stockley, M. Tropak, *et al.*, The natural history of juvenile or subacute GM2 gangliosidosis: 21 new cases and literature review of 134 previously reported, Pediatrics 118 (2006) e1550–e1562.

[19] R. Rozenberg, F. Kok, M.G. Burin, M.C. Sa Miranda, *et al.*, Diagnosis and molecular characterization of non-classic forms of Tay-Sachs disease in Brazil, J. Child Neurol. 21 (2006) 540–544.

[20] S.B. Wortmann, D.J. Lefeber, G. Dekomien, *et al.*, Substrate deprivation therapy in juvenile Sandhoff disease, J. Inherit. Metab. Dis. 32 (Suppl. 1) (2009) S307–S311.

[21] A. Levit, D. Nutman, E. Osher, E. Kamhi, R. Navon, Two novel exonic point mutations in HEXA identified in a juvenile Tay-Sachs patient: role of alternative splicing and nonsense-mediated mRNA decay, Mol. Genet. Metab. 100 (2010) 176–183.

[22] N.J. Smith, A.M. Winstone, L. Stellitano, T.M. Cox, C.M. Verity, GM2 gangliosidosis in a UK study of children with progressive neurodegeneration: 73 cases reviewed, Dev. Med. Child Neurol. 54 (2012) 176–182.

[23] T. Georgiou, G. Christopoulos, V. Anastasiadou, *et al.*, The first family with Tay-Sachs disease in Cyprus: genetic analysis reveals a nonsense (c.78G > A) and a silent (c.1305C > T) mutation and allows preimplantation genetic diagnosis, Meta Gene 2 (2014) 200–205.

[24] L.E. Maquat, When cells stop making sense: effects of nonsense codons on RNA metabolism in vertebrate cells, RNA 1 (1995) 453–465.

[25] J.A. Holbrook, G. Neu-Yilik, M.W. Hentze, A.E. Kulozik, Nonsense-mediated decay approaches the clinic, Nat. Genet. 36 (2004) 801–808.

[26] C.S. Wright, S.C. Li, F. Rastinejad, Crystal structure of human GM2-activator protein with a novel beta-cup topology, J. Mol. Biol. 304 (2000) 411–422.

[27] D.J. Mahuran, Biochemical consequences of mutations causing the GM2 gang- liosidoses, Biochim. Biophys. Acta 1455 (1999) 105–138.

[28] D. Renaud, M. Brodsky, GM2-gangliosidosis, AB variant: clinical, ophthalmological, MRI, and molecular findings, JIMD Rep. (2015). http://dx.doi.org/10.1007/8904_ 2015_469.

[29] M. Schroder, D. Schnabel, K. Suzuki, K. Sandhoff, A mutation in the gene of a glycolipid-binding protein (GM2 activator) that causes GM2-gangliosidosis variant AB, FEBS Lett. 290 (1991) 1-3.

[30] C.M. de Baecque, K. Suzuki, I. Rapin, A.B. Johnson, D.L. Whethers, GM2-gangliosidosis, AB variant: clinico-pathological study of a case, Acta Neuropathol. 33 (1975) 207–226.

[31] B. Xie, B. Rigat, N. Smiljanic-Georgijev, H. Deng, D. Mahuran, Biochemical characterization of the Cys138Arg substitution associated with the AB variant form of GM2 gangliosidosis: evidence that Cys138 is required for the recognition of the GM2 activator/GM2 ganglioside complex by beta-hexosaminidase A, Biochemistry 37 (1998) 814–821.

[32] K. Sandhoff, My journey into the world of sphingolipids and sphingolipidoses, Proc. Jpn. Acad. Ser. B Phys. Biol. Sci. 88 (2012) 554–582.

[33] J.T. Clarke, D.J. Mahuran, S. Sathe, E.H. Kolodny, B.A. Rigat, J.A. Raiman, M.B. Tropak, An open-label phase I/II clinical trial of pyrimethamine for the treatment of patients affected with chronic GM2 gangliosidosis (Tay-Sachs or Sandhoff variants), Mol. Genet. Metab. 102 (2011) 6–12.

## Figures

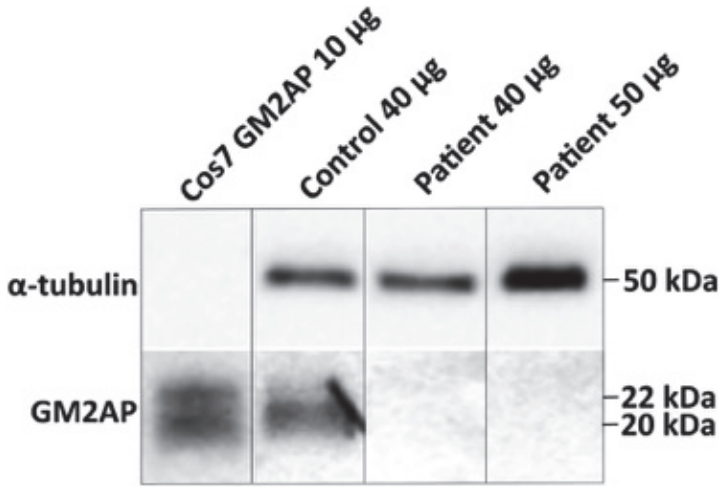


**Fig. 1**. GM2AP is not detected in the patient's cultured fibroblasts by Western blot. Either 40 or 50 µg of total protein extracted from cultured fibroblasts of the patient or normal healthy controls (N = 2) were resolved on SDS PAGE gels, transferred to nitrocellulose membrane and hybridized with anti-GM2AP antibody. A mature ~ 20 kDa GM2AP band was detected in control fibroblasts but not in the patient's fibroblasts. The two bands detected in the protein extract of Cos7 cells transfected with a plasmid encoding GM2AP correspond to the mature ~ 20 kDa protein and its ~ 22 kDa precursor. α-Tubulin was used as a loading control.

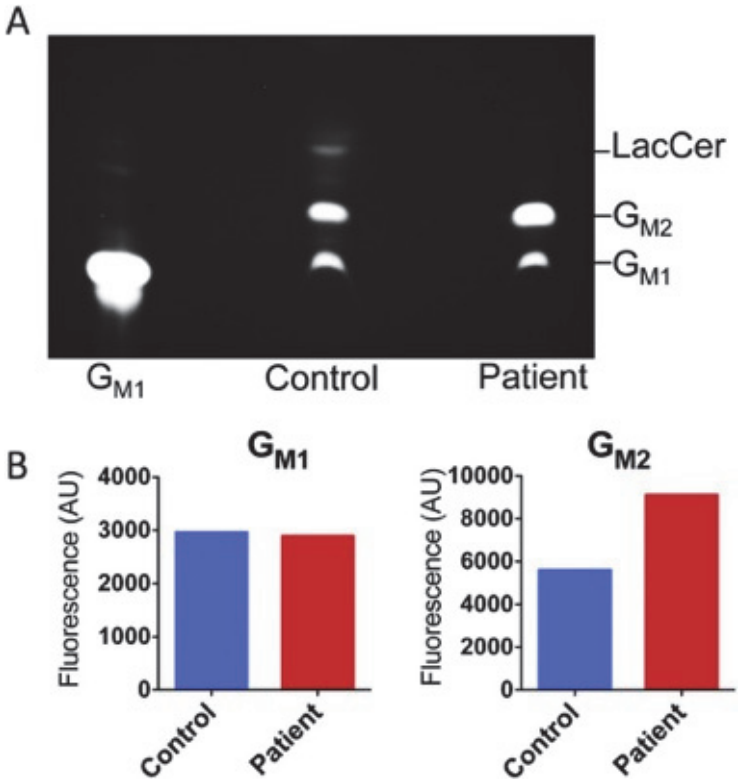


**Fig. 2**. Thin-layer chromatography of fluorescently labeled gangliosides reveals accumulation of GM2 ganglioside in the patient's cultured fibroblasts. Fibroblasts of the patient or a normal healthy control subject were cultured in DMEM containing 1.45 μM of fluorescently labeled BODIPY® FL C5 GM1 ganglioside for 72 h. Total lipids were extracted from cell pellets with 1:1 chloroform/methanol mixture and the gangliosides were separated from neutral lipids and analysed by TLC on silica plates.(A) The fluorescence image of the TLC plate acquired on G:Box Chemi XQR system. The position of fluorescent GM1 ganglioside used as a standard is shown.(B) GM1 and GM2 ganglioside bands were quantified in control and patient's fibroblasts by ImageJ software.

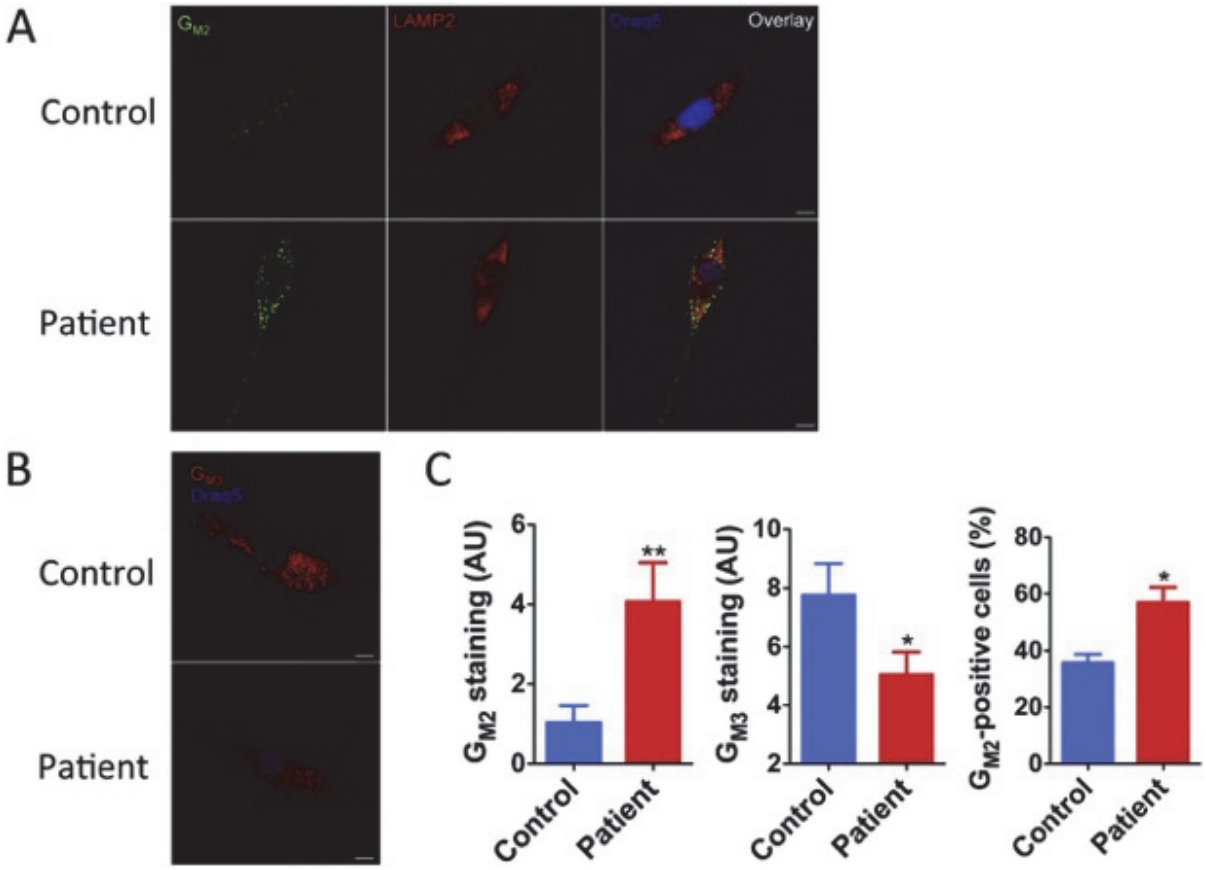


**Fig. 3.** Increased lysosomal GM2 and reduced GM3 ganglioside in the patient's cultured fibroblasts. (A) Fibroblasts from the patient and two normal healthy controls cultured on glass coverslips were fixed and stained with monoclonal humanized anti-GM2 and mouse anti-LAMP-2 antibodies followed by anti-human IgG Alexa 488-labeled (green) and anti-mouse IgG Alexa 555-labeled (red) secondary antibodies. Nuclei were stained with Draq5 (blue). The patient's fibroblasts show a higher intensity of GM2 staining (green) than control fibroblasts and increased co-localization of GM2 and LAMP-2 staining. (B) Fibroblasts from the patient and two normal healthy controls were stained with monoclonal mouse anti-GM3 antibody followed by anti-mouse IgG Alexa-555-labeled secondary antibody (red). Nuclei were stained with Draq5 (blue).The images were acquired in a Leica SP8 confocal microscope with a 63× objective. Bar represents 10 μM. The panels show representative images of at least 40 studied for each cell type. (C) Mean GM2 and GM3 staining intensity and a fraction of GM2-positive cells in control and patient's fibroblasts. Mean staining intensities per μm2 were measured with ImageJ software. Data show

mean (± SEM) of individual values measured for 35 randomly selected cells. **P < 0.01, *P < 0.05 in unpaired two-tailed t-test. GM2-positive cells were manually counted in three randomly selected microscope fields (~ 150 cells each). Data show mean values (± SEM) of 3 independent experiments. *P < 0.05 in unpaired two-tailed t-test. (For interpretation of the references to colour in this figure legend, the reader is referred to the web version of this article.)

## Supplementary figure

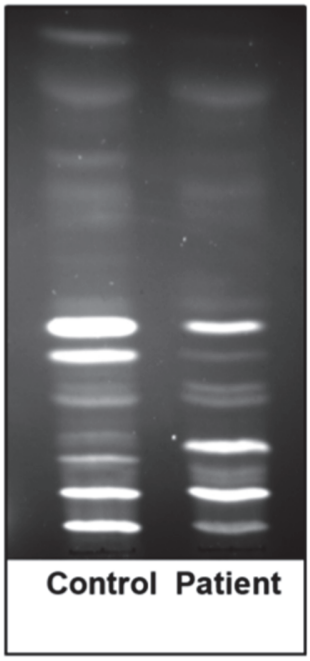


**Supplementary Figure 1.** Fluorescently labeled neutral glycosphingolipids are decreased in patient's fibroblasts. Fibroblasts of the patient or normal healthy control subject were cultured in the presence of 1.45 μM fluorescently labelled BODIPY® FL C5 GM1 ganglioside for 72 h. Total lipids were extracted from cell pellets with 1:1 chloroform/methanol mixture and the neutral lipids were separated from gangliosides and analysed by TLC on silica plates. The fluorescence image of the TLC plate was acquired on G:Box Chemi XQR system.

## 6.3 Supplementary article 2

# A novel adeno-associated virus capsid with enhanced neurotropism corrects a lysosomal transmembrane enzyme deficiency

(Manuscript published in Brain, July 2018)

### Context

The validation of *Hgsnat-Geo* mouse as a *bona fide* animal model of MPS IIIC mouse model (chapter II) enabled the development of therapeutic approaches and evaluation of their efficacy. We have collaborated in first gene therapy study for MPS IIIC with the University of Manchester, based on the intrastriatal delivery of a neurotropic AAV vector expressing WT HGSNAT to the *Hgsnat-Geo* mouse. The results were reported by Tordo *et al*. in a research article published in the journal Brain in July 2018 (Brain. 2018 Jul 1;141(7):2014-2031).

### Personal contribution

Carla Martins quantified the content of GM2 and GM3 gangliosides (by thin-layer chromatography) and studied the regional and subcellular distribution of these gangliosides in the brains (by IHC) of WT, treated and untreated MPS IIIC mice. I have contributed to the writing and final revision of the manuscript.

# A novel adeno-associated virus capsid with enhanced neurotropism corrects a lysosomal transmembrane enzyme deficiency

Julie Tordo[1], Claire O'Leary[2], Andre´ S. L. M. Antunes[1], Nuria Palomar[1], Patrick AldrinKirk[3], Mark Basche[4], Antonette Bennett[5], Zelpha D'Souza[2], Hélène Gleitz[2], Annie Godwin[2], Rebecca J. Holley[2], Helen Parker[2], Ai Yin Liao[2], Paul Rouse[2], Amir Saam Youshani[2], Larbi Dridi[6], Carla Martins[6], Thierry Levade[7], Kevin B. Stacey[8], Daniel M. Davis[8], Adam Dyer[1], Nathalie Clément[9], Tomas Björklund[3], Robin R. Ali[4], Mavis Agbandje-McKenna[5], Ahad A. Rahim[10], Alexey Pshezhetsky[6], Simon N. Waddington[11,12], R. Michael Linden[1], Brian W. Bigger[2], and Els Henckaerts[1]

[1] Department of Infectious Diseases, School of Immunology and Microbial Sciences, King's College London, London, UK

[2] Stem Cell and Neurotherapies, Division of Cell Matrix Biology and Regenerative Medicine, School of Biological Sciences, Faculty of Biology Medicine and Health, University of Manchester, Manchester, UK

[3] Molecular Neuromodulation, Wallenberg Neuroscience Center, Lund University, Lund, Sweden

[4] Department of Genetics, UCL Institute of Ophthalmology, London, UK

[5] Department of Biochemistry and Molecular Biology, Center for Structural Biology, McKnight Brain Institute, College of Medicine, University of Florida, Gainesville, FL, USA

[6] CHU Ste-Justine, University of Montreal, Montreal, Canada

[7] Centre Hospitalo-Universitaire de Toulouse, Institut Fédératif de Biologie, Laboratoire de Biochimie Métabolique, and Unité Mixte de Recherche (UMR) 1037 Institut National de la Santé et de la Recherche Médicale (INSERM), Centre de Recherche en Cancérologie de Toulouse, Toulouse, France

[8] Manchester Collaborative Centre for Inflammation Research, Division of Infection, Immunity and Respiratory Medicine, School of Biological Sciences, Faculty of Biology Medicine and Health, University of Manchester, Manchester, UK

[9] Department of Pediatrics, Powell Gene Therapy Center, University of Florida, Gainesville, FL, USA

[10] Department of Pharmacology, UCL School of Pharmacy, University College London, London, UK

[11] Gene Transfer Technology Group, Institute for Women's Health, University College London, London, UK

[12] Wits/SAMRC Antiviral Gene Therapy Research Unit, Faculty of Health Sciences, University of the Witwatersrand, Johannesburg, South Africa

Correspondence to: Els Henckaerts, Department of Infectious Diseases, School of Immunology and Microbial Sciences, King's College London, London, UK. E-mail: els.henckaerts@kcl.ac.uk
Correspondence may also be addressed to: Brian W. Bigger, Stem Cell and Neurotherapies, Division of Cell Matrix Biology and Regenerative Medicine, School of Biological Sciences, Faculty of Biology Medicine and Health, University of Manchester, Manchester, UK. E-mail: brian.bigger@manchester.ac.uk

Keywords: adeno-associated virus; capsid engineering; neurotropism; mucopolysaccharidosis; lysosomal transmembrane enzyme
Abbreviations: AAV = adeno-associated virus; GlcNS = N-sulpho-glucosamine; HS = heparan sulphate; HSPG = heparan sulphate proteoglycan; IgG = immunoglobulin G; MPSIIIC = mucopolysaccharidosis type IIIC; UA = uronic acid

## Introduction

Recent clinical trials have demonstrated safety and efficacy of adeno-associated virus (AAV)-mediated gene therapies targeting the eye, muscle and liver (Nathwani *et al.*, 2014; Bainbridge *et al.*, 2015; Russell *et al.*, 2017; Sparks Therapeutics, 2017). However, despite recent unparalleled results in an AAV gene therapy trial for spinal muscular atrophy (Mendell *et al.*, 2017), other AAV gene therapies directed at the brain of patients with rare neurological diseases have shown only limited efficacy (Worgall *et al.*, 2008; Tardieu *et al.*, 2014, 2017). One of the main difficulties associated with gene therapy for CNS diseases is the inefficient AAV distribution to neurons from injection sites in patients. To overcome this hurdle, various strategies have been used to identify or generate more suitable AAV capsids for CNS transduction. These include the discovery of new AAV serotypes in humans and non-human primates and the thorough characterization of their brain tropism (Gao *et al.*, 2002, 2004; Cearley and Wolfe, 2006; Foust *et al.*, 2009; Bevan *et al.*, 2011). Concurrently, diverse capsid engineering strategies emerged as approaches to direct the AAV vectors to defined cell types (Müller *et al.*, 2003; Chen *et al.*, 2009; Adachi *et al.*, 2014). AAV capsids can be improved through rational design, directed evolution techniques and *in vivo* selection in mouse or humanized mouse models (Asokan *et al.*, 2010; Shen *et al.*, 2013; Kotterman and Schaffer, 2014; Lisowski *et al.*, 2014; Tervo *et al.*, 2016; Kanaan *et al.*, 2017). Recently, a novel engineering approach based on *in silico* reconstruction of ancestral viruses has yielded a promising vector for gene therapy of diseases that affect liver, muscle or retina (Zinn *et al.*, 2015). Here we report an alternative evolutionary approach to AAV capsid design based on the introduction of amino acids conserved in AAV2 variants that are currently circulating in the human population (Chen *et al.*, 2005).

This yields a potent neurotropic vector, which may be ideally suited to treat human neurological diseases such as mucopolysaccharidosis type IIIC (MPSIIIC). This disease is caused by mutations in the heparan sulphate acetyl-CoA: α-glucosaminide *N*-acetyltransferase (*HGSNAT*) gene, resulting in a deficiency in the lysosomal enzyme HGSNAT (EC 2.3.1.78). Deficiency of HGSNAT causes progressive accumulation of

undegraded heparan sulphate (HS) in all cells of the body (Ruijter *et al.*, 2008). Patients with MPSIIIC have mild visceral manifestations; however, neurological symptoms are severe, characterized by behavioural problems, cognitive decline and, eventually, dementia and death in early adulthood (Ruijter *et al.*, 2008; Valstar *et al.*, 2008). Neuroinflammation and storage of secondary substrates contribute to the pathology of the disease (Archer *et al.*, 2014). The HGSNAT protein is a transmembrane lysosomal *N*-acetyltransferase, and thus enzyme replacement therapy approaches relying on cellular uptake of exogenous enzyme by mannose 6 phosphate receptors that are effective in other lysosomal diseases, cannot be used in this setting. Alternatives, including haematopoietic stem cell transplantation, or gene modification of these cells, also rely on cross-correction and therefore will also most likely prove ineffectual (Durand *et al.*, 2010). The majority of the clinical phenotype is neurological in MPSIIIC, with global neuropathology (Martins *et al.*, 2015), therefore direct transgene delivery to the brain using AAV ensuring distribution to the largest number of cells possible may prove beneficial. This approach has been used in both preclinical studies and clinical trials for the cross-correctable diseases MPSIIIA (Tardieu *et al.*, 2014; Winner *et al.*, 2016) and MPSIIIB (Ellinwood *et al.*, 2011; Tardieu *et al.*, 2017) caused by deficiencies of soluble secreted enzymes using serotypes rhesus 10 (rh10) and 5, respectively, but even in this case clinical efficacy has been limited. Improved vector distribution in the brain is paramount to overcome these issues, particularly in the case of non-secreted neurological proteins, such as the one deficient in MPSIIIC. Here we present data demonstrating that an alternative approach to capsid engineering, drawing on the natural evolution of the virus, yields a potent neurotropic vector that is more effectively distributed within the brain than the benchmark vectors AAV9 and AAVrh10, and displays an improved ability to correct the neurological phenotype in MPSIIIC mice. The utilization of AAV-TT paves the way for more effective clinical correction of neurological diseases such as MPSIIIC.

## Material and methods

### AAV-TT model generation

The AAV2-TT monomer model was generated with Swiss- model (https://swissmodel.expasy.org) (Biasini *et al.*, 2014) using the AAV2 crystal structure (RSCB PDB ID no. 1LP3) supplied as a template and the AAV-TT sequence. The AAV-TT VP3 60-mer capsid coordinates were generated by icosahedral matrix multiplication using the Oligomer Generator subroutine available on the VIPERdb online server (http://viperdb.scripps.edu) (Carrillo-Tripp *et al.*, 2009) and visualized by the program Pymol (The PyMOL Molecular Graphics System, Version 1.8 Schrödinger, LLC.).

### Animals

Outbred CD1 mice were time mated to produce neonatal animals. Female Sprague Dawley rats (225–250 g) were purchased from Charles River and were housed with free access to food and water under a 12-hour light/dark cycle in a temperature-controlled room. All experimental proced- ures were approved by the Ethical Committee for Use of Laboratory Animals in the Lund-Malmoü region.

Mice used for ocular injections were female C57Bl/6J mice and were housed at University College London facilities. All animal experiments were conducted according to the ARVO Statement for the Use of Animals for Vision and Ophthalmic Research.

The MPSIIIC mouse model with targeted disruption of the *Hgsnat* gene was generated previously (Martins *et al.*, 2015). MPSIIIC and wild-type mice were maintained at 21 ± 1˚C, with a constant humidity of 45–65%, on a 12 h light/dark cycle with ad libitum access to food and water. These studies were approved by the Ethics Committee of the University of Manchester. All studies performed on mice were approved by the UK Home Office for the conduct of regulated procedures under license according to the Animals (Scientific Procedures) Act 1986.

### Recombinant AAV vector production

The AAV-CAG coHGSNAT transgene plasmid was constructed by replacing the GFP coding sequence in the pTRUF-11 plasmid (ATCC, MBA-331) with a human codon-optimized HGSNAT cDNA (including a Kozak sequence) into the SbfI and SphI sites. Recombinant AAV was produced, purified and titred using standard procedures (Supplementary material). The vectors were titre-matched before injection.

**Intracranial injections**

Intracranial injections in neonatal mice were carried out as previously described (Kim *et al.*, 2013). Neonatal CD1 mice were prepared for injection by cryoanaesthesia at Day 1 post-gestation (P1) and 5 x 1010 vector genomes (vg) were injected via intracerebroventricular injection in a volume of 5 ml per brain using a 33-gauge needle (Hamilton). The experimental groups existed of equal mixes of male and female animals.

Adult female wild-type rats were injected in the substantia nigra or in the striatum at a dose of 3.5 x 109 vg per injection. Rats were anaesthetized with fentanyl-dormitor (Apoteksbolaget) and placed in the stereotactic frame with the tooth bar individually adjusted for flat skull (bregma-lambda; tooth bar: -3 to -4 mm). A hole was drilled through the skull and the viral vectors were infused unilaterally into the brain. Injections were performed using a pulled glass capillary (60–80 mm internal diameter and 120–160 mm outer diameter) attached to a 25 ml Hamilton syringe connected to an automated infusion pump system. Infusions into the striatum used 3 ml of viral vector preparations at the following coordinates relative to the bregma: antero-posterior (AP) = + 0.4; medio-lateral (ML) = -3.5; dorso-ventral (DV) = -5.0/-4.0, with an infusion rate of 0.4 ml/min. Infusion into the ventral midbrain used 3 ml of viral vector at AP = -5.3; ML = -1.7; DV = -7.2, with an infusion rate of 0.2 ml/min. The capillary was left in position for 2 min before retraction. Eight-week-old female MPSIIIC and wild-type mice were anaesthetized and placed in a stereotactic frame. The stereotactic coordinates used were: striatal, located 2 mm lateral and 3 mm deep to bregma. Using 26-gauge Hamilton syringe, 2.6 x 109 vg/hemisphere were delivered into each striatum at a rate of 0.5 ml/min (3 ml/hemisphere). Sham treated mice received either phosphate-buffered saline (PBS) or AAV-GFP (3 ml/hemisphere). The needle was left in place for 5 min after each infusion before retraction.

**Intraocular injections**

Intraocular injections were performed under general anaesthesia using an operating microscope (Supplementary material). Six-week-old female mice were injected with viral vectors at a dose of 2 x 109 vg per eye, in a volume of 2 ml per eye, and each mouse received an injection of AAV-TT in one eye and an injection of AAV2 in the contralateral eye.

**Tissue preparation**

Mice that received vector as neonates were sacrificed at 28 days post-injection by terminal isoflurane anaesthesia followed by exsanguination perfusion with PBS. The brains were removed and fixed for

48 h at 4˚C in 4% paraformaldehyde (PFA) and then transferred to 30% sucrose for cryoprotection. Brains were sectioned at -20˚C using a cryostat microtome to 40 mm thickness. Sections were stored in anti-freeze buffer (50 mM sodium azide, pH 7.4 containing 25% glycerol and 30% ethylene glycol) at 4oC until use.

Adult rats were sacrificed 28 days' post-injection by sodium pentobarbital overdose (Apoteksbolaget) and transcardially perfused with 150 ml PBS followed by 250 ml of ice-cold 4% PFA in 0.1 M phosphate buffer (pH 7.4). The brains were removed and post-fixed for 2 h in ice-cold PFA before storing in 25% buffered sucrose. Brains were cut into coronal sections to 35 mm thickness using a sliding microtome (HM 450, Thermo Scientific). Sections were stored in anti-freeze solution (0.5 M sodium phosphate buffer, 30% glycerol and 30% ethylene glycol) at -20˚C until use. Adult mice were sacrificed 6 weeks after intra-ocular injections. Tissues were fixed in 4% PFA for 1 h and then embedded in O.C.T. medium (R.A. Lamb) and frozen in pre-cooled isopentane. Specimens were stored at -20˚C and 18 mm thick sections were cut using a Bright cryostat. Slides were stored at -20˚C. Sections were air dried for 10 min before immunostaining.

MPSIIIC and wild-type adult mice were anaesthetized and transcardially perfused with 37oC PBS to remove blood from organs. Samples of liver, lung, kidneys and spleen tissue and one hemisphere of brain were frozen at -80˚C. The other brain hemisphere was fixed in 4% PFA for 24 h then treated with 30% sucrose 2 mmol/l MgCl2/PBS for 48 h before freezing at -80˚C. For HGSNAT assays, brain tissue was dissected into precise hemicoronal fifths (R1–R5). The injection site was in section R2 (rostral to caudal) close to the border of R2/R3. For HS quantification, vector copy number determination and thin-layer chromatography, a full hemisphere was used. For HGSNAT and HS assays, samples were homogenized and sonicated in homogenization buffer (0.5 mol/l NaCl, 0.02 mol/l Tris pH 7–7.5), then centrifuged at 2200g for 15 min at 4˚C, and the supernatant was collected. Protein concentration was determined using Pierce BCA assay kit (Fisher Scientific). All brain sections were cut from O.C.T. embedded tissues using a freezing microtome.

**Immunohistochemical staining**

Immunohistochemical staining of neonatal mouse brain sections to detect GFP was performed as previously described (Rahim *et al.*, 2012) using the following antibodies: anti-GFP (1:4000, ab290, Abcam), biotinylated secondary antibody (1:1000, BA-1000, Vector Laboratories) (Supplementary material). Representative images were captured using a live video camera (Nikon, DS-Fil) mounted

onto a Nikon Eclipse E600 microscope. For immunohistochemical analysis in adult rat brains, a standard free-floating protocol was used with an anti-GFP primary antibody (1:20 000, ab13970, Abcam). Biotinylated secondary antibody (1:250, BA-9010, Vector Laboratories) was used for DAB immunohistochemistry and amplified by Vector Labs ABC kit (Supplementary material). Images were captured using an Olympus BX53 microscope and analysed using cellSens Dimension v. 1.11 software. For Isolectin B4 (ILB4) staining in adult mouse brains, coronal sections (30 mm) were stained as previously described (Wilkinson *et al.*, 2012).

**Quantitative analysis of immunohistochemical staining**

Levels of GFP immunohistochemical staining were measured by quantitative thresholding image analysis as previously described (Rahim *et al.*, 2012). Data were separately plotted graphically as the mean percentage area of immunoreactivity per field [± standard error of the mean (SEM)].

**Immunofluorescence staining and confocal microscopy**

For immunofluorescence analysis of neonatal mouse brain sections, the following primary antibodies were used: anti-GFP (1:1000, ab13970, Abcam), anti-calbindin (1:20 000, CB38, Swant), anti-TH; (1:500; AB152, Millipore), anti-GFP (1:4000, ab290, Abcam), anti-ChAT (1:100, AB144P, Millipore), anti-S100b (1:500, ab52642, Abcam). For immunofluorescence, Alexa-conjugated secondary antibodies were used. After washing in TBS, sections were counter- stained with DAPI, mounted and coverslipped with Fluoromount G® (SouthernBiotech). Sections were visualized with a laser scanning confocal microscope (Nikon, Eclipse Ti-E Inverted, A1R-Si confocal) and images were processed using NIS Elements and Photoshop software.

Eye sections were counterstained with DAPI using a 5 mg/ml solution in Tris-buffered saline (TBS) for 15 min and coverslipped using Dako mounting medium. Microscopy of specimens was performed using an upright confocal laser scanning microscope (Leica TCS SPE DM5500 Q, Leica Microsystems) and the manufacturer's software (Leica LAS AF, Version 2.4.1). All images presented are confocal z-projections through 18 mm sections with DAPI in blue and eGFP in green. For immunofluorescence staining of 30 mm brain sections from adult wild-type and MPSIIIC mice, the following primary antibodies were used: anti-GFP (1:1000, ab13970, Abcam), anti-NeuN (1:500, ab177487, Abcam), anti- GFAP (1:1500, Z-0334, Dako), anti-LAMP2 (1:200, ab13524, Abcam). Alexa-conjugated secondary antibodies were used. Sections were mounted using ProLong® Gold Antifade medium with DAPI (Life Technologies). Images were acquired on a 3D-

Histech Pannoramic-250 micro- scope slide-scanner using a 20 x/0.30 Plan Achromat objective (Zeiss) and the DAPI, FITC and TRITC filter sets and processed using Case Viewer software (3D-Histech). GFP immunofluorescence was visualized at x 100 on a confocal laser scanning microscope (Leica TCS SP8). For analysis of $G_{M2}$ and $G_{M3}$ gangliosides, 40 mm sagittal brain sections were incubated with anti-$G_{M2}$ (KM966, 1:500) or anti-$G_{M3}$ (M2590, Cosmo Bio Co., Ltd., 1:100). Alexa-conjugated secondary antibodies and Draq5TM solution (ThermoFisher Scientific) were used. Sections were mounted using Vectashield® medium. The images were first analysed at low magnification using Zeiss Slide Scanner Axio Scan.Z1 (10x /0.45) for $G_{M2}$ staining and Nikon Eclipse E800 fluorescence microscope (5x) for $G_{M3}$ staining. For quantification of $G_{M2}$ ganglioside, images were acquired using a LSM510 Meta Laser inverted confocal microscope (Zeiss, 20 x/0.4) or a Leica TCS SPE confocal microscope (10 x/0.3). Quantification of immunofluorescence was assessed by ImageJ software (National Institutes of Health, Bethesda, MD, USA).

**Quantification of NeuN/GFP co-localization**

To demonstrate that GFP was primarily located within neurons, automated counting was performed using the analysed particles plugin in FIJI. NeuN/GFP double positive cells were counted using FIJI in a representative 40 x section for each brain area (n = 4 individual mice/group).

**HGSNAT enzyme assay**

HGSNAT enzyme activity was measured using 4-methylum-belliferyl-b-D-N-glucosaminide (MU-bGlcNH2, Moscerdam) as a substrate (Supplementary material).

**Open-field behaviour**

Open field behaviour was analysed as previously described (Langford-Smith *et al.*, 2011; Martins *et al.*, 2015). Outliers were removed using the Tukey outlier method of 1.5 x interquartile range (IQR).

**Spontaneous alternation**

Spontaneous alternation was assessed during one continuous 10-min session in a Y-maze consisting of three identical arms as previously described (O'Leary *et al.*, 2014). All animals fell within the minimal 33% alternation for outlier identification.

**Indirect enzyme-linked immunosorbent assay detection of anti-AAV IgG antibodies**

Total IgG antibody responses against AAV capsid proteins were measured with an enzyme-linked immunosorbent assay (ELISA) assay, using several brain homogenate dilutions, biotinylated goat anti-mouse IgG antibody (Vector) and the Vectastain ABC kit (Vector) (Supplementary material).

**Vector copy number determination**

Analysis of vector biodistribution was performed by quantitative PCR (qPCR) (Supplementary material).

**Analysis of brain gangliosides by thin-layer chromatography**

Briefly, frozen brain tissues were homogenized in water (10% v/w) using a FastPrep-24 MP homogenizer. Lipids were extracted by addition of two volumes of methanol and one volume of chloroform to one volume of the homogenate. After 10 min centrifugation at 1000g the organic phase was collected, and used to analyse gangliosides by phase separation as previously described (Seyrantepe *et al.*, 2008).

**Glycosaminoglycan analysis**

Glycosaminoglycan chains were purified, 2-aminoacridone (AMAC)-labelled and analysed by reversed-phase high-performance liquid chromatography (RP-HPLC) as previously described (Holley, 2018).

**Statistical analysis**

Statistical analysis was performed using Graphpad Prism software. All data were analysed by either Student's t-tests or ANOVA and Tukey and Sidak's post hoc test for analysis. Where standard deviations (SDs) were unequal, data were log transformed to achieve normal distributions. Significance was determined as $p < 0.05$. All the test results are given as exact values, with confidence intervals in the main text.

**Experimental design**

The MPSIIIC mice treated showed no phenotype at treatment age. The treatment groups were randomly assigned at weaning. MPSIIIC n-numbers were based on previous power calculations for biochemical and histological changes as seen in the MPSIIIA mouse model (Sergijenko *et al.*, 2013) and behavioural changes in the MPSIIIB mouse model (Langford-Smith *et al.*, 2011). It was

impossible to blind treatment groups because of the nature of the treatments and the size of the experiment, with treatments staggered over several months. Analysis was carried out in a blinded fashion for biochemical, histological and behavioural analyses. The nature of the analyses was such that unconscious bias is difficult to introduce in any case, as automated quantification methods were used for the most part. Data exclusion: outliers were removed from open field behaviour using the Tukey outlier method of 1.5 x IQR. No other mice were removed from any analysis.

## Results

### Engineering of a novel AAV2 capsid

We substituted 14 amino acids in the AAV2 capsid gene to create a novel vector, designated AAV-TT, based on the conserved amino acid changes present in natural AAV2 isolates sampled from human paediatric tissues (Chen *et al.*, 2005). These were one amino acid change in the VP1 unique region (VP1u), two in the VP1/VP2 common region, and 11 in VP3 (Fig. 1A). Most notably, arginine (R) at positions 585 and 588 was substituted to serine (S) and threonine (T), respectively (Fig. 1A and B). These changes have been previously shown to abolish heparan sulphate proteoglycan (HSPG) binding (Grifman *et al.*, 2001; Kern *et al.*, 2003; Opie *et al.*, 2003). The majority of substitutions in VP3 are located on the AAV2 capsid surface and cluster around the icosahedral 3-fold axis (Fig. 1C and D). Ribbon diagrams show that most of the substituted amino acids within the structurally ordered VP3 region localize to variable regions IV–VIII (Fig. 1C and E–G), which are involved in receptor binding and determine the antigenic properties of AAV capsids (Gurda et al., 2013; Tseng *et al.*, 2015). To characterize the physical properties of the AAV-TT capsid, its stability was determined by differential scanning fluorimetry (DSF). The melting temperature of AAV-TT is 7oC greater than AAV2 (Supplementary Fig. 1A and B); the melting temperature of AAV2 is consistent with previous reports (Rayaprolu *et al.*, 2013). A recent publication reported that AAV capsid stability has no correlation to AAV1, AAV2, or AAV5 transduction in HEK293 cells and that the stability of the virus is determined by its pI (Bennett *et al.*, 2017). This implies that the increased melting temperature of AAV-TT compared to AAV2 is

based on the difference in the number of charged residues between the two viruses. AAVs have been shown to use different proteoglycans as their primary receptors. AAV-TT exhibits a high sequence homology to AAV2 and AAV3, serotypes that are both dependent on HSPG binding for viral uptake in vitro (Summerford and Samulski, 1998). Recombinant AAV-TT and AAV2 were assessed for their ability to transduce various cell lines in vitro. Not surprisingly, AAV-TT displayed a lower transduction efficiency than AAV2 and the efficiency of transduction of AAV-TT varied significantly depending on the cell type transduced [effect of treatment, F(7,13) = 15.82, P 5 0.0001] (Supplementary Fig. 2A). The independence of HSPG binding of AAV-TT was further confirmed in a cell-based heparin competition assay showing that AAV-TT transduction efficiency in vitro is not affected by the presence of heparin [effect of treatment x vector type, F(5,24) = 4.047, P 5 0.01] (Supplementary Fig. 2B); this was further substantiated by a heparin column-binding assay. Virus-like particles were assembled from AAV5, AAV2 or AAV-TT capsid proteins and were loaded in excess on a heparin column (Supplementary Fig. 2C). AAV2 virus-like particles bind the heparin column and elute with increasing NaCl concentrations, AAV5 virus-like particles flow through the column without binding to heparin and none were further eluted when high concentrations of NaCl were applied. AAV-TT virus-like particles showed a similar profile to AAV5 and were only detected in the flow-through and the wash fractions. These data confirm that AAV-TT capsids do not interact with heparin.

**AAV-TT enables widespread transduction in neonatal and adult rodent brains**

Prompted by previous reports that high levels of HSPG expression in the brain parenchyma limit vector spread (Nguyen *et al.*, 2001; Mastakov *et al.*, 2002; Kanaan *et al.*, 2017), we assessed AAV-TT's potential for an increased ability to spread in the brain. GFP reporter viruses were delivered via unilateral intracerebroventricular administration [5 x 1010 vector genomes (vg) total] in neonatal mice and biodistribution was assessed using GFP immunohistochemistry. Figure 2A–C shows that increased transduction levels were observed with AAV-TT as com- pared to AAV2 in the majority of brain sections analysed; quantification of GFP expression in the striatum highlights the strongly enhanced transduction capacity of AAV-TT (two-tailed Student's t-test; t = 13.88 df = 4, P 5 0.001). Further analysis of the tissues by immunofluorescence mi- croscopy demonstrates that both glial and neuronal cells are targeted by AAV-TT (Fig. 2D and E). The improved in vivo transduction

profile was further confirmed in adult rats where intrastriatal (Fig. 3A and B) as well as nigral injections of 3.5 x 109 vg (Supplementary Fig. 3A and B) of AAV-TT result in markedly enhanced transduction throughout the hemisphere, whereas the delivery of AAV2 leads to transduction of a small area of cells situated along the needle track. Delivery of AAV-TT into the striatum appears to mediate transduction across the corpus callosum into the cortex, into the intralaminar nuclei of the thalamus, and into the substantia nigra pars compacta (Fig. 3A). All these regions have afferents to the striatum (Fig. 3B), suggesting that retrograde transport may be occurring (Salegio *et al.*, 2013).

**AAV-TT efficiently transduces photoreceptors**

Given the ability of AAV-TT to target various neuronal cell types, we investigated if this new capsid would show improved transduction of photoreceptors. AAV2 has been used to treat a number of hereditary diseases of the eye that cause blindness, with clinical trials showing improved visual acuity for severalyears posttreatment (Ripamonti *et al.*, 2015; Russell *et al.*, 2017). However, this serotype has now been eclipsed by a number of other serotypes that have shown improved photoreceptor tropism in preclinical animal studies (Vandenberghe and Auricchio, 2012; Georgiadis *et al.*, 2016). Sub-retinal injections in mice of AAV-TT (2 x 109 vg) and AAV2 (2 x 109 vg, contralateral eye) allowed for side-to-side comparison of both capsid variants; confocal microscopy of transverse sections of the eye showed that AAV-TT has a strongly improved ability to transduce photoreceptors as compared to AAV2. AAV-TT transduced retinal pigment epithelium at least as well as AAV2 (Fig. 4A). Conversely, AAV-TT vectors administered via intravitreal injection showed decreased transduction abilities (Fig. 4B), in line with previous observations that HSPG binding is required for transduction of the retina via this injection route (Boye *et al.*, 2016; Woodard *et al.*, 2016).

In summary, our data show that the introduction of a select number of specific mutations in the AAV2 capsid results in a potent neurotropic vector that could be used to treat diseases of the eye as well as therapeutically more challenging neurological diseases, such as MPSIII, which would benefit by provision of more effective CNS transduction.

**AAV-TT exceeds the transduction abilities of AAV9 and AAVrh10 in adult mouse brains**

Many AAV serotypes have previously been assessed for their CNS transduction properties in rodents and have shown different expression patterns in the brain (Burger *et al.*, 2004; Cearley and Wolfe, 2006; Klein *et al.*, 2006, 2008; Foust *et al.*, 2009). In preparation for preclinical studies, intracerebral injection of GFP reporter virus of AAV-TT was assessed against AAV serotypes AAV9 and AAVrh10, which had shown particularly good transduction capabilities within the CNS in these studies. For each serotype, relatively low but equivalent viral titres were injected bilaterally into the caudate putamen of adult mouse brains ($2.6 \times 10^9$ vg/hemisphere) and GFP expression assessed after 3 weeks (Fig. 5A–C). AAV-TT resulted in greater global transduction of cells throughout the brain compared to either AAV9 or AAVrh10; in which spread of vector was limited to areas within the caudate putamen and thalamus (Fig. 5D). AAV9 gave intense staining in the areas close to the injection site, especially around the needle track (Fig. 5A and D) with limited distribution in other areas. In contrast, GFP expression of AAV-TT was less intense than AAV9 and AAVrh10 but more widely distributed in the brain resulting in a greater number of areas transduced; including the cingulate cortex, thalamus, amygdala, hippocampus, somatosensory cortex and the external capsule, respectively (Fig. 5B and D). GFP expression was exclusively seen in neurons with expression in both the soma and processes (Fig. 5E). We could not detect GFP in GFAP + astrocytes or Iba1+ microglia/macrophages (Supplementary Fig. 4A and B). The percentages of GFP/ NeuN double positive cells were similar for AAV-TT and AAV9 serotypes in the thalamus, an area close to the injection site (Fig. 5F). However, in areas further away from the injection site such as the amygdala and somatosensory cortex, the percentage of GFP/NeuN double positive cells was markedly higher in AAV-TT-treated mice compared to AAV9-treated mice (Fig. 5G and H). We subsequently compared the therapeutic efficacy of AAV vectors expressing the codon optimized human HGSNAT (coHGSNAT) trans- gene using the two best performing serotypes; AAV9 and AAV-TT.

Relative HGSNAT activity measured in transiently transfected HEK293T cells with a plasmid containing coHGSNAT confirmed that increased HGSNAT enzyme activity was detected intracellularly but not in the supernatant, thereby confirming that the enzyme cannot be secreted [effect of treatment, $F(5,15) = 66.75$, $P < 0.0001$] (Supplementary Fig. 5B).

**AAV-TT, but not AAV9 corrects pathological behaviour in MPSIIIC mice**

Four months after bilateral intracranial injections (2.6 x 109 vg/hemisphere) of coHGSNAT expressing AAV9 and AAV-TT vectors into MPSIIIC mice, we measured behavioural outcomes; biochemical and histological outcomes were measured 6 months posttreatment (Fig. 6A–C). MPSIIIC mice have a hyperactive phenotype in the 1 h open field test (Martins *et al.*, 2015) (Fig. 6D). The hyperactive phenotype, assessed by total distance moved was corrected in AAV-TT treated MPSIIIC mice at 4 months posttreatment, but not in AAV9-treated mice [effect of treatment, $F(3,30) = 7.68$, $P < 0.001$] (Fig. 6D). Impaired cognitive abilities in MPSIIIC mice can be evaluated by assessing working memory as determined by the number of correct entries into the different arms of a Y-maze (Hughes, 2004) (Fig. 6E). This spontaneous alternation task takes advantage of the natural tendency for the mouse to explore novel environments; measurement of working memory in this task consists of an increase in exploration of a novel arm compared to a recently explored arm of the maze (Deacon *et al.*, 2002). Consistent with correction of hyperactivity, AAV-TT treated mice showed significant improvements in immediate spatial working memory and correction to wild-type levels in the Y-maze [effect of treatment, $F(3,35) = 3.806$, $P < 0.05$] (Fig. 6F). AAV9 had a more variable effect that was not significantly improved over MPSIIIC sham. No statistically significant differences in vector copy numbers in the brain were found among the groups with average numbers of 39.15 ± 16.91 and 45.09 ± 16.29 for AAV9 and AAV-TT, respectively (Fig. 6G). Little to no off-target transduction of AAV9 and AAV-TT to peripheral organs was observed in treated mice with vg/cell values generally under 0.5 vg/cell (Supplementary Fig. 6A, C, E and G). Consistent with vector genome results, no HGSNAT enzyme was detected in spleen, lung and kidney, in all treated animals (Supplementary Fig. 6B, D, F and H).

**AAV-TT further improves brain-specific HGSNAT activity at 6 months in MPSIIIC mice**

At 6 months post-treatment, AAV-TT and AAV9 vectors expressing coHGSNAT increased overall brain enzyme activity levels to above wild-type levels [effect of treatment, $F(3,97) = 14.19$, $P$ 5 0.0001]; but higher levels were obtained in AAV-TT (266.5%) treated mice compared to AAV9-treated mice (185.2%) (Fig. 6H). The brain was divided into hemicoronal fifths (anterior to posterior R1–R5; Fig. 6B), with enzyme activity detected throughout the brain but highest around the injection site in R2 [effect of treatment x brain region, $F(12,97) = 4.91$, $P < 0.0001$] (Fig. 6I). In

contrast to earlier observations at 1 week and 3 weeks post-treatment (Supplementary Fig. 5C and D), enzyme levels mediated by AAV-TT at 6 months post-treatment were significantly greater than AAV9 ($P < 0.001$) in R2 at 767.78% and 453.03%, respectively (Fig. 6I). Despite supra-physiological enzyme levels in treated brains, both AAV9 (Fig. 6J) and AAV-TT (Fig. 6K) capsids produced no detectable levels of anti-AAV IgG anti- bodies in the brains of all treated mice, in contrast to positive control mice that received a mixture of adjuvant and either AAV9 or AAV-TT to stimulate significant IgG responses.

**AAV-TT and AAV9 reduce primary storage of heparan sulphate, while AAV-TT improves heparan sulphate patterning in vivo**

MPSIIIC mice display a 13.4-fold increase in primary storage of HS in the brain compared to wild-type (Fig. 7A). Overall, AAV9 and AAV-TT both reduced total HS levels by ""46% [effect of treatment, $F(3,20) = 10.03$, $P < 0.001$]. Abnormal highly sulphated UA(2S)-GlcNS(6S) ($P < 0.0001$) and UA(2S)-GlcNS ($P < 0.0001$) HS species were seen in the brains of MPSIIIC mice; with a reduction in the unsulphated UA-N-acetyl-glucosamine (GlcNAc) ($P < 0.0001$) groups. AAV-TT reduced UA(2S)-GlcNS(6S) residues compared to MPSIIIC ($P < 0.01$), whereas levels in AAV9 treated mice remained unchanged. AAV-TT was significantly better at correcting abnormal UA(2S)-GlcNS ($P < 0.01$) and UA-GlcNAc ($P < 0.0001$) disaccharide composition than AAV9 (Fig. 7B).

**AAV-TT and AAV9 reduce secondary storage of GM2 and GM3 gangliosides in the brain of MPSIIIC mice**

It has been previously reported that both GM3 and GM2 gangliosides are significantly increased in the brains of MPSIIIC mice (Martins *et al.*, 2015). GM3 storage is observed (in the order of storage level) in the hypothalamus, amygdala, midbrain, medial entorhinal cortex (MEnt), secondary motor cortex (M2), secondary visual cortex mediolateral, and hippocampus including the molecular layer of the dentate gyrus. AAV treatment with both serotypes significantly reduced overall levels of GM3 gangliosides in the brains of MPSIIIC mice at 6 months' post-injection ($P < 0.01$) (Fig. 7C) including the secondary motor cortex (M2) (Fig. 7E and F) and the medial entorhinal cortex (Supplementary Fig. 7B). GM2 ganglioside levels are abnormally elevated throughout the MPSIIIC

brain but particularly (in the order of storage level) in the amygdala, pons, medulla, midbrain, hypothalamus, reticular nucleus of the thalamus, medial entorhinal cortex, cortex, hippocampus and cerebellum. These were reduced in the hippocampus in both groups of treated mice compared to untreated mice (Fig. 7D) and appear reduced in other brain areas (Supplementary Fig. 7C).

**AAV-TT and AAV9 reduce astrocytosis and lysosomal burden in the brain of MPSIIIC mice**

Astrocytosis was observed in the thalamus of MPSIIIC mice with non-significant reductions of GFAP (Fig. 7G and H) in both AAV9 and AAV-TT treated groups; no differences were observed in GFAP-positive astrocytes between MPSIIIC and both treated groups in the external capsule (Supplementary Fig. 8A), caudate putamen (Supplementary Fig. 8B), amygdala (Supplementary Fig. 8C) and the cortex (Supplementary Fig. 8D). Levels of LAMP2 lysosomal storage were significantly decreased by both vectors ($P < 0.01$) in the caudate putamen, an area close to the injection site [effect of treatment, $F(3,11) = 16.52$, $P < 0.001$] (Fig. 7I and J). A similar trend was observed in areas distant from the injection site including the external capsule (Supplementary Fig. 9A) and cortex (Supplementary Fig. 9D) and less so in the thalamus (Supplementary Fig. 9B) and amygdala (Supplementary Fig. 9C).

**AAV-TT corrects neuroinflammation over AAV9 in the caudate putamen and amygdala of MPSIIIC mice**

Immunohistochemical analysis of the brain showed a better correction of inflammation in terms of the number of isolectin B4-positive microglial cells in AAV-TT than AAV9 treated ($P < 0.05$) mice in the caudate putamen [effect of treatment, $F(3,12) = 88.27$, $P < 0.0001$] (Fig. 7K and L) and in the amygdala [effect of treatment, $F(3,12) = 264$, $P < 0.0001$] (Supplementary Fig. 10C). AAV-TT reduced inflammation ($P < 0.001$) similarly to AAV9 (P 5 0.05) in the cortex [effect of treatment, $F(3,12) = 92.8$, $P < 0.0001$] (Supplementary Fig. 10D); with no improvements in the hippocampus (Supplementary Fig. 10A), thalamus (Supplementary Fig. 10B) and amygdala (Supplementary Fig. 10C).

## Discussion

We used an alternative capsid design approach to generate a variant of AAV2, which is closely related to natural variants that presumably have evolved to efficiently infect human tissues. Intriguingly, when injected in rodents, vectors based on this new capsid show strong tropism for the CNS, including photoreceptors in the eye, rather than for peripheral organ systems, which may be due to changes in the receptor footprint (Asokan *et al.*, 2010; Drouin and Agbandje-McKenna, 2013). One of the most notable changes is the abolished HSPG binding site (Wu *et al.*, 2000; Grifman *et al.*, 2001; Kern *et al.*, 2003; Opie *et al.*, 2003), which steers the AAV-TT capsid away from its tissue culture adapted tropism features and contributes to an increased spread in the CNS in vivo. In general, it is thought that high expression levels of HSPG on cell surfaces and extracellular matrix leads to reduced spread and sequestration of AAV2 in 'off target' tissues (Perabo *et al.*, 2006). In the CNS particularly, it has been shown that high affinity for HSPG is detrimental for the spread of transduction by AAV2 (Mastakov *et al.*, 2002; Kanaan *et al.*, 2017). However, preliminary experiments indicate that mutation of the HSPG binding site in AAV2 (R585S and R588S) increases transduction spread and efficiency compared to wild-type AAV2 but to a lower extent than observed for AAV-TT, arguing that additional amino acid changes con- tribute to the observed phenotype (data not shown). The combined effect of all amino acid replacements is likely to contribute to the increased thermal stability observed for AAV-TT as the difference in stability between AAV-TT and AAV2 is larger than the previously described increase in an AAV2-HSPG null variant, which harbours mutations at positions 585 and 588 (Pacouret *et al.*, 2017). However, the mechanistic link between enhanced capsid stability and increased transduction ability is not entirely understood; primary differences between the capsid variants in various aspects of vector biology, ranging from uptake to genome release in the nucleus, could potentially contribute to the observed differences in transduction efficacy.

Given the encouraging results achieved in AAV2/AAV-TT comparative biodistribution studies, we assessed the efficacy of AAV-TT in correcting neurological deficits in the mouse model of MPSIIIC by comparing it to preferred neurological serotypes. Preparatory GFP distribution studies suggested that at the indicated dose, AAV9 yields very high transduction of cells in localized areas and is not well distributed. In contrast, AAV-TT has less intense levels of staining with a larger proportion of neurons throughout the brain transduced. In adult rodents, neurons are the major cell type

transduced with all vectors within both the white and grey matter (Herculano-Houzel, 2014), in keeping with data from AAV9 and AAVrh10 (Cearley and Wolfe, 2006).

It should be noted that AAV-TT and AAVrh10 were affinity-purified and therefore contained a higher number of empty capsids compared to AAV9, which was purified using density gradient centrifugation. The previously described role for empty capsids as decoy for AAV-specific antibodies is unlikely to play a role in the brain given the fact that we could not even detect AAV-specific antibodies after treatment (Mingozzi *et al.*, 2013). However, empty capsids could potentially compete for receptor binding and uptake thereby putting AAV-TT and AAVrh10 at a disadvantage compared to AAV9. Nevertheless, our results show that AAV-TT performed better than AAV9 in the biodistribution studies and was more efficient in correcting the disease in MPSIIIC mice.

Both short-term and long-term data from MPSIIIC mice showed supra-physiological enzyme levels in areas close to the injection site, a distribution pattern seen in other preclinical studies using AAV vectors to treat MPSIIIA (Winner *et al.*, 2016) or MPSIIIB (Fu *et al.*, 2002). Importantly, the treatment did not elicit an antibody response in the brains of MPSIIIC mice.

Although the neuropathology of the brain was corrected in only some regions, we were able to achieve correction of hyperactive behaviour and working memory in AAV-TT treated mice over AAV9 treated mice. It is unclear which brain area is responsible for hyperactivity in MPS, however, the frontostriatal pathway has been implicated in ADHD (Cubillo *et al.*, 2012), as it is involved in control of impulsivity, locomotion, affect, attention and emotion (Takamatsu *et al.*, 2015). This pathway connects the cortex, striatum and thalamus (Morris *et al.*, 2016), areas in which we have observed improvement in LAMP2, GFAP and ILB4 levels with AAV-TT treatment. Hyperactivity could also be a circadian effect controlled from the nucleus as we have hypothesized earlier (Canal *et al.*, 2010), or from areas projecting from the suprachiasmiatic nucleus such as the thalamus (Schwartz *et al.*, 2011). The Y-maze is a widely used test measuring working memory and has been used to study hippocampal function as performance of rodents in this test is disrupted by hippocampal lesions (Rawlins and Olton, 1982; Hock and Bunsey, 1998). The results obtained from the Y-maze test correlate with GFP expression data showing hippocampal vector expression and suggest that effectively transducing these areas can restore hippocampal based learning.

HS has been implicated for its role in neuroinflammation (Zhang *et al.*, 2014), interestingly, AAV-TT treatment improved both HS sulphation patterning and neuroinflammation over AAV9 in several areas. We hypothesize that the sulphation patterning of HS may contribute to neuroin- flammation in MPSIIIC potentially resulting in subsequent behavioural abnormalities. These data are consistent with previous findings that suggest that restoring sulphation patterning of HS and reducing inflammation may be key in improving behavioural outcomes in MPSIII (Sergijenko *et al.*, 2013).

$G_{M2}$ and $G_{M3}$ gangliosides have a still undefined role in MPSIIIC neuropathology, and respond differentially to AAV treatment. It has been previously reported that $G_{M2}$ and $G_{M3}$ gangliosides showed only modest levels of co-localization by both region and subcellular compartment in the brains of MPSIII mice (McGlynn et al., 2004; Martins *et al.*, 2015) with storage also observed in the medial entorhinal cortex in MPSIIIB mice (Ryazantsev *et al.,* 2007; Ohmi *et al.*, 2011). This suggests that different pathological mechanisms underlie storage of $G_{M2}$ and $G_{M3}$ gangliosides in MPSIIIC potentially explaining why they respond differently to restoration of the primary HGSNAT deficiency by AAV-mediated gene correction.

In a disease with global pathology such as MPSIIIC where the enzyme is not secreted and thus cannot cross- correct other cells, maximum cell transduction is required. A similar AAV-based approach has been developed in the non-cross correctable neurological disease CLN3, resulting in some disease correction, although neonatal delivery of AAV is often much more effective than delivery to adult mice (Sondhi *et al.*, 2014). Notably an intravenous AAV9 approach in CLN3 was only partly effective, underlining the difficulty of treating non-cross correctable neurological diseases (Bosch *et al.*, 2016).

Our data for the first time show that the neurological non cross-correctable lysosomal disease MPSIIIC can be treated via AAV-mediated gene therapy suggesting that this may be a therapeutic option for patients.

**Acknowledgements**

A baculovirus expressing AAV2 virus-like particles was generously donated by Sergei Zolotukhin (Department of Pediatrics, University of Florida). We also thank Dr. Nobuo Hanai, Dr. Akiko Furuya and Kyowa Hakko Kirin Co., Ltd. for a generous gift of monoclonal antibodies against $G_{M2}$ ganglioside.

**Funding**

R.R.A. received funding from European Union Horizon 2020 (grant No. 66691), RP Fighting Blindness, UK (GR576). R.R.A. is partially supported by the NIHR Biomedical Research Centre at Moorfields Eye Hospital. A.A.R. is funded by the UK Medical Research Council (MR/N026101/1), EU Horizon2020; BATCure 666918 and Action Medical Research (GN2485). S.N.W. received funding from MRC grants MR/P026494/1 and MR/N026101/1. T.B. received funding from a Swedish Research Council (ÄR-MH-2016-01997) Starting grant. M.A.-M. and M.L. were supported by a joined MRC grant to King's College London (MC_PC_13065 'A novel platform for adeno-associated virus vectors for gene therapy'). B.W.B. received funding from Jonah's Just Begun and Vaincre les Maladies Lysosomales. E.H. received funding from King's Commercialisation Institute, the Pfizer Rare Disease Consortium and UK Medical Research Council (MR/N022890/1).

**Conflict of interest**

E.H. is funded by a Rare Disease Consortium Award from Pfizer Inc. to further develop AAV-TT vector technology. A patent #WO2015121501 on 'Adeno-associated virus vector' has been deposited by M.L., E.H. and J.T. M.L. is a consultant to various gene therapy companies. M.L. is an SAB member of Spark Therapeutics. M.A.-M. is an SAB member for AGTC, StrideBio, Inc., and Voyager Therapeutics, Inc., is a consultant for Intima Biosciences, and has a sponsored research agreement with AGTC and Voyager Therapeutics, Inc. These companies have interest in the development of AAV for gene delivery applications. M.A.-M. is an inventor of AAV patents licensed to various biopharmaceutical companies. M.A.-M. is a co-founder of StrideBio, Inc. This is a biopharmaceutical company with interest in developing AAV vectors for gene delivery application. The MPSIIIC work in this paper has been patented and licenced to Phoenix Nest Inc, in which B.W.B. is a shareholder.

**Supplementary material**

Supplementary material is available at Brain online.

## References


Adachi K, Enoki T, Kawano Y, Veraz M, Nakai H. Drawing a high-resolution functional map of adeno-associated virus capsid by massively parallel sequencing. Nat Commun 2014; 5: 3075.

Archer LD, Langford-Smith KJ, Bigger BW, Fildes JE. Mucopolysaccharide diseases: a complex interplay between neuroinflammation, microglial activation and adaptive immunity. J Inherit Metab Dis 2014; 37: 1–12.

Asokan A, Conway JC, Phillips JL, Li C, Hegge J, Sinnott R, *et al.* Reengineering a receptor footprint of adeno-associated virus enables selective and systemic gene transfer to muscle. Nat Biotech 2010; 28: 79–82.

Bainbridge JWB, Mehat MS, Sundaram V, Robbie SJ, Barker SE, Ripamonti C, *et al.* Long-term effect of gene therapy on Leber's congenital amaurosis. N Engl J Med 2015; 372: 1887–97.

Bennett A, Patel S, Mietzsch M, Jose A, Lins-Austin B, Yu JC, *et al.* Thermal stability as a determinant of AAV serotype identity. Mol Ther Methods Clin Dev 2017; 6: 171–82.

Bevan AK, Duque S, Foust KD, Morales PR, Braun L, Schmelzer L, *et al.* Systemic gene delivery in large species for targeting spinal cord, brain, and peripheral tissues for pediatric disorders. Mol Ther 2011; 19: 1971–80.

Biasini M, Bienert S, Waterhouse A, Arnold K, Studer G, Schmidt T, *et al.* SWISS-MODEL: modelling protein tertiary and quaternary structure using evolutionary information. Nucleic Acids Res 2014; 42: W252–8.

Bosch ME, Aldrich A, Fallet R, Odvody J, Burkovetskaya M, Schuberth K, *et al.* Self-complementary AAV9 gene delivery partially corrects pathology associated with juvenile neuronal ceroid lipofuscinosis (CLN3). J Neurosci 2016; 36: 9669–82.

Boye SL, Bennett A, Scalabrino ML, McCullough KT, Van Vliet K, Choudhury S, *et al.* Impact of heparan sulfate binding on transduction of retina by recombinant adeno-associated virus vectors. J Virol 2016; 90: 4215–31.

Burger C, Gorbatyuk OS, Velardo MJ, Peden CS, Williams P, Zolotukhin S, *et al.* Recombinant AAV viral vectors pseudotyped with viral capsids from serotypes 1, 2, and 5 display differential efficiency and cell tropism after delivery to different regions of the central nervous system. Mol Ther 2004; 10: 302–17.

Canal MM, Wilkinson FL, Cooper JD, Wraith JE, Wynn R, Bigger BW. Circadian rhythm and suprachiasmatic nucleus alterations in the mouse model of mucopolysaccharidosis IIIB. Behav Brain Res 2010; 209: 212–20.

Carrillo-Tripp M, Shepherd CM, Borelli IA, Venkataraman S, Lander G, Natarajan P, *et al.* VIPERdb2: an enhanced and web API enabled relational database for structural virology. Nucleic Acids Res 2009; 37: D436–42.

Cearley CN, Wolfe JH. Transduction characteristics of adeno-associated virus vectors expressing cap serotypes 7, 8, 9, and Rh10 in the mouse brain. Mol Ther 2006; 13: 528–37.

Chen C-L, Jensen RL, Schnepp BC, Connell MJ, Shell R, Sferra TJ, *et al.* Molecular characterization of adeno-associated viruses infecting children. J Virol 2005; 79: 14781–92.

Chen YH, Chang M, Davidson BL. Molecular signatures of disease brain endothelia provide new sites for CNS-directed enzyme therapy. Nat Med 2009; 15: 1215–18.

Cubillo A, Halari R, Smith A, Taylor E, Rubia K. A review of fronto- striatal and fronto-cortical brain abnormalities in children and adults with Attention Deficit Hyperactivity Disorder (ADHD) and new evidence for dysfunction in adults with ADHD during motivation and attention. Cortex 2012; 48: 194–215.

Deacon RMJ, Bannerman DM, Kirby BP, Croucher A, Rawlins JNP. Effects of cytotoxic hippocampal lesions in mice on a cognitive test battery. Behav Brain Res 2002; 133: 57–68.

Drouin LM, Agbandje-McKenna M. Adeno-associated virus structural biology as a tool in vector development. Future Virol 2013; 8: 1183–99.

Durand S, Feldhammer M, Bonneil E, Thibault P, Pshezhetsky AV. Analysis of the biogenesis of heparan sulfate acetyl-coA:α-glucosaminide N-acetyltransferase provides insights into the mechanism underlying its complete deficiency in mucopolysaccharidosis IIIC. J Biol Chem 2010; 285: 31233-42.

Ellinwood NM, Ausseil J, Desmaris N, Bigou S, Liu S, Jens JK, *et al.* Safe, efficient, and reproducible gene therapy of the brain in the dog models of Sanfilippo and Hurler syndromes. Mol Ther 2011; 19: 251–59.

Foust KD, Nurre E, Montgomery CL, Hernandez A, Chan CM, Kaspar BK. Intravascular AAV9 preferentially targets neonatal neurons and adult astrocytes. Nat Biotech 2009; 27: 59.

Fu H, Samulski RJ, McCown TJ, Picornell YJ, Fletcher D, Muenzer J. Neurological correction of lysosomal storage in a mucopolysaccharidosis IIIB mouse model by adeno-associated virus-mediated gene delivery. Mol Ther 2002; 5: 42–9.

Gao G-P, Alvira MR, Wang L, Calcedo R, Johnston J, Wilson JM. Novel adeno-associated viruses from rhesus monkeys as vectors for human gene therapy. Proc Natl Acad Sci USA 2002; 99: 11854–59. Gao G, Vandenberghe LH, Alvira MR, Lu Y, Calcedo R, Zhou X, *et al.* Clades of adeno-associated viruses are widely disseminated in human tissues. J Virol 2004; 78: 6381–88.

Georgiadis A, Duran Y, Ribeiro J, Abelleira-Hervas L, Robbie SJ, Sunkel-Laing B, *et al.* Development of an optimized AAV2/5 gene therapy vector for Leber congenital amaurosis owing to defects in RPE65. Gene Ther 2016; 23: 857–62.

Grifman M, Trepel M, Speece P, Gilbert LB, Arap W, Pasqualini R, *et al.* Incorporation of tumor-targeting peptides into recombinant adeno-associated virus capsids. Mol Ther 2001; 3: 964–75.

Gurda BL, DiMattia MA, Miller EB, Bennett A, McKenna R, Weichert WS, *et al.* Capsid antibodies to different adeno-associated virus serotypes bind common regions. J Virol 2013; 87: 9111–24.

Herculano-Houzel S. The glia/neuron ratio: how it varies uniformly across brain structures and species and what that means for brain physiology and evolution. Glia 2014; 62: 1377–91.

Hock BJJ, Bunsey MD. Differential effects of dorsal and ventral hippocampal lesions. J Neurosci 1998; 18: 7027–32.

Holley RJ, Ellison SM, Fil D, O'Leary C, McDermott J, Senthivel N, *et al.* Macrophage enzyme and reduced inflammation drive brain correction of mucopolysaccharidosis IIIB by stem cell gene therapy. Brain 2018; 141: 99–116.

Hughes RN. The value of spontaneous alternation behavior (SAB) as a test of retention in pharmacological investigations of memory. Neurosci Biobehav Rev 2004; 28: 497–505.

Kanaan NM, Sellnow RC, Boye SL, Coberly B, Bennett A, Agbandje McKenna M, *et al.* Rationally engineered AAV capsids improve transduction and volumetric spread in the CNS. Mol Ther Nucleic Acids 2017; 8: 184–97.

Kern A, Schmidt K, Leder C, Müller OJ, Wobus CE, Bettinger K, *et al.* Identification of a heparin-binding motif on adeno-associated virus type 2 capsids. J Virol 2003; 77: 11072–81.

Kim J-Y, Ash RT, Ceballos-Diaz C, Levites Y, Golde TE, Smirnakis SM, *et al.* Viral transduction of the neonatal brain delivers controllable genetic mosaicism for visualizing and manipulating neuronal circuits in vivo. Eur J Neurosci 2013; 37: 1203–20.

Klein RL, Dayton RD, Tatom JB, Henderson KM, Henning PP. AAV8, 9, Rh10, Rh43 vector gene transfer in the rat brain: effects of serotype, promoter and purification method. Mol Ther 2008; 16: 89–96.

Klein RL, Dayton RD, Leidenheimer NJ, Jansen K, Golde TE, Zweig RM. Efficient neuronal gene transfer with AAV8 leads to neurotoxic levels of tau or green fluorescent proteins. Mol Ther 2006; 13: 517-27.

Kotterman MA, Schaffer DV. Engineering adeno-associated viruses for clinical gene therapy. Nature Rev Genet 2014; 15: 445–51.

Langford-Smith A, Langford-Smith KJ, Jones SA, Wynn RF, Wraith JE, Wilkinson FL, *et al.* Female mucopolysaccharidosis IIIA mice exhibit hyperactivity and a reduced sense of danger in the open field test. PLoS One 2011; 6: e25717.

Lisowski L, Dane AP, Chu K, Zhang Y, Cunningham SC, Wilson EM, *et al.* Selection and evaluation of clinically relevant AAV variants in a xenograft liver model. Nature 2014; 506: 382–86.

Martins C, Hulkova H, Dridi L, Dormoy-Raclet V, Grigoryeva L, Choi Y, *et al.* Neuroinflammation, mitochondrial defects and neurodegeneration in mucopolysaccharidosis III type C mouse model. Brain 2015; 138 (Pt 2): 336–55.

Mastakov MY, Baer K, Kotin RM, During MJ. Recombinant adeno-associated virus serotypes 2- and 5-mediated gene transfer in the mammalian brain: quantitative analysis of heparin co-infusion. Mol Ther 2002; 5: 371–80.

McGlynn R, Dobrenis K, Walkley SU. Differential subcellular localization of cholesterol, gangliosides, and glycosaminoglycans in murine models of mucopolysaccharide storage disorders. J Comp Neurol 2004; 480: 415–26.

Mendell JR, Al-Zaidy S, Shell R, Arnold WD, Rodino-Klapac LR, Prior TW, *et al.* Single-dose gene-replacement therapy for Spinal Muscular Atrophy. N Engl J Med 2017; 377: 1713–22.

Mingozzi F, Anguela XM, Pavani G, Chen Y, Davidson RJ, Hui DJ, *et al.* Overcoming preexisting humoral immunity to AAV using capsid decoys. Sci Transl Med 2013; 5: 194ra92.

Morris LS, Kundu P, Dowell N, Mechelmans DJ, Favre P, Irvine MA, *et al.* Fronto-striatal organization: defining functional and microstructural substrates of behavioural flexibility. Cortex 2016; 74: 118–33. Müller OJ, Kaul F, Weitzman MD, Pasqualini R, Arap W, Kleinschmidt JA, et al. Random peptide libraries displayed on adeno-associated virus to select for targeted gene therapy vectors. Nat Biotech 2003; 21: 1040–6.

Nathwani AC, Reiss UM, Tuddenham EGD, Rosales C, Chowdary P, McIntosh J, *et al.* Long-term safety and efficacy of factor IX gene therapy in hemophilia B. N Engl J Med 2014; 371: 1994–2004.

Nguyen JB, Sanchez-Pernaute R, Cunningham J, Bankiewicz KS. Convection-enhanced delivery of AAV-2 combined with heparin increases TK gene transfer in the rat brain. Neuroreport 2001;12: 1961-4.

O'Leary C, Desbonnet L, Clarke N, Petit E, Tighe O, Lai D, *et al.* Phenotypic effects of maternal immune activation and early postnatal milieu in mice mutant for the schizophrenia risk gene neuregulin-1. Neuroscience 2014; 277: 294–305.

Ohmi K, Zhao HZ, Neufeld EF. Defects in the medial entorhinal cortex and dentate gyrus in the mouse model of Sanfilippo syndrome type B. PLoS One 2011; 6: e27461.

Opie SR, Warrington JKH, Agbandje-McKenna M, Zolotukhin S, Muzyczka N. Identification of amino acid residues in the capsid proteins of adeno-associated virus type 2 that contribute to heparan sulfate proteoglycan binding. J Virol 2003; 77: 6995–7006.

Pacouret S, Bouzelha M, Shelke R, Andres-Mateos E, Xiao R, Maurer A, *et al.* AAV-ID: a rapid and robust assay for batch-to-batch consistency evaluation of AAV preparations. Mol Ther 2017; 25: 1375–86.

Perabo L, Goldnau D, White K, Endell J, Boucas J, Humme S, *et al.* Heparan sulfate proteoglycan binding properties of adeno-associated virus retargeting mutants and consequences for their in vivo tropism. J Virol 2006; 80: 7265–9.

Rahim AA, Wong AM, Ahmadi S, Hoefer K, Buckley SMK, Hughes DA, *et al.* In utero administration of Ad5 and AAV pseudotypes to the fetal brain leads to efficient, widespread and long-term gene expression. Gene Ther 2012; 19: 936–46.

Rawlins JNP, Olton DS. The septo-hippocampal system and cognitive mapping. Behav Brain Res 1982; 5: 331–58.

Rayaprolu V, Kruse S, Kant R, Venkatakrishnan B, Movahed N, Brooke D, *et al.* Comparative analysis of adeno-associated virus capsid stability and dynamics. J Virol 2013; 87: 13150–60.

Ripamonti C, Henning GB, Robbie SJ, Sundaram V, van den Born LI, Casteels I, *et al.* Spectral sensitivity measurements reveal partial success in restoring missing rod function with gene therapy. J Vis 2015; 15: 20.

Ruijter GJ, Valstar MJ, van de Kamp JM, van der Helm RM, Durand S, van Diggelen OP, *et al.* Clinical and genetic spectrum of Sanfilippo type C (MPS IIIC) disease in The Netherlands. Mol Genet Metab 2008; 93: 104–11.

Russell S, Bennett J, Wellman JA, Chung DC, Yu Z-F, Tillman A, *et al.* Efficacy and safety of voretigene neparvovec (AAV2- hRPE65v2) in patients with RPE65-mediated inherited retinal dystrophy: a randomised, controlled, open-label, phase 3 trial. Lancet 2017; 390: 849–60.

Ryazantsev S, Yu WH, Zhao HZ, Neufeld EF, Ohmi K. Lysosomal accumulation of SCMAS (subunit c of mitochondrial ATP synthase) in neurons of the mouse model of mucopolysaccharidosis III B. Mol Genet Metab 2007; 90: 393–401.

Salegio EA, Samaranch L, Kells AP, Mittermeyer G, San Sebastian W, Zhou S, *et al.* Axonal transport of adeno-associated viral vectors is serotype-dependent. Gene Ther 2013; 20: 348–52.

Schwartz MD, Urbanski HF, Nunez AA, Smale L. Projections of the suprachiasmatic nucleus and ventral subparaventricular zone in the Nile grass rat (Arvicanthis niloticus).Brain Res 2011; 1367: 146-61.

Sergijenko A, Langford-Smith A, Liao AY, Pickford CE, McDermott J, Nowinski G, *et al.* Myeloid/microglial driven autologous hematopoi- etic stem cell gene therapy corrects a neuronopathic lysosomal disease. Mol Ther 2013; 21: 1938–49.

Seyrantepe V, Canuel M, Carpentier S, Landry K, Durand S, Liang F, *et al.* Mice deficient in Neu4 sialidase exhibit abnormal ganglioside catabolism and lysosomal storage. Hum Mol Genet 2008; 17: 1556–68.

Shen S, Horowitz ED, Troupes AN, Brown SM, Pulicherla N, Samulski RJ, *et al.* Engraftment of a galactose receptor footprint onto adeno-associated viral capsids improves transduction efficiency. J Biol Chem 2013; 288: 28814–23.

Sondhi D, Scott EC, Chen A, Hackett NR, Wong AM, Kubiak A, *et al.* Partial correction of the CNS lysosomal storage defect in a mouse model of juvenile neuronal ceroid lipofuscinosis by neonatal CNS administration of an adeno-associated virus serotype rh.10 vector expressing the human CLN3 gene. Hum Gene Ther 2014; 25: 223–39.

Sparks Therapeutics. Spark Therapeutics presents updated preliminary data from hemophilia B phase 1/2 trial suggesting consistent and sustained levels of factor IX activity at the Hemostasis and Thrombosis Research Society (HTRS) 2017 Scientific Symposium. Press Release, 2017.

Summerford C, Samulski RJ. Membrane-associated heparan sulfate proteoglycan is a receptor for adeno-associated virus type 2 virions. J Virol 1998; 72: 1438–45.

Takamatsu Y, Hagino Y, Sato A, Takahashi T, Nagasawa SY, Kubo Y, *et al.* Improvement of learning and increase in dopamine level in the frontal cortex by methylphenidate in mice lacking dopamine transporter. Curr Mol Med 2015; 15: 245–52.

Tardieu M, Zerah M, Husson B, de Bournonville S, Deiva K, Adamsbaum C, *et al.* Intracerebral administration of adeno-associated viral vector serotype rh.10 carrying human SGSH and SUMF1 cDNAs in children with mucopolysaccharidosis type IIIA disease: results of a phase I/II trial. Hum Gene Ther 2014; 25: 506–16.

Tardieu M, Zerah M, Gougeon ML, Ausseil J, de Bournonville S, Husson B, *et al.* Intracerebral gene therapy in children with mucopolysaccharidosis type IIIB syndrome: an uncontrolled phase 1/2 clinical trial. Lancet Neurol 2017; 16: 712–20.

Tervo DG, Hwang BY, Viswanathan S, Gaj T, Lavzin M, Ritola KD, *et al.* A designer AAV variant permits efficient retrograde access to projection neurons. Neuron 2016; 92: 372–82.

Tseng Y-S, Gurda BL, Chipman P, McKenna R, Afione S, Chiorini JA, *et al.* Adeno-associated virus serotype 1 (AAV1) and AAV5-antibody complex structures reveal evolutionary commonalities in parvovirus antigenic reactivity. J Virol 2015; 89: 1794–808.

Valstar MJ, Ruijter GJ, van Diggelen OP, Poorthuis BJ, Wijburg FA. Sanfilippo syndrome: a mini-review. J Inherit Metab Dis 2008; 31: 240–52.

Vandenberghe LH, Auricchio A. Novel adeno-associated viral vectors for retinal gene therapy. Gene Ther 2012; 19: 162–68.

Wilkinson FL, Holley RJ, Langford-Smith KJ, Badrinath S, Liao A, Langford-Smith A, *et al.* Neuropathology in mouse models of mucopolysaccharidosis type I, IIIA and IIIB. PLoS One 2012; 7: e35787. Winner LK, Beard H, Hassiotis S, Lau AA, Luck AJ, Hopwood JJ, *et al.* A preclinical study evaluating AAVrh10-based gene therapy for Sanfilippo syndrome. Hum Gene Ther 2016; 27: 363–75.

Woodard KT, Liang KJ, Bennett WC, Samulski RJ. Heparan sulfate binding promotes accumulation of intravitreally delivered adeno-associated viral vectors at the retina for enhanced transduction but weakly influences tropism. J Virol 2016; 90: 9878–88.

Worgall S, Sondhi D, Hackett NR, Kosofsky B, Kekatpure MV, Neyzi N, *et al.* Treatment of late infantile neuronal ceroid lipofuscinosis by CNS administration of a serotype 2 adeno-associated virus express- ing CLN2 cDNA. Hum Gene Ther 2008; 19: 463–74.

Wu P, Xiao W, Conlon T, Hughes J, Agbandje-McKenna M, Ferkol T, *et al.* Mutational analysis of the adeno-associated virus type 2 (AAV2) capsid gene and construction of AAV2 vectors with altered tropism. J Virol 2000; 74: 8635–47.

Zhang X, Wang B, Li JP. Implications of heparan sulfate and heparanase in neuroinflammation. Matrix Biol 2014; 35: 174–81.

Zinn E, Pacouret S, Khaychuk V, Turunen HT, Carvalho LS, Andres-Mateos E, *et al.* In silico reconstruction of the viral evolutionary lineage yields a potent gene therapy vector. Cell Rep 2015; 12: 1056–68.

## Figures

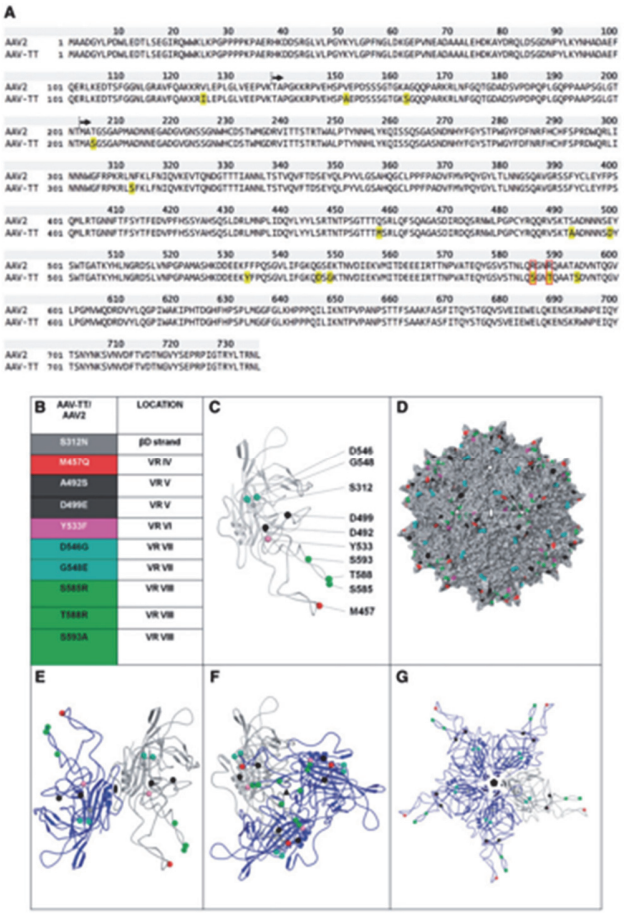


**Figure 1:** AAV-TT capsid sequence and 3D model. (A) Protein alignment of AAV-TT and AAV2 (NCBI, accession number: NC_001401.2). VP1 is shown, with residues in yellow highlighting the amino acids that differ between the two capsids. Residues boxed in red correspond to the amino acid belonging to the basic patch that constitutes the HSPG binding site. Black arrows indicate the start sites of the VP2 and VP3 capsid proteins. (B) List of AAV-TT/AAV2 differing residues located in VP3 (the amino acid change at position 205 in AAV-TT is not listed as the 3D structure of the N-terminal end of VP3 is currently unknown). The positions of these residues within VP3 variable regions (VR) are indicated. (C) Ribbon diagram of VP3 monomer with AAV-TT/AAV2 differing residues shown as spheres and coloured according to list in B. (D) Surface representation of the 3D structure of AAV2 VP3 with the position of the residues which differ from AAV-TT coloured as in B. The icosahedral 2-, 3-, and 5-fold axes are indicated by an oval, triangle and pentagon, respectively. (E–G) Ribbon diagrams of VP3 dimer, trimer and pentamer with the reference monomer coloured grey and the symmetry related monomers coloured blue.

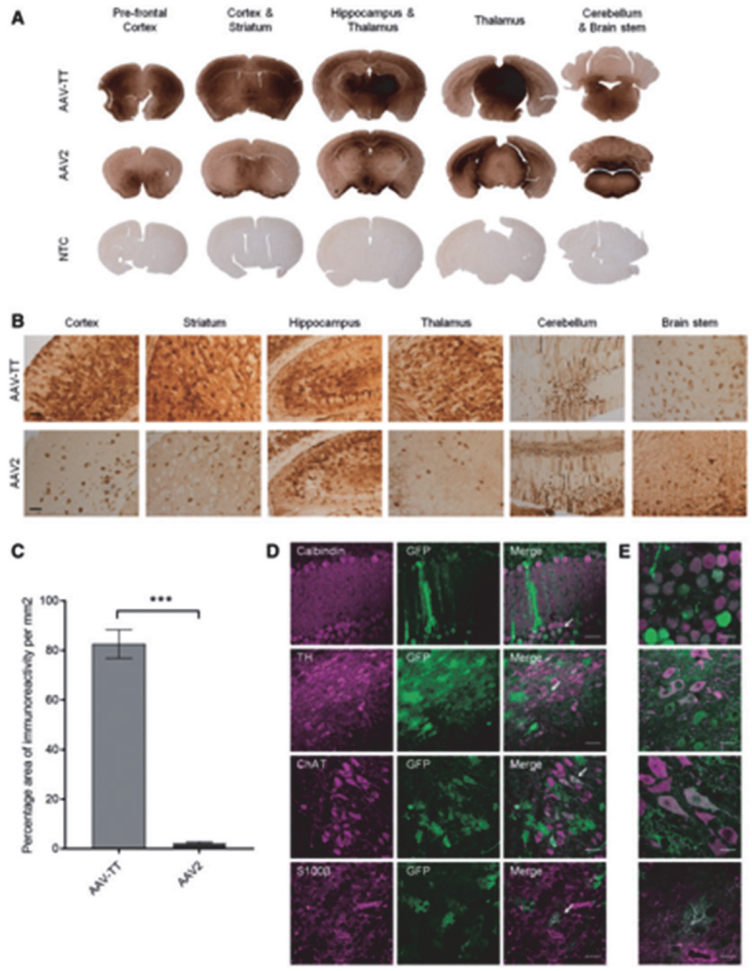


**Figure 2:** Intracerebroventricular injections in neonatal mice show superior transduction ability of AAV-TT across the CNS. $5 \times 10^{10}$ vg of GFP-expressing AAV-TT or AAV2 vectors were injected unilaterally into the lateral ventricle of neonatal mice at postnatal Day 1 (P1) ($n$ = 3 per condition). (A) Representative images of GFP signal observed 4 weeks post-injection in the different brain areas indicated. Brain sections derived from an untreated animal were used as negative control (NTC, non-transduced control, $n$ = 3). (B) High magnification images of the sections shown in A. Scale bar = 100 mm. (C) GFP signal quantified as the percentage area of immunoreactivity measured in the striatum of the injected hemisphere. Signal was significantly higher in AAV-TT as compared to AAV2 treated animals. Unpaired Student's $t$-test, two-tailed, $n$ = 3 per group. The data are presented as mean ± SEM; ***$P < 0.001$. (D) Representative images of native GFP fluorescence and calbindin, tyrosine hydroxylase (TH), choline acetyltransferase (ChAT) or S100b taken at 40 x magnification show that AAV-TT has the ability to transduce Purkinje cells, dopaminergic neurons, cholinergic neurons and astrocytes, respectively. Scale bars =

50 mm. White arrows indicate the areas magnified in E. (E) Representative images taken at 100 x magnification showing GFP expression in the areas indicated by white arrows in the corresponding panels in D. Scale bars = 20 mm.

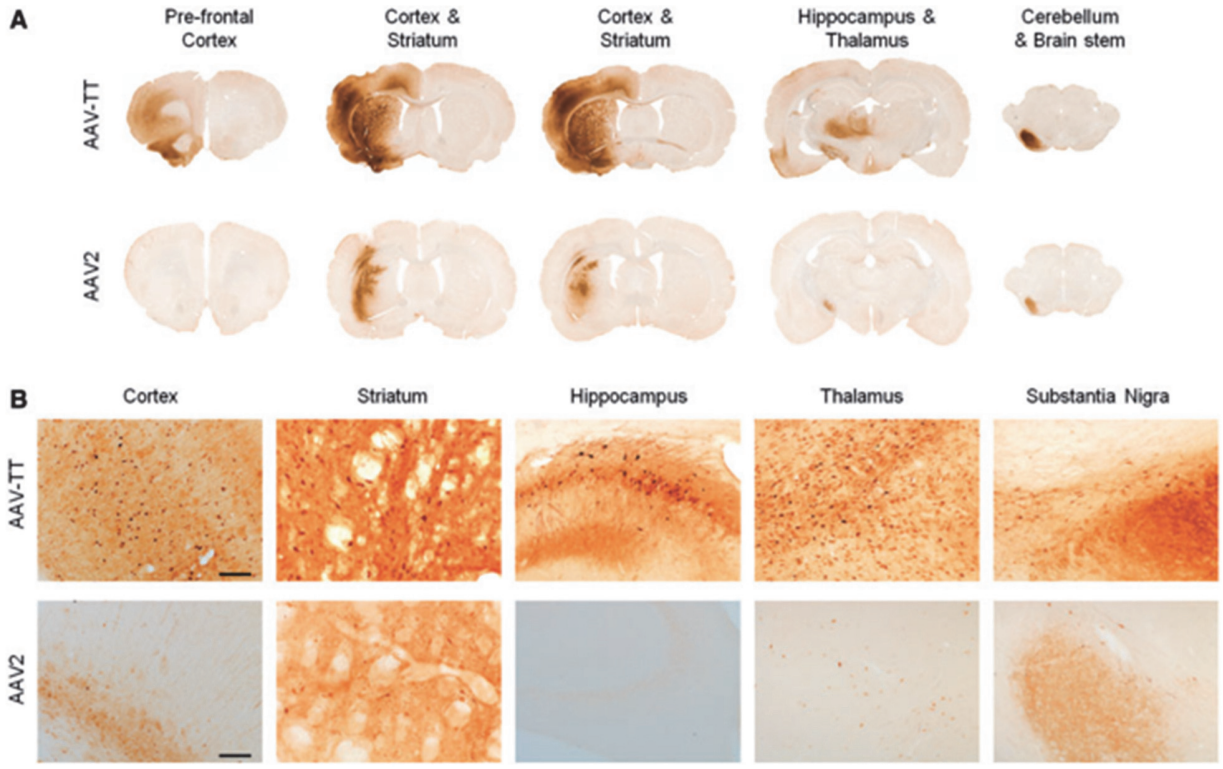


**Figure 3:** Intrastriatal injections in adult rats show superior transduction ability and vector spread of AAV-TT across large areas of the CNS. GFP-expressing AAV-TT or AAV2 (both 3.5 x 109 vg) were injected into the striatum of adult rat brains (n = 3). (A) Representative images of GFP signal 4 weeks post-injection in the different brain areas indicated. (B) High magnification images of the sections shown in A. Scale bar = 100 mm.

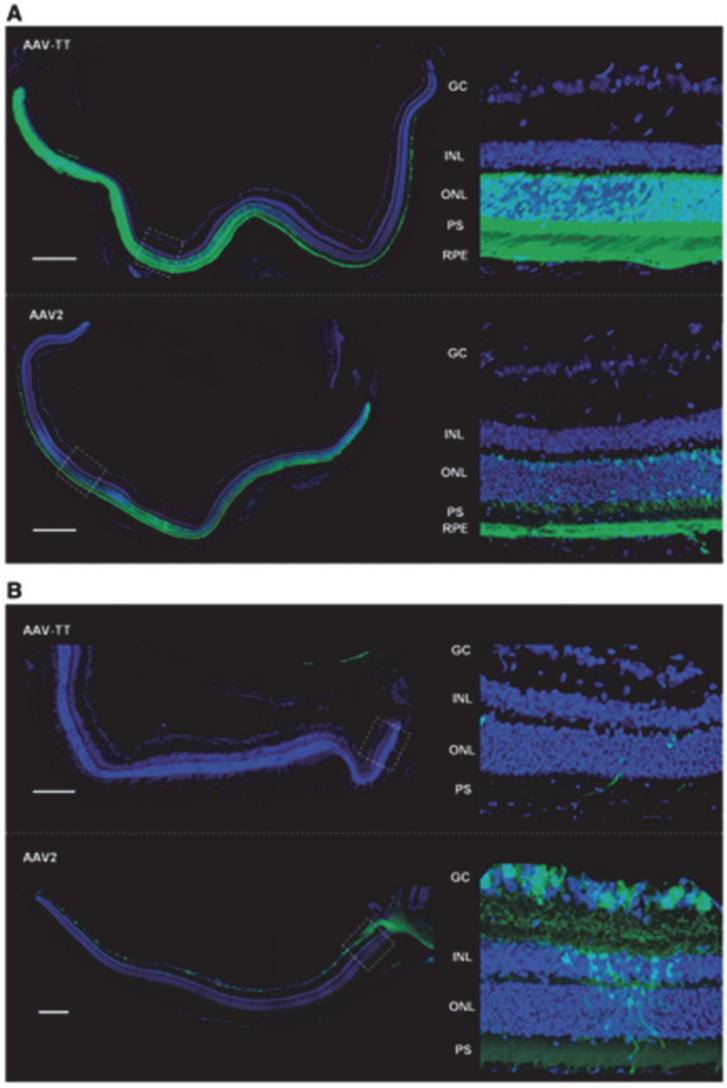


**Figure 4:** Sub-retinal injections in adult mice show superior transduction ability of AAV-TT throughout different layers of the retina. GFP expressing AAV2 and AAV-TT were injected contralaterally in adult mice at a dose of $2 \times 10^9$ vg per eye ($n = 4$ per condition).

(A) Representative confocal z-projections of transverse sections of the retina taken 4 weeks after sub-retinal injections show that AAV-TT targets a higher number of RPE and photoreceptor cells and mediates increased transgene expression as compared to AAV2. (B) AAV-TT cannot efficiently penetrate the retina when injected via the intra-vitreal route; intra-vitreal injection of AAV2 leads to transduction of retinal ganglion cells. GC = ganglion cell layer; INL = inner nuclear layer; ONL = outer nuclear layer; PS = photoreceptor segments; RPE = retinal pigment epithelium. Scale bar = 200 mm.

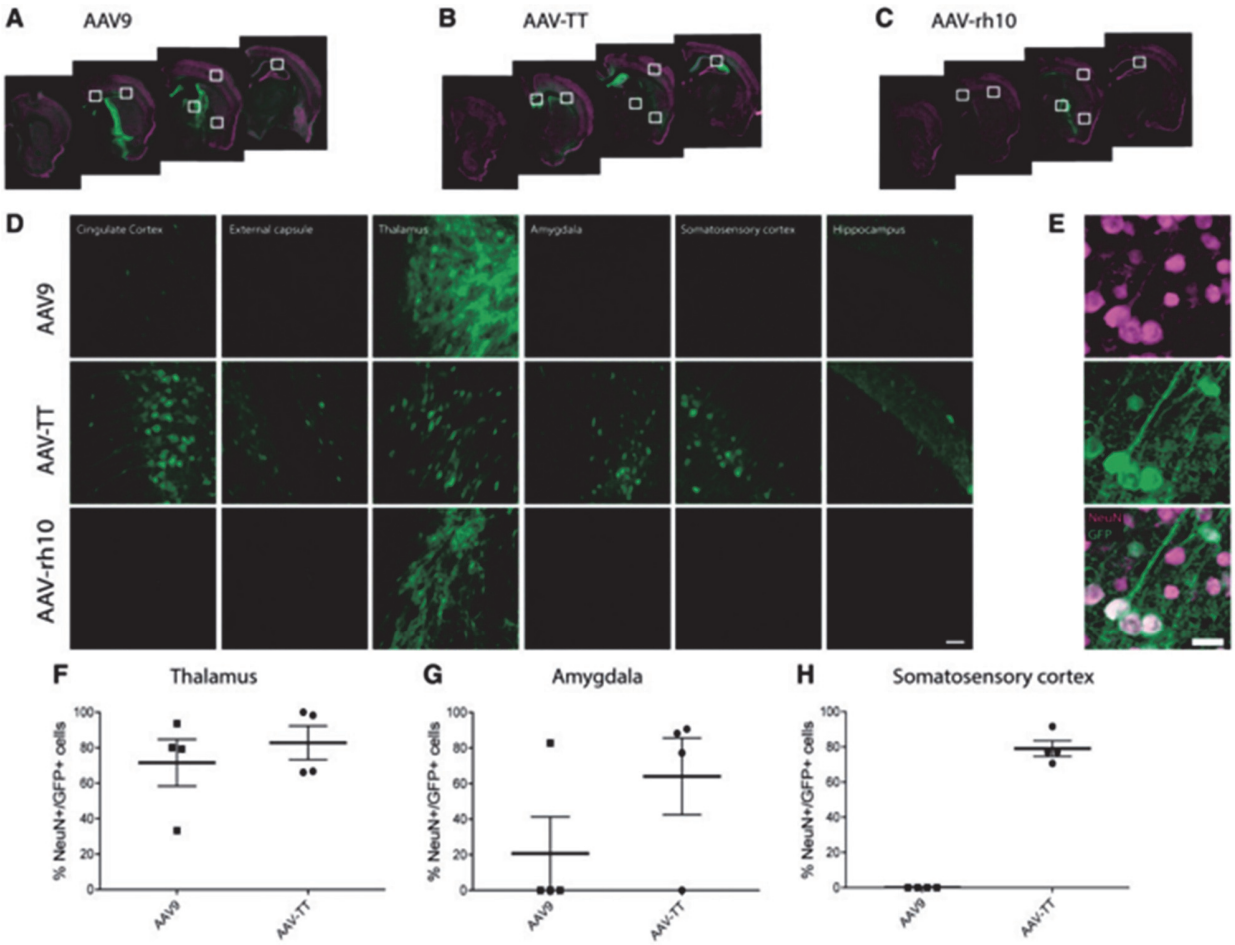


**Figure 5:** AAV-TT outperforms AAV9 and AAVrh10 in GFP biodistribution studies. GFP vectors were packaged into AAV9, AAVrh10 or AAV-TT capsids and used for comparative biodistribution studies. (A-C) Representative confocal microscopy images showing GFP expression in the CNS of mice 3 weeks after they were injected with the three different marker viruses. The white squares indicate the areas that are shown at higher magnification in D. (D) Representative confocal images showing GFP expression in the areas indicated in (A–C). Scale bar = 50 mm. (E) NeuN staining of brain sections of adult mice treated with AAV-TT shows that AAV-TT specifically transduces neurons. Scale bar = 20 mm. The percentage of NeuN/GFP co-localizing cells in the (F) thalamus (G) amygdala and (H) somatosensory cortex in AAV9- and AAV-TT-treated mice.

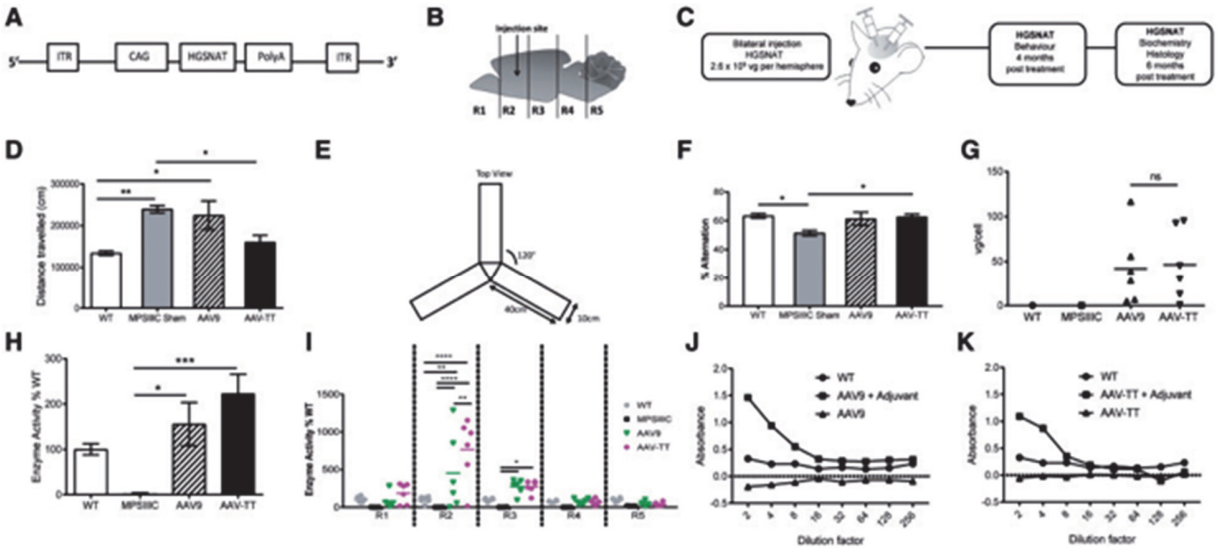


**Figure 6:** AAV-TT effectively corrects disease phenotype in MPSIIIC mice. (A) AAV-HGSNAT vectors, packaged into AAV9 or AAV-TT capsids, were used to treat MPSIIIC mice. (B) Schematic of injection site and brain sectioning used for enzyme level determination. (C) Overview of treatment and analysis scheme. (D) Hyperactivity as measured by distance travelled by wild-type (wt, n = 8) and MPSIIIC sham (n = 11), AAV9 (n = 8) and AAV-TT (n = 7) treated MPSIIIC mice. (E) Configuration of Y-maze. (F) Cognitive ability as measured by the percentage of alternation in the Y- maze of wild-type (n = 10) and MPSIIIC sham (n = 12), AAV9 (n = 9) and AAV-TT (n = 9) treated MPSIIIC mice. (G) Vector genome copy numbers (vg/cell) measured by qPCR in whole brain tissue preparations from wild-type (n = 1), MPSIIIC (n = 1), AAV9 (n = 6) and AAV-TT (n = 6) treated MPSIIIC mice. (H) HGSNAT enzyme activity measured in whole brain preparations of wild-type (n = 6), MPSIIIC (n = 6), AAV9 (n = 6) and AAV-TT (n = 6) treated MPSIIIC mice. (I) HGSNAT enzyme activity measured in brain sections R1–R5. (J) Total IgG antibody responses against AAV9 capsid proteins as measured by ELISA. Absence of capsid-specific antibodies in brain homogenates of AAV9-coHGSNAT (n = 6) treated mice. (K) Total IgG antibody responses against AAV-TT capsid proteins as measured by ELISA. Absence of capsid-specific antibodies in brain homogenates of AAV-TT-HGSNAT (n = 6) treated mice. Positive controls consist of mice treated with vectors and adjuvant. ANOVA followed by Tukey's post hoc multiple comparison test. Data are presented as mean ± SEM; $*P < 0.05$; $**P < 0.01$; $***P < 0.001$; $****P < 0.0001$.

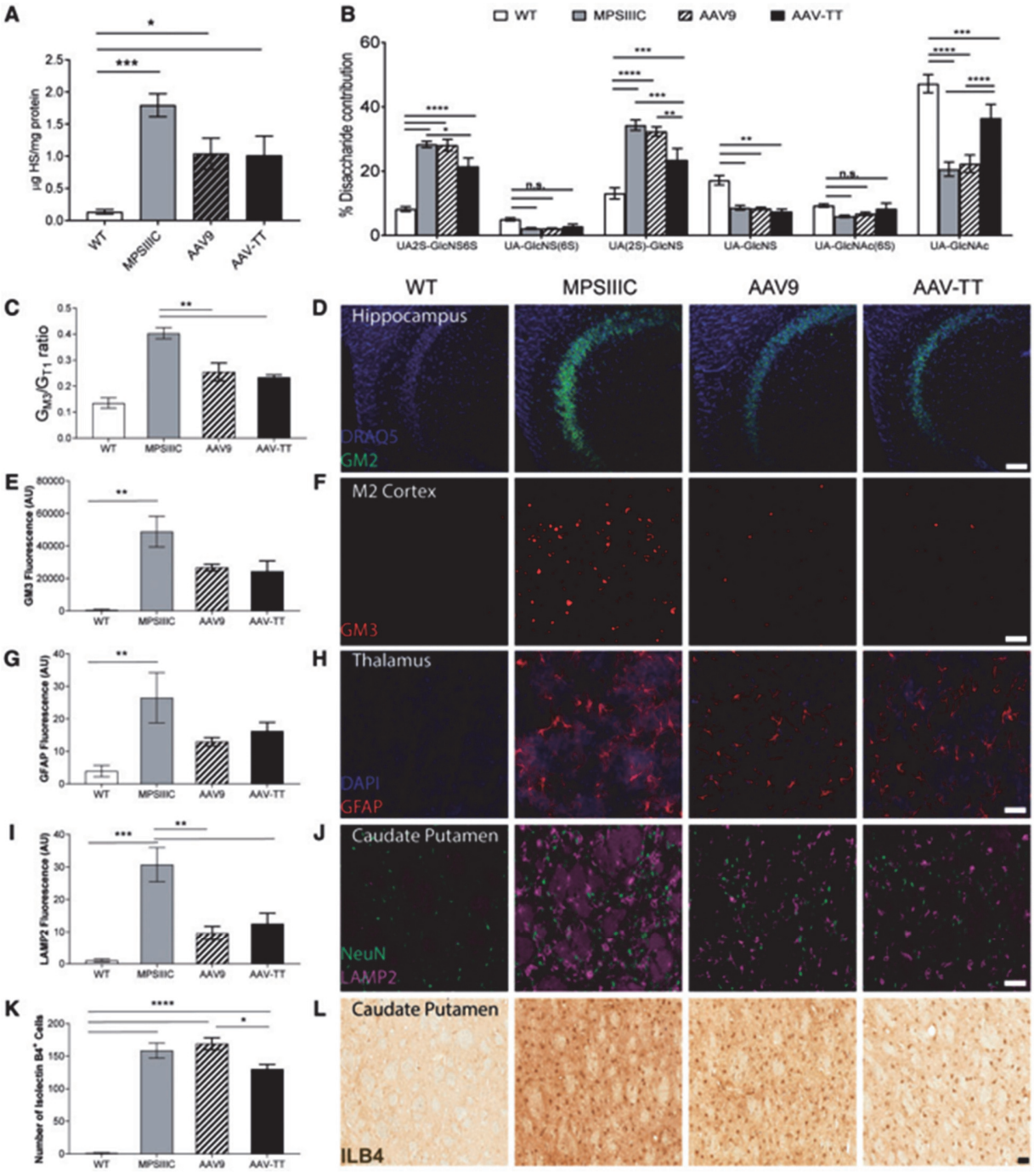


**Figure 7:** AAV-TT reduces primary and secondary storage molecules leading to a reduction in neuroinflammation in MPSIIIC mice. (A) Primary storage i.e. total HS measured by reversed phase chromatography in brains in wild-type (wt, n = 6), untreated MPSIIIC (n = 6), AAV9 (n = 6) and AAV-TT (n = 6) treated MPSIIIC mice. (B) Measurement of the different disaccharide contributions in HS in wild-type (n = 6), untreated MPSIIIC (n = 6), AAV9 (n = 6) and AAV-TT

(n = 6) treated MPSIIIC mice shows normalization of the relative proportion of HS that is NAc, 6S and 2S sulphated. (C) Secondary storage i.e. GM3 gangliosides measured by thin layer chromatography in homogenized brain tissues of wild-type (n = 4), untreated MPSIIIC (n = 3), AAV9 (n = 4) and AAV-TT (n = 4) treated MPSIIIC mice, which is reduced in treated MPSIIIC mice. (D) Storage of GM2 ganglioside in the hippocampus of wild-type (n = 2), untreated MPSIIIC (n = 6), AAV9 (n = 3) and AAV-TT (n = 4) treated MPSIIIC mice, which is reduced in treated MPSIIIC mice. (E and F) Storage of GM3 stained brain sections in the M2 cortex of wild-type (n = 2), untreated MPSIIIC (n = 6), AAV9 (n = 3) and AAV-TT (n = 4), which is reduced in treated MPSIIIC mice. Scale bar = 20 mm. (G and H) Confocal microscopy of GFAP stained brain sections in wild-type (n = 4), untreated MPSIIIC (n = 3), AAV9 (n = 4) and AAV-TT (n = 4) treated MPSIIIC mice shows trend towards reduction in the accumulation of GFAP positive astrocytes in the thalamus of treated MPSIIIC mice. (I and J) Confocal microscopy of LAMP2 stained brain sections in wild-type (n = 4), untreated MPSIIIC (n = 3), AAV9 (n = 4) and AAV-TT (n = 4) treated MPSIIIC mice shows reduction in lysosomal LAMP2 staining in the caudate putamen in treated MPSIIIC mice. (K and L) Confocal microscopy of ILB4 stained brain sections in wild-type (n = 4), untreated MPSIIIC (n = 4), AAV9 (n = 4) and AAV-TT (n = 4) treated MPSIIIC mice shows improvement in neuroinflammation in the caudate putamen in AAV-TT-HGSNAT treated mice. ANOVA followed by Tukey's post hoc multiple comparison test. Data are mean ± SEM; *$P < 0.05$; **$P < 0.01$; ***$P < 0.001$; ****$P < 0.0001$. Scale bar = 50 mm.

## Supplementary figure

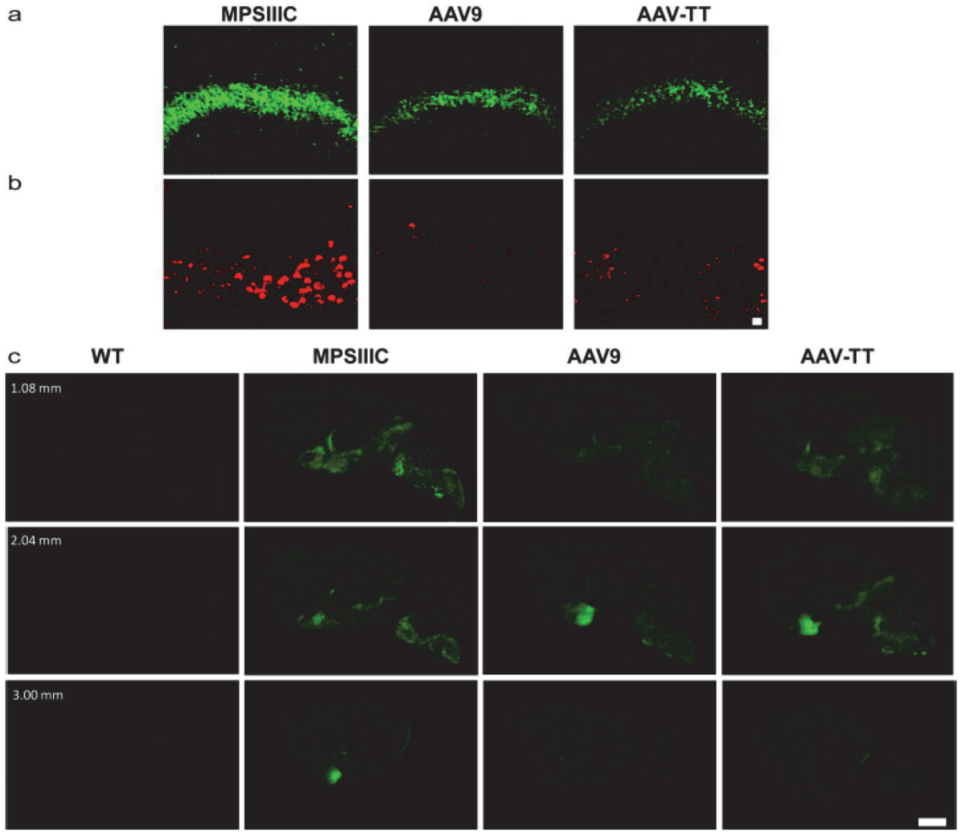


**Supplementary figure 7.** AAV-TT and AAV-9 correct storage of GM2 and GM3 gangliosides in specific brain regions.

GM2 and GM3 accumulation is reduced in specific brain areas of AAV-coHGSNAT treated MPS IIIC mice as compared to untreated mice. (a) Treatment of MPS IIIC with both AAV9-coHGSNAT and AAV-TT-coHGSNAT vectors leads to a decreased in the accumulation of GM2 in the field CA3 of the hippocampus, as compared with untreated animals. (b) GM3 was significantly reduced in Medial Entorhinal cortex (MEnt) of mice treated with both AAV9-coHGSNAT and AAV-TT-coHGSNAT. Scale bar: 20µm. (c) Representative images of GM2 ganglioside levels in wt, MPS IIIC, AAV9-coHGSNAT and AAV-TT-coHGSNAT treated mice. As the site of injection was 2mm lateral to the bregma the images were acquired in the saggital sections 2.04mm and two other sections equidistant to the site of injection, 1.08mm and at 3.00mm lateral from the bregma as indicated in the picture using Slide Scanner Axio Scan Z1 from Zeiss (objective 10x/0.45). Scale bar: 500µm.